MODIFIED MONOTERPENE INDOLE ALKALOID PRODUCTION IN THE YEAST *SACCHAROMYCES CEREVISIAE*

A Dissertation
Presented to
The Academic Faculty

by

Amy M. Ehrenworth

In Partial Fulfillment
of the Requirements for the Degree
Doctor of Philosophy in the
School of Chemistry and Biochemistry

Georgia Institute of Technology
December, 2017

MODIFIED MONOTERPENE INDOLE ALKALOID PRODUCTION IN THE YEAST *SACCHAROMYCES CEREVISIAE*

Approved by:

Dr. Pamela Peralta-Yahya, Advisor
School of Chemistry and Biochemistry
Georgia Institute of Technology

Dr. Francesca Storici
School of Biological Studies
Georgia Institute of Technology

Dr. M.G. Finn
School of Chemistry and Biochemistry
Georgia Institute of Technology

Dr. Loren Williams
School of Chemistry and Biochemistry
Georgia Institute of Technology

Dr. Wendy L. Kelly
School of Chemistry and Biochemistry
Georgia Institute of Technology

Date Approved: August 14, 2017

ACKNOWLEDGEMENTS

I would like to thank all those who've guided me on my scientific and personal journey. I was blessed by the circumstances that have led me to this point, and I hope to make those who have influenced and inspired me proud.

I want to express gratitude to my advisor Pamela Peralta-Yahya for all she has done for me in my time at Georgia Tech- from introducing me to the incredible field of synthetic biology and sharing her knowledge to helping make me a better scientist. I admire her dedication and ambition, and I am honored to have helped establish the Peralta-Yayha lab. I also appreciate the guidance I've received from all of my committee members throughout the years, be it via scientific discussions, mentorship, or personal inspiration.

I value the friendships and experiences I've gained with all of the past and current members of the Peralta-Yahya lab. I want to express special thanks to Stephen Sarria, who has been through this journey with me from day one, and Emily Yasi for their companionship through years of joys and frustrations and to Dr. Kuntal Mukherjee for sharing his insights and knowledge. I'd also like to recognize the undergraduates and research technicians that have worked with me. I've grown as a person through my interactions with all of you and I am eager to see what you all accomplish.

In addition to labmates, I've had a number of other friends that helped accompany me through this time. While relationships change over time, I cherish all of my interactions and memories of the last five years. I want to express special thanks to Udita

Brahmachari. I treasure your unwavering confidence, support, and friendship. I couldn't have done it without you. I also appreciate the continuing friendships from earlier chapters in my life that have helped support me throughout my time at Georgia Tech.

I can't express in words my thanks to my parents and grandparents for their constant support every day of my life. I am blessed with your presence and love in my life.

Finally, I express my deepest gratitude to my fiancé Donovan. You are my rock in every way. You've stood by me through my good days and bad and always drive me to be a better person. I can't wait to take the next steps in my career and in life together with you.

TABLE OF CONTENTS

LIST OF TABLES

LIST OF FIGURES

LIST OF ABBREVIATIONS

µg	Microgram
µL	Microliter
µM	Micromolar
4-HPAA	4-Hydroxyphenylacetaldehyde
5-HIAA	5-Hydroxyindoleacetic acid
5-HTP	5-Hydroxytryptophan
ADMET	Absorption, Distribution, Metabolism, Excretion, and Toxicity
BH_4	Tetrahydrobiopterin
BH_4-OH	BH_4-4a-carbinolamine
BBIA	Bisbenzylisoquinoline Alkaloid
BIA	Benzylisoquinoline Alkaloid
°C	Degree Celcius
CloA	Clavine Oxidase
CV	Coefficient of Variation
DDC	Aromatic L-Amino Acid Decarboxylase
DDMM	8,14-Didehydro-3-methoxymorphinan
DHPR	Dihydropteridine Reductase
DMAPP	Dimethylallylpyrophosphate
DmaW	Tryptophan Dimethylallyltransferase
DOPA	L-3,4-Dihydroxyphenylalanine
EasA_Nl	Chanoclavine-I Aldehyde Reductase from *Neotyphodium lolii*
EasC	Catalase

EasE	FAD-linked Oxidoreductase
EasF	4-Dimethylallyltryptophan *N*-Methyltransferase
EasG	Agroclavine Dehydrogenase
FDA	US Food and Drug Administration
FgaDH	Chanoclavine-I Dehydrogenase
g	Gram
g	Gravity
GFLOMT2	*O*-Methyltransferase from *Glaucium flavum*
GFP	Green Fluorescent Protein
GPCR	G-Protein Coupled Receptor
GTP	Guanosine Triphosphate
GTPCH	GTP Cyclohydrolase
h	Hour
HTR	Serotonin (5-Hydroxytryptamine) Receptor
L	Liter
LC/MS	Liquid Chromatography/Mass Spectrometry
L-DOPA	L-3,4-Dihydroxyphenylalanine
M	Molar
MH_4	Tetrahydromonapterin
mg	Milligram
MIA	Monoterpene Indole Alkaloid
min	Minute
mL	Milliliter
mM	Millimolar
MRM	Multple Reaction Monitoring

m/z	Mass-to-charge Ratio
N4OMT	Norbelladine 4′-*O*-Methyltransferase
NCS	Norcoclaurine Synthase
NR	Noroxomaritidine Reductase
OD	Optical Density
PCD	Pterin-4a-carbinolamine Dehydratase
PTPS	Pyruvoyl Tetrahydropterin Synthase
rt	Retention Time
s	Second
SalR	Salutaridine Reductase
SalS	Salutaridine Synthase
Sero	Serotonin
SR	Sepiapterin Reductase
STR	Strictosidine Synthase
TH	Tyrosine Hydroxylase
TPH	Tryptophan Hydroxylase
Trp	Tryptophan
WHO	World Health Organization

SUMMARY

Alkaloids are a large group of nitrogen containing natural products found throughout nature, in particular in plants, which tend to possess a variety of medical uses. These include pain killers such as morphine and codeine, anti-cancer agents such as vinblastine and camptothecin, anti-malarial drugs such as quinine, anti-microbial agents, and drugs that affect the cardiovascular or nervous system. The usefulness of these compounds make them very desirable, however their complex chemical syntheses force us to rely on plant-extraction to obtain the molecules of interest. This process is hindered due to low natural abundances and difficult separation due to other similar compounds present in the native plants. The synthesis of plant alkaloids in microbes would enable their rapid and scalable production. Microbial production has the advantages of short doubling time, rapid extraction of the alkaloid from the culture medium, easier isolation of the desired alkaloid due to the absence of similar natural products, and a lack of endogenous pathway regulation.

Often times, microbial production of a modified natural product can be more beneficial than production of the natural product, especially when looking at therapeutic molecules. Modifications can lead to pharmaceuticals with improved or novel uses. In addition, microbially-produced modified natural products can accelerate the semi-synthesis of known and novel drugs. **Chapter 1** reports the enzymatic steps that must be discovered, engineered, or evolved to develop microbes to produce modified alkaloids that would aid in the semisynthesis of FDA-approved drugs currently on the market in the United States.

Chapter 2 focuses on microbial production of the modified monoterpene indole alkaloid hydroxystrictosidine in the yeast *Saccharomyces cerevisiae*, which could enable the accelerated semisynthesis of known and novel camptothecin-derived anti-cancer pharmaceuticals. This chapter reports the use of a pterin-dependent mono-oxidation strategy for the microbial synthesis of the biogenic amines dopamine and serotonin and the leveraging of serotonin to produce hydroxystrictosidine.

Improving the biosynthetic performance of microbes for the synthesis of non-colorimetric chemicals, such as serotonin, is slow due to reliance on low-throughput technologies for chemical detection. Chemical biosensors, which convert chemical detection into a fluorescent signal, have the potential to accelerate this screening process. Recently, we developed G-protein-coupled receptor (GPCR)-based sensors in yeast for this purpose. **Chapter 3** reports the engineering of a GPCR-based sensor to detect serotonin in the spent medium of a serotonin-producing microbe in a medium-throughput fashion. This work showcases the ease of generating GPCR-based chemical sensors and their ability to detect specific chemicals in complex aqueous solutions. Further, this work sets the stage for the rapid engineering of serotonin-producing microbes, which can result in higher yielding alkaloid-producing microbes.

Compartmentalization of metabolic pathways into organelles of the yeast *S. cerevisiae* is a useful way to improve microbial production of chemicals. While several translocation tags have been used to localize proteins to various organelles, there was no quantitative data on their translocation efficiencies. **Chapter 4**, reports the quantification of translocation efficiencies of multiple signal tags. This work will enable metabolic

engineers to rationally choose translocation tags for the compartmentalization of metabolic pathway enzymes and to understand the limitations of the chosen tag.

In **Chapter 5**, I propose future directions related to the preceding chapters.

CHAPTER 1. Accelerating the Semisynthesis of Alkaloid-based Drugs through Metabolic Engineering

Reprinted by permission from MacMillan Publishers Ltd.:
Ehrenworth, A.M. and Peralta-Yahya, P. Accelerating the Semisynthesis of Alkaloid-based Drugs through Metabolic Engineering *Nature Chemical Biology* 13, 249-258.

1.1 Abstract

Alkaloid-derived pharmaceuticals are commonly semisynthesized from plant-extracted starting materials, which often limits their availability and final price. Recent advances in synthetic biology have enabled the introduction of complete plant pathways into microbes for the production of plant alkaloids. Microbial production of modified alkaloids has the potential to accelerate the semisynthesis of alkaloid-derived drugs by providing advanced intermediates that are structurally closer to the final pharmaceuticals and could be used as advanced intermediates for the synthesis of novel drugs. Here, we analyze the scientific and engineering challenges that must be overcome to generate microbes to produce modified plant alkaloids that can provide more suitable intermediates to US Food and Drug Administration–approved pharmaceuticals. We highlight modified alkaloids that currently could be produced by leveraging existing alkaloid microbial platforms with minor variations to accelerate the semisynthesis of seven pharmaceuticals on the market.

1.2 Introduction

Natural products are a prime source of lead compounds for use in small-molecule drug discovery. Indeed, of all new small-molecule-based pharmaceuticals approved between 1981 and 2014, 51% were based on natural products whereas 49% were synthetic. Of the natural product-based drugs, most were natural product-derived or synthetic drugs with natural product backbones, while only a small minority were natural products or botanical mixtures[1]. Natural product-derived pharmaceuticals are often semisynthesized, starting with a microbially produced or plant-extracted natural product, which is then chemically modified to improve therapeutic properties including absorption, distribution, metabolism, excretion, and toxicity (ADMET)[2]. For example, commercial synthesis of the anticancer drugs topotecan and irinotecan starts with plant-extracted camptothecin, while commercial production of the anticancer drug vinorelbine starts from plant-extracted catharanthine[3]. Access to plant natural products for use as starting materials in the semisynthesis of pharmaceuticals is challenging because of the low levels at which these products accumulate in native plants, the long doubling times of plants and plant cultures, and the difficult isolation of the desired natural products from other metabolites with similar chemical properties[4]. Substantial efforts in plant breeding and plant metabolic engineering have increased the yields of pharmaceutically relevant plant natural products, including plant alkaloids[5-8], which have a wide range of therapeutic uses from anticancer and antipsychotic agents to analgesics and antimalarials. Nevertheless, the lack of high-throughput plant transformation and screening technologies, compounded by the difficulty in overcoming endogenous plant pathway

regulation, makes the engineering of plants for the increased production of specific natural products slow moving.

Advances in metabolic engineering and synthetic biology have enabled the reconstruction of plant metabolic pathways in rapidly dividing microbes (0.5–3 h doubling time) such as *Escherichia coli* and *Saccharomyces cerevisiae*. The reduced cost of DNA synthesis and sequencing[9], together with the availability of more efficient DNA assembly technologies[10], has made the engineering of microbes for the low-level production of plant natural products routine, at least for compounds for which the biosynthetic enzymes are known[11]. The appeal of using microbes for the production of plant natural products includes the simplified purification process—no similar metabolites are endogenously produced by the microbe—and the sidestepping of native plant pathway regulation, which enable overproduction of the desired natural product or intermediate thereof. The vision for engineering microbes to produce plant natural products is to provide greater access to natural products or natural product intermediates for use in the semisynthesis of final therapeutics. The most successful realization of this vision has been the production of the antimalarial artemisinin using artemisinic acid produced by an engineered microbe[12]. After multiyear optimizations that resulted in microbial titers of 25 g/L for artemisinic acid, semisynthetic artemisinin was produced commercially in 2014[13]. While market demand for artemisinin has steadied lately as a result of changes in global malaria treatment, semisynthetic artemisinin has contributed to long-term price stability and has provided a key alternative source for a plant-derived natural product pharmaceutical[14].

In some instances, improvements in economic value, for example, lower production costs, and therapeutic value, for example, access to novel structures, may be achieved by engineering microbes to produce alkaloids that more closely resemble current pharmaceuticals (Figure 1.1). Analysis of commercial alkaloid-based therapeutics shows that production of modified plant alkaloids that carry functional groups amenable to rapid chemical derivatization has the potential to enable faster semisynthesis of known or novel pharmaceuticals[15,16]. In the last seven years, initial efforts to leverage plants to produce modified alkaloids have taken place, specifically in the production of modified monoterpene indole alkaloids, where non-natural substrates were fed to plants to incorporate halogen, azido, and methyl groups in the final product or engineered heterologous halogenases were introduced for the addition of chlorine or bromine to the natural product *in situ*[17-20]. Nevertheless, production of modified alkaloids in planta suffers from the same obstacles as production of natural products in plants.

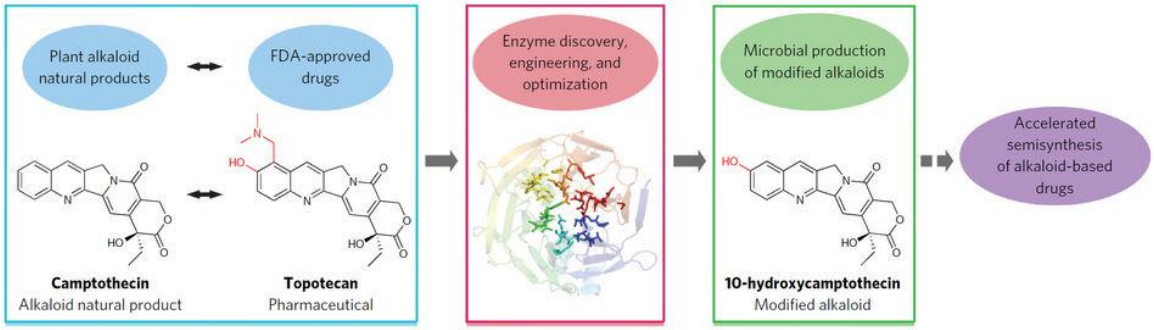

Figure 1.1. Microbial production of advanced intermediates for plant-alkaloid-based pharmaceuticals. By dissecting similarities between natural products and current FDA-approved pharmaceuticals, microbes can be engineered for the production of modified alkaloids that can serve as more suitable advanced intermediates for the semisyntheses of known and novel pharmaceuticals when compared to natural products.

Outstanding progress in plant pathway reconstruction in microbes has not majorly translated to the production of modified natural products in microbes. Recently, the majority of the work in plant pathway reconstruction in microbes has centered on alkaloid-based natural products. Since 2014, microbes have been engineered to produce over a dozen plant alkaloid natural products, including strictosidine, berberine, noscapine, stylopine, caffeine, cycloclavine, and various morphinans such as morphine and codeine[20-36]. In the same time period, microbes have been engineered to produce at least six modified plant alkaloids, including *N*-methylcheilanthifoline, 1-hydroxycanadine, 10-hydroxystrictosidine, and current semisynthetic opioids such as hydrocodone[23,29,30,34,35,37].

In this chapter, we analyze how structurally far microbially produced plant alkaloids are from the closest US Food and Drug Administration (FDA)-approved pharmaceuticals and the challenges that must be overcome to engineer microbes to produce modified plant alkaloids that more closely resemble final pharmaceuticals (Table 1-1). Specifically, we focus on production in *E. coli* and *S. cerevisiae*, as these platforms have been leveraged

for the biosynthesis of complex plant alkaloids. We define a 'modified alkaloid' as a natural product alkaloid that has additional functional groups (for example, hydroxyl or halogen groups) or an unnatural alkaloid generated using promiscuous enzymes to achieve, for example, a different stereochemistry. As the microbial production of plant alkaloids has centered on phenylalanine- and tyrosine- or tryptophan-derived alkaloids, these are the major alkaloid classes covered in this chapter (Figure 1.2, Figure 1.3). Furthermore, we focus on the alkaloid subclasses that result in chemical cores used in FDA-approved pharmaceuticals. We analyze the enzymatic steps that must be discovered, engineered, or evolved to develop microbes to produce alkaloids that would aid in the semisynthesis of FDA-approved non-peptide small-molecule drugs currently on the market in the United States. We do not include in our analysis commonly used supplements without FDA approval (for example, melatonin and yohimbine), compounds with reported medical activities or that are currently only in clinical trials (for example, norcoclaurine and berberine), drugs only approved outside the United States (for example, noscapine), or drugs with discontinued marketing (for example, tubocurarine) (Drugs@FDA, https://www.accessdata.fda.gov/scripts/cder/daf/)[38]. This chapter strives to provide a roadmap for the enzymatic steps that would need to be discovered or engineered to achieve the microbial production of alkaloid-based pharmaceuticals or their semisynthetic intermediates.

Table 1-1. FDA approved drugs mentioned in this chapter with chemical structures and selected uses, listed by class.

Drug Name	Alkaloid Class	Structure	Uses/Treatments
Dopamine[a]	Phenylethylamine	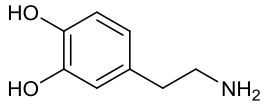	Heart failure, stimulant
Ephedrine[a]	Phenylethylamine	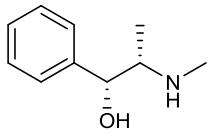	Hypotension during spinal anaesthesia
Epinephrine[a]	Phenylethylamine	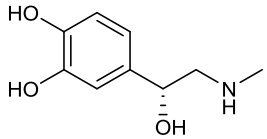	Anaphylaxis, asthma, cardiac arrest
Formoterol	Phenylethylamine	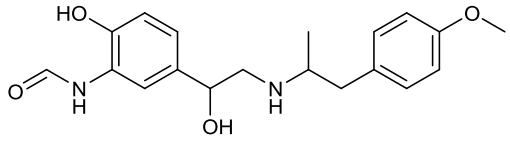	Asthma, COPD
Phenelzine	Phenylethylamine	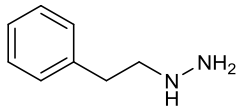	Major depressive disorder
Pseudoephedrine	Phenylethylamine	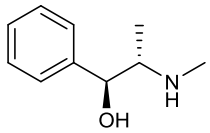	Decongestant

Table 1-1 (continued)

Drug Name	Alkaloid Class	Structure	Uses/Treatments
Praziquantel[a]	Tetrahydroisoquinoline	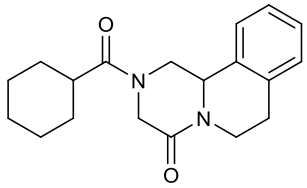	Anthelmintic
Solifenacin	Tetrahydroisoquinoline	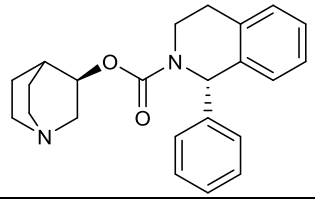	Overactive bladder
Tetrabenazine	Tetrahydroisoquinoline	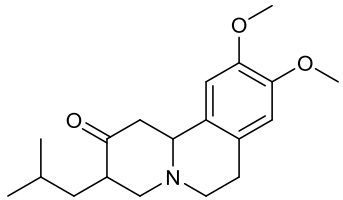	Chorea associated with Huntington's disease
Trabectedin	Tetrahydroisoquinoline	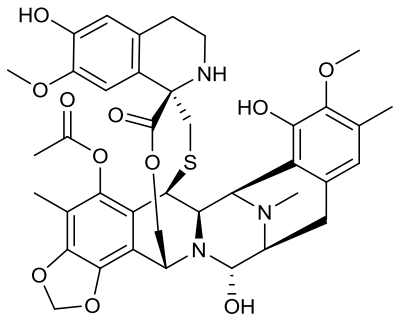	Soft tissue sarcomas, anticancer

Table 1-1 (continued)

Drug Name	Alkaloid Class	Structure	Uses/Treatments
Galantamine	Amaryllidaceae	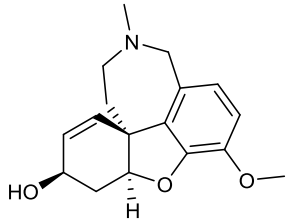	Alzheimer's disease
Colchicine	Phenylethylisoquinoline	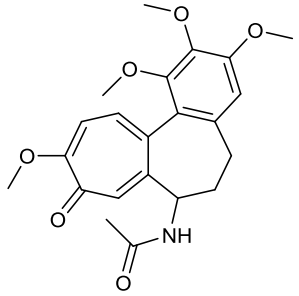	Gout
Atracurium[a]	Bisbenzylisoquinoline	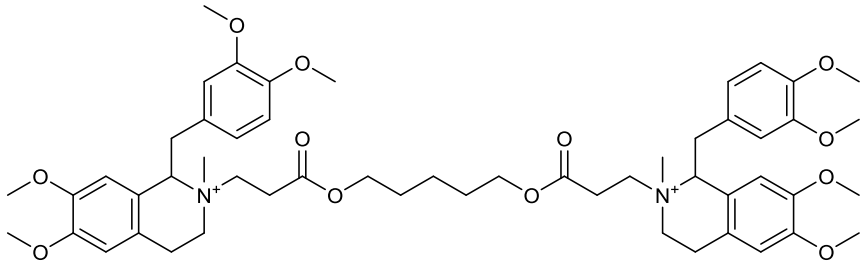	Skeletal muscle relaxant

Table 1-1 (continued)

Drug Name	Alkaloid Class	Structure	Uses/Treatments
Cisatracurium	Bisbenzylisoquinoline	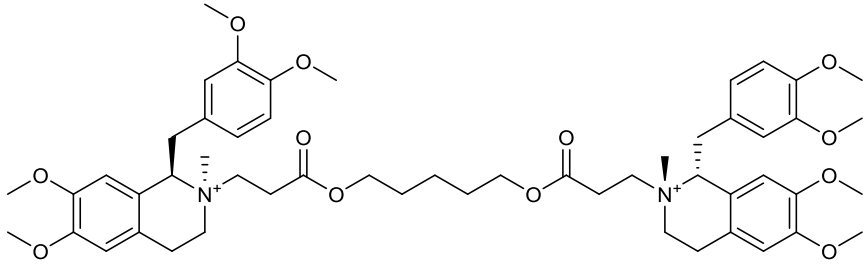	Skeletal muscle relaxant
Mivacurium	Bisbenzylisoquinoline	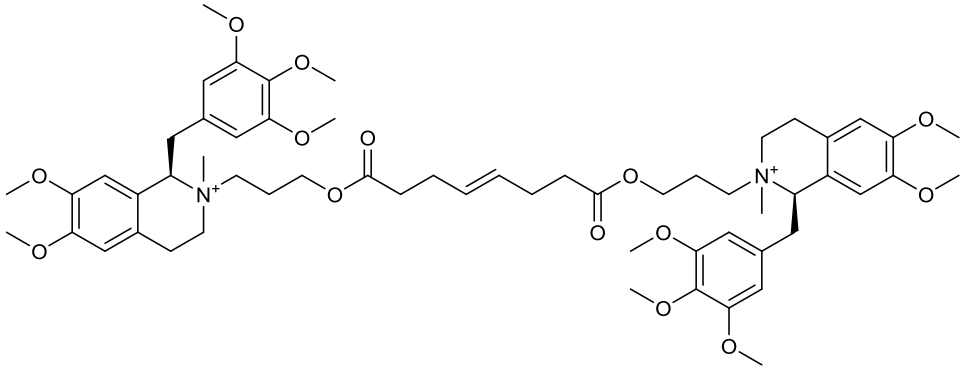	Skeletal muscle relaxant
Apomorphine	Aporphine	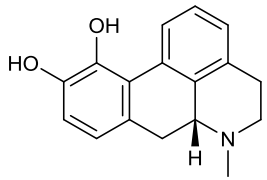	Parkinson's Disease

Table 1-1 (continued)

Drug Name	Alkaloid Class	Structure	Uses/Treatments
Buprenorphine[a]	Morphinan	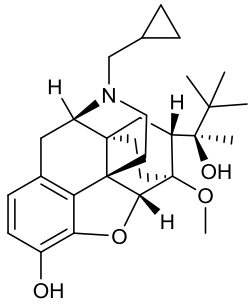	Analgesic, opioid addiction
Butorphanol	Morphinan	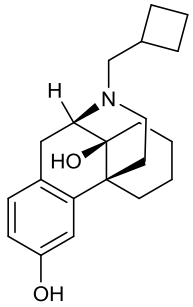	Analgesic
Codeine[a]	Morphinan	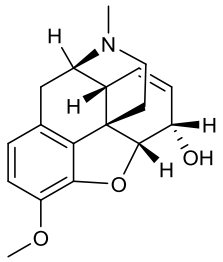	Analgesic, cough suppressant

Table 1-1 (continued)

Drug Name	Alkaloid Class	Structure	Uses/Treatments
Dihydrocodeine	Morphinan	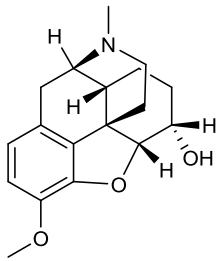	Analgesic
Hydrocodone	Morphinan	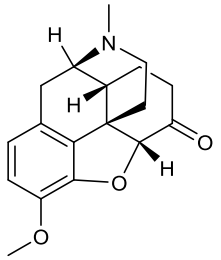	Analgesic, cough suppressant
Hydromorphone[a]	Morphinan	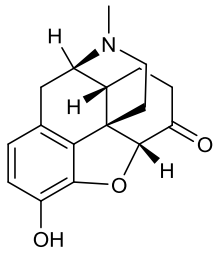	Analgesic

Table 1-1 (continued)

Drug Name	Alkaloid Class	Structure	Uses/Treatments
Levorphanol	Morphinan	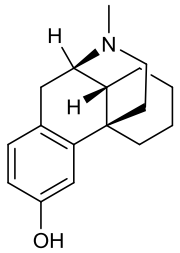	Analgesic
Methylnaltrexone	Morphinan	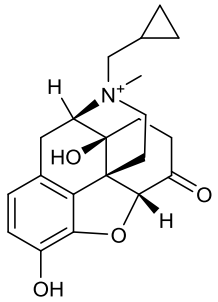	Opioid induced constipation
Morphine[a]	Morphinan	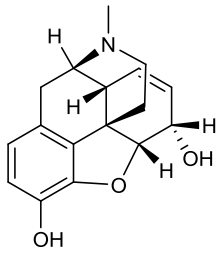	Analgesic

Table 1-1 (continued)

Drug Name	Alkaloid Class	Structure	Uses/Treatments
Nalbuphine	Morphinan	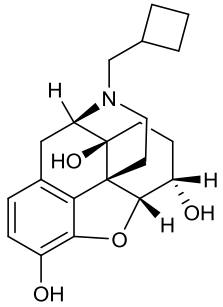	Analgesic
Naloxegol	Morphinan	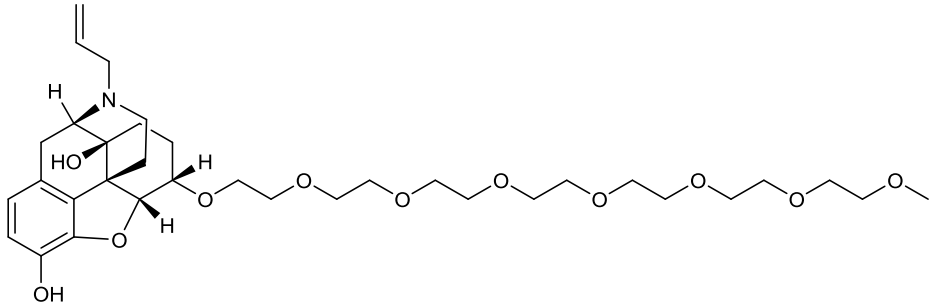	Opioid induced constipation
Naloxone[a]	Morphinan	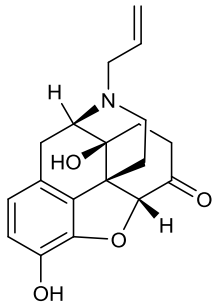	Opioid overdose

Table 1-1 (continued)

Drug Name	Alkaloid Class	Structure	Uses/Treatments
Naltrexone	Morphinan	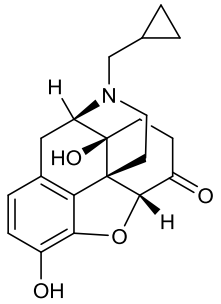	Opioid addiction and alcohol dependence
Oxycodone[a]	Morphinan	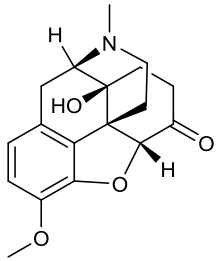	Analgesic
Oxymorphone	Morphinan	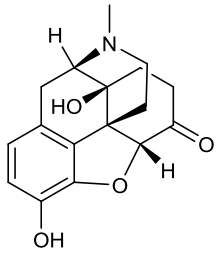	Analgesic

Table 1-1 (continued)

Drug Name	Alkaloid Class	Structure	Uses/Treatments
Rizatriptan	Indole	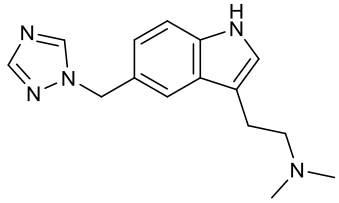	Migraines
Sumatriptan	Indole	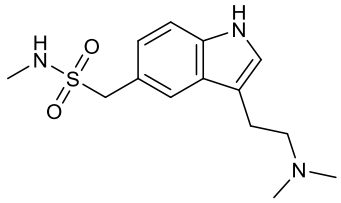	Migraines
Tadalafil	Beta-carboline	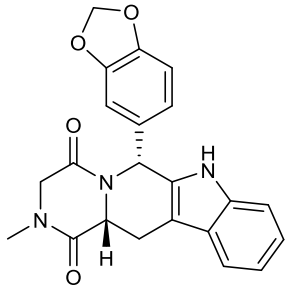	Male erectile dysfunction

Table 1-1 (continued)

Drug Name	Alkaloid Class	Structure	Uses/Treatments
Reserpine	Monoterpene indole	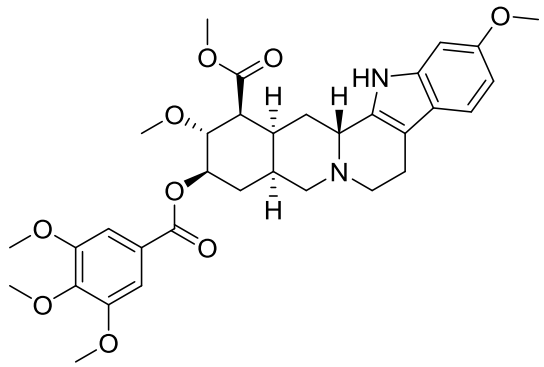	Antihypertensive
Vinblastine[a]	Monoterpene indole	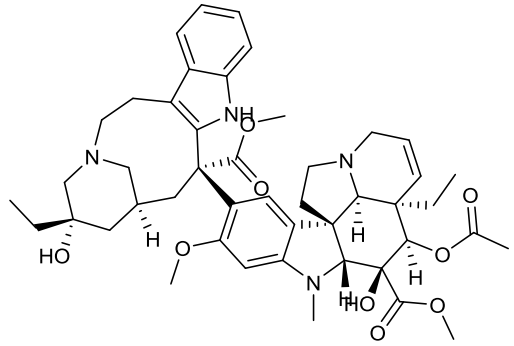	Anticancer

Table 1-1 (continued)

Drug Name	Alkaloid Class	Structure	Uses/Treatments
Vincristine[a]	Monoterpene indole	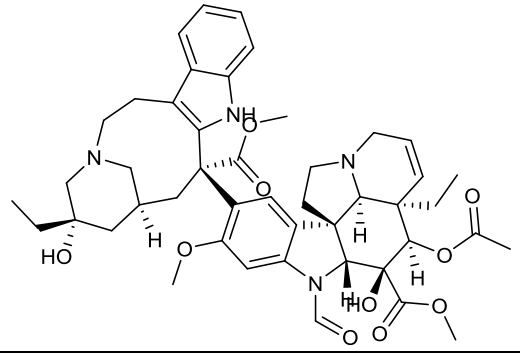	Anticancer
Vinorelbine[a]	Monoterpene indole	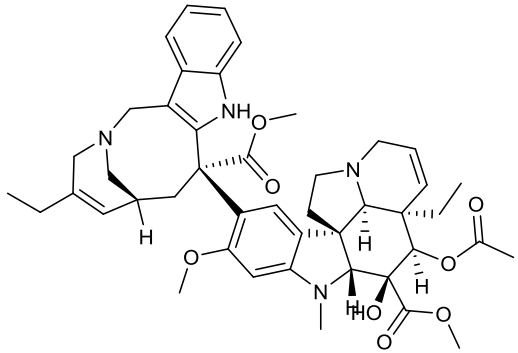	Anticancer
Quinidine	Quinoline	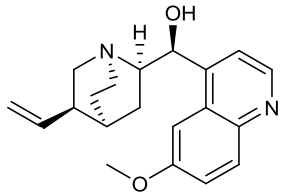	Antiarrhythmic

Table 1-1 (continued)

Drug Name	Alkaloid Class	Structure	Uses/Treatments
Quinine[a]	Quinoline	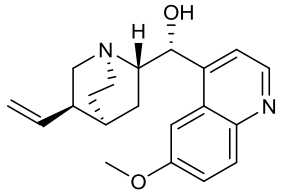	Antimalarial
Irinotecan[a]	Pyrroloquinoline	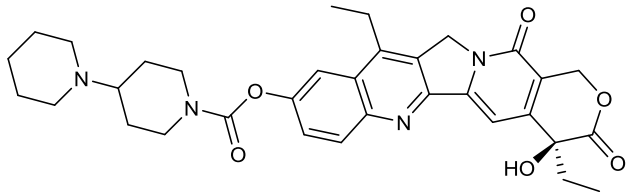	Anticancer
Topotecan	Pyrroloquinoline	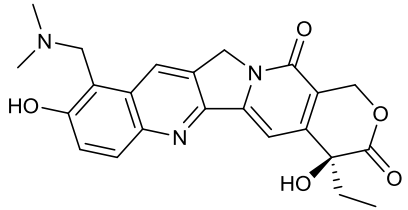	Anticancer
Bromocryptine	Ergot	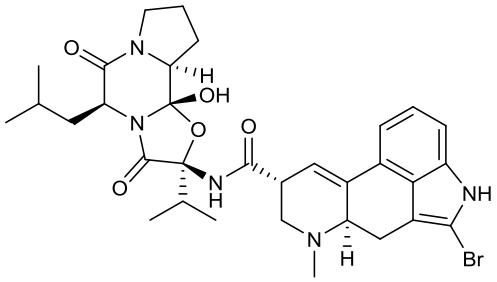	Hyperprolactinemia, Parkinsonian Syndrome

Table 1-1 (continued)

Drug Name	Alkaloid Class	Structure	Uses/Treatments
Cabergoline	Ergot	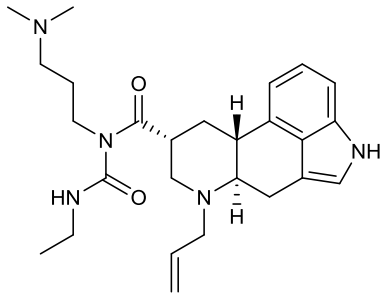	Hyperprolactinemia, Parkinsonian Syndrome
Dihydroergotamine	Ergot	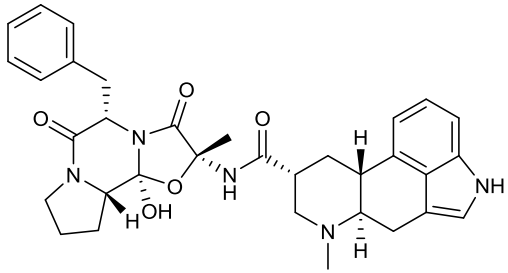	Migraines
Ergoloid mesylate (dihydroergocornine, dihydroergocristine, alpha-dihydroergocryptine, beta-dihydroergocryptine)	Ergot	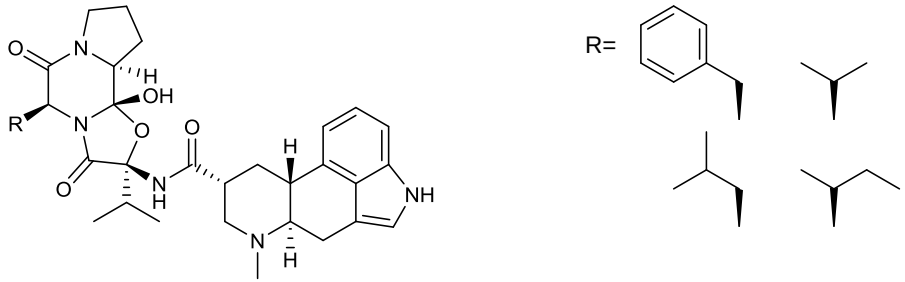	Dementia

Table 1-1 (continued)

Drug Name	Alkaloid Class	Structure	Uses/Treatments
Ergotamine	Ergot	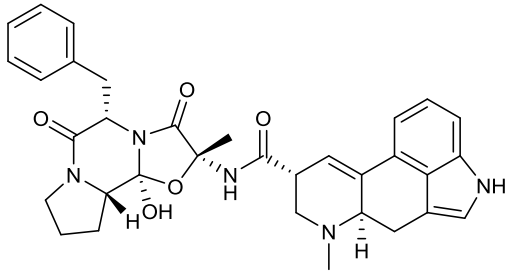	Migraines, post-partum hemorrhage
Methylergonovine	Ergot	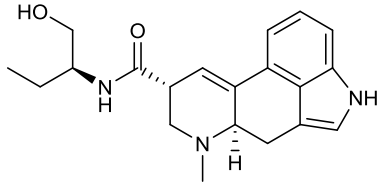	Migraines, post-partum hemorrhage

[a]Listed on the WHO Model List of Essential Medicines

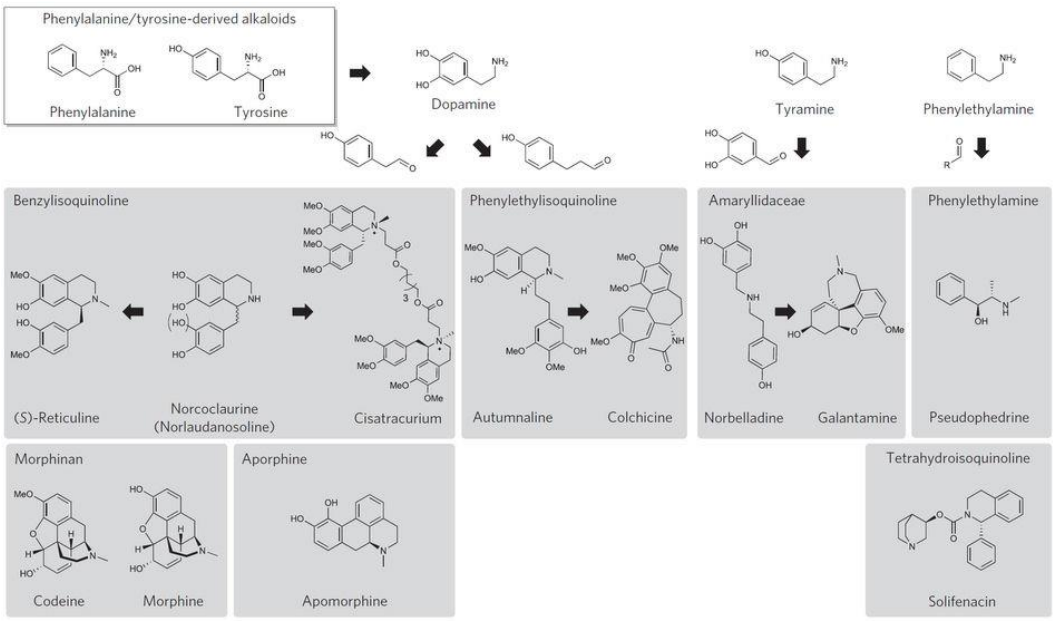

Figure 1.2. Phenylalanine- and tyrosine-derived pharmaceuticals. Representative phenylalanine- and tyrosine-derived FDA-approved alkaloid-based pharmaceuticals and key biosynthetic intermediates discussed in this chapter.

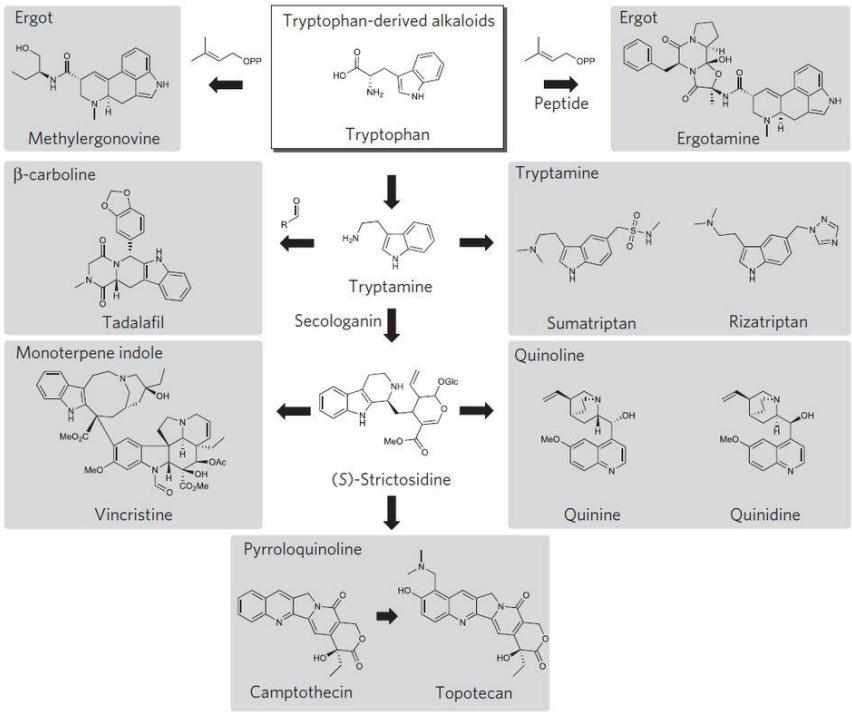

Figure 1.3. Tryptophan-derived pharmaceuticals. Representative tryptophan-derived FDA-approved alkaloid-based pharmaceuticals and key biosynthetic intermediates discussed in this chapter.

1.3 Phenylalanine- and Tyrosine-derived Alkaloid-based Pharmaceuticals

1.3.1 Phenylethylamines

Decarboxylation of phenylalanine and tyrosine results in phenylethylamine and tyramine, respectively (Figure 1.2). There are over 30 derivatives of phenylethylamine and tyramine among FDA-approved drugs, including epinephrine, used in the emergency treatment of anaphylaxis; formoterol, used for the treatment of asthma; and phenelzine, used to treat depression. Phenylethylamines, such as dopamine (Figure 1.2), are often microbially produced as precursors or intermediates to more complex plant alkaloids[20,30,32,37]. Industrially, however, yeast is used to produce the amphetamine-derived drugs pseudoephedrine (Figure 1.2) and ephedrine, which contain a methyl group adjacent to the nitrogen, by feeding yeast benzaldehyde to produce phenylacetylcarbinol, which is then chemically converted to the final products[39]. Biosynthetic production of phenylethylamine-derived pharmaceuticals would involve enzyme discovery and/or engineering as has previously been proposed for amphetamine-derived pharmaceuticals[39].

1.3.2 Tetrahydroisoquinoline Alkaloids

Condensation of phenylethylamine with an aldehyde via a Pictet–Spengler reaction results in tetrahydroisoquinoline alkaloids. The four tetrahydroisoquinoline-derived FDA-approved pharmaceuticals are trabectedin, used to treat soft tissue sarcomas; the antihelmitic praziquantel; tetrabenazine, used to treat Huntington's disease symptoms; and solifenacin (Figure 1.2), used to treat overactive bladder. Trabectedin is obtained via semisynthesis using cyanosafracin B produced by *Pseudomonas fluorescens*[40]. Praziquantel[41] and tetrabenazine[42] are sold as racemates, and biological production of

intermediates may not be justifiable. Solifenacin, however, is a single stereoisomer for which the specificity of enzymes could be leveraged. A key intermediate in the synthesis of solifenacin is (1*S*)-phenyl-tetrahydroisoquinoline (Figure 1.4a), which is produced industrially in three chemical steps, including a chiral resolution step in which >50% of the material is discarded[43]. Biologically, (1*S*)-phenyl-tetrahydroisoquinoline could be generated stereospecifically via enzymatic coupling of phenylethylamine and benzaldehyde using the Pictet–Spenglerase norcoclaurine synthase (NCS). Wild-type NCS condenses dopamine and 4-hydroxyphenylacetaldehyde (4-HPAA) to form (*S*)-norcoclaurine, but it does not condense phenylethylamine with 4-HPAA or dopamine with benzaldehyde[44]. Engineering NCS to accept the substrates needed to generate (1*S*)-phenyl-tetrahydroisoquinoline has the potential to accelerate the commercial synthesis of solifenacin (Figure 1.4a).

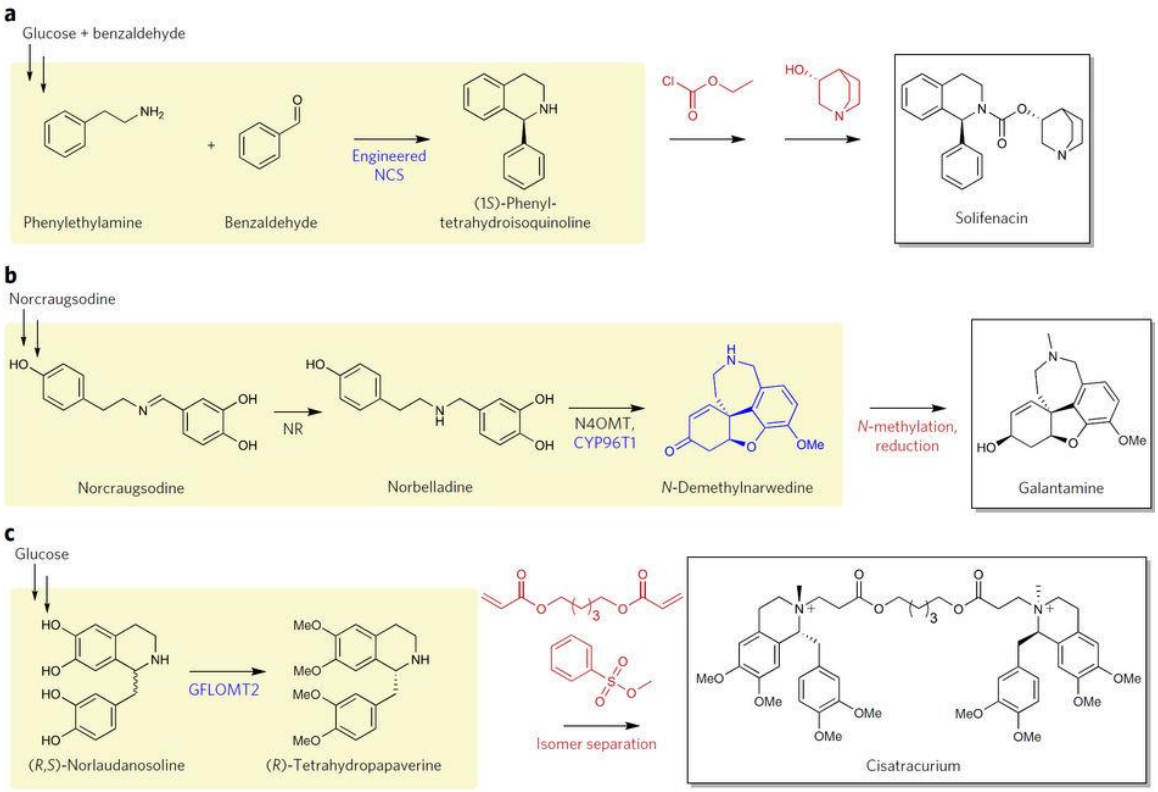

Figure 1.4. Proposed semisyntheses of benzylisoquinoline alkaloid-derived FDA-approved pharmaceuticals. Yellow box, microbe; blue, enzymes to be engineered, elucidated, or optimized and newly proposed semisynthetic intermediates; red, chemical modifications. (a) Proposed semisynthesis of solifenacin. Glucose and benzaldehyde can be fed to a microbe expressing an engineered norcoclaurine synthase (NCS) to produce (1*S*)-phenyl-tetrahydroisoquinoline, which can be converted to solifenacin in two chemical steps[43]. (b) Proposed semisynthesis of galantamine. Norcraugsodine can be fed to a microbe expressing noroxomaritidine reductase (NR), norbelladine 4′-*O*-methyltransferase (N4OMT), and CYP96T1 to produce *N*-demethylnarwedine, which can be converted to galantamine via *N*-methylation and reduction. (c) Proposed semisynthesis of cisatracurium. Existing (*R*,*S*)-norlaudanosoline-producing microbes expressing *G. flavum* *O*-methyltransferase (GFLOMT2) could produce (*R*)-tetrahydropapaverine, which can be converted to cisatracurium using established synthetic routes[53].

1.3.3 Amaryllidaceae Alkaloids

Condensation of tyramine with 3,4-dihydroxybenzaldehyde followed by reduction results in norbelladine (Figure 1.2), the common precursor to amaryllidaceae alkaloids. The natural product galantamine (Figure 1.2), used for the treatment of Alzheimer's

disease, is the only FDA-approved amaryllidaceae-based pharmaceutical. Galantamine is produced by various plant species, *Galanthus sp.* in particular, and plant-extracted galantamine is used commercially[45]. The low levels of galantamine accumulation in natural sources and high cost of isolating it ($50,000/kg) have resulted in substantial efforts toward its chemical synthesis[46]. The crux in the chemical synthesis of galantamine is introduction of the correct stereochemistry at the tricyclic benzofuran core[47], which in nature is installed by the phenol-phenol coupling enzyme CYP96T1 that produces *N*-demethylnarwedine as a minor product[48] (Figure 1.4b). *N*-Demethylnarwedine can be chemically converted to the final galantamine via reduction of the conjugated ketone into a conjugated alcohol and methylation of the only amine. Microbial production of *N*-demethylnarwedine could be achieved today by engineering a microbe to express noroxomaritide reductase[49], norbelladine 4′-*O*-methyltransferase[45], and CYP96T1[48] and feeding it chemically synthesized norcraugsodine (Figure 1.4b), which is one chemical step from tyramine and 3,4-dihydroxybenzaldehyde[50]. Improving the product specificity of CYP96T1 so that this enzyme preferentially produces *N*-demethylnarwedine would further increase the production of galantamine.

1.3.4 Phenylethylisoquinoline Alkaloids

Hydroxylation of tyrosine to L-3,4-dihydroxyphenylalanine (DOPA) followed by decarboxylation results in dopamine (Figure 1.2). Condensation of dopamine and 4-hydroxydihydrocinnamaldehyde generates the scaffold of phenylethylisoquinoline alkaloids[51]. Colchicine (Figure 1.2), the only approved phenylethylisoquinoline-based pharmaceutical, is used in the treatment of acute gout and is obtained from *Gloriosa superba* for commercial production[51]. The colchicine biosynthetic pathway from

dopamine and 4-hydroxydihydrocinnamaldehyde is not known, and the only elucidated step is the P450-dependent oxidation of autumnaline (Figure 1.2) to isoandrocymbine[52]. Genome sequencing of *G. superba* would aid in the discovery of colchicine biosynthetic enzymes, which catalyze steps including oxidation, ring formation and cleavage, methylation and demethylation, and amide hydrolysis and formation.

1.3.5 Benzylisoquinoline Alkaloids

Condensation of dopamine and 4-HPAA results in (*S*)-norcoclaurine, which is eventually converted to (*S*)-reticuline, the common precursor to all benzylisoquinoline alkaloids (BIAs) (Figure 1.2). The engineering of microbes for the production of BIAs has been extremely successful in the last eight years[7,11]. Briefly, simple BIAs, including norcoclaurine, norlaudanosoline, and reticuline, have been microbially produced from simple sugars, while more complex BIAs, including morphine, magnoflorine, canadine, and noscapine, have been produced from simple sugars or advanced intermediates. Dimerization of two simple BIAs via one or two ether linkages results in bisbenzylisoquinoline alkaloids (BBIAs). Synthetic BBIA cores, however, are connected via a polymethylene chain[51]. Three synthetic BBIA-based drugs, atracurium, mivacurium, and cisatracurium (Figure 1.2), have been approved as muscle relaxants. Atracurium, which is on the World Health Organization (WHO) Model List of Essential Medicines (http://www.who.int/medicines/publications/essentialmedicines/en/), is an isomeric mixture, while cisatracurium, the *R-cis*, *R-cis* isomer of atracurium, has superior pharmacodynamics and fewer side effects in comparison to atracurium[53]. Cisatracurium is chemically synthesized in two steps from (*R*)-tetrahydropapaverine (Figure 1.4c)[53], which is obtained via optical resolution of (*R,S*)-tetrahydropapaverine, with ~60% of the

starting material discarded[53]. Although (*S*)-tetrahydropapaverine is the natural product, non-natural (*R*)-tetrahydropapaverine could be produced from (*R*)-norlaudanosoline starting from glucose by engineering a single enzyme (Figure 1.4c). Racemic (*R,S*)-norlaudanosoline has been produced in *E. coli* via spontaneous Pictet–Spengler condensation of dopamine and 3,4-dihydroxyphenylacetaldehyde starting from supplied glucose[36], and many BIA O-methyltransferases accept both the *R* and *R,S* forms of their respective substrates[54, 55]. Indeed, feeding (*R,S*)-norlaudanosoline to *E. coli* expressing *Glaucium flavum* GFLOMT2 resulted in tetrahydropapaverine production[56]. As no norlaudanosoline was found after the reaction, it is hypothesized that the enzyme converted both *R* and *S* isomers. Analysis of this and related methyltransferases to understand their substrate and product specificities and improve their activity on the *R* stereoisomer should further enable the biological production of (*R*)-tetrahydropapaverine and accelerate the large-scale semisynthesis of cisatracurium.

1.3.6 Aporphines and Morphinans

Oxidative coupling within the scaffold of the BIA (*S*)-reticuline results in aporphines, while coupling within the scaffold of (*R*)-reticuline, a downstream intermediate, results in morphinans. The semisynthetic aporphine apomorphine has been approved for the treatment of Parkinson's disease and is made via chemical rearrangement of morphine[57] (Figure 1.2). Morphinans are a major class of alkaloid-based FDA-approved pharmaceuticals with 16 compounds, most of which are analgesics. Among the 16 compounds are found the natural product morphine, four pharmaceuticals that are semisynthesized from morphine (including the natural product codeine; Figure 1.2), eight pharmaceuticals that are semisynthesized from thebaine, and three fully synthetic

pharmaceuticals[58]. Morphine and thebaine are currently obtained from poppy (*Papaver somniferum* and *Papaver bracteatum*[58]) and, while plant-extracted morphinan alkaloids meet current demand (United Nations International Control Board, http://www.incb.org/documents/Publications/AnnualReports/AR2015/English/Supp/AR15_Availability_E_Chapter_II.pdf), microbial production represents an alternative supply that is attractive because of the drawbacks associated with plant harvesting and unpredictable environmental factors. The natural product morphine has been microbially produced in yeast from thebaine or codeine[28,34], and morphine-derived drugs have also been produced in yeast from either thebaine (codeine, dihydrocodeine, hydromorphone, hydrocodone, and oxycodone)[34], (*R*)-reticuline (codeine)[28], or simple carbon sources (hydrocodone)[29,30]. As the remaining semisynthesized morphinans (buprenorphine, methylnaltrexone, nalbuphine, naloxegol, naloxone, naltrexone, and oxymorphone) are chemically synthesized from thebaine and thebaine has been microbially made from simple carbon sources[29,30], there is the possibility of an alternative microbial source for all the natural and semisynthetic morphinans on the market. Today, a key issue with microbially produced morphinan-based alkaloids is the low yields. Morphine has been microbially produced from thebaine at 1.5% molar yield, while thebaine has been produced at <0.001% molar yield from glucose[29,34].

An as yet unexplored idea has been to provide late intermediates for the semisynthesis of fully synthetic morphinan-derived drugs. Levorphanol (Figure 1.5a) is chemically synthesized in eight steps from cyclohexanone[58]. The closest natural product to levorphanol is salutaridinol, an intermediate in the thebaine–morphine pathway (Figure 1.5a). Salutaridinol contains multiple hydroxyls, methoxys, and alkenes, and it could be

demethylated and chemically reduced to form levorphanol or only partially chemically modified to generate levorphanol derivatives. Butorphanol (Figure 1.5a) is chemically synthesized in 13 steps from 7-methoxy-3,4-dihydronaphthalen-1(2H)-one via the intermediate 8,14-didehydro-3-methoxymorphinan (DDMM), which is produced after nine steps[58]. The closest natural product to DDMM is also salutaridinol (Figure 1.5a). Unlike DDMM, salutaridinol is *N*-methylated, which would hinder the current strategy of chemically adding the cyclobutylmethyl group found in butorphanol. As salutaridine synthase has shown activity toward *N*-desmethylated (*R*)-norreticuline to produce norsalutaridine[59], it is likely that either the previously elucidated salutaridine reductase or novel homologs could produce *N*-desmethylated norsalutaridinol (Figure 1.5a). Norsalutaridinol could be demethylated and reduced chemically to form DDMM or only partially modified to generate butorphanol derivatives.

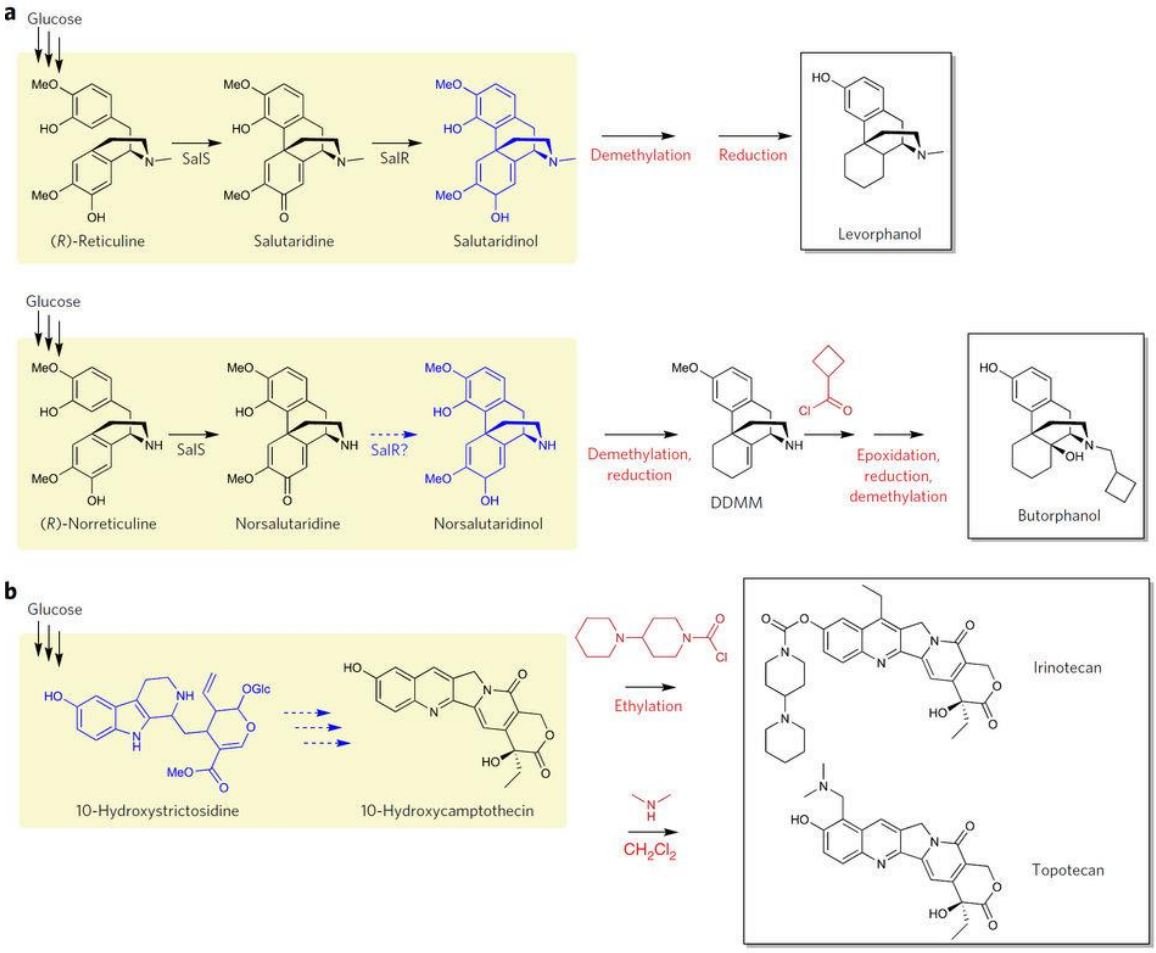

Figure 1.5. Proposed semisyntheses of morphinan- and pyrroloquinoline-derived FDA-approved pharmaceuticals. Yellow box, microbe; blue, enzymes to be engineered, elucidated, or optimized and newly proposed semisynthetic intermediates; red, chemical modifications. (a) Proposed semisynthesis of levorphanol and butorphanol. Top, existing microbial strains produce salutaridinol, which requires chemical demethylation and reduction to produce levorphanol. Bottom, existing microbial strains expressing salutaridine synthase (SalS) and homologs of salutaridine reductase (SalR) could produce norsalutaridinol, which can be converted to 8,14-didehydro-3-methoxymorphinan (DDMM) via chemical demethylation and reduction steps. DDMM is a late intermediate in the chemical synthesis of butorphanol[58]. (b) Proposed semisynthesis of irinotecan and topotecan. The modified alkaloid 10-hydroxystrictosidine has been produced in yeast[37]. Camptothecin pathway enzymes from strictosidine need to be elucidated and their promiscuity assessed to produce 10-hydroxycamptothecin, which can be dropped into existing commercial syntheses of irinotecan and topotecan, which currently rely on camptothecin[76,77]. Dotted arrows, unknown enzymes.

1.4 Tryptophan-derived Alkaloid-based Pharmaceuticals

1.4.1 Tryptamines and β-Carbolines

Decarboxylation of tryptophan results in tryptamine, and eight simple tryptamine derivatives including six 'triptans' such as sumatriptan and rizatriptan are on the market (Figure 1.3). Tryptamine derivatives, such as serotonin, and tryptamine itself are common intermediates in microbial productions[21,37], and some have also been produced as end products[60,61]. However, simple tryptamine derivatives can be efficiently produced chemically[62]. Condensation of tryptamine and aldehydes results in β-carbolines. Tadalafil (Cialis®; Figure 1.3), a vasodilator used for male erectile dysfunction, is the only approved β-carboline drug on the market. The key structural features of tadalafil are the cis arrangements of the benzodioxole and piperazinedione moieties of the β-carboline scaffold. Although enzymes could provide the desired enantiomeric selectivity, the commercial synthesis of tadalafil is three steps starting from commercially available starting materials and leverages the fact that the desired cis isomer precipitates out of the reaction while the *trans* isomer stays in solution[63].

1.4.2 Monoterpene Indole Alkaloids

Condensation of tryptamine with the monoterpene secologanin generates (*S*)-strictosidine, the key intermediate to monoterpene indole alkaloids (MIAs)[64] (Figure 1.3). The four FDA-approved MIA-based pharmaceuticals on the market comprise the antihypertensive agent reserpine and the anticancer drugs vinorelbine, vinblastine, and vincristine (Figure 1.3). Reserpine is a natural product and is extracted from *Rauwolfia vomitoria* for commercial production[65]. The biosynthetic pathway for reserpine is yet to

be elucidated, and an intriguing feature of this chemical is the (*R*) stereochemistry at the C3 position, which hints that (*R*)-strictosidine might be the key biosynthetic precursor to reserpine rather than (*S*)-strictosidine[51]. Vinorelbine is a semisynthetic drug made in two steps from anhydrovinblastine obtained chemically or enzymatically from plant-extracted catharanthine and vindoline[51]. Similar to vinorelbine, vinblastine and vincristine are also bisindoles formed via the condensation of catharanthine and vindoline, although they are natural products.

Unlike the microbial production of morphinans, in which microbes are now available for the production of complex morphinan-derived alkaloids, the engineering of microbes for the production of complex bisindole MIAs has lagged behind, mainly because of incomplete elucidation of MIA biosynthetic pathways. Specifically, microbial bisindole MIA production has been limited to early intermediates, up to strictosidine[21], or conversion of later intermediates such as tabersonine into vindoline[31]. This is due to the limited pathway knowledge beyond strictosidine other than (i) strictosidine-β-glucosidase, which converts strictosidine to a common intermediate that spontaneously converts to cathenamine *in vitro*; (ii) the enzymes converting tabernosine to vindoline; and (iii) α-3,4-anhydrovinblastine synthase, which dimerizes vindoline and catharanthine to form anhydrovinblastine[64]. As a point of reference, only in 2014 was the complete upstream secologanin biosynthetic pathway elucidated[66]. Just one year later, the secologanin pathway was refactored in yeast for the *de novo* production of strictosidine[21], underscoring the idea that the engineering of microbes for the production of MIAs is limited by biosynthetic pathway discovery. MIA pathway elucidation will open the door to the engineering of microbes for the production of naturally occurring and modified

MIAs. With recent transcriptomic[67,68] and genomic[69] knowledge, we can really start to utilize microbes that produce key intermediates or feed microbes key intermediates to screen for potential pathway enzymes[20,29,70].

1.4.3 Quinoline Alkaloids

Rearrangement of the indole ring in (*S*)-strictosidine to a quinoline ring results in quinoline alkaloids. The natural product diastereomers quinine, used to treat malaria, and quinidine, used to treat arrhythmia, are the only two MIA-derived quinolines approved on the market (Figure 1.3). *Cinchona* bark is the sole commercial source of these compounds, with 300–500 tons of alkaloids extracted per year, ~40% of which go to pharmaceutical production[71]. Chemical synthesis of quinine has a long history, with the first stereoselective total synthesis of quinine accomplished in 2001, involving 13 steps and giving <10% yield[72]. Although plant-extracted quinine is sufficient for pharmaceutical production[71], quinine and quinidine production in *Cinchona* trees takes years of growth and leads to destructive harvesting of the trees[51]. The lack of biosynthetic pathway knowledge for quinine or quinidine hinders the reconstruction of these pathways in microbes. Today, only one of the final enzymes in the quinoline biosynthetic pathway, cinchoninone:NADPH oxidoreductase, has been isolated and characterized[73], yet its protein sequence is unknown.

1.4.4 Pyrroloquinoline Alkaloids

A different rearrangement of (*S*)-strictosidine results in pyrroloquinoline alkaloids, which include the natural product, and topoisomerase I inhibitor, camptothecin (Figure 1.3). As a result of toxicity and low solubility, camptothecin itself is a poor drug[2]. Two

camptothecin derivatives, the anticancer agents irinotecan and topotecan (Figure 1.3), are the only approved pyrroloquinoline-based drugs on the market, while three other camptothecin derivatives are in active clinical trials or development (https://clinicaltrials.gov/ and http://adisinsight.springer.com/)[38]. Despite several reports on the total synthesis of camptothecin and its derivatives[74,75], irinotecan and topotecan are semisynthesized from plant-extracted camptothecin for commercial use[76,77]. Today, plant-extracted camptothecin (600 kg/year) does not meet the demand for the synthesis of camptothecin derivatives (3,000 kg/year)[78], which leads to destructive harvesting of *Camptotheca acuminata* and *Nothapodytes foetida* trees[79], potentially restricting the future supply of camptothecin-derived drugs. The slow growth of the woody trees *C. acuminata* and *N. foetida* has led to the engineering of hairy-root cultures of these and other plants that accumulate camptothecin, such as *Ophirriza pumila*[80,81]. As the camptothecin biosynthetic pathway has not been fully elucidated, plant engineering efforts rely solely on upregulation of early MIA pathway enzymes[80]. Knowledge of the camptothecin biosynthetic pathway from strictosidine would not only aid plant engineering efforts for high-level camptothecin production but also enable the engineering of microbial platforms for the production of camptothecin. After lactam formation of strictosidine, or strictosidinic acid, to form strictosamide, the proposed camptothecin biosynthetic pathway consists of multiple oxidations and reductions, a dehydration, and a deglycosylation and includes an unknown conversion of the β-carboline to the pyrroloquinoline scaffold[51,82]. A currently accessible strategy for pathway elucidation is to engineer a microbe for the production of a late intermediate, such as strictosidine, and screen for potential enzymes in the pathway[6,37]. While

biosynthetic pathway knowledge would allow the bioproduction of camptothecin, both irinotecan and topotecan are modified at the 10′ position by introduction of a hydroxyl group or a bipiperidine moiety via an ester bond, and their semisyntheses proceed through a 10-hydroxycamptothecin intermediate (Figure 1.5b)[76,77]. Therefore, microbial production of 10-hydroxycamptothecin instead of camptothecin may be more appealing for the semisynthesis of camptothecin derivatives (Figure 1.5b). Indeed, we have recently demonstrated that production of modified MIAs such as 10-hydroxystrictosidine (Figure 1.5b) is possible by using plant, mammalian, fungal, and bacterial enzymes expressed in *S. cerevisiae*[37]. Given that 10-hydroxylated MIAs have been produced in *Catharanthus roseus* hairy-root culture fed with serotonin[83], it is likely that enzymes downstream in the camptothecin pathway would accept 10-hydroxystrictosidine to generate 10-hydroxycamptothecin in microbes as well.

1.4.5 Ergot Alkaloids

Ergot alkaloids are derived from the combination of tryptophan and dimethylallyl pyrophosphate (Figure 1.3). While mainly of fungal origin, ergot alkaloids are often found in fungi that infect grains or in fungi-associated plants[84] and are thus included in this chapter. There are currently six approved ergot alkaloids on the market, including treatments for parkinsonian syndrome and vasoconstrictors. The four ergopeptides (ergotamine (Figure 1.3), dihydroergotamine, ergoloid mesylate, and bromocriptine) are synthesized from lysergic acid and synthetic peptides[85], although they can be obtained by other production or isolation routes as well. The two ergoamides cabergoline and methylergonovine (Figure 1.3) can also be synthesized from lysergic acid. Today, most lysergic acid is semisynthesized from paspalic acid (Figure 1.6) or lysergic acid

hydroxyethylamide obtained from *Claviceps* fermentation broth[85]. As the compounds isolated from ergot fermentation can be impure because of the abundance of similar metabolites, heterologous production of lysergic acid in a non-ergot-producing microbe could be beneficial for the production of ergot-based pharmaceuticals. Conversion of tryptophan and dimethylallyl pyrophosphate to lysergic acid can be catalyzed by eight enzymes (Figure 1.6). Although heterologous microbial production of lysergic acid in a non-ergot-producing microbe has not been shown, all enzymes in this pathway are known. The early ergot intermediate chanoclavine-I (Figure 1.6) has been produced from glucose in *S. cerevisiae*[33] and from sucrose in *Aspergillus nidulans*[86] and has been converted in vitro to chanoclavine-I aldehyde[87], and subsequently to agroclavine[88] (Figure 1.6). Agroclavine has also been produced through reprogramming of the fumigaclavine ergot producer *Aspergillus fumigatus*[89]. Expression of clavine oxidase (CloA) in the reprogrammed *A. fumigatus* resulted in production of lysergic acid, although the final conversion of paspalic acid to lysergic acid may be catalyzed by another isomerase or be completed spontaneously[84]. Microbially produced lysergic acid could be used in the semisynthesis of current drugs or could be microbially converted to ergoamides and ergopeptides via two non-ribosomal peptide synthases and, in the case of ergopeptides, a dioxygenase.

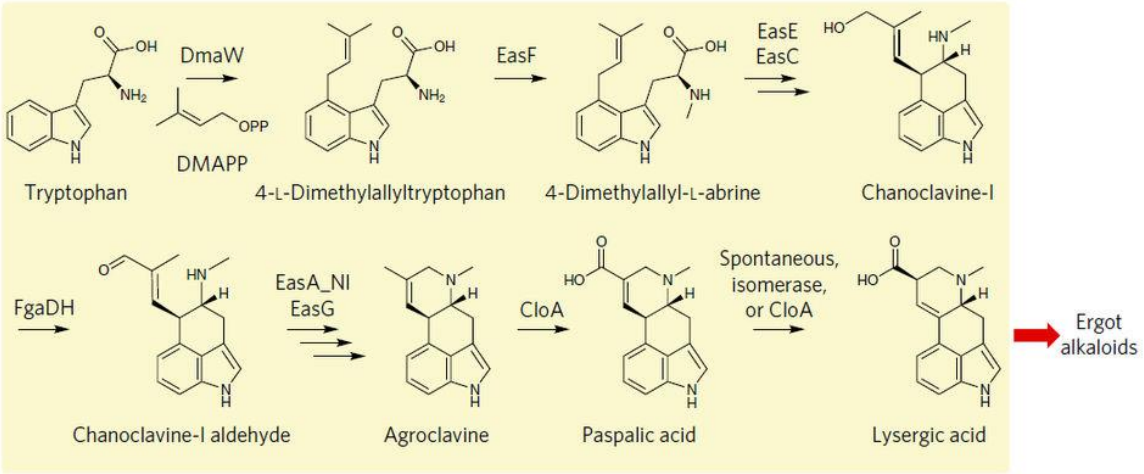

Figure 1.6. Proposed microbial production of lysergic acid for the semisynthesis of ergot alkaloids. Yellow box, non-ergot-producing microbe; red arrow, chemical modification to reach ergot alkaloids. The early ergot intermediate chanoclavine-I has been produced in *S. cerevisiae* and *A. nidulans* and, although microbial conversion of chanoclavine-I to lysergic acid has not been shown in a non-ergot-producing microbe, all enzymes in this pathway are known. Microbially produced lysergic acid can be used in current chemical syntheses of ergoamides and ergopeptides. Abbreviations: DmaW, tryptophan dimethylallyltransferase; DMAPP, dimethylallylpyrophosphate; EasF, 4-dimethylallyltryptophan *N*-methyltransferase; EasE, FAD-linked oxidoreductase; EasC, catalase; FgaDH, chanoclavine-I dehydrogenase; EasA_Nl, chanoclavine-I aldehyde reductase from *Neotyphodium lolii*; EasG, agroclavine dehydrogenase; CloA, clavine oxidase.

1.5 Enzymatic Production of Modified Alkaloids

Many natural product derivatives are obtained through chemical modifications; however, engineering microbes to produce modified alkaloids has the potential to supply more advanced intermediates for the semisynthesis of natural product-derived pharmaceuticals, to supply alternative production sources for currently semisynthesized drugs, or to speed up the generation of novel drug analogs[15,16]. Taking advantage of biosynthetic enzyme promiscuity and removal of plant pathway regulation, modified BIAs have been produced microbially[23,34,35]. Furthermore, the broad substrate specificity of the BIA Pictet–Spenglerase NCS has enabled the condensation of substrates carrying

fluoride, methyl, and methoxy modifications as well as the condensation of drastically different analogs, such as thiophene[44]. Substantial headway has also been made in the production of modified MIAs, including the incorporation of a hydroxyl group in strictosidine in yeast[37] and halogens (chlorine and bromine) in *C. roseus* root cultures[17,18]. Hydroxyls and halogens, as well as azido and methyl groups, are accepted by downstream enzymes in *C. roseus* root and cell cultures to produce modified complex MIAs, including modified ajmalicine, serpentine, tabersonine, and vindoline[17,18,19,83]. As with NCS, strictosidine synthase (the MIA Pictet–Spenglerase) has been shown to promiscuously accept a range of unnatural substrates, including benzofuran, benzothiophene, and aza-indole tryptamine derivatives[90,91], and enzymes in the upstream iridoid pathway exhibit promiscuity as well[92,93]. Enzymes have also been engineered to accept modified substrates for modified MIA production4. For example, tryptophan halogenases have been engineered for substrate specificity[18] and regiospecificity[94], being able to produce both chlorinated and brominated compounds, such as 7-chlorotryptamine and 5-bromotryptophan. Enzymatic halogenation is not only more environmentally friendly than chemical halogenation but also enables the incorporation of halogens at key chemical positions, which may be difficult using chemical methods[95]. Strategic incorporation of modifications such as hydroxyls, alkenes, or halogens can facilitate regiospecific chemical reactions without major concerns of cross-reactivity. An example of this can be seen in the semisynthesis of MIA analogs wherein chlorinated or brominated tryptamines were either fed to or formed *in situ* in *C. roseus* hairy-root cultures to produce halogenated MIAs, which were then chemically cross-coupled to boronic acid derivatives[96].

Although fluorinated natural products remain rare, fluorinated pharmaceuticals are highly represented on the market (~20.25%)[95]. Fluorine modifications can improve many drug characteristics, including potency and ADMET properties[97]. While multiple classes of halogenases exist[95], fluorinases are still difficult to identify, with only one enzyme currently known: 5′-fluoro-5′-deoxyadenosine synthase, which converts *S*-adenosylmethionine (SAM) and a fluoride ion into 5′fluoro-5′deoxyadenosine and L-methionine, a reaction in the biosynthesis of fluoroacetate[98]. Fluoroacetate is a promising building block in fluorinated compounds such as polyketides[99,100]. Given the pharmaceutical importance of fluorine modifications and the ability of downstream alkaloid enzymes to accept fluorinated intermediates[83], one can envision discovery of new fluorinases and/or engineering of other halogenases for the fluorination of plant alkaloids.

1.6 Conclusion

Microbial production of strategically modified plant alkaloids has the capability to accelerate the production and reduce the cost of FDA-approved drugs and open the door for the rapid generation of potentially new pharmaceuticals. Although many alkaloids on the market are natural products, natural product-derived alkaloids such as topotecan and irinotecan often have improved therapeutic properties, including better solubility, chemical stability, metabolic stability, and potency[2]. The limited presence of natural product derivatives among alkaloid-based pharmaceuticals may stem from (i) the difficulty of generating derivatives starting with the plant-extracted terminal natural product, which is often highly hydroxylated, making it difficult to selectively modify specific positions in the molecule; (ii) the limited availability of natural product starting

material for chemical modification; or (iii) the expensiveness of total synthesis of natural product-like compounds. Although alkaloid derivatives are now obtained via chemical modifications, engineering microbes to produce modified alkaloids has the potential to supply more advanced intermediates to aid the semisynthesis of alkaloid-derived pharmaceuticals or enable the generation of novel drug analogs[15,16].

With the advent of synthetic biology technologies, microbes are poised to start generating a number of modified alkaloids in coming years because of their fast doubling times, their efficient uptake of modified substrates, and the ease of downstream processing in isolating the plant-derived products due to the lack of similar metabolites in the microbial medium. Furthermore, reconstruction of heterologous plant pathways in microbes has the advantage of bypassing endogenous plant regulation and the ability to rapidly mix and match enzymes from different species. A key challenge that remains in achieving the vision of high-level microbial production of modified plant alkaloids is biosynthetic pathway elucidation. This is exemplified by the fact that, for products where the biosynthetic pathway has been elucidated, an increasing number of works use promiscuous or engineered enzymes to incorporate useful chemical handles that would allow synthesis or semisynthesis of known and novel pharmaceuticals. This is seen in the numerous works published on microbial BIA production, which have culminated in the microbial production of final pharmaceuticals, current semisynthetic intermediates, and modified natural products. Yet, when the pathways are unknown, microbial engineering of modified alkaloids is severely limited, as can be seen in the lack of progress for MIAs (which has thus far culminated in early intermediates in the natural product pathways) and other alkaloid classes that have little to no microbial reconstruction work completed.

However, notable work focused on modifications of these early intermediates provides optimism for the rapid production of useful modified alkaloids and/or final pharmaceuticals upon further pathway elucidation.

1.7 References

1 Newman, D.J. and Cragg, G.M. (2016) Natural products as sources of new drugs from 1981 to 2014. *J. Nat. Prod.* 79, 629–661.

2 Chen, J., Li, W., Yao, H. and Xu, J. (2015) Insights into drug discovery from natural products through structural modification. *Fitoterapia* 103, 231–241.

3 Rahier, N.J., Thomas, C.J. and Hecht, S.M. in *Anticancer Agents from Natural Products*. 2nd edn. (eds. Cragg, G., Kingston, D. and Newman, D.) 5–26 (CRC Press, 2011).

4 Leonard, E., Runguphan, W., O'Connor, S. and Prather, K.J. (2009) Opportunities in metabolic engineering to facilitate scalable alkaloid production. *Nat. Chem. Biol.* 5, 292–300.

5 Dehghan, E., Hosseini, B., Naghdi Badi, H. and Shahriari Ahmadi, F. (2010) Application of conventional and new biotechnological approaches for improving of morphinane alkaloids production. *J. Med. Plants* 9, 33–50.

6 Glenn, W.S., Runguphan, W. and O'Connor, S.E. (2013) Recent progress in the metabolic engineering of alkaloids in plant systems. *Curr. Opin. Biotechnol.* 24, 354–365.

7 Diamond, A. and Desgagné-Penix, I. (2016) Metabolic engineering for the production of plant isoquinoline alkaloids. *Plant Biotechnol. J.* 14, 1319–1328.

8 Kulkarni, R.N., Baskaran, K. and Jhang, T. (2016) Breeding medicinal plant, periwinkle [*Catharanthus roseus* (L) G. Don]: a review. *Plant Genet. Resour.* 14, 283–302.

9 Kosuri, S. and Church, G.M. (2014) Large-scale *de novo* DNA synthesis: technologies and applications. *Nat. Methods* 11, 499–507.

10 Chao, R., Yuan, Y. and Zhao, H. (2015) Recent advances in DNA assembly technologies. *FEMS Yeast Res.* 15, 1–9.

11 Narcross, L., Fossati, E., Bourgeois, L., Dueber, J.E. and Martin, V.J. (2016) Microbial factories for the production of benzylisoquinoline alkaloids. *Trends Biotechnol.* 34, 228–241.

12 Ro, D.K. *et al.* (2006) Production of the antimalarial drug precursor artemisinic acid in engineered yeast. *Nature* 440, 940–943.

13 Paddon, C.J. and Keasling, J.D. (2014) Semi-synthetic artemisinin: a model for the use of synthetic biology in pharmaceutical development. *Nat. Rev. Microbiol.* 12, 355–367.

14 Peplow, M. (2016) Synthetic biology's first malaria drug meets market resistance. *Nature* 530, 389–390.

15 Pickens, L.B., Tang, Y. and Chooi, Y.H. (2011) Metabolic engineering for the production of natural products. *Annu. Rev. Chem. Biomol. Eng.* 2, 211–236.

16 O'Connor, S.E. (2012) Strategies for engineering plant natural products: the iridoid-derived monoterpene indole alkaloids of *Catharanthus roseus*. *Methods Enzymol.* 515, 189–206.

17 Runguphan, W., Qu, X. and O'Connor, S.E. (2010) Integrating carbon–halogen bond formation into medicinal plant metabolism. *Nature* 468, 461–464.

18 Glenn, W.S., Nims, E. and O'Connor, S.E. (2011) Reengineering a tryptophan halogenase to preferentially chlorinate a direct alkaloid precursor. *J. Am. Chem. Soc.* 133, 19346–19349.

19 Friedrich, A., Bräse, S. and O'Connor, S.E. (2009) Synthesis of 4-, 5-, 6-, and 7-azidotryptamines. *Tetrahedr. Lett.* 50, 75–76.

20 Trenchard, I.J., Siddiqui, M.S., Thodey, K. and Smolke, C.D. (2015) *De novo* production of the key branch point benzylisoquinoline alkaloid reticuline in yeast. *Metab. Eng.* 31, 74–83.

21 Brown, S., Clastre, M., Courdavault, V. and O'Connor, S.E. (2015) *De novo* production of the plant-derived alkaloid strictosidine in yeast. *Proc. Natl. Acad. Sci. U.S.A.* 112, 3205–3210.

22 Galanie, S. and Smolke, C.D. (2015) Optimization of yeast-based production of medicinal protoberberine alkaloids. *Microb. Cell Fact.* 14, 144.

23 Li, Y. and Smolke, C.D. (2016) Engineering biosynthesis of the anticancer alkaloid noscapine in yeast. *Nat. Commun.* 7, 12137.

24 Trenchard, I.J. and Smolke, C.D. (2015) Engineering strategies for the fermentative production of plant alkaloids in yeast. *Metab. Eng.* 30, 96–104.

25 Hori, K., Okano, S. and Sato, F. (2016) Efficient microbial production of stylopine using a *Pichia pastoris* expression system. *Sci. Rep.* 6, 22201.

26 McKeague, M., Wang, Y.H., Cravens, A., Win, M.N. and Smolke, C.D. (2016) Engineering a microbial platform for *de novo* biosynthesis of diverse methylxanthines. *Metab. Eng.* 38, 191–203.

27 Jakubczyk, D. *et al.* (2015) Discovery and reconstitution of the cycloclavine biosynthetic pathway—enzymatic formation of a cyclopropyl group. *Angew. Chem. Weinheim Bergstr. Ger.* 127, 5206–5210.

28 Fossati, E., Narcross, L., Ekins, A., Falgueyret, J.P. and Martin, V.J. (2015) Synthesis of morphinan alkaloids in *Saccharomyces cerevisiae*. *PLoS One* 10, e0124459.

29 Galanie, S., Thodey, K., Trenchard, I.J., Filsinger Interrante, M. and Smolke, C.D. (2015) Complete biosynthesis of opioids in yeast. *Science* 349, 1095–1100.

30 Nakagawa, A. *et al*. (2016) Total biosynthesis of opiates by stepwise fermentation using engineered *Escherichia coli*. *Nat. Commun.* 7, 10390.

31 Qu, Y. *et al*. (2015) Completion of the seven-step pathway from tabersonine to the anticancer drug precursor vindoline and its assembly in yeast. *Proc. Natl. Acad. Sci. U.S.A.* 112, 6224–6229.

32 DeLoache, W.C. *et al*. (2015) An enzyme-coupled biosensor enables (S)-reticuline production in yeast from glucose. *Nat. Chem. Biol*. 11, 465–471.

33 Nielsen, C.A. *et al*. (2014) The important ergot alkaloid intermediate chanoclavine-I produced in the yeast *Saccharomyces cerevisiae* by the combined action of EasC and EasE from *Aspergillus japonicus*. *Microb. Cell Fact*. 13, 95.

34 Thodey, K., Galanie, S. and Smolke, C.D. (2014) A microbial biomanufacturing platform for natural and semisynthetic opioids. *Nat. Chem. Biol*. 10, 837–844.

35 Fossati, E. *et al*. (2014) Reconstitution of a 10-gene pathway for synthesis of the plant alkaloid dihydrosanguinarine in Saccharomyces cerevisiae. *Nat. Commun*. 5, 3283.

36 Nakagawa, A. *et al*. (2014) (R,S)-tetrahydropapaveroline production by stepwise fermentation using engineered *Escherichia coli*. *Sci. Rep*. 4, 6695.

37 Ehrenworth, A.M., Sarria, S. and Peralta-Yahya, P. (2015) Pterin-dependent mono-oxidation for the microbial synthesis of a modified monoterpene indole alkaloid. *ACS Synth. Biol*. 4, 1295–1307.

38 Wishart, D.S. *et al*. (2006) DrugBank: a comprehensive resource for in silico drug discovery and exploration. *Nucleic Acids Res*. 34, D668–D672.

39 Hagel, J.M., Krizevski, R., Marsolais, F., Lewinsohn, E. and Facchini, P.J. (2012) Biosynthesis of amphetamine analogs in plants. *Trends Plant Sci*. 17, 404–412.

40 Cuevas, C. *et al*. (2000) Synthesis of ecteinascidin ET-743 and phthalascidin Pt-650 from cyanosafracin B. *Org. Lett.* 2, 2545–2548.

41 Meyer, T. *et al*. (2009) Taste, a new incentive to switch to (*R*)-praziquantel in schistosomiasis treatment. *PLoS Negl. Trop. Dis*. 3, e357.

42 Yu, Q.S. *et al*. (2010) Preparation and characterization of tetrabenazine enantiomers against vesicular monoamine transporter 2. *ACS Med. Chem. Lett*. 1, 105–109.

43 Naito, R. *et al*. (2005) Synthesis and antimuscarinic properties of quinuclidin-3-yl 1,2,3,4-tetrahydroisoquinoline-2-carboxylate derivatives as novel muscarinic receptor antagonists. *J. Med. Chem*. 48, 6597–6606.

44 Ruff, B.M., Bräse, S. and O'Connor, S.E. (2012) Biocatalytic production of tetrahydroisoquinolines. *Tetrahedr. Lett*. 53, 1071–1074.

45 Kilgore, M.B. and Kutchan, T.M. (2016) The Amaryllidaceae alkaloids: biosynthesis and methods for enzyme discovery. *Phytochem. Rev*. 15, 317–337.

46 Marco-Contelles, J., do Carmo Carreiras, M., Rodríguez, C., Villarroya, M. and García, A.G. (2006) Synthesis and pharmacology of galantamine. *Chem. Rev*. 106, 116–133.

47 Chen, J.Q., Xie, J.H., Bao, D.H., Liu, S. and Zhou, Q.L. (2012) Total synthesis of (−)-galanthamine and (−)-lycoramine via catalytic asymmetric hydrogenation and intramolecular reductive Heck cyclization. *Org. Lett*. 14, 2714–2717.

48 Kilgore, M.B., Augustin, M.M., May, G.D., Crow, J.A. and Kutchan, T.M. (2016) CYP96T1 of *Narcissus sp. aff. pseudonarcissus* catalyzes formation of the Para-Para′ C–C phenol couple in the Amaryllidaceae alkaloids. *Front. Plant Sci.* 7, 225.

49 Kilgore, M.B., Holland, C.K., Jez, J.M. and Kutchan, T.M. (2016) Identification of a noroxomaritidine reductase with Amaryllidaceae alkaloid biosynthesis related activities. *J. Biol. Chem.* 291, 16740–16752.

50 Wang, R. *et al*. (2013)Chemical synthetic method for norbelladine. CN patent 103,408,439.

51 Dewick, P.M. *Medicinal Natural Products: A Biosynthetic Approach* 3rd edn, 311–420 (Wiley, 2009).

52 Nasreen, A., Rueffer, M. and Zenk, M.H. (1996) Cytochrome P-450-dependent formation of isoandrocymbine from autumnaline in colchicine biosynthesis. *Tetrahedr. Lett.* 37, 8161–8164.

53 Hill, D.A. and Turner, G.L. Neuromuscular blocking agents. US Patent 5,453,510 (1995).

54 Morishige, T., Tsujita, T., Yamada, Y. and Sato, F. (2000) Molecular characterization of the *S*-adenosyl-L-methionine:3′-hydroxy-*N*-methylcoclaurine 4′-*O*-methyltransferase involved in isoquinoline alkaloid biosynthesis in *Coptis japonica. J. Biol. Chem*. 275, 23398–23405.

55 Ounaroon, A., Decker, G., Schmidt, J., Lottspeich, F. and Kutchan, T.M. (2003) (*R*,*S*)-Reticuline 7-*O*-methyltransferase and (*R*,*S*)-norcoclaurine 6-*O*-methyltransferase of *Papaver somniferum*—cDNA cloning and characterization of methyl transfer enzymes of alkaloid biosynthesis in opium poppy. *Plant J*. 36, 808–819.

56 Chang, L., Hagel, J.M. and Facchini, P.J. (2015) Isolation and characterization of *O*-methyltransferases involved in the biosynthesis of glaucine in *Glaucium flavum*. *Plant Physiol*. 169, 1127–1140.

57 Gurusamy, N. Process for making apomorphine and apocodeine. EP patent 2,007,730 (2008).

58 Schaefer, B. in *Natural Products in the Chemical Industry* 260–296 (Springer-Verlag, 2014).

59 Gesell, A. *et al*. (2009) CYP719B1 is salutaridine synthase, the C–C phenol-coupling enzyme of morphine biosynthesis in opium poppy. *J. Biol. Chem*. 284, 24432–24442.

60 Park, S. *et al*. (2011) Production of serotonin by dual expression of tryptophan decarboxylase and tryptamine 5-hydroxylase in *Escherichia coli*. *Appl. Microbiol. Biotechnol*. 89, 1387–1394.

61 Germann, S.M. *et al*. (2016) Glucose-based microbial production of the hormone melatonin in yeast *Saccharomyces cerevisiae*. *Biotechnol. J*. 11, 717–724.

62 Baumann, M., Baxendale, I.R., Ley, S.V. and Nikbin, N. (2011) An overview of the key routes to the best selling 5-membered ring heterocyclic pharmaceuticals. *Beilstein J. Org. Chem.* 7, 442–495.

63 Dunn, P.J. (2005) Synthesis of commercial phosphodiesterase(V) inhibitors. *Org. Process Res. Dev.* 9, 88–97.

64 O'Connor, S.E. and Maresh, J.J. (2006) Chemistry and biology of monoterpene indole alkaloid biosynthesis. *Nat. Prod. Rep.* 23, 532–547.

65 Hoareau, L. and DaSilva, E. (1999) Medicinal plants: a re-emerging health aid. *Electron. J. Biotechnol.* 2, http://dx.doi.org/10.2225/vol2-issue2-fulltext-2.

66 Miettinen, K. *et al*. (2014) The seco–iridoid pathway from *Catharanthus roseus*. *Nat. Commun*. 5, 3606.

67 Góngora-Castillo, E. *et al*. (2012) Development of transcriptomic resources for interrogating the biosynthesis of monoterpene indole alkaloids in medicinal plant species. *PLoS One* 7, e52506.

68 Xiao, M. *et al*. (2013) Transcriptome analysis based on next-generation sequencing of non-model plants producing specialized metabolites of biotechnological interest. *J. Biotechnol.* 166, 122–134.

69 Kellner, F. *et al*. (2015) Genome-guided investigation of plant natural product biosynthesis. *Plant J*. 82, 680–692.

70 Hawkins, K.M. and Smolke, C.D. (2008) Production of benzylisoquinoline alkaloids in *Saccharomyces cerevisiae. Nat. Chem. Biol*. 4, 564–573.

71 Kaufman, T.S. and Rúveda, E.A. (2005) The quest for quinine: those who won the battles and those who won the war. *Angew. Chem. Int. Edn Engl*. 44, 854–885.

72 Stork, G. *et al*. (2001) The first stereoselective total synthesis of quinine. *J. Am. Chem. Soc.* 123, 3239–3242.

73 Isaac, J.E., Robins, R.J. and Rhodes, M.J.C. (1987) Cinchoninone:NADPH oxidoreductases i and ii—novel enzymes in the biosynthesis of quinoline alkaloids in *Cinchona ledgeriana*. *Phytochemistry* 26, 393–399.

74 Comins, D.L. and Nolan, J.M. (2001) A practical six-step synthesis of (*S*)-camptothecin. *Org. Lett*. 3, 4255–4257.

75 Rao, A.V.R., Rao, R., Yadav, J.S. and Khagga, M. (2013) Scalable synthetic route to 2-amino-5-hydroxypropiophenone: efficient formal synthesis of irinotecan. *Synth. Commun*. 43, 1661–1667.

76 Zabudkin, A. Method for the synthesis of irinotecan. EP patent 2,881,396 (2015).

77 Puri, S.C., Handa, G., Dhar, K.L., Suri, O.P. and Qazi, G.N. Process for preparing topotecan from 10-hydroxy-4-(*S*) camptothecin. EP patent 1,608,660 (2007).

78 Lorence, A. and Nessler, C.L. (2004) Camptothecin, over four decades of surprising findings. *Phytochemistry* 65, 2735–2749.

79 Pu, X. *et al*. (2013) Camptothecin-producing endophytic fungus *Trichoderma atroviride* LY357: isolation, identification, and fermentation conditions optimization for camptothecin production. *Appl. Microbiol. Biotechnol.* 97, 9365–9375.

80 Cui, L. *et al*. (2015) Co-overexpression of geraniol-10-hydroxylase and strictosidine synthase improves anti-cancer drug camptothecin accumulation in *Ophiorrhiza pumila*. *Sci. Rep.* 5, 8227.

81 Ni, X.H. *et a*l. (2011) Enhancement of camptothecin produciton in *Camptotheca acuminara* hairy roots by overexpressing ORCA3 gene. *J. Appl. Pharm. Sci*. 1, 85–88.

82 Sadre, R. *et al.* (2016) Metabolite diversity in alkaloid biosynthesis: a multi-lane (diastereomer) highway for camptothecin synthesis in *Camptotheca acuminata*. *Plant Cell* 28, 1926–1944.

83 McCoy, E. and O'Connor, S.E. (2006) Directed biosynthesis of alkaloid analogs in the medicinal plant *Catharanthus roseus*. *J. Am. Chem. Soc.* 128, 14276–14277.

84 Gerhards, N., Neubauer, L., Tudzynski, P. and Li, S.M. (2014) Biosynthetic pathways of ergot alkaloids. *Toxins (Basel)* 6, 3281–3295.

85 Cvak, L. in *Ergot: The Genus Claviceps* (eds. Kren, V. and Cvak, L.) 373–408 (Harwood Academic Publishers, 1999).

86 Ryan, K.L., Moore, C.T. and Panaccione, D.G. (2013) Partial reconstruction of the ergot alkaloid pathway by heterologous gene expression in *Aspergillus nidulans*. *Toxins (Basel)* 5, 445–455.

87 Wallwey, C., Matuschek, M. and Li, S.M. (2010) Ergot alkaloid biosynthesis in *Aspergillus fumigatus*: conversion of chanoclavine-I to chanoclavine-I aldehyde catalyzed by a short-chain alcohol dehydrogenase FgaDH. *Arch. Microbiol.* 192, 127–134.

88 Cheng, J.Z., Coyle, C.M., Panaccione, D.G. and O'Connor, S.E. (2010) Controlling a structural branch point in ergot alkaloid biosynthesis. *J. Am. Chem. Soc.* 132, 12835–12837.

89 Robinson, S.L. and Panaccione, D.G. (2014) Heterologous expression of lysergic acid and novel ergot alkaloids in *Aspergillus fumigatus*. *Appl. Environ. Microbiol.* 80, 6465–6472.

90 McCoy, E., Galan, M.C. and O'Connor, S.E. (2006) Substrate specificity of strictosidine synthase. *Bioorg. Med. Chem. Lett.* 16, 2475–2478.

91 Lee, H.Y., Yerkes, N. and O'Connor, S.E. (2009) Aza-tryptamine substrates in monoterpene indole alkaloid biosynthesis. *Chem. Biol.* 16, 1225–1229.

92 Geu-Flores, F. *et al.* (2012) An alternative route to cyclic terpenes by reductive cyclization in iridoid biosynthesis. *Nature* 492, 138–142.

93 Campbell, A. *et al.* (2016) Engineering of a nepetalactol-producing platform strain of *Saccharomyces cerevisiae* for the production of plant seco–iridoids. *ACS Synth. Biol.* 5, 405–414.

94 Lang, A. *et al.* (2011) Changing the regioselectivity of the tryptophan 7-halogenase PrnA by site-directed mutagenesis. *Angew. Chem. Int. Edn Engl.* 50, 2951–2953.

95 Brown, S. and O'Connor, S.E. (2015) Halogenase engineering for the generation of new natural product analogues. *ChemBioChem* 16, 2129–2135.

96 Runguphan, W. and O'Connor, S.E. (2013) Diversification of monoterpene indole alkaloid analogs through cross-coupling. *Org. Lett.* 15, 2850–2853.

97 Gillis, E.P., Eastman, K.J., Hill, M.D., Donnelly, D.J. and Meanwell, N.A. (2015) Applications of fluorine in medicinal chemistry. *J. Med. Chem.* 58, 8315–8359.

98 O'Hagan, D. and Deng, H. (2015) Enzymatic fluorination and biotechnological developments of the fluorinase. *Chem. Rev.* 115, 634–649.

99 Hong, H., Spiteller, D. and Spencer, J.B. (2008) Incorporation of fluoroacetate into an aromatic polyketide and its influence on the mode of cyclization. *Angew. Chem. Int. Edn Engl.* 47, 6028–6032.

100 Walker, M.C. *et al.* (2013) Expanding the fluorine chemistry of living systems using engineered polyketide synthase pathways. *Science* 341, 1089–1094.

CHAPTER 2. Pterin-dependent Mono-oxidation for the Microbial Synthesis of a Modified Monoterpene Indole Alkaloid

2.1 Abstract

Monoterpene indole alkaloids (MIAs) have important therapeutic value, including as anticancer and antimalarial agents. Because of their chemical complexity, therapeutic MIAs, or advanced intermediates thereof, are often isolated from the native plants. The microbial synthesis of MIAs would allow for the rapid and scalable production of complex MIAs and MIA analogues for therapeutic use. Here, we produce the modified MIA hydroxystrictosidine from glucose and the monoterpene secologanin via a pterin-dependent mono-oxidation strategy. Specifically, we engineered the yeast *Saccharomyces cerevisiae* for the high-level synthesis of tetrahydrobiopterin to mono-oxidize tryptophan to 5-hydroxytryptophan, which, after decarboxylation to serotonin, is coupled to exogenously fed secologanin to produce 10-hydroxystrictosidine in an eight-enzyme pathway. We selected hydroxystrictosidine as our synthetic target because hydroxylation at the 10′ position of the alkaloid core strictosidine provides a chemical handle for the future chemical semisynthesis of therapeutics. We show the generality of the pterin-dependent mono-oxidation strategy for alkaloid synthesis by hydroxylating tyrosine to L-DOPA—a key intermediate in benzylisoquinoline alkaloid (BIA) biosynthesis—and, thereafter, further converting it to dopamine. Together, these results present the first

microbial synthesis of a modified alkaloid, the first production of tetrahydrobiopterin in yeast, and the first use of a pterin-dependent mono-oxidation strategy for the synthesis of L-DOPA. This work opens the door to the scalable production of MIAs as well as the production of modified MIAs to serve as late intermediates in the semisynthesis of known and novel therapeutics. Further, the microbial strains in this work can be used as plant pathway discovery tools to elucidate known MIA biosynthetic pathways or to identify pathways leading to novel MIAs.

2.2 Introduction

Alkaloids are the largest group of nitrogen-containing secondary metabolites, with more than 20 000 structures[1], are present in roughly 20% of plant species[2], and are important because of their medicinal use[3]. Of particular importance are monoterpene indole alkaloids (MIAs), which include anticancer agents such as camptothecin (**1**) and vinblastine (**2**), antimalarial agents such as quinine, and antiarrhythmic agents such as ajmalicine. Another important alkaloid family is benzylisoquinoline alkaloids (BIAs), which include the antibiotic berberine (**3**) and the analgesic morphine (**4**)[4]. Due to their chemical complexity, alkaloids often require multistep chemical syntheses, which, coupled with the necessity of enantiopure material, make them a challenging synthetic target[5-8]. Therefore, medically important alkaloids, or advanced intermediates thereof, are frequently isolated directly from the native plants[5,7,9]. Although effective, isolation of alkaloids from plants is often limited by their low accumulation in plant tissue and their difficult separation from other natural products, thus resulting in the high cost of alkaloid-derived pharmaceuticals, especially those based on MIAs[5,7]. Via plant breeding and, more recently, plant metabolic engineering, the production of BIAs and MIAs in planta has

been increased[10-13]. Further, plants have been engineered to produce halogenated MIAs, with potentially higher bioactivity, which can serve as late intermediates in the semisynthesis of other alkaloids[14-16]. Nevertheless, limited understanding of plant secondary metabolite regulation and slow plant growth rate cloud the future of engineering plants to overproduce alkaloids[2,5,7]. These limitations result in the underrepresentation of alkaloid-derived compounds in pharmaceutical drug screenings[17]. The synthesis of plant alkaloids in microbes would enable the rapid and scalable production of known alkaloids and open the door to the biosynthesis of novel alkaloids using engineered enzymes or combinatorial enzyme assembly. Plant alkaloid production in microbes has the advantages of short doubling time, rapid extraction of the alkaloid from the culture medium, easier isolation of the desired alkaloid due to the absence of similar natural products, and a lack of endogenous pathway regulation, which allows for deregulation of alkaloid biosynthesis.

Many alkaloids are obtained via the hydroxylation and decarboxylation of amino acids[18]. Specifically, BIAs are derived from tyrosine (**5**) and MIAs are derived from tryptophan (**6**). In the last 10 years, full elucidation of many BIA biosynthetic pathways[4], in conjunction with advances in synthetic biology, have enabled the reconstruction of BIA pathways in both *Escherichia coli* and *Saccharomyces cerevisiae*[19-25]. Although MIA biosynthetic pathways have been extensively engineered in planta[14-15], the engineering of MIA alkaloids in microbes has been limited. A major problem in engineering microbes for the synthesis of plant alkaloids is the amino acid hydroxylation step. Tyrosinase, the most common enzyme used to hydroxylate tyrosine, not only oxidizes tyrosine into L-3,4-dihydroxyphenylalanine (L-DOPA, **7**), but its *o*-diphenolase

activity also results in further oxidation of L-DOPA to L-dopaquinone, a melanin precursor[26-28], thus reducing the availability of L-DOPA for alkaloid production. Nevertheless, tyrosinase has been used to produce the BIA reticuline from glycerol[21,25]. Recently, a P450 enzyme from beet was engineered for reduced *o*-diphenolase activity to increase the specificity of tyrosine hydroxylation to L-DOPA[29]. There is no equivalent to tyrosinase for tryptophan hydroxylation. To circumvent this problem, microbial synthesis of 5-hydroxytryptophan (**8**) has been achieved by indole hydroxylation followed by coupling to serine[30] or using an engineered phenylalanine hydroxylase with changed substrate specificity[31]. Hydroxytrytophan has not been converted to serotonin (**9**) or to MIAs microbially from glucose. Specific mono-oxygenases for tyrosine and tryptophan exist in higher eukaryotes; however, they require the pterin cofactor tetrahydrobiopterin (BH_4, **10**), which is not present in *E. coli* or *S. cerevisiae*.

We hypothesized that a pterin-dependent oxidation strategy to specifically mono-oxidize tyrosine or tryptophan would provide an alternative route for MIA and BIA biosynthesis (Figure 2.2). The difficulty in this strategy is that neither *E. coli* nor *S. cerevisiae* endogenously produces BH_4, which is necessary for the activity of mono-oxygenases found in higher eukaroytes[32,33]. Although BH_4 has been previously produced in *E. coli*[34], it was not coupled to amino acid mono-oxidation. The endogenous *E. coli* BH_4 analogue, tetrahydromonapterin (MH_4), has been promiscuously used as a cofactor for BH_4-dependent mono-oxygenases in the production of hydroxytyrosol[35] and 5-hydroxytryptophan[31]. However, MH_4 does not have the correct composition or stereochemistry when compared to BH_4 (Figure 2.1), which is likely to be accepted with higher efficiency by amino acid mono-oxygenases from higher eukaryotes[32,36], such as

those in this study. To establish a microbial platform for the synthesis of plant alkaloids via the pterin-dependent mono-oxidation strategy, we engineered *S. cerevisiae* for BH_4 production. We selected *S. cerevisiae* as the microbial host because yeast, like plants, is eukaryotic. A yeast platform for amino acid mono-oxidation will facilitate the synthesis of complex plant alkaloids, as expression of downstream alkaloid pathway enzymes are thought to be mainly transmembrane cytochrome P450s, which are difficult to functionally express in bacteria such as *E. coli*[20,37] without protein engineering[38-40]. In addition, *S. cerevisiae*'s robustness, tolerance to industrial conditions, including low pH and high sugar concentrations, and insusceptibility to phage infection make it the ideal host for chemical production[41-43].

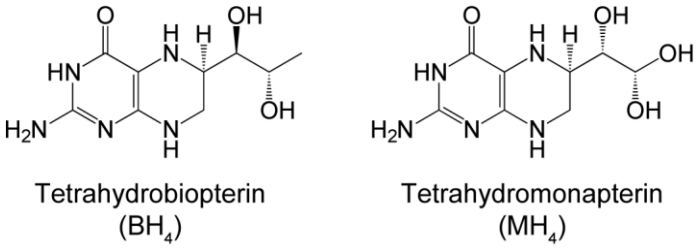

Figure 2.1. Stereochemistry of pterin co-factors. Chemical structures of tetrahydrobiopterin (BH_4), the natural amino acid mono-oxygenase co-factor, and tetrahydromonapterin (MH_4), the BH_4 analogue found in *E. coli*. BH_4 and MH_4 vary in stereochemistry and composition.

Here, we report the use of a pterin-dependent mono-oxidation strategy for the microbial synthesis of the biogenic amines dopamine and serotonin and the leveraging of serotonin to produce a modified MIA. Specifically, we engineered BH_4-producing yeast to mono-oxidize tryptophan to 5-hydroxytryptophan, which, after decarboxylation to serotonin, is condensed with the monoterpene secologanin (**11**) to produce the modified MIA hydroxystrictosidine (**12**). First, we combinatorially screened BH_4 biosynthetic

enzymes to identify the enzyme assembly leading to the highest BH_4 production. Next, we introduced a BH_4 recycling pathway to guarantee supply of BH_4 to the amino acid mono-oxygenases. Then, we showed that pterin-dependent oxidation of tryptophan followed by decarboxylation results in serotonin, a key MIA intermediate. Finally, we introduced the MIA biosynthetic pathway to ultimately produce hydroxystrictosidine from glucose and secologanin. We show the generality of the pterin-dependent mono-oxidation strategy for the microbial synthesis of alkaloids by using a tyrosine mono-oxygenase to convert tyrosine into L-DOPA, which is subsequently decarboxylated to dopamine (**13**), a key BIA intermediate. This is the first production of BH_4 in *S. cerevisiae* and the first microbial synthesis of a modified MIA. Further, this is the first time that *S. cerevisiae* has been engineered to produce the key BIA biogenic amine, dopamine, and the key MIA biogenic amine, serotonin, from glucose via pterin-dependent mono-oxidation. The microbial strains presented in this work open the door to the scalable production of MIAs, as well as the production of modified MIAs to serve as late intermediates in the semisynthesis of known and novel therapeutics. Further, the microbial strains in this work can be used as plant pathway discovery tools to elucidate known MIA biosynthetic pathways or to identify pathways leading to novel MIAs.

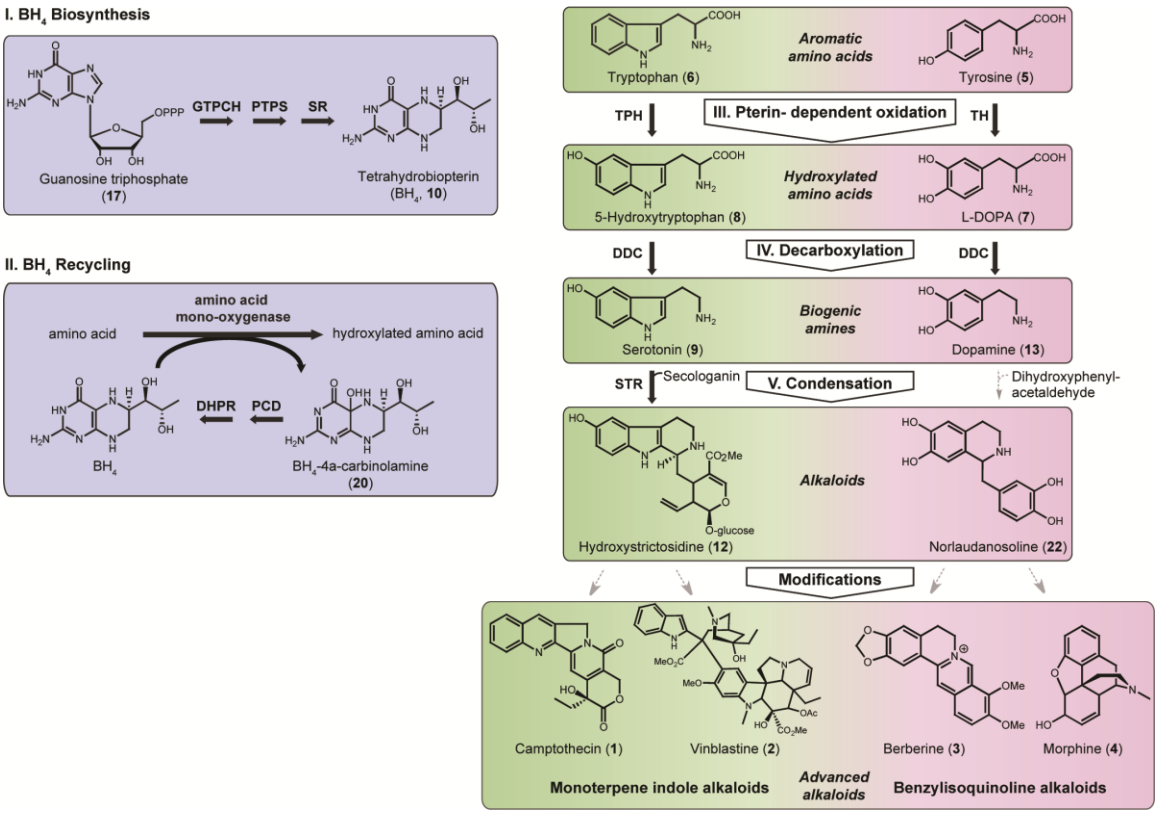

Figure 2.2. Pterin-dependent microbial synthesis of monoterpene indole alkaloids (MIAs) in *Saccharomyces cerevisiae*. General schematic of MIA and benzylisoquinoline alkaloid microbial synthesis via pterin-dependent mono-oxidation. The engineered strains of *S. cerevisiae* presented in this work contain one or more of the following: (I) the BH_4 biosynthetic pathway, (II) the BH_4 recycling pathway, (III) a pterin-dependent mono-oxygenase, (IV) a decarboxylase, or (V) a Pictet–Spenglerase. Gray arrows represent future potential of the system. GTPCH, GTP cyclohydrolase; PTPS, pyruvoyl tetrahydropterin synthase; SR, sepiapterin reductase; PCD, pterin-4a-carbinolamine dehydratase; DHPR, dihydropteridine reductase; TPH, tryptophan hydroxylase; TH, tyrosine hydroxylase; DDC, aromatic-L-amino-acid decarboxylase; STR, strictosidine synthase.

2.3 Results

2.3.1 Target Choice: Hydroxystrictosidine

While the natural branch point in MIA biosynthesis is strictosidine[44], we pursued instead the biosynthesis of 10-hydroxystrictosidine, an MIA that can be produced by *Camptotheca acuminata*[45], the major producer of the anticancer agent camptothecin. We

were interested in the biosynthesis of 10′ functionalized strictosidine as it provides a chemical handle for the rapid derivatization of strictosidine-derived MIAs. 10-hydroxystrictosidine is synthesized via the condensation of 5-hydroxytryptamine (serotonin) and secologanin, rather than tryptamine and secologanin as in the case of strictosidine. Modifications at the 5′ position of tryptophan have been shown to be processed by MIA enzymes in *Catharanthus roseus* to produce 10′ modified ajmalicine, serpentine, and tabersonine[46]. In this spirit, 10-hydroxystrictosidine may enable the biosynthesis of modified MIAs, such as 10-hydroxycamptothecin (**14**), which has higher anticancer activity than camptothecin[18] (Figure 2.3). Modified MIAs such as 10-hydroxycamptothecin can serve as better semisynthesis intermediates than camptothecin for the chemical synthesis of more water-soluable derivatives[18], such as the colon anticancer drug irinotecan (**15**) and the ovarian and lung cancer drug topotecan (**16**). More generally, modified MIAs can serve as synthons for the semisynthesis of novel complex alkaloids with potential therapeutic activities.

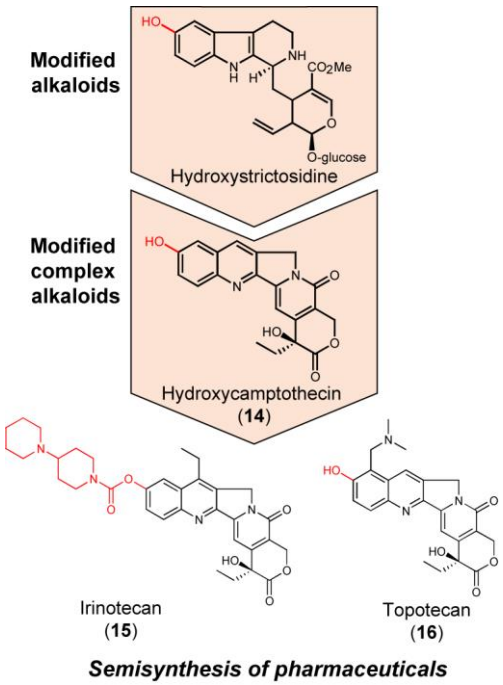

Figure 2.3. Modified MIAs for the semisynthesis of pharmaceuticals. Modified alkaloids, such as hydroxystrictosidine, have the potential to be biosynthetically converted to advanced alkaloids, such as hydroxycamptothecin, via the MIA biosynthetic pathway. These alkaloids can be used as functionalized starting materials for the semisynthesis of pharmaceuticals. In particular, hydroxycamptothecin, which is the 10′ hydroxylated version of camptothecin, could enable rapid access to the anticancer drugs topotecan and irinotecan.

2.3.2 Microbial Synthesis of Tetrahydrobiopterin in S. cerevisiae

S. cerevisiae does not produce BH_4, but guanosine triphosphate (GTP, **17**) can be rerouted to produce BH_4 through the intermediates dihydroneopterin triphosphate (**18**) and pyruvoyl tetrahydropterin (**19**) using three enzymes: GTP cyclohydrolase I (GTPCH), pyruvoyl tetrahydropterin synthase (PTPS), and sepiapterin reductase (SR) (Figure 2.4a). Given that BH_4 oxidizes to dihydrobiopterin and, subsequently, to biopterin in water[47], we screened for the presence of biopterin in the medium. GTPCH is the first committed step in BH_4 biosynthesis[48]. *S. cerevisiae* has an endogenous GTPCH as part of the folate biosynthetic pathway and thus requires only expression of

heterologous PTPS and SR to produce BH_4. *Mortierella alpina* is the only fungus shown to carry the full BH_4 biosynthetic pathway from GTP[49], and, given that *S. cerevisiae* is also a fungus, *M. alpina* enzymes may be efficiently expressed in this organism. Overexpression of *M. alpina* PTPS and SR in *S. cerevisiae* produced 0.74 mg/L of BH_4, measured as biopterin (Figure 2.4b, Figure 2.5). Concerned that this would be an insufficient amount of BH_4, even for use as a cofactor only, we set out to determine if BH_4 levels have a limiting effect on alkaloid production. We exogenously fed BH_4 to yeast cells expressing only a pterin-dependent tyrosine mono-oxygenase to convert tyrosine into L-DOPA. No L-DOPA was seen when feeding 0–50 mg/L of BH_4, suggesting that BH_4 oxidizes to dihydrobiopterin or biopterin before reaching the tyrosine mono-oxygenase. BH_4 must be synthesized intracellularly rather than exogenously fed to determine whether 0.74 mg/L BH_4 limits alkaloid biosynthesis.

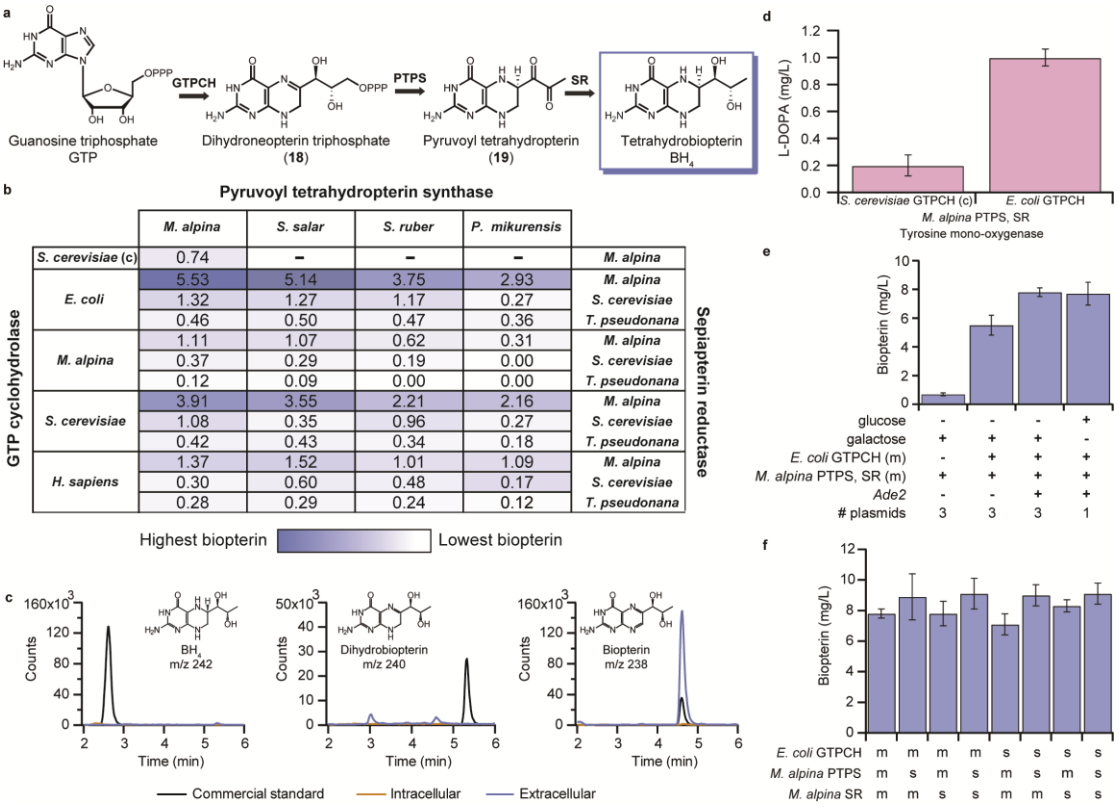

Figure 2.4. Microbial synthesis of tetrahydrobiopterin (BH_4) in *S. cerevisiae*. (a) BH_4 biosynthetic pathway from guanosine triphosphate (GTP), which is endogenously made by *S. cerevisiae*. (b) Heat map of biopterin titers (mg/L), as a proxy for BH_4 titers, from the 49 BH_4-producing yeast strains. Except for *S. cerevisiae* chromosomal (c), where the chromosomal copy of *S. cerevisiae* GTPCH was used, each enzyme was expressed from a multi-copy plasmid from an inducible galactose promoter (P_{GAL1}). Biopterin was quantified using liquid chromatography–mass spectrometry (LC/MS). Biopterin titers reported as (-) were not determined. Biopterin titers reported as 0.00 were either too low to quantify or undetectable. A control strain expressing green fluorescent protein in a three-plasmid system showed no biopterin production. The experiments were run in triplicate and shown are the means. Standard deviations can be found in Figure 2.5. (c) LC/MS traces (extracted ion chromatograms) of BH_4 (*m/z* 242) and oxidation products dihydrobiopterin (*m/z* 240) and biopterin (*m/z* 238) found intracellularly and in the production medium. Standard retention times: BH_4 = 2.6 min, dihydrobiopterin = 5.3 min, biopterin = 4.6 min. Only biopterin was observed in the production medium. Full windows of the spectra can be found in Figure 2.5. (d) Pterin-dependent mono-oxidation of tyrosine to L-DOPA using the original BH_4 synthesis strain (*S. cerevisiae* GTPCH, *M. alpina* PTPS and SR) and the combinatorially optimized BH_4 synthesis strain (*E. coli* GTPCH, *M. alpina* PTPS and SR), both strains carrying tyrosine mono-oxygenase. Improving BH_4 production improves amino acid mono-oxidation. (e) Optimization of BH_4 biosynthesis. BH_4 synthesis pathway: *E. coli* GTPCH, *M. alpina* PTPS and SR. For the glucose system, all three

enzymes were expressed from a single multi-copy plasmid under control of constitutive promoters (P_{ADH1}, P_{TEF1}, and P_{HXT7}). (f) BH_4 biosynthetic pathway bottleneck identification. Biopterin production from galactose in yeast expressing each BH_4 biosynthetic enzyme from either a single-copy (s) or a multi-copy (m) plasmid. All experiments were run in triplicate and shown are the means and standard deviations. GTPCH, GTP cyclohydrolase; PTPS, pyruvoyl tetrahydropterin synthase; SR, sepiapterin reductase.

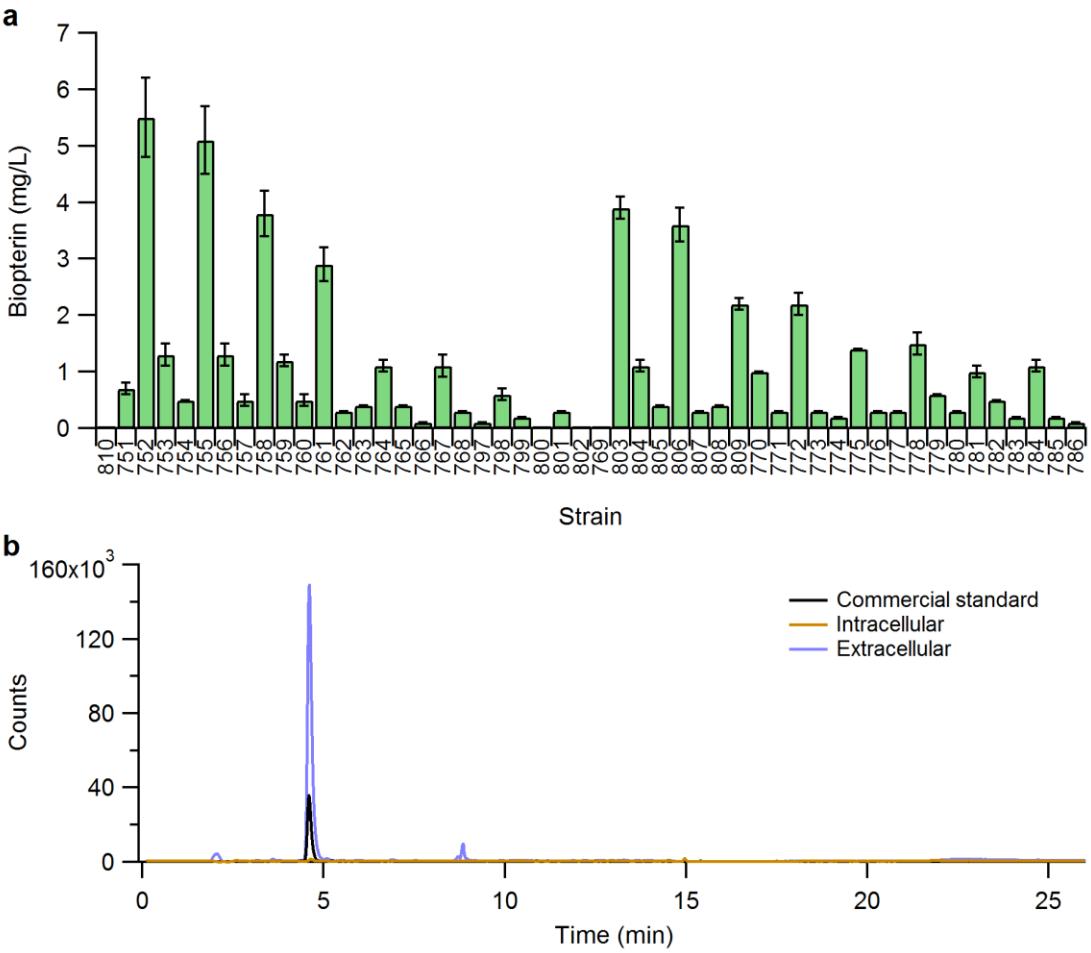

Figure 2.5. Combinatorial production of biopterin. (a) Production levels of biopterin were quantified using LC/MS. Production levels reported as 0.00 were either too low to quantify or undetectable. Strain PPY810 represents a control strain expressing green fluorescent protein in a three-plasmid system. The experiments were run in triplicate and shown are the mean and standard deviation. (b) Full window of LC traces representing biopterin production in Figure 2.4c.

So as not to limit alkaloid production due to insufficient BH_4, we combinatorially overexpressed four GTPCHs, four PTPSs, and three SRs in *S. cerevisiae* to identify a

high-level BH_4-producing yeast strain. Among GTPCHs, we screened the enzymes from *E. coli*, *M. alpina*, *Homo sapiens*, and *S. cerevisiae*. *E. coli* GTPCH has a low K_M (0.02[50]–100[51] μM) and has been previously expressed in *S. cerevisiae*[52]. *H. sapiens* GTPCH has a pI of 5.6[53], which could aid in its solubility, and it has also been expressed in *S. cerevisiae*[52]. Among PTPSs, we screened the enzymes from *M. alpina*, *Salmo salar*, the halophile *Salinibacter ruber*, and the bacteria *Phycisphaera mikurensis*. *S. salar* PTPS has a specific activity that is 50 times higher, and a K_M that is five times lower, than that of the canonical human PTPS[54]. We screened the putative PTPS from *S. ruber* because a structural homology model alignment with *S. salar* PTPS revealed that these enzymes have an almost identical active site, except that *S. ruber* PTPS has a catalytic aspartate rather than a cysteine residue[55] (Figure 2.6). We hypothesized that the aspartate's carboxylate functions as a better acid–base catalyst compared to cysteine's thiol group. We screened the predicted PTPS from *P. mikurensis* because its active site is almost identical to the well-studied *Rattus rattus* PTPS[56]; however, the *P. mikurensis* PTPS N-terminus has an additional ~100 amino acids. A bioinformatics search revealed that *S. cerevisiae* lacked any PTPS homologue. Among SRs, we screened the SR from *M. alpina*, a predicted SR from the diatom *Thalassiosira pseudonana*, which, based on structural homology models is hypothesized to be NADH- rather than NADPH-dependent (Figure 2.7), and a putative SR from *S. cerevisiae* identified using bioinformatics.

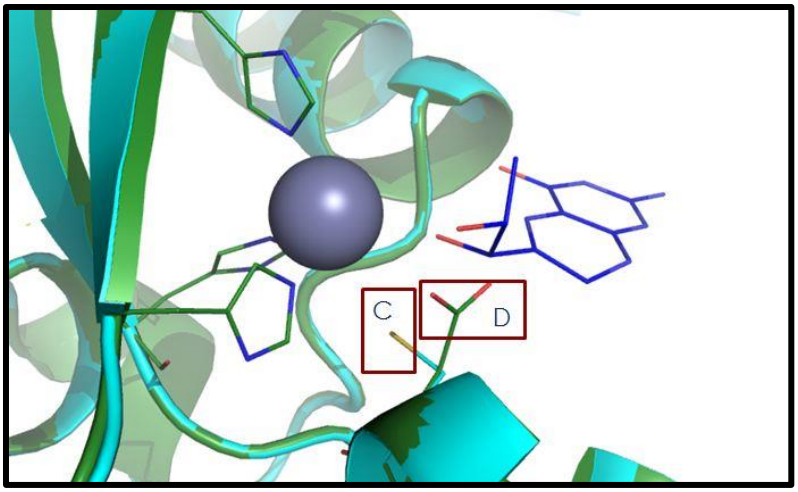

Figure 2.6. Structural alignment of *Salinibacter ruber* and *Salmo salar* pyruvoyl tetrahydropterin synthase (PTPS). Structural alignment of homology models of *S. salar* PTPS (cyan) and *S. ruber* (green) PTPS obtained via structural homology to rat PTPS (PDB:1B66) using SWISS-MODEL[81-83]. Presented is a monomer of the active site of PTPS (which is composed of three monomers) showing the catalytic cysteine residue of *S. salar* PTPS and corresponding aspartate residue of *S. ruber* PTPS. Biopterin (blue) and Zn(II) (purple) were obtained from the crystal structure from rat. Alignment was completed with PyMOL.

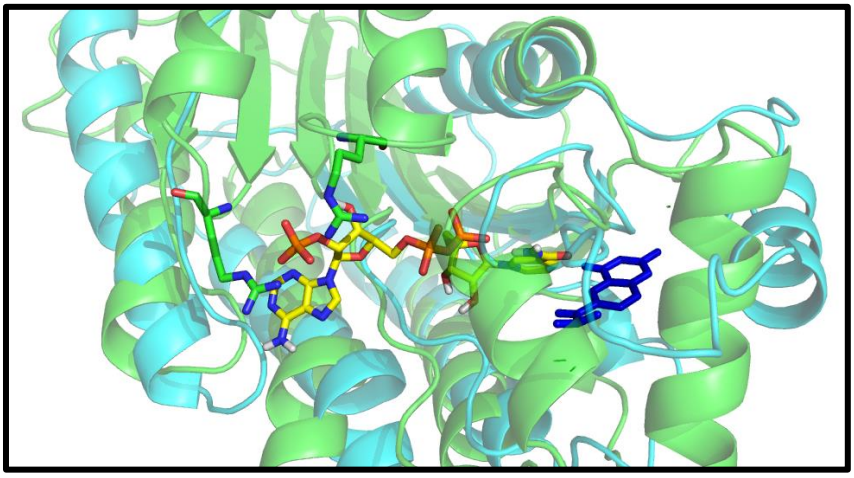

Figure 2.7. Structural alignment of *Mortierella alpina* and *Thalassiosira pseudonana* sepiapterin reductase (SR). Structural alignment of homology models of *M. alpina* SR (green) and *T. pseudonana* (cyan) SR obtained via structural homology to PDB:1Z6Z and 3ICC, respectively, using SWISSMODEL[81-83]. NADPH (yellow) and biopterin (dark blue) were obtained from the crystal structure of mouse SR (PDB:1SEP). While arginine residues are present in the *M. alpina* structure to stabilize the phosphate group of NADPH, there are no stabilizing residues present in the *T. pseudonana* structure. Alignment was completed with PyMOL.

The combination of *E. coli* GTPCH, *M. alpina* PTPS, and *M. alpina* SR resulted in the highest biopterin microbial synthesis, at 5.53 mg/L (Figure 2.4b, Figure 2.5). *E. coli* GTPCH outperformed all other GTPCHs, including the endogenous *S. cerevisiae* GTPCH. *H. sapiens* and *M. alpina* GTPCH resulted in the lowest biopterin production, with 3 of the 12 strains expressing *M. alpina* GTPCH producing undetectable levels of biopterin. PTPS expression showed graded levels of biopterin production with *M. alpina* ≈ *S. salar* > *S. ruber* > *P. mikurensis* in most cases. Expression of *M. alpina* SR resulted in statistically significant higher production of biopterin than the *S. cerevisiae* or *T. pseudonana* SRs in all 32 cases (all P-values < 0.015). No BH_4 or dihydrobiopterin were found in the medium or inside the cell, and negligible amounts of biopterin were found inside the cell, supporting diffusion of biopterin out of the cell (Figure 2.4c). As suspected, BH_4 levels had a limiting effect on pterin-dependent amino acid hydroxylation, judging by the performance of tyrosine mono-oxygenase in different BH_4-producing strains. L-DOPA production from the combinatorially optimized BH_4 synthesis strain (*E. coli* GTPCH, *M. alpina* PTPS and SR) resulted in 5-fold higher L-DOPA levels when compared to the initial BH_4 synthesis yeast strain (*S. cerevisiae* GTPCH (chromosomal), *M. alpina* PTPS and SR) (Figure 2.4d).

2.3.3 Optimization of Tetrahydrobiopterin Biosynthesis

We hypothesized that increasing the flux through the purine pathway should increase GTP levels and, in turn, BH_4 production. The parent yeast strain, W303, has a nonfunctional phosphoribosylaminoimidazole carboxylase (*ade2*) gene located upstream of GTP in the purine biosynthetic pathway (Figure 2.8). We generated a functional *Ade2* yeast strain and introduced the combinatorially optimized BH_4 synthesis pathway,

achieving 7.81 mg/L of biopterin, a statistically significant improvement over the combinatorially optimized BH_4 synthesis pathway in the *ade2* strain (5.53 mg/L, P value < 0.04) (Figure 2.4e). To identify bottlenecks within the BH_4 pathway, we dosed the expression of each gene in the combinatorially optimized BH_4 synthesis pathway by expressing each gene from a single- or multi-copy plasmid using galactose-inducible promoters. The highest biopterin production was obtained when GTPCH was expressed from a multi-copy plasmid with PTPS and SR expressed from single-copy plasmids, producing 9.13 mg/L of biopterin (Figure 2.4f). To help rationalize this result, we measured GTPCH, PTPS, and SR mRNA levels when expressed from single- or multi-copy plasmids (Figure 2.9). GTPCH mRNA levels were lowest when expressed from a multi-copy plasmid, while PTPS and SR mRNA levels were lowest when expressed from a single-copy plasmid. Thus, the best BH_4-producing strain had the lowest mRNA levels for each of the three genes, hinting that overexpression of the three enzymes may be a burden to the system. Nevertheless, the increase in biopterin production was not statistically different from the 7.81 mg/L of biopterin produced when all enzymes were expressed from multi-copy plasmids in the *Ade2* strain (Figure 2.4f). To produce BH_4 from glucose and to reduce plasmid burden[57,58], the best enzyme combination was expressed in the *Ade2* strain from a single multi-copy plasmid using constitutive promoters. Surprisingly, the single-plasmid BH_4 synthesis pathway resulted in only 7.69 mg/L of biopterin (Figure 2.4e), not statistically different from the biopterin production obtained from the three-plasmid galactose induced system (7.81 mg/L). It is possible that GTPCH, PTPS, and SR overexpression burden is more important than plasmid maintenance burden.

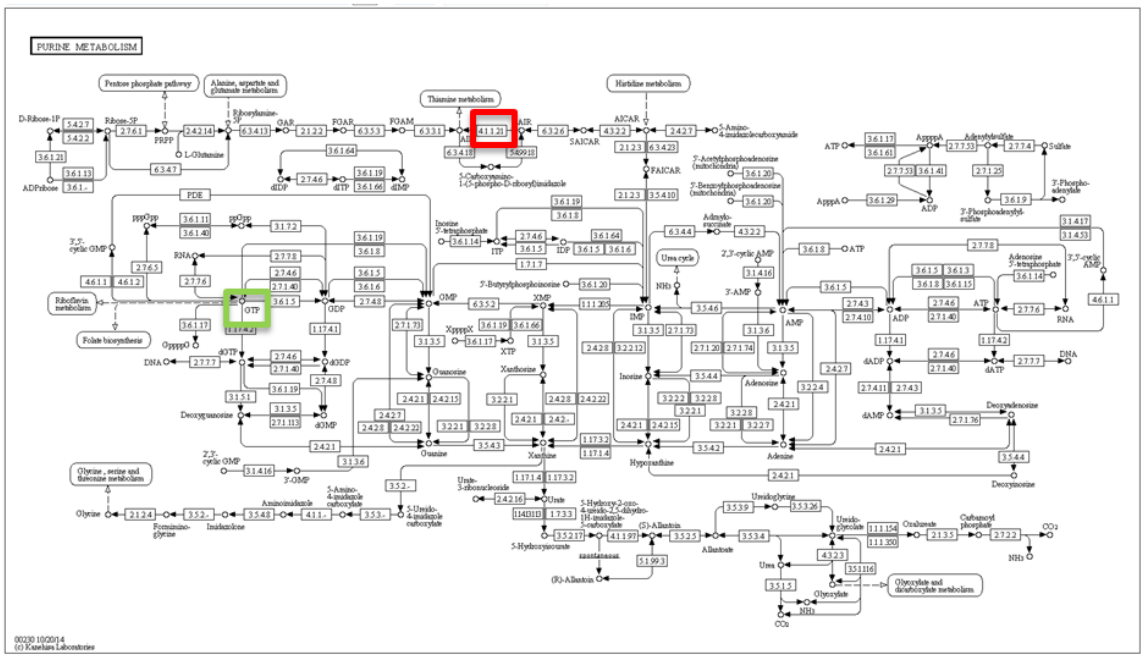

Figure 2.8. Purine biosynthetic pathway from the Kyoto Encyclopedia of Genes and Genomes (KEGG)[84]. The enzyme encoded by *Ade2* is boxed in red. GTP is boxed in green.

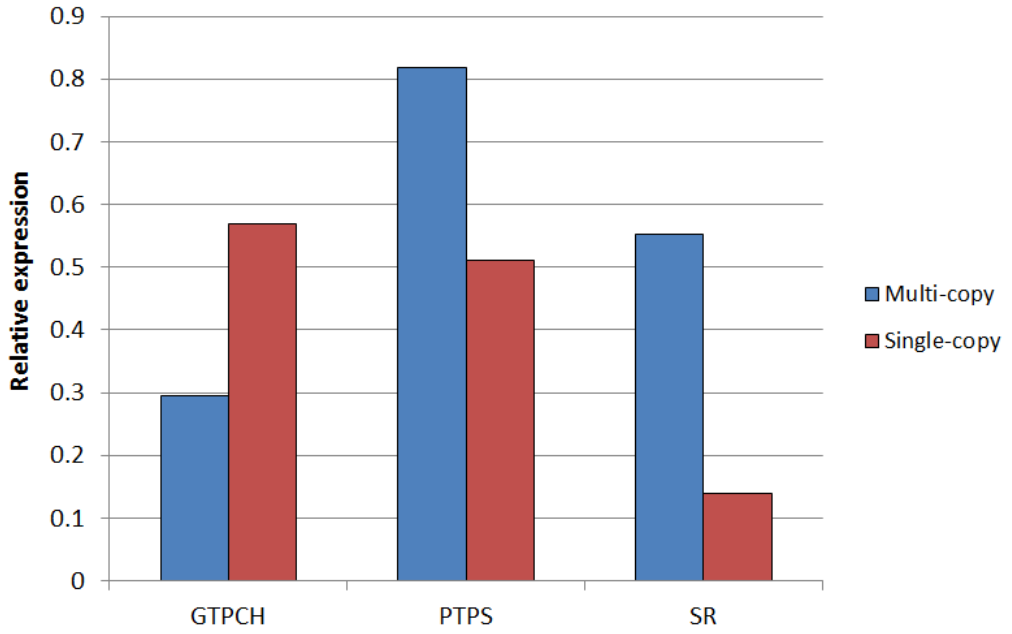

Figure 2.9. GTPCH, PTPS and SR mRNA levels. Multi-copy: multi-copy plasmid. Single-copy: single-copy plasmid. Values represent the mean of two reactions.

2.3.4 Tetrahydrobiopterin Recycling for Pterin-dependent Amino Acid Mono-oxidation

Upon amino acid mono-oxidation, BH_4 is converted to BH_4-4a-carbinolamine (**20**). Previous work in *E. coli* has shown the BH_4 recycling pathway to be critical to ensure continuous supply of the BH_4 analogue MH_4 in pterin-dependent amino acid mono-oxidation[31,35]. To provide a continuous supply of BH_4 to the amino acid mono-oxygenases, we established a BH_4 recycling pathway in *S. cerevisiae*. In the recycling pathway, BH_4-4a-carbinolamine is converted back to BH_4 via the intermediate quinoid dihydrobiopterin (**21**) through consecutive reactions by pterin-4a-carbinolamine dehydratase (PCD) and dihydropteridine reductase (DHPR) (Figure 2.10a). We measured the effect of the *H. sapiens* BH_4 recycling pathway on the pterin-dependent mono-oxidation of tyrosine to L-DOPA, using the codon optimized *Mus musculus* tyrosine hydroxylase, in (1) the absence of the BH_4 biosynthetic and recycling pathways, (2) the presence of only the BH_4 biosynthetic pathway, and (3) the presence of both the BH_4 biosynthetic and recycling pathways (Figure 2.10b,c, Figure 2.11a). As expected, no L-DOPA was produced in the absence of the BH_4 biosynthetic and recycling pathways. In the presence of only the BH_4 biosynthetic pathway, L-DOPA was produced at 0.27 mg/L, while in the presence of both the BH_4 biosynthetic and recycling pathways, L-DOPA was produced at 0.33 mg/L. This increase in L-DOPA was not statistically significant, and the difference in biopterin levels in the presence or absence of the recycling pathway was not statistically significant either (Figure 2.10d). We conclude that high-level BH_4 synthesis eliminates the necessity of the BH_4 recycling pathway at the current rate of tyrosine mono-oxidation. To determine if tyrosine was limiting L-DOPA production, we

supplemented the media with tyrosine and observed a slight increase in L-DOPA levels (Figure 2.12). Thus, improving tyrosine biosynthesis should increase L-DOPA.

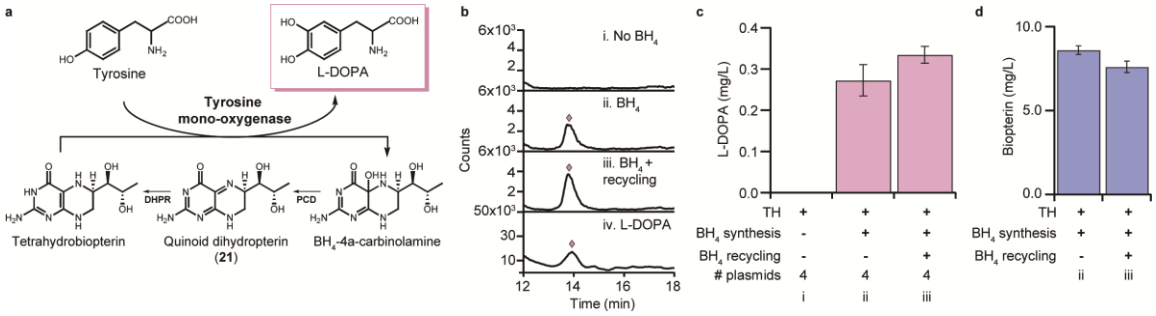

Figure 2.10. Microbial synthesis of L-DOPA via pterin-dependent tyrosine mono-oxidation. (a) Schematic representation of the BH_4 recycling pathway. (b) Representative LC/MS traces for various L-DOPA production strains (extracted ion chromatograms for L-DOPA = *m/z* 198). Traces represent strains expressing (i) only tyrosine hydroxylase (TH), (ii) TH and the BH_4 synthesis pathway, and (iii) TH, the BH_4 synthesis pathway, and the BH_4 recycling pathway. Trace iv is commercial L-DOPA standard. Full windows of the spectra can be found in Figure 2.11a. (c) Production levels of L-DOPA from galactose in the presence (+) or absence (−) of the BH_4 synthesis pathway and/or BH_4 recycling pathway. (d) Production levels of biopterin from galactose in the presence (+) or absence (−) of the BH_4 recycling pathway. All experiments were run in triplicate and shown are the means and standard deviations. Strains carried four multi-copy plasmids in which each gene was expressed from galactose inducible promoters (P_{GAL1} or P_{GAL10}). PCD, pterin-4a-carbinolamine dehydratase; DHPR, dihydropteridine reductase.

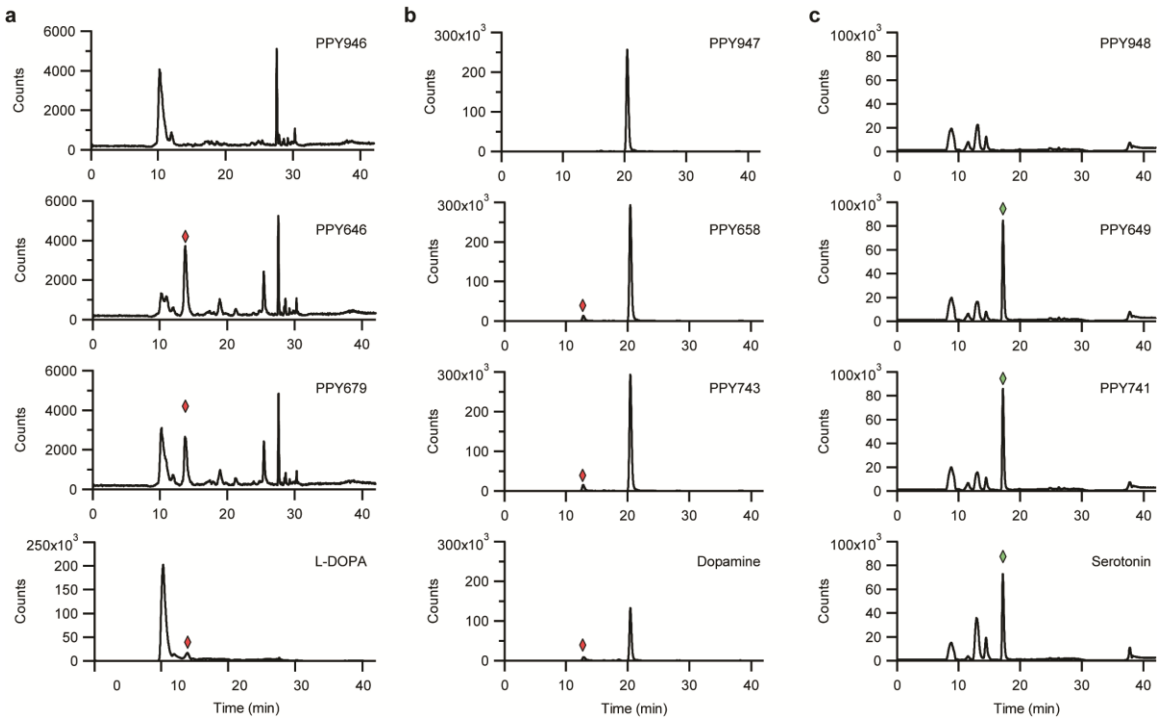

Figure 2.11. Full windows of LC/MS traces in Figure 2.10b, Figure 2.13b, Figure 2.13f. L-DOPA, dopamine and serotonin highlighted with a pink (L-DOPA, dopamine) or green diamond (serotonin). (a) L-DOPA (13.8 min), (b) dopamine (12.8 min), and (c) serotonin (17.2 min).

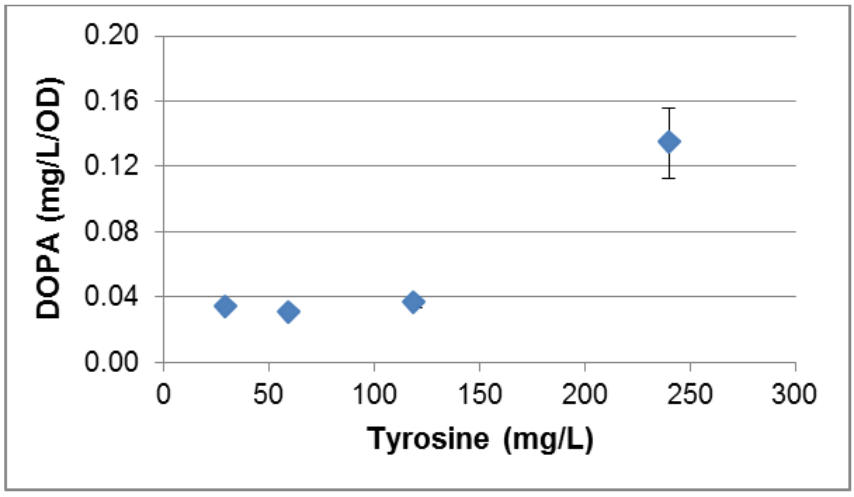

Figure 2.12. Effect of tyrosine on L-DOPA production. In our experiments, 30 mg/L of tyrosine is present when producing L-DOPA or dopamine.

2.3.5 Microbial Synthesis of Biogenic Amines via Pterin-dependent Mono-oxidation

Biogenic amines are the immediate precursors to both MIAs and BIAs.(5) To microbially synthesize the BIA biogenic amine precursor dopamine from galactose, we engineered a yeast strain carrying the BH_4 biosynthetic and recycling pathways, tyrosine mono-oxygenase, and the codon optimized *Sus scrofa* aromatic L-amino-acid decarboxylase (DDC) (Figure 2.13a). This strain produced dopamine at 1.52 mg/L, while no dopamine was produced in the absence of the BH_4 biosynthetic and recycling pathways (Figure 2.13b,c, Figure 2.11b). To microbially synthesize the MIA biogenic amine serotonin from galactose, we engineered a yeast strain carrying the BH_4 biosynthetic and recycling pathways, a truncated codon optimized *H. sapiens* tryptophan hydroxylase[59], and DDC (Figure 2.13e). This strain produced serotonin at 5.72 mg/L, while no serotonin was produced in the absence of the BH_4 synthesis and recycling pathways (Figure 2.13f,g, Figure 2.11c). In the presence of the amino acid mono-oxygenase, DDC, and the BH_4 biosynthetic pathway, but in the absence of the BH_4 recycling pathway, dopamine was produced at 1.73 mg/L, while serotonin was produced at 5.18 mg/L (Figure 2.13c,g). As with the production of L-DOPA, the BH_4 recycling pathway had no statistically significant effect on biogenic amine production. The dopamine- and serotonin-producing strains had similar levels of biopterin with and without the BH_4 recycling pathway (Figure 2.13d,h). To determine if tryptophan was limiting serotonin production, we supplemented the media with tryptophan. Indeed, increasing extracellular tryptophan levels increased serotonin production (Figure 2.14). Thus, improving yeast tryptophan biosynthesis should increase serotonin levels.

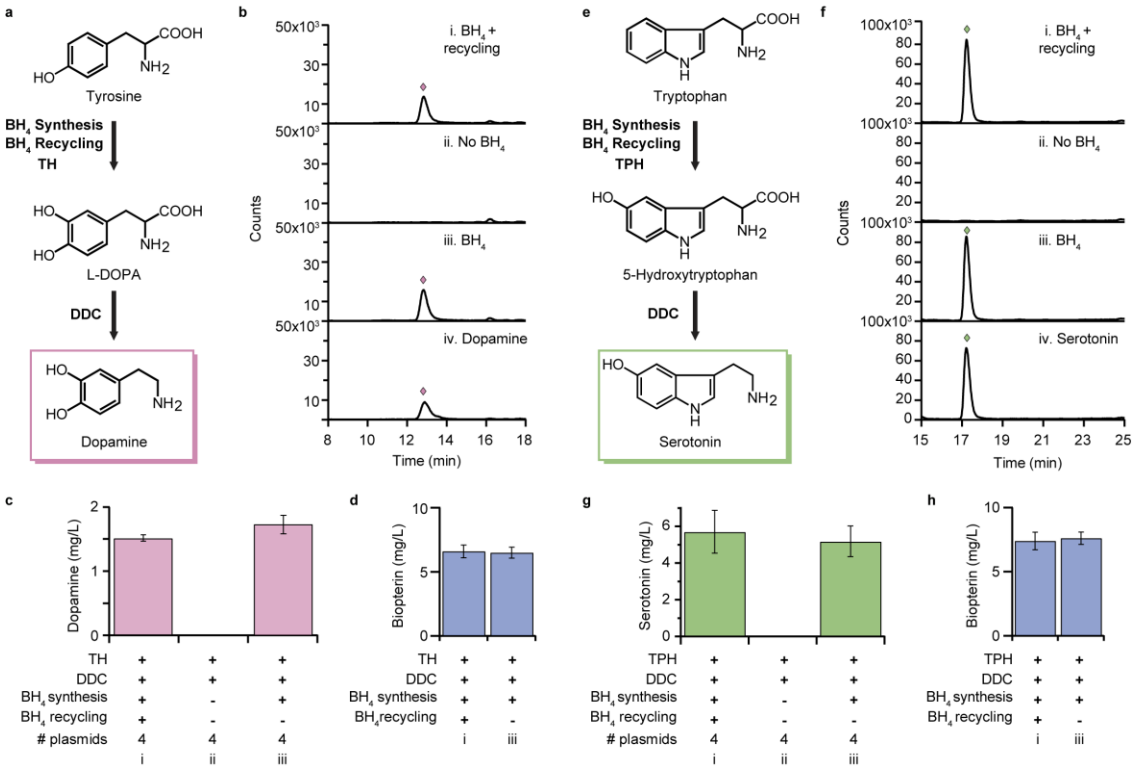

Figure 2.13. Microbial synthesis of biogenic amines via pterin-dependent mono-oxidation. (a) Schematic representation of dopamine biosynthesis. (b) Representative LC/MS traces for various production strains (extracted ion chromatograms (EIC) for dopamine = *m*/*z* 154). Traces represent strains expressing (i) tyrosine hydroxylase (TH), aromatic-l-amino-acid decarboxylase (DDC), the BH_4 synthesis pathway, and the BH_4 recycling pathway, (ii) TH and DDC, and (iii) TH, DDC, and the BH_4 synthesis pathway. Trace iv is commercial dopamine standard. Full windows of the spectra can be found in Figure 2.11b. (c) Production levels of dopamine in the presence (+) or absence (−) of the BH_4 synthesis pathway, and/or the BH_4 recycling pathway. (d) Production levels of biopterin in the presence (+) or absence (−) of the BH_4 recycling pathway. (e) Schematic representation of serotonin biosynthesis. (f) Representative LC traces for various production strains (EIC for serotonin = *m*/*z* 177). Traces represent strains expressing (i) tryptophan hydroxylase (TPH), DDC, the BH_4 synthesis pathway, and the BH_4 recycling pathway, (ii) TPH and DDC, and (iii) TPH, DDC, and the BH_4 synthesis pathway. Trace iv is commercial serotonin standard. Full windows of the spectra can be found in Figure 2.11c. (g) Production levels of serotonin in the presence (+) or absence (−) of the BH_4synthesis pathway and/or BH_4 recycling pathway. (h) Production levels of biopterin in the presence (+) or absence (−) of the BH_4 recycling pathway. All experiments were run in triplicate and shown are the means and standard deviations. Strains carried four multi-copy plasmids in which each gene was expressed from galactose inducible promoters (P_{GAL1} or P_{GAL10}).

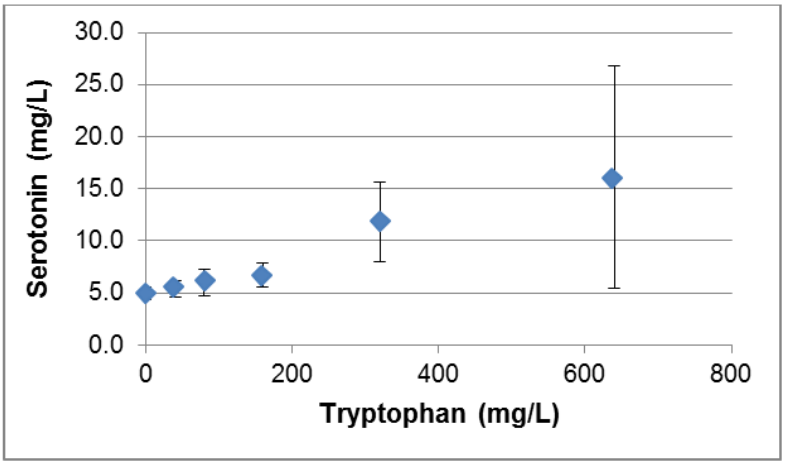

Figure 2.14. Effect of tryptophan on serotonin production. In our experiments, tryptophan is not supplemented when producing serotonin or hydroxystrictosidine.

2.3.6 Microbial Synthesis of the Modified MIA 10-Hydroxystrictosidine

Although several microbial strains have been engineered for the production of BIAs[19-25], engineering of MIA microbial platforms has lagged behind[60]. Further, to our knowledge no modified alkaloid has been produced microbially to date. Microbial synthesis of modified alkaloids has the potential to generate more amenable intermediates for chemical derivatization to obtain final therapeutics. Therefore, we focused our pterin-dependent biogenic amine-producing strain toward the production of the modified MIA hydroxystrictosidine. To microbially synthesize hydroxystrictosidine from galactose and secologanin, we used the serotonin-producing strain, carrying the BH_4 recycling pathway and expressing the *Ophiorrhiza pumila* strictosidine synthase[61] with the vacuolar tag removed so as to avoid enzyme secretion[62] (Figure 2.15a). The strain produced both *R*- and *S*-hydroxystrictosidine isomers. (Figure 2.15b, Figure 2.16). Given that hydroxystrictosidine is not commercially available, we characterized the compounds using tandem mass spectrometry and high resolution mass spectrometry (Figure 2.15c,d,

Figure 2.17). To improve upon the inducible four-plasmid system, which has drawbacks in terms of carbon source, plasmid burden, stability, and the reuse of promoters, we engineered a three-plasmid system using multi-copy plasmids with the enzymes under control of constitutive promoters. The four- and three-plasmid systems produced similar levels of hydroxystrictosidine (Figure 2.15e,Table 2-1). Interested in whether the BH_4 recycling pathway had an effect on hydroxystrictosidine levels, we removed the recycling pathway in both the four- and three-plasmid systems and saw that the BH_4 recycling pathway had no significant impact on hydroxystrictosidine production. Given this observation, we engineered a two-plasmid system without the BH_4 recycling pathway; however, this system also failed to improve hydroxystrictosidine production. Interestingly, all the hydroxystrictosidine-producing yeast strains resulted in a mixture of *R*- and *S*-hydroxystrictosidine isomers even though previous *in vitro* work feeding tryptamine and secologanin to strictosidine synthase at pH = 7 resulted in the stereoselective synthesis of *S*-strictosidine[61]. Removing strictosidine synthase from the hydroxystrictosidine-producing strain resulted in similar *R*- and *S*-hydroxystrictosidine levels (Figure 2.18). This indicated that, at the low pH of the yeast medium (pH = 5–3), secologanin and serotonin were coupling chemically rather than enzymatically to produce a mixture of hydroxystrictosidine isomers[63]. Indeed, strictosidine synthase retains less than one tenth of its activity at pH = 4–3[64] and has 3 orders of magnitude less catalytic activity with serotonin when compared to tryptamine[65].

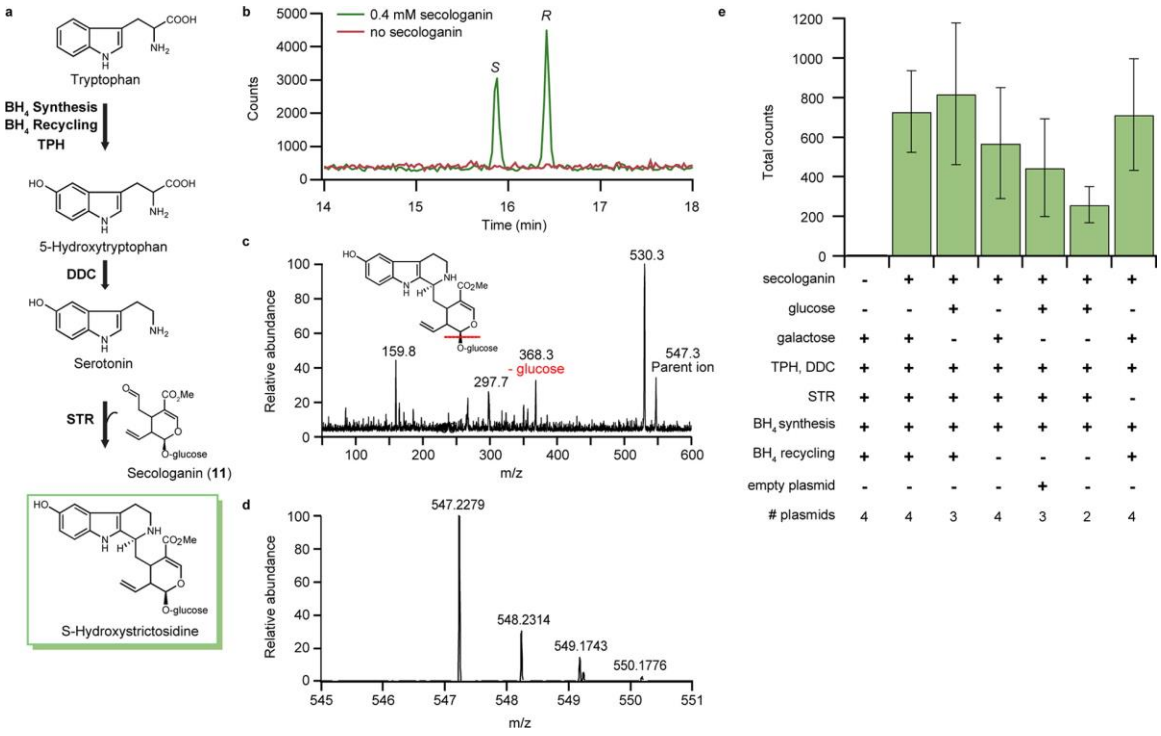

Figure 2.15. Microbial synthesis of the modified MIA 10-hydroxystrictosidine. (a) Schematic of hydroxystrictosidine biosynthesis. (b) Representative LC/MS trace (multiple reaction monitoring hydroxystrictosidine 547.60 → 530.00 transition) for the yeast strain (PPY650) carrying tryptophan hydroxylase, aromatic-L-amino-acid decarboxylase, strictosidine synthase, and the BH_4 biosynthesis and recycling pathways in the presence or absence of 0.4 mM secologanin. S = (*S*)-hydroxystrictosidine; R = (*R*)-hydroxystrictosidine. Full window of the spectra can be found in Figure 2.16. (c) Tandem mass spectrum of microbially synthesized *S*-hydroxystrictosidine. (d) High-resolution mass spectrum of microbially produced *S*-hydroxystrictosidine. (e) (*S*) and (*R*)-hydroxystrictosidine production in *S. cerevisiae*. DDC, aromatic-l-amino-acid decarboxylase; TPH, tryptophan hydroxylase; STR, strictosidine synthase.

Table 2-1. Overview of alkaloid and precursor production.

Strain	BH_4 Synthesis Pathway	BH_4 Recycling Pathway	Alkaloid Synthesis Patway	# Plasmids	Substrate(s)	Product	Production
PPY946			TH	4	Galactose	L-DOPA	nd
PPY646	GTPCH PTPS SR	PCD DHPR	TH	4	Galactose	L-DOPA	0.33 ± 0.02 mg/L
PPY679	GTPCH PTPS SR		TH	4	Galactose	L-DOPA	0.27 ± 0.04 mg/L
PPY947			TH DDC	4	Galactose	Dopamine	nd
PPY658	GTPCH PTPS SR	PCD DHPR	TH DDC	4	Galactose	Dopamine	1.52 ± 0.05 mg/L
PPY743	GTPCH PTPS SR		TH DDC	4	Galactose	Dopamine	1.73 ± 0.14 mg/L
PPY948			TPH DDC	4	Galactose	Serotonin	nd
PPY649	GTPCH PTPS SR	PCD DHPR	TPH DDC	4	Galactose	Serotonin	5.72 ± 1.18 mg/L
PPY741	GTPCH PTPS SR		TPH DDC	4	Galactose	Serotonin	5.18 ± 0.84 mg/L
PPY650	GTPCH PTPS SR	PCD DHPR	TPH DDC STR	4	Galactose Secologanin	Hydroxystrictosidine	728.8 ± 206.2 counts
PPY955	GTPCH PTPS SR		TPH DDC STR	4	Galactose Secologanin	Hydroxystrictosidine	570.6 ± 280.6 counts
PPY744	GTPCH PTPS SR	PCD DHPR	TPH DDC STR	3	Glucose Secologanin	Hydroxystrictosidine	819.4 ± 357.3 counts
PPY748	GTPCH PTPS SR		TPH DDC STR	3	Glucose Secologanin	Hydroxystrictosidine	444.7 ± 246.5 counts
PPY740	GTPCH PTPS SR		TPH DDC STR	2	Glucose Secologanin	Hydroxystrictosidine	258.7 ± 91.3 counts
PPY649	GTPCH PTPS SR	PCD DHPR	TPH DDC	4	Galactose Secologanin	Hydroxystrictosidine	713.9 ± 281.9 counts

Arrows represent presence of the enzyme. nd = not detectable. Amount produced is represented by the mean ± standard deviation for samples run in triplicate. GTPCH: GTP cyclohydrolase; PTPS: pyruvoyl tetrahydropterin synthase; SR: sepiapterin reductase; PCD: pterin-4a-carbinolamine dehydratase; DHPR: dihydropteridine reductase; TPH: tryptophan hydroxylase; TH: tyrosine hydroxylase; DDC: aromatic-L-amino-acid decarboxylase; STR: strictosidine synthase.

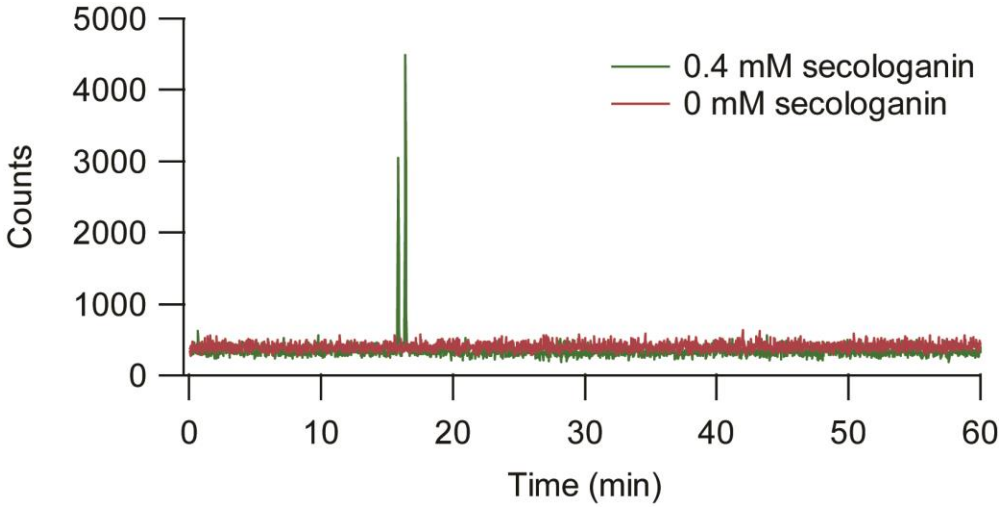

Figure 2.16. Full window of multiple reaction monitoring for Figure 2.15b. Shown hydroxystrictosidine transition: 547.60 → 530.00 transition.

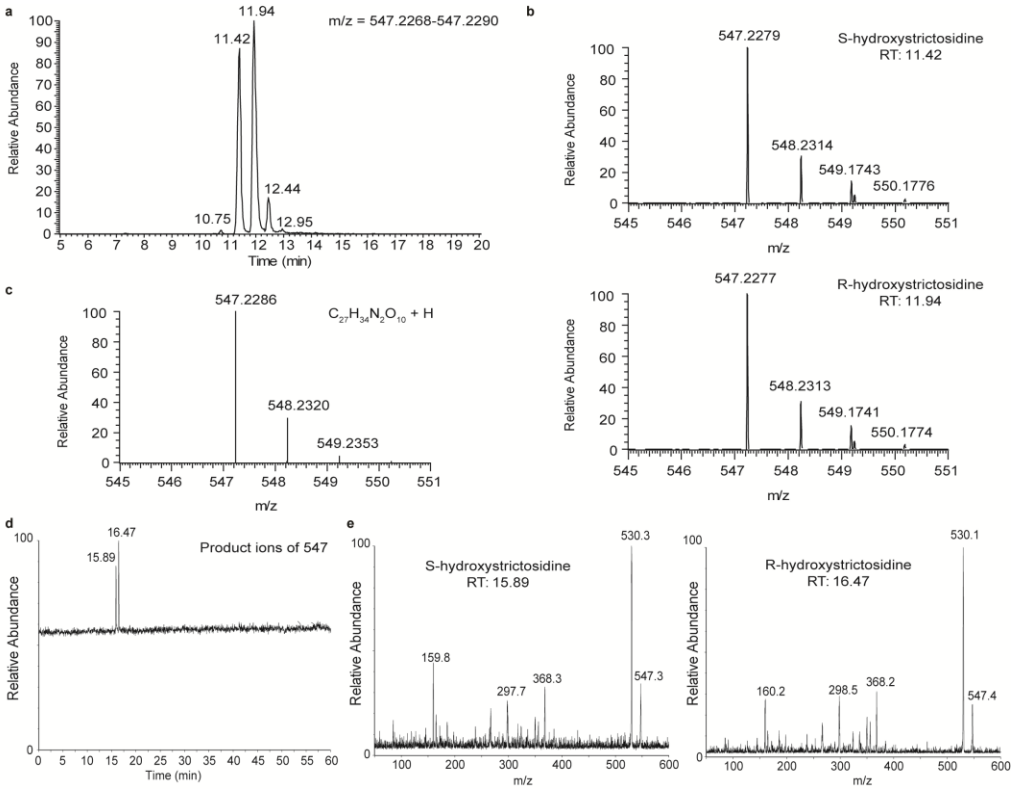

Figure 2.17. Mass spectral characterization of hydroxystrictosidine isomers. (a) LC trace (extracted ion chromatogram corresponding to hydroxystrictosidine, *m/z* 547, extracted from full scan data) from high resolution mass spectrometry analysis. (b) High-resolution mass spectrum of microbially-produced *S*-hydroxystrictosidine and *R*-hydroxystrictosidine. (c) Theoretical high-resolution mass spectrum of hydroxystrictosidine. (d) LC trace for product ions of *m/z* 547 from tandem mass spectrometry analysis. (e) Tandem mass spectra of microbially-produced *S*-hydroxystrictosidine and *R*-hydroxystrictosidine.

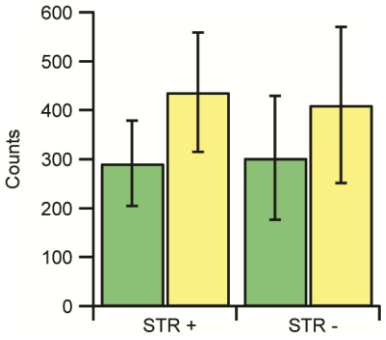

Figure 2.18. Isomer ratios produced in the presence (STR +, PPY650) or absence (STR -, PPY649) of strictosidine synthase using yeast synthetic media (pH=5-3). Green: *S*-hydroxystrictosidine; Yellow: *R*-hydroxystrictosidine.

2.3.7 Determining Strictosidine Synthase Functionality

To determine if strictosidine synthase was functionally expressed in the hydroxystrictosidine-producing yeast strain, we examined the level of spontaneous and enzymatic hydroxystrictosidine synthesis under different conditions. First, we confirmed that spontaneous condensation of serotonin and secologanin does not occur at pH = 7, but does at pH = 3, producing both hydroxystrictosidine isomers (Figure 2.19a, Figure 2.20a), explaining why *in vitro* strictosidine synthase studies at pH = 7 do not exhibit spontaneous condensation and produce only the *S*-isomer. Next, we tested hydroxystrictosidine formation using the lysate of yeast cells expressing strictosidine synthase. When the lysate was placed at pH = 3 and fed serotonin and secologanin, both hydroxystrictosidine isomers were formed, while the same experiment at pH = 7 resulted in only the *S*-isomer (Figure 2.19b, Figure 2.20b), demonstrating that strictosidine synthase is functionally expressed in yeast. Isomer identification was determined due to the fact that strictosidine synthase is known to form only the *S*-isomer[61] while the spontaneous chemical condensation produces both *R*- and *S*-isomers, with the *R*-isomer being the major product[63]. Next, we used intact yeast cells expressing strictosidine synthase, fed serotonin and secologanin, and cultured the cells for 136 h using standard (pH = 4–2.5, Figure 2.21) or buffered (pH = 7–5, Figure 2.21) synthetic complete media. Yeast cells in the buffered media resulted in the synthesis of only *S*-hydroxystrictosidine (Figure 2.19c, Figure 2.20c). Finally, we showed that strictosidine synthase is necessary for *S*-hydroxystrictosidine production in yeast and that the reaction was not catalyzed by an endogenous yeast enzyme (Figure 2.19d, Figure 2.20d, Figure 2.22). These results demonstrate that strictosidine synthase is functionally expressed in the

hydroxystrictosidine-producing yeast strain, that the enzymatic reaction leading to the *S*-isomer is taking place intracellularly, and that secologanin is crossing the yeast cell membrane. In standard yeast synthetic complete media, however, the spontaneous coupling of serotonin and secologanin is the predominant hydroxystrictosidine forming reaction.

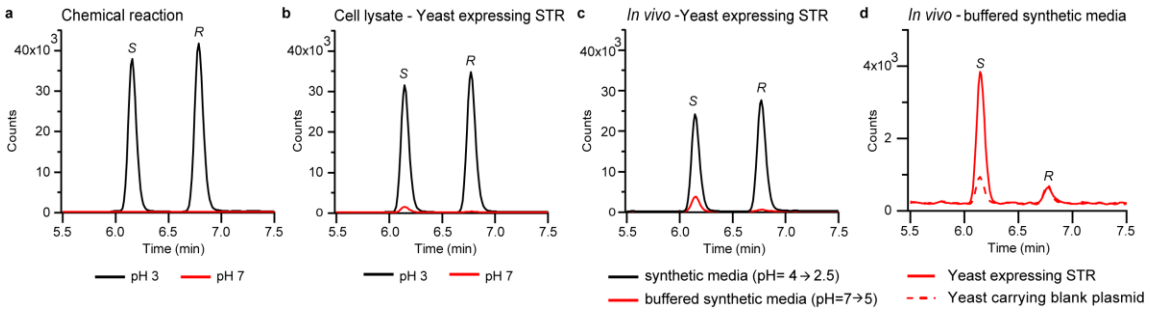

Figure 2.19. Analysis of the 10-hydroxystrictosidine isomer ratio. All reactions contain 0.4 mM each of secologanin and serotonin. LC traces (extracted ion chromatograms for hydroxystrictosidine = *m/z* 547) for (a) the chemical reaction in phosphate buffer at pH = 3 (black) or pH = 7 (red); (b) the reaction in cell lysate of yeast expressing strictosidine synthase (PPY827) adjusted to pH = 3 (black) or pH = 7 (red); (c) *in vivo* reaction using intact yeast cells expressing strictosidine synthase (PPY827) in standard yeast media (black) or pH = 7 buffered media (red); and (d) *in vivo* reaction using intact yeast cells expressing either strictosidine synthase (PPY827, solid red line) or yeast expressing a blank plasmid (PPY828, dotted red line) in pH = 7 buffered media. Full windows of the spectra can be found in Figure 2.20. Multiple reaction monitoring of panel d can be found in Figure 2.22. STR, strictosidine synthase.

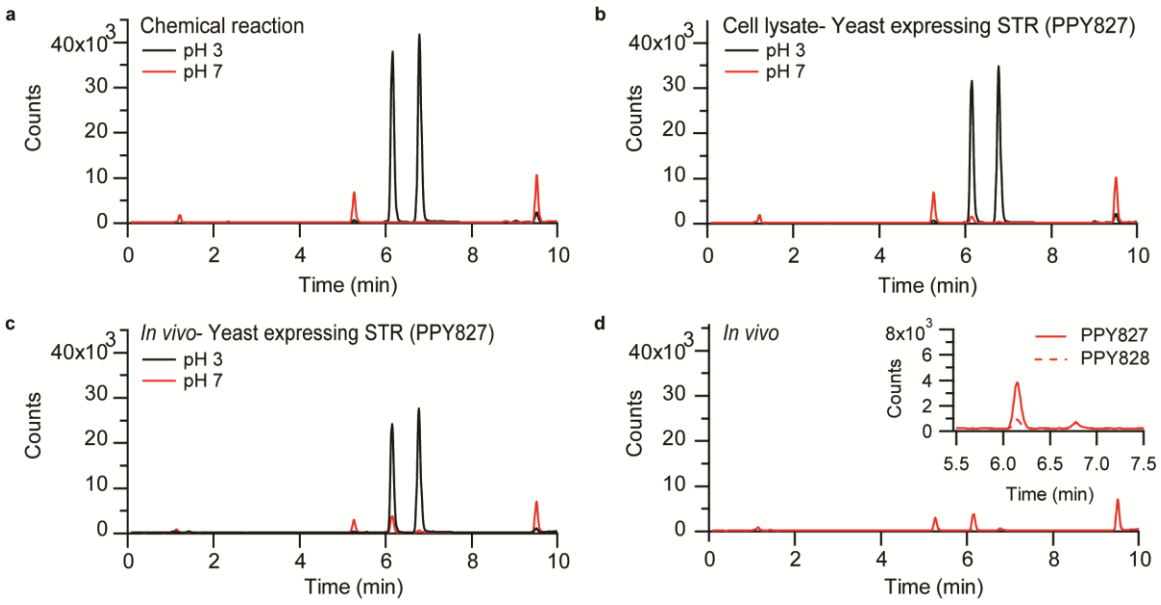

Figure 2.20. Full windows of LC/MS traces in Figure 2.19 (extracted ion chromatograms for hydroxystrictosidine, *m/z* 547). *S*-hydroxystrictosidine, rt=6.1 min. *R*-hydroxystrictosidine, rt=6.8 min. Isomer identification was determined due to the fact that strictosidine synthase is known to form only the *S*-isomer. A single isomer is formed *in vivo* in buffered synthetic media (pH=7 → 5).

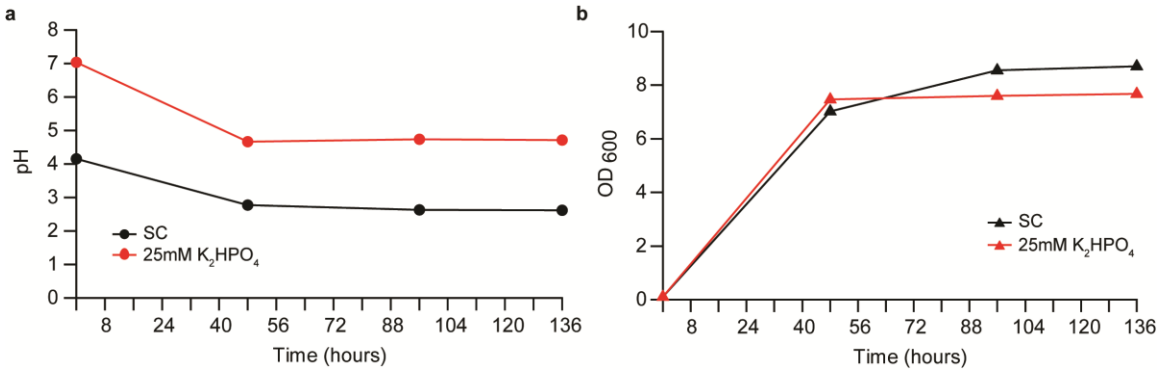

Figure 2.21. pH of media over time. (a) pH of wild-type W303 yeast grown in synthetic complete media (black) or buffered synthetic complete media (25mM K_2HPO_4, red). (b) Cell growth monitored by absorption at OD_{600}.

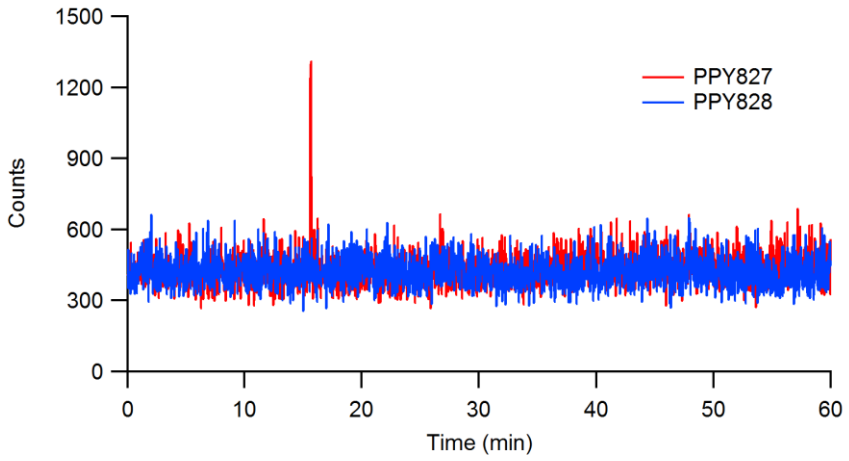

Figure 2.22. Full window for multiple reaction monitoring (MRM) analysis for Figure 2.19d. Only one peak can be found in the MRM spectrum corresponding to the characteristic hydroxystrictosidine transition 547.60 → 530.00. All other peaks in the Figure 2.19d (and Figure 2.20d) LC/MS trace have *m/z* value of 547, but do not have the characteristic hydroxystrictosidine transition 547.60→530.

2.4 Discussion

Together, these results establish the first microbial synthesis of a modified alkaloid, specifically a modified MIA, representing an alkaloid family with important medicinal compounds, including anticancer, antimalarial, and antiarrhythmic agents. We produced hydroxystrictosidine from glucose and secologanin in *S. cerevisiae* by leveraging the pterin-dependent mono-oxidation of tryptophan using microbially produced BH_4 as a cofactor. Pterin-dependent mono-oxidation of tryptophan was necessary as no known natural enzyme oxidizes tryptophan akin to how tyrosinase oxidizes tyrosine, and plant enzymes used to convert tryptophan to serotonin can be promiscuous. We chose *S. cerevisiae* as the microbial host due to its robustness to industrial conditions, which makes this MIA-producing platform attractive for continued use. Further, the presence of compartments in *S. cerevisiae* with unique pH values and metal concentrations can be exploited to express downstream MIA pathway enzymes at the ideal conditions for

maximal enzymatic activity or to prevent byproduct formation. Finally, although in this work we fed secologanin to the microbe, in the future, secologanin can also be biosynthesized from glucose as the nine-step secologanin biosynthetic pathway from geranyldiphosphate is known and has been reconstituted in yeast[60,66].

We were surprised by the non-necessity of the BH_4 recycling pathway for amino acid mono-oxidation and ultimately hydroxystrictosidine production, even though a BH_4 recycling pathway was shown to be necessary for the production of hydroxytyrosol[35] and hydroxytryptophan[31] in *E. coli* when using the cofactor analogue MH_4. In our engineered yeast strain, BH_4 synthesis alone is sufficient to drive robust amino acid mono-oxidation, and aromatic amino acid levels are currently limiting alkaloid production. Using the pterin-dependent mono-oxidation strategy, L-DOPA is produced to 0.33 mg/L, which is comparable to L-DOPA production in yeast using a tyrosinase at ~0.1 mg/L[29]. Interestingly, L-DOPA production was higher (~1 mg/L) in the BH_4-producing strain synthesizing slightly less BH_4 (5.53 mg/L vs 7.81 mg/L) due to a nonfunctional mutation in the *ade2* gene. The resource allocation for the increased BH_4 production may be detrimental to the production of tyrosine, and, thus limiting for L-DOPA. Therefore, matching the levels of the BH_4 cofactor supply to the demand of the amino acid mono-oxygenase should enable further improvement in the yield of amino acid mono-oxidation and, in turn, in BIA or MIA production. Increasing the tyrosine supply and dynamically regulating the BH_4 levels to match the demand of the amino acid mono-oxygenase may enable the production of L-DOPA at the levels achieved in *E. coli*, 293 mg/L[21].

Using standard yeast media, both *R*- and *S*-hydroxystrictosidine isomers are produced; through testing various reaction conditions, we conclude that strictosidine

synthase is functional in our strain, although at the low pH of the yeast media the chemical condensation of serotonin and secologanin prevails. While the enzymes in the MIA pathway are likely to prefer one isomer over the other for further processing, synthesis of both hydroxystrictosidine isomers may not be detrimental to the production of more complex MIAs as later enzymes in MIA pathways, such as strictosidine glucosidase, are able to turn over the *R*-isomer, albeit at lower rates when compared to the *S*-isomer[67,68]. Further, enzymes capable of turning over alkaloid isomer mixtures have also been seen in other alkaloid families, such as BIAs[19]. Alternatively, later enzymes in the MIA pathway may be able to convert only one isomer, as in the case of the berberine bridge enzyme in the BIA pathway[69], thus reducing the concerns of producing a mixture of hydroxystrictosine isomers early on in the pathway.

There are several opportunities and some key challenges to improving the yield of amino acid mono-oxidation and, in turn, MIA production. First, we show that tyrosine and tryptophan levels limit the system; thus, increasing aromatic amino acid supply via introduction of feedback-resistant enzyme mutants in aromatic amino acid metabolism, such as *Aro4*[70], or utilizing a tyrosine overproducing strain[71], should enable straightforward increases in amino acid mono-oxidation. Second, our system does not currently take advantage of the power of the BH_4 recycling system, as biogenic amine levels are similar in the presence and absence of the recycling system. Screening or engineering aromatic amino acid mono-oxidases with increased *in vivo* activity should also increase aromatic amino acid mono-oxidation. Finally, the BH_4 synthesis and recycling pathways could be integrated to reduce plasmid burden, and the MIA pathway enzymes could be colocalized to increase flux through the pathway[72]. The major

challenge with any of these potential approaches to improving the yield of aromatic amino acid mono-oxidation is the low-throughput of the chromatography-based screens required to detect and quantify these compounds, which take close to one hour per sample. Biosensors for key compounds in the pathway, such as hydroxylated amino acids[29], biogenic amines, or, ideally, the terminal MIAs, should enable the faster optimization of this and other metabolic pathways with products that are neither colorimetric nor fluorescent. A general obstacle is that a new biosensor must be engineered for every chemical of interest, and current strategies to rapidly engineer user-specified chemical biosensors are at the proof-of-principal stage[73] or still on the drawing board.

The strains reported in this work could be further optimized for production of (1) BH_4, itself being a treatment for phenylketonuria[74], (2) hydroxytryptophan, serotonin, and serotonin derivatives, key compounds in depression treatment and studies[75-77], (3) DOPA and dopamine, important compounds related to Parkinson's disease[78], and (4) advanced alkaloids, including anticancer agents. The BH_4-producing yeast strain could be used for the synthesis of both MIAs and BIAs, by introducing different amino acid mono-oxygenases. For example, the dopamine-producing strain can be rapidly adapted to produce BIAs by using norcoclaurine synthase and hydroxyphenylacetaldehyde to produce norcoclaurine (**22**). Ultimately, we envision the MIA-producing strain being used in the biosynthesis of modified and non-natural MIAs or as a plant pathway discovery tool to identify unknown steps in MIA biosynthetic pathways. For instance, we can use the hydroxystrictosidine platform to screen cDNA libraries of plant tissues

known to overproduce MIAs to rapidly identify missing steps in MIA biosynthetic pathways to medically important alkaloids.

2.5 Materials and Methods

2.5.1 Reagents

Tetrahydrobiopterin, dihydrobiopterin, and biopterin were purchased from Cayman Chemical (81880, 81882, and 10007662). Dopamine and vanillin were purchased from Alfa Aesar (A11136 and A11169). L-DOPA and serotonin were purchased from TCI America (D0600 and S0370). Secologanin and tryptophan were purchased from Sigma-Aldrich (50741-5MG-F and T0254). 5-Chlorotryptamine was purchased from Ark Pharm, Inc. (AK-32281).

2.5.2 Construction of W303-Ade2$^+$ Strain

S. cerevisiae W303 were transformed with AME245 and AME246 via an adapted electroporation protocol. Transformed cells were plated and subsequently patched on synthetic complete media with 2% glucose lacking adenine (SD (Ade-)). To confirm the presence of a functional *Ade2*, genomic DNA from multiple patches was isolated, the mutation was amplified by PCR using primers AME128/AME247, and the PCR product sequenced with AME247.

2.5.3 Plasmid Construction

To construct pAME18, 20, 22-26, and 28, genes were amplified from plasmids carrying codon-optimized nucleotide sequences of *M. alpina* GTPCH, *H. sapiens*

GTPCH, *M. alpina* PTPS, *S. salar* PTPS, *S. ruber* PTPS, *P. mikurensis* PTPS, *M. alpina* SR, and *T. pseudonana* SR with primers AME143/AME144, AME141/AME139, AME149/AME150, AME147/AME148, AME151/AME152, AME153/AME154, AME165/AME166, or AME165/AME167, respectively, and cloned into pESC-Leu2 at *Bam*HI/*Hind*III (pAME18, 20), pESC-Trp1 at *Bam*HI/*Sac*II (pAME22-25), or pESC-His3 at *Bam*HI/*Sac*II (pAME26, 28). To construct pAME17, *E. coli* GTPCH was amplified from the *E. coli* DH10B genome with primers AME163/164. The gene product was re-amplified with primers AME135/140 and cloned into pESC-Leu2 at *Bam*HI/*Hind*III. To construct pAME19, *S. cerevisiae* GTPCH was amplified from *S. cerevisiae* W303 genome with primers AME161/162, and re-amplified with primers AME137/142. The gene product was cloned into pESC-Leu2 at *Bam*HI/*Hind*III. To construct pAME27, *S. cerevisiae* SR was amplified from *S. cerevisiae* W303 genome with primers AME168/169, and re-amplified with primers AME180/183. The gene product was cloned into pESC-His3 at *Bam*HI/*Sac*II. To construct pAME3, 29-30, green fluorescent protein (GFP) was amplified from pEGFP with primers AME123/124 and cloned into pESC-Leu2, pESC-Trp1, or pESC-His3, respectively, at *Bam*HI/*Hind*III (Leu2) or *Bam*HI/*Sac*II (Trp1, His3). Constructs were sequence verified using primers AME104 and AME105.

To construct pAME53-55, the region between terminators T_{ADH1} and T_{CYC1} was amplified from pAME26, 22, or 17 using primers AME184/AME185 and cloned into pRS413, pRS414, or pRS415, respectively, at *Bam*HI/*Hind*III. Constructs were sequence verified using primers MH100 and MH101.

To construct pAME22PCD and pAME26DHPR, PCD and DHPR genes were amplified from plasmids carrying the codon optimized genes with primers SS152/SS153 or AME241/AME242, respectively, and cloned into pAME22 or pAME26, respectively, at *Not*I/*Sac*I. Constructs were sequence verified using primers AME229 and AME104.

To construct pSS61, the STR gene was amplified from pSS42 with primers SS159/SS160 and cloned into pESC-Ura3 at *Bam*HI/*Hind*III. To construct pSS66, the DDC gene was amplified from pSS62 with primers SS157/SS158 and cloned into pAME17 at *Not*I/*Sac*I. To construct pSS68, the TH gene was amplified from pSS64 with primers SS179/SS180 and cloned into pESC-Ura3 at *Not*I/*Sac*I. To construct pSS70, the TPH gene was amplified from pSS44 with primers SS207/SS208 and cloned into pESC-Ura3 at *Bam*HI/*Hind*III. To construct pSS71, the TPH gene was amplified from pSS44 with primers SS177/SS178 and cloned into pSS61 at *Not*I/*Sac*I. Constructs were sequence verified using primer SS112. To construct pAME63, the DDC gene was amplified from pSS62 with primers SS157/SS158 and cloned into pESC-Leu2 at *Not*I/*Sac*I. To construct pAME64, the STR gene was amplified from pSS42 with primers SS159/AME406 and cloned into pESC-Ura3 at *Bam*HI/*Hind*III. Constructs were sequence verified using primers AME229/AME230 (pAME63) or AME104/AME105 (pAME64).

To construct pAME56-58, assembly similar to sewing PCR was utilized. Fragments were amplified from template plasmids using primers as follows (fragment-primer/primer/template): SR-AME373/AME374/pAME26; P_{TEF1}_P_{HXT7}-AME365/AME366/pSS102; PTPS-AME363/AME364/pAME22; T_{HXT7}-AME369/AME370/pSS102 P_{ADH1g}-AME371/AME372/pSS43; P_{ADH1ng}-

AME371/AME383/pSS43; GTPCH-AME367/AME368/pAME17; PCD-AME375/AME376/pAME22PCD; DHPR-AME377/AME378/pAME26DHPR; DDC-AME384/AME385/pSS66; TPH-AME386/AME387/pSS70; STR-AME388/AME389/pSS61; vector-AME394/AME395/pAME26DHPR,pAME22PCD,pSS67. After amplification, PCR products were gel purified. To create pAME56-58, fragments were sewn together using primers AME384/AME389 (P_{TEF1}_P_{HXT7}, T_{HXT7}, P_{ADH1g}, DDC, TPH, STR), AME363/AME374 (P_{TEF1}_P_{HXT7}, T_{HXT7}, P_{ADH1g}, GTPCH, PTPS, SR), and AME375/AME383 (P_{TEF1}_P_{HXT7}, T_{HXT7}, PA_{DH1ng}, PCD, DHPR), respectively, using a typical PCR protocol and equimolar amounts of fragments. Resulting products were gel purified and combined with respective vector fragments (from pAME22PCD, pAME26DHPR, pSS67, respectively) via Gibson assembly[79]. Sequencing was obtained using primers AME105/AME229/AME396/AME397/AME369/AME370/AME372.

2.5.4 Yeast Transformation

A modified electroporation method[80] was utilized to transform *S. cerevisiae* W303 or W303-Ade2^{+}. Modifications included no DNA precipitation step and immediately after electroporation, cells were rescued with YPD and left at room temperature overnight before plating on selection media plates.

2.5.5 Microbial Synthesis of Tetrahydrobiopterin

Overnight cultures of strains PPY750, 752–793, and 797–810 in synthetic complete media with 2% glucose lacking histidine, tryptophan, and leucine (SD (HWL^{-})) were used to inoculate 5 mL of synthetic complete media with 2% galactose lacking histidine,

tryptophan, and leucine (SCgal (HWL^-)) to OD_{600} = 0.1 and incubated for 136 h at 30°C (250 rpm). Overnight culture of strain PPY749 in synthetic complete media with 2% glucose lacking histidine (SD (H^-)) was used to inoculate 5 mL of synthetic complete media with 2% galactose lacking histidine (SCgal (H^-)) to OD_{600} = 0.1 and incubated for 136 h at 30°C (250 rpm). Overnight culture of strain PPY751 in synthetic complete media with 2% glucose lacking histidine and tryptophan (SD (HW^-)) was used to inoculate 5 mL of synthetic complete media with 2% galactose lacking histidine and tryptophan (SCgal (HW^-)) to OD_{600} = 0.1 and incubated for 136 h at 30°C (250 rpm). After incubation, cultures were centrifuged for 5 min at 3230 x *g*, the supernatant was filtered, vanillin was added as an internal standard and samples were analyzed via LC/MS. For quantification of biopterin in L-DOPA, dopamine, and serotonin-producing strains, 5-chlorotryptamine was used as an internal standard.

2.5.6 Microbial Synthesis of L-DOPA, Dopamine, Serotonin, and Hydroxystrictosidine

Overnight cultures of strains PPY646, 649–650, 658, 679, 741, 743, 946−948, and 955 in synthetic complete media with 2% glucose lacking histidine, tryptophan, leucine, and uracil (SD ($HWLU^-$)) were used to inoculate 5 mL of synthetic complete media with 2% galactose lacking histidine, tryptophan, leucine, and uracil (SCgal ($HWLU^-$)) to OD_{600} = 0.1. Overnight cultures of strains PPY744 and 748 in SD (HWU^-) were used to inoculate 5 mL of fresh SD (HWU^-) to OD_{600}= 0.1. Overnight culture of strain PPY740 in SD (HW^-) was used to inoculate 5 mL of fresh SD (HW^-) to OD_{600} = 0.1. For hydroxystrictosidine production (strains PPY649, 650, 740, 744, 748, and 955), secologanin (solution in water) was added at the time of inoculation to a final concentration of 0.4 mM (150 mg/L). After inoculation, all strains were incubated for 136

h at 30°C (250 rpm). The cultures were then centrifuged for 5 min at 3230 x *g*, the supernatant was filtered, 5-chlorotryptamine (L-DOPA, dopamine, serotonin) or vanillin (hydroxystrictosidine) was added as an internal standard, and the samples were analyzed via LC/MS.

2.5.7 Biopterin Quantification

LC/MS analysis was completed using an Agilent 1100/1260 series system equipped with a 1260 ALS autosampler and a 6120 Single Quadrupole LC/MS with a Poroshell 120 SB-Aq 3.0 mm × 100 mm × 2.7 μm column and an electrospray ion source. LC conditions: solvent A—150 mM acetic acid with 0.1% formic acid; solvent B—methanol with 0.1% formic acid. Gradient: 4 min ramp from 95%:5%:0.2 (A:B:flow rate in mL/min) to 70%:30%:0.2, 6 min ramp to 40%:60%:0.2, 2 min ramp to 2%:98%:0.2, 2 min ramp to 2%:98%:0.5, 4 min at 2%:98%:0.5, 1 min ramp to 95%:5%:0.5, 7 min at 95%:5%:0.5, and 1.5 min post time. MS acquisition (positive ion mode) included 25% scan from *m*/*z* 100–600, 25% scan from *m*/*z* 230–260, 25% scan from *m*/*z* 145–165, and 25% selected ion monitoring (SIM) for BH_4 (*m*/*z* 242.1), dihydrobiopterin (*m*/*z* 240.1), biopterin (*m*/*z* 238.1), and vanillin (*m*/*z* 153.1). Quantitation was performed by obtaining the area under the peak in the extracted ion chromatogram (EIC) for the desired *m*/*z* value from the SIM signal. For biopterin quantification in L-DOPA-, dopamine-, and serotonin-producing strains, 5-chlorotryptamine (*m*/*z* 195.1) was used as an internal standard instead of vanillin. Area was converted to concentration using standard curves produced from commercially available biopterin. Retention times were determined using commercially available standards.

2.5.8 Quantification of L-DOPA, Dopamine, and Serotonin

LC/MS system and solvent composition was the same as the one used in the analysis of biopterin. LC gradient: 8 min ramp from 95%:5%:0.05 to 70%:30%:0.05, 6 min ramp to 40%:60%:0.05, 1 min ramp to 40%:60%:0.1, 9 min ramp to 2%:98%:0.1, 1 min at 2%:98%:0.1, 5 min ramp to 2%:98%:0.3, 0.1 min ramp to 2%:98%:0.5, 3.9 min at 2%:98%:0.5, 1 min ramp to 95%:5%:0.5, 7 min at 95%:5%:0.5, and 3.5 min post time. MS acquisition (positive ion mode) included 33% scan from *m*/*z* 100–600, 33% scan from *m*/*z* 120–240, and 33% SIM for L-DOPA (*m*/*z* 198.2), dopamine (*m*/*z* 154.2), hydroxytryptophan (*m*/*z* 221.2), serotonin (*m*/*z* 177.2), and 5-chlorotryptamine (*m*/*z* 195.1). Quantitation was performed by obtaining the area under the peak in the EIC for the desired *m*/*z* value from the SIM signal. Area was converted to concentration using standard curves produced from commercially available L-DOPA, dopamine and serotonin dissolved in media taken from a culture of strain PPY810 grown under the same conditions as production samples. Traces used for the L-DOPA standard curve were background subtracted using just media. Retention times were determined using commercially available standards.

2.5.9 Mass Spectral Analysis of Hydroxystrictosidine

High resolution mass spectrometry (HRMS) and tandem mass spectrometry (MS–MS) analysis of hydroxystrictosidine was performed at the Mass Spectrometry Facility at Georgia Tech. MS–MS was done using a Waters Quattro LC mass spectrometer with a Gemini 2 mm × 150 mm × 5 μm C18 column from Phenomenex. LC conditions: solvent A—95%:5% water:acetonitrile; solvent B—5%:95% water:acetonitrile. Gradient: 7 min

at 100%:0% (A:B), 37 min ramp to 0%:100%, 8 min at 0%:100%, 1 min ramp to 100%:0%, and 7 min at 100%:0%. Flow rate was 0.2 mL/min. HRMS was done using a Thermo LTQ Orbitrap XL equipped with a Nano ACQUITY UPLC with a BEH130 300 μm × 100 mm × 1.7 μm C8 column from Waters. Solvent A—10 mM ammonium acetate in water; solvent B—acetonitrile. Gradient: 5 min at 95%:5% (A:B), 40 min ramp to 70%:30%, 5 min at 70%:30%, 2 min ramp to 5%:95%, 3 min at 5%:95%, 1 min ramp to 95%:5%, and 4 min at 95%:5%. Flow rate was 8 μL/min. Multiple Reaction Monitoring (MRM) was done on the Waters Quattro LC mass spectrometer using the same column and LC gradient using solvent A—95%:5%:0.1% water:acetonitrile:formic acid; solvent B—5%:95%:0.1% water:acetonitrile:formic acid. MRM parameters: hydroxystrictosidine: transition 547.60 → 530.00, cone voltage 20 V, collision energy 35 eV; transition 547.60 → 298.00, cone voltage 20 V, collision energy 35 eV. Vanillin: transition 152.80 → 92.80, cone voltage 25 V, collision energy 15 eV; transition 152.80 → 124.80, cone voltage 25 V, collision energy 15 eV. Camptothecin: transition 349.10 → 305.00, cone voltage 45 V, collision energy 35 eV; transition 349.10 → 220.00, cone voltage 45 V, collision energy 40 eV. Reported hydroxystrictosidine counts were obtained using 547.60 → 530.00 transition. Vanillin internal standard transition used 152.80 → 92.80.

2.5.10 Hydroxystrictosidine Isomer Ratios

For the chemical reactions, secologanin and serotonin were mixed to a final concentration of 0.4 mM each in pH = 3 or pH = 7 phosphate buffer (135 mM NaCl, 2.7 mM KCl, 4.3 mM Na_2HPO_4, 1.4 mM KH_2PO_4). Solutions were mixed and incubated for 136 h at 30°C (250 rpm). After incubation, solutions were analyzed using LC/MS. For

lysate experiments, an overnight culture of PPY827 in synthetic complete media with 2% glucose lacking uracil (SD(U^-)) was used to inoculate 5 mL of synthetic complete media with 2% galactose lacking uracil SCgal (U^-) to OD_{600} = 0.1. The culture was incubated for 24 h at 30 °C (250 rpm). After incubation, the culture was centrifuged at 3230 x *g* for 5 min, the supernatant was removed, and the pellet was resuspended in 1.5 mL phosphate buffer. The pellet was lysed by sonication using a Misonix Sonicator 3000 at 5.0 output level for 20 s, 20 s rest, for a total six pulses. The lysate was centrifuged, and supernatant was collected. The pH of the lysate was adjusted to either pH = 3 or pH = 7, and secologanin and serotonin were added to a final concentration of 0.4 mM each. After mixing, the lysates were incubated for 136 h at 30°C (250 rpm), after which the lysates were analyzed using LC/MS. For *in vivo* intact cell experiments, overnight cultures of strains PPY827 and PPY828 in SD (U^-) were used to inoculate 5 mL of SCgal (U^-) or SCgal (U^-) buffered with 25 mM K_2HPO_4 (pH = 7) to OD_{600} = 0.1. Secologanin and serotonin were added to a final concentration of 0.4 mM each and the cultures were incubated for 136 h at 30 °C (250 rpm). After incubation, all cultures were centrifuged for 5 min at 3230 x *g*, and the supernantant was filtered and analyzed via LC/MS. The column compartment was kept constant at 28°C. LC/MS analysis was completed on the Agilent system described above. Gradient: 0.25 min ramp from 95%:5% (A:B) to 70%:30%, 4.75 min ramp to 68%:32%, 2 min ramp to 30%:70%, 1 min at 30%:70%, 0.50 min ramp to 95%:5%, and 5.5 min at 95%:5%. Flow rate was 0.4 mL/min. MS acquisition (positive ion mode) included 30% scan from *m*/*z* 100–600 and 70% SIM for ions related to alkaloid formation (dopamine, *m*/*z* 154; tryptamine, *m*/*z* 161;

serotonin, *m*/*z* 177; tyrosine, *m*/*z* 182; L-DOPA, *m*/*z* 198; tryptophan, *m*/*z* 205; 5-hydroxytryptophan, *m*/*z* 221; strictosidine, *m*/*z* 531; hydroxystrictosidine, *m*/*z* 547).

2.5.11 Statistical Analysis

Two-tailed, paired T-tests were performed in Microsoft Excel.

2.5.12 Yeast Cell Lysis for Intracellular Biopterin Determination

After 136 h of microbial production, cultures were centrifuged at 3230 x *g* for 5 min. The supernatant was removed and filtered with a 0.2 µm filter. The pellet was frozen at -80°C, thawed, washed with 1 mL water, and resuspended in 250 µL water. 250 µL 0.2M NaOH was mixed in and the cells remained at room temperature for 10 minutes. The lysate was centrifuged and filtered. Both supernatant and lysate were analyzed using liquid chromatography/ mass spectrometry (LC/MS).

2.5.13 Determination of SR Open Reading Frame from T. pseudonana

As only a portion of the amino acid sequence is known for the predicted SR from *T. pseudonana*, we searched upstream and downstream of the sequence in the genome to obtain a complete open reading frame.

2.5.14 Determiniation of GTPCH, PTPS, and SR mRNA Levels

Overnight cultures of strain PPY949-950 in synthetic complete media with 2% glucose lacking leucine (SD (L-)) was used to inoculate 5mL of synthetic complete media with 2% galactose lacking leucine (SCgal (L-)) to OD_{600}=0.1 and incubated overnight at 30°C (250 rpm). Overnight cultures of strain PPY951-952 in synthetic complete media

with 2% glucose lacking tryptophan (SD (W-)) was used to inoculate 5mL of synthetic complete media with 2% galactose lacking tryptophan (SCgal (W-)) to OD_{600}=0.1 and incubated overnight at 30°C (250 rpm). Overnight cultures of strain PPY953-954 in synthetic complete media with 2% glucose lacking histidine (SD (H-)) was used to inoculate 5mL of synthetic complete media with 2% galactose lacking histidine (SCgal (H-)) to OD_{600}=0.1 and incubated overnight at 30°C (250 rpm). Total RNA for all cultures was extracted using a RNeasy Mini Kit (Qiagen) following the manufacturer's protocol for isolation from yeast using $3x10^7$ cells per culture. RNA quantity was measured using a NanoDrop Lite. 1 µg of total RNA was taken from each strain and converted into cDNA using QuantiTect® reverse transcription kit (Qiagen) using manufacturer's instructions. Relative expression levels of GFP were quantified using QuantiTect® SYBR Green PCR kit (Qiagen) using manufacturer's instructions for LightCyclers 1.x and 2.0 with 150ng cDNA per reaction. Duplicate reactions were set up for each strain. Quantification was completed using a StepOnePlus Real-time PCR system (Applied Biosystems) with primers AME443/AME444 (GTPCH), AME441/AME442 (PTPS), AME445/AME446 (SR), and ACT-F/ACT-R. Cycling conditions: 15 min activation at 95°C followed by 40 cycles of 15 s 95°C, 15 s 57°C, and 15 s 72°C. ACT1, a gene that encodes actin, was used to normalize the amount of the mRNA for the gene of interest in all samples.

2.5.15 Amino Acid Limiting Experiments

Overnight cultures of strain PPY649 and PPY646 in synthetic media containing 2% glucose and lacking histidine, leucine, uracil, and tryptophan (SD (HWUL-)) was used to inoculate 5mL of synthetic media containing 2% galactose and lacking histidine, leucine,

uracil, and tryptophan (SCgal (HWUL-)) to OD_{600}=0.1. Tryptophan was added to strain PPY649 (final concentrations 0-640 mg/L) and tyrosine was added to strain PPY646 (final concentrations 30-960 mg/L). Cultures were incubated for 136 hours at 30°C (250 rpm). After incubation, cultures were centrifuged for 5 min at 3230 x *g*. Supernatant was removed, filtered and analyzed via LC/MS analysis. 5-chlorotryptamine was used as an internal standard.

2.6 References

1 Schafer, H., and Wink, M. (2009) Medicinally important secondary metabolites in recombinant microorganisms or plants: progress in alkaloid biosynthesis. *Biotechnol. J.* 4, 1684-1703.

2 Minami, H. (2013) Fermentative production of plant benzylisoquinoline alkaloids in microbes. *Biosci. Biotech. Bioch.* 77, 1617-1622.

3 Yang, L. Q., and Stockigt, J. (2010) Trends for diverse production strategies of plant medicinal alkaloids. *Nat. Prod. Rep.* 27, 1469-1479.

4 Hagel, J. M., and Facchini, P. J. (2013) Benzylisoquinoline alkaloid metabolism: a century of discovery and a brave new world. *Plant Cell Physiol.* 54, 647-672.

5 Leonard, E., Runguphan, W., O'Connor, S., and Prather, K. J. (2009) Opportunities in metabolic engineering to facilitate scalable alkaloid production. *Nat. Chem. Biol.* 5, 292-300.

6 Winter, J. M., and Tang, Y. (2012) Synthetic biological approaches to natural product biosynthesis. *Curr. Opin. Biotechnol.* 23, 736-743.

7 Chemler, J. A., and Koffas, M. A. (2008) Metabolic engineering for plant natural product biosynthesis in microbes. *Curr. Opin. Biotechnol.* 19, 597-605.

8 Kuboyama, T., Yokoshima, S., Tokuyama, H., and Fukuyama, T. (2004) Stereocontrolled total synthesis of (+)-vincristine. *Proc. Natl. Acad. Sci. U.S.A.* 101, 11966-11970.

9 Murata, J., Roepke, J., Gordon, H., and De Luca, V. (2008) The leaf epidermome of *Catharanthus roseus* reveals its biochemical specialization. *Plant Cell* 20, 524-542.

10 Sato, F., Hashimoto, T., Hachiya, A., Tamura, K., Choi, K. B., Morishige, T., Fujimoto, H., and Yamada, Y. (2001) Metabolic engineering of plant alkaloid biosynthesis. *Proc. Natl. Acad. Sci. U.S.A.* 98, 367-372.

11 Frick, S., Kramell, R., and Kutchan, T. M. (2007) Metabolic engineering with a morphine biosynthetic P450 in opium poppy surpasses breeding. *Metab. Eng.* 9, 169-176.

12 Allen, R. S., Millgate, A. G., Chitty, J. A., Thisleton, J., Miller, J. A. C., Fist, A. J., Gerlach, W. L., and Larkin, P. J. (2004) RNAi-mediated replacement of morphine with the nonnarcotic alkaloid reticuline in opium poppy. *Nat. Biotechnol.* 22, 1559-1566.

13 Glenn, W. S., Runguphan, W., and O'Connor, S. E. (2013) Recent progress in the metabolic engineering of alkaloids in plant systems. *Curr. Opin. Biotechnol.* 24, 354-365.

14 Runguphan, W., and O'Connor, S. E. (2009) Metabolic reprogramming of periwinkle plant culture. *Nat. Chem. Biol.* 5, 151-153.

15 Runguphan, W., Qu, X. D., and O'connor, S. E. (2010) Integrating carbon-halogen bond formation into medicinal plant metabolism. *Nature* 468, 461-464.

16 Glenn, W. S., Nims, E., and O'Connor, S. E. (2011) Reengineering a tryptophan halogenase to preferentially chlorinate a direct alkaloid precursor. *J. Am. Chem. Soc.* 133, 19346-19349.

17 Harvey, A. L. (2008) Natural products in drug discovery. *Drug Discovery Today* 13, 894-901.

18 Dewick, P. M. *Medicinal natural products: a biosynthetic approach*, 2nd ed.; John Wiley and Sons Ltd.: 2002.

19 Hawkins, K. M., and Smolke, C. D. (2008) Production of benzylisoquinoline alkaloids in *Saccharomyces cerevisiae*. *Nat. Chem. Biol.* 4, 564-573.

20 Minami, H., Kim, J. S., Ikezawa, N., Takemura, T., Katayama, T., Kumagai, H., and Sato, F. (2008) Microbial production of plant benzylisoquinoline alkaloids. *Proc. Natl. Acad. Sci. U.S.A.* 105, 7393-7398.

21 Nakagawa, A., Minami, H., Kim, J. S., Koyanagi, T., Katayama, T., Sato, F., and Kumagai, H. (2011) A bacterial platform for fermentative production of plant alkaloids. *Nat. Commun.* 2, 326.

22 Fossati, E., Ekins, A., Narcross, L., Zhu, Y., Falgueyret, J. P., Beaudoin, G. A. W., Facchini, P. J., and Martin, V. J. J. (2014) Reconstitution of a 10-gene pathway for synthesis of the plant alkaloid dihydrosanguinarine in *Saccharomyces cerevisiae*. *Nat. Commun.* 5, 3283.

23 Thodey, K., Galanie, S., and Smolke, C. D. (2014) A microbial biomanufacturing platform for natural and semisynthetic opioids. *Nat. Chem. Biol.* 10, 837–844

24 Fossati, E., Narcross, L., Ekins, A., Falgueyret, J. P., and Martin, V. J. J. (2015) Synthesis of morphinan alkaloids in *Saccharomyces cerevisiae*. *PloS One* 10, DOI: 10.1371/journal.pone.0124459.

25 Nakagawa, A., Matsuzaki, C., Matsumura, E., Koyanagi, T., Katayama, T., Yamamoto, K., Sato, F., Kumagai, H., and Minami, H. (2014) (*R*, *S*)-Tetrahydropapaveroline production by stepwise fermentation using engineered *Escherichia coli*. *Sci. Rep.* 4, DOI:10.1038/srep06695.

26 Hernandez-Romero, D., Sanchez-Amat, A., and Solano, F. (2006) A tyrosinase with an abnormally high tyrosine hydroxylase/dopa oxidase ratio - Role of the seventh histidine and accessibility to the active site. *FEBS J.* 273, 257-270.

27 Luetke-Eversloh, T., Santos, C. N. S., and Stephanopoulos, G. (2007) Perspectives of biotechnological production of L-tyrosine and its applications. *Appl. Microbiol. Biotechnol.* 77, 751-762.

28 Land, E. J., Ramsden, C. A., and Riley, P. A. (2003) Tyrosinase autoactivation and the chemistry of ortho-quinone amines. *Acc. Chem. Res.* 36, 300-308.

29 DeLoache, W. C., Russ, Z. N., Narcross, L., Gonzales, A. M., Martin, V. J., and Dueber, J. E. (2015) An enzyme-coupled biosensor enables (*S*)-reticuline production in yeast from glucose. *Nat. Chem. Biol.* 11, 465–471.

30 Sun, X., Lin, Y., Yuan, Q., and Yan, Y. (2014) Precursor-directed biosynthesis of 5-hydroxytryptophan using metabolically engineered *E. coli*. *ACS Synth. Biol.* 4, 554-558.

31 Lin, Y. H., Sun, X. X., Yuan, Q. P., and Yan, Y. J. (2014) Engineering bacterial phenylalanine 4-hydroxylase for microbial synthesis of human neurotransmitter precursor 5-hydroxytryptophan. *ACS Synth. Biol.* 3, 497-505.

32 Fitzpatrick, P. F. (1999) Tetrahydropterin-dependent amino acid hydroxylases. *Annu. Rev. Biochem.* 68, 355-381.

33 Werner-Felmayer, G., Golderer, G., and Werner, E. R. (2002) Tetrahydrobiopterin biosynthesis, utilization and pharmacological effects. *Curr. Drug Metab.* 3, 159-173.

34 Yamamoto, K., Kataoka, E., Miyamoto, N., Furukawa, K., Ohsuye, K., and Yabuta, M. (2003) Genetic engineering of *Escherichia coli* for production of tetrahydrobiopterin. *Metab. Eng.* 5, 246-254.

35 Satoh, Y., Tajima, K., Munekata, M., Keasling, J. D., and Lee, T. S. (2012) Engineering of L-tyrosine oxidation in *Escherichia coli* and microbial production of hydroxytyrosol. *Metab. Eng.* 14, 603-610.

36 Leiros, H. K. S., Pey, A. L., Innselset, M., Moe, E., Leiros, I., Steen, I. H., and Martinez, A. (2007) Structure of phenylalanine hydroxylase from *Colwellia psychrerythraea* 34H, a monomeric cold active enzyme with local flexibility around the active site and high overall stability. *J. Biol. Chem.* 282, 21973-21986.

37 Siddiqui, M. S., Thodey, K., Trenchard, I., and Smolke, C. D. (2012) Advancing secondary metabolite biosynthesis in yeast with synthetic biology tools. *FEMS Yeast Res.* 12, 144-170.

38 Chang, M. C. Y., Eachus, R. A., Trieu, W., Ro, D. K., and Keasling, J. D. (2007) Engineering *Escherichia coli* for production of functionalized terpenoids using plant P450s. *Nat. Chem. Biol.* 3, 274-277.

39 Miki, Y., and Asano, Y. (2014) Biosynthetic pathway for the cyanide-free production of phenylacetonitrile in *Escherichia coli* by utilizing plant cytochrome P450 79A2 and bacterial aldoxime dehydratase. *Appl. Environ. Microbiol.* 80, 6828-6836.

40 Barnes, H. J., Arlotto, M. P., and Waterman, M. R. (1991) Expression and enzymatic-activity of recombinant cytochrome-P450 17-alpha-hydroxylase in *Escherichia-coli*. *Proc. Natl. Acad. Sci. U.S.A.* 88, 5597-5601.

41 Hong, K. K., and Nielsen, J. (2012) Metabolic engineering of *Saccharomyces cerevisiae*: a key cell factory platform for future biorefineries. *Cell Mol. Life Sci.* 69, 2671-2690.

42 Peralta-Yahya, P. P., Zhang, F. Z., del Cardayre, S. B., and Keasling, J. D. (2012) Microbial engineering for the production of advanced biofuels. *Nature* 488, 320-328.

43 Da Silva, N. A., and Srikrishnan, S. (2012) Introduction and expression of genes for metabolic engineering applications in *Saccharomyces cerevisiae*. *FEMS Yeast Res.* 12, 197-214.

44 O'Connor, S. E., and Maresh, J. J. (2006) Chemistry and biology of monoterpene indole alkaloid biosynthesis. *Nat. Prod. Rep.* 23, 532-547.

45 Silvestrini, A., Pasqua, G., Botta, B., Monacelli, B., van der Heijden, R., and Verpoorte, R. (2002) Effects of alkaloid precursor feeding on a *Camptotheca acuminata* cell line. *Plant Physiol. Bioch.* 40, 749-753.

46 Friedrich, A., Brase, S., and O'Connor, S. E. (2009) Synthesis of 4-, 5-, 6-, and 7-azidotryptamines. *Tetrahedron Lett.* 50, 75-76.

47 Davis, M. D., Kaufman, S., and Milstien, S. (1988) The auto-oxidation of tetrahydrobiopterin. *Eur. J. Biochem.* 173, 345-351.

48 Thony, B., Auerbach, G., and Blau, N. (2000) Tetrahydrobiopterin biosynthesis, regeneration and functions. *Biochem. J.* 347, 1-16.

49 Wang, H. C., Yang, B., Hao, G. F., Feng, Y., Chen, H. Q., Feng, L., Zhao, J. X., Zhang, H., Chen, Y. Q., Wang, L., and Chen, W. (2011) Biochemical characterization of the tetrahydrobiopterin synthesis pathway in the oleaginous fungus *Mortierella alpina*. *Microbiology.* 157, 3059-3070.

50 Yim, J. J., and Brown, G. M. (1976) Characteristics of guanosine triphosphate cyclohydrolase-I purified from *Escherichia-coli*. *J. Biol. Chem.* 251, 5087-5094.

51 Schoedon, G., Redweik, U., Frank, G., Cotton, R. G. H., and Blau, N. (1992) Allosteric characteristics of GTP cyclohydrolase-I from *Escherichia-coli*. *Eur. J. Biochem.* 210, 561-568.

52 Mancini, R., Saracino, F., Buscemi, G., Fischer, M., Schramek, N., Bracher, A., Bacher, A., Gutlich, M., and Carbone, M. L. A. (1999) Complementation of the *fol2* deletion in *Saccharomyces cerevisiae* by human and *Escherichia coli* genes encoding GTP cyclohydrolase I. *Biochem. Biophys. Res. Commun.* 255, 521-527.

53 Blau, N., and Niederwieser, A. (1986) The application of 8-aminoguanosine triphosphate, a new inhibitor of GTP cyclohydrolase I, to the purification of the enzyme from human liver. *Biochim. Biophys. Acta* 880, 26-31.

54 Hasler, T., and Curtius, H. C. (1989) Purification and characterization of 6-pyruvoyl tetrahydropterin synthase from salmon liver. *Eur. J. Biochem.* 180, 205-211.

55 Burgisser, D. M., Thony, B., Redweik, U., Hess, D., Heizmann, C. W., Huber, R., and Nar, H. (1995) 6-Pyruvoyl tetrahydropterin synthase, an enzyme with a novel type of active-site involving both zinc-binding and an intersubunit catalytic triad motif - site-directed mutagenesis of the proposed active-center, characterization of the metal-binding site and modeling of substrate-binding. *J. Mol. Biol.* 253, 358-369.

56 Ploom, T., Thony, B., Yim, J., Lee, S., Nar, H., Leimbacher, W., Richardson, J., Huber, R., and Auerbach, G. (1999) Crystallographic and kinetic investigations on the mechanism of 6-pyruvoyl tetrahydropterin synthase. *J. Mol. Biol.* 286, 851-860.

57 Glick, B. R. (1995) Metabolic load and heterologous gene-expression. *Biotechnol. Adv.* 13, 247-261.

58 Jones, K. L., Kim, S. W., and Keasling, J. D. (2000) Low-copy plasmids can perform as well as or better than high-copy plasmids for metabolic engineering of bacteria. *Metab. Eng.* 2, 328-338.

59 Carkaci-Salli, N., Flanagan, J. M., Martz, M. K., Salli, U., Walther, D. J., Bader, M., and Vrana, K. E. (2006) Functional domains of human tryptophan hydroxylase 2 (hTPH2). *J. Biol. Chem.* 281, 28105-28112.

60 Brown, S., Clastre, M., Courdavault, V., and O'Connor, S. E. (2015) *De novo* production of the plant-derived alkaloid strictosidine in yeast. *Proc. Natl. Acad. Sci. U.S.A.* 112, 3205-3210.

61 Bernhardt, P., Usera, A. R., and O'Connor, S. E. (2010) Biocatalytic asymmetric formation of tetrahydro-beta-carbolines. *Tetrahedron Lett.* 51, 4400-4402.

62 Geerlings, A., Redondo, F. J., Contin, A., Memelink, J., van der Heijden, R., and Verpoorte, R. (2001) Biotransformation of tryptamine and secologanin into plant terpenoid indole alkaloids by transgenic yeast. *Appl. Microbiol. Biotechnol.* 56, 420-424.

63 Battersby A.R., Burnett, A. R., and Parsons, P. G. (1969) Alkaloid Biosynthesis Part XV. Partial synthesis and isolation of vincoside and isovincoside - biosynthesis of 3 major classes of indole alkaloids from vincoside. *J. Chem. Soc. C*, 1193-1200.

64 Maresh, J. J., Giddings, L. A., Friedrich, A., Loris, E. A., Panjikar, S., Trout, B. L., Stockigt, J., Peters, B., and O'Connor, S. E. (2008) Strictosidine synthase: mechanism of a Pictet-Spengler catalyzing enzyme. *J. Am. Chem. Soc.* 130, 710-723.

65 McCoy, E., Galan, M. C., and O'Connor, S. E. (2006) Substrate specificity of strictosidine synthase. *Bioorg. Med. Chem. Lett.* 16, 2475-2478.

66 Miettinen, K., Dong, L. M., Navrot, N., Schneider, T., Burlat, V., Pollier, J., Woittiez, L., van der Krol, S., Lugan, R., Ilc, T., Verpoorte, R., Oksman-Caldentey, K. M., Martinoia, E., Bouwmeester, H., Goossens, A., Memelink, J., and Werck-Reichhart, D. (2014) The seco-iridoid pathway from *Catharanthus roseus*. *Nat. Commun.* 5:3606.

67 Yerkes, N., Wu, J. X., McCoy, E., Galan, M. C., Chen, S., and O'Connor, S. E. (2008) Substrate specificity and diastereoselectivity of strictosidine glucosidase, a key enzyme in monoterpene indole alkaloid biosynthesis. *Bioorg. Med. Chem. Lett.* 18, 3095-3098.

68 Bernhardt, P., Yerkes, N., and O'Connor, S. E. (2009) Bypassing stereoselectivity in the early steps of alkaloid biosynthesis. *Org. Biomol. Chem.* 7, 4166-4168.

69 Dittrich, H., and Kutcham, T.M. (1991) Molecular clonin, expression, and induction of berberine bridge enzyme, and enzyme essential to the formation of benzyophenanthridine alkaloids in the response of plants to pathogenic attack. *Proc. Natl. Acad. Sci. U.S.A.* 88, 9969-9973.

70 Luttik, M. A. H., Vuralhan, Z., Suir, E., Braus, G. H., Pronk, J. T., and Daran, J. M. (2008) Alleviation of feedback inhibition in *Saccharomyces cerevisiae* aromatic amino acid biosynthesis: Quantification of metabolic impact. *Metab. Eng.* 10, 141-153.

71 Gold, N. D., Gowen, C. M., Lussier, F. X., Cautha, S. C., Mahadevan, R., and Martin, V. J. (2015) Metabolic engineering of a tyrosine-overproducing yeast platform using targeted metabolomics. *Microb. Cell Fact.* 14, 73.

72 Sarria, S., Wong, B., Martin, H. G., Keasling, J. D., and Peralta-Yahya, P. (2014) Microbial synthesis of pinene. *ACS Synth. Biol.* 3, 466-475.

73 Mukherjee, K., Bhattacharyya, S., and Peralta-Yahya, P. (2015) GPCR-based chemical biosensors for medium-chain fatty acids. *ACS Synth. Biol.* 4, 1261–1269.

74 Belanger-Quintana, A., Burlina, A., Harding, C. O., and Muntau, A. C. (2011) Up to date knowledge on different treatment strategies for phenylketonuria. *Mol. Genet. Metab.* 104, S19-S25.

75 Byerley, W. F., Judd, L. L., Reimherr, F. W., and Grosser, B. I. (1987) 5-Hydroxytryptophan - a review of its antidepressant efficacy and adverse-effects. *J. Clin. Psychopharm.* 7, 127-137.

76 Birdsall, T. C. (1998) 5-Hydroxytryptophan: a clinically-effective serotonin precursor. *Alt. Med. Rev.* 3, 271-280.

77 Bloom, F.; Kupfer, D. *Psychopharmacology, the Fourth Generation of Progress*; Raven Press: 1995; pp 933−944.

78 Connolly, B. S., and Lang, A. E. (2014) Pharmacological treatment of Parkinson Disease a review. *JAMA, J. Am. Med. Assoc.* 311, 1670-1683.

79 Gibson, D.G., Young, L., Chuang, R-Y., Venter, J.C., Hutchison III, C.A. and Smith, H.O. (2009) Enzymatic assembly of DNA molecules up to several hundred kilobases. *Nat. Methods* 6, 343 - 345.

80 Peralta-Yahya, P., Carter, B.T., Lin, H., Tao, H. and Cornish, V.W (2008) High-throughput selection for cellulase catalysts using chemical complementation. *J. Am. Chem. Soc.* 130 (51), 17446–17452.

81 Arnold K., Bordoli L., Kopp J. and Schwede T. (2006) The SWISS-MODEL Workspace: A web-based environment for protein structure homology modelling. *Bioinformatics* 22,195-201.

82 Kiefer F., Arnold K., Künzli M., Bordoli L. and Schwede T. (2009) The SWISS-MODEL Repository and associated resources. *Nucleic Acids Res*. 37, D387-D392.

83 Peitsch, M. C. (1995) Protein modeling by E-mail *Nat. Biotechnol.* 13, 658-660.

84 Kanehisa, M. and Goto, S. (2000) KEGG: Kyoto encyclopedia of genes and genomes. *Nucleic Acids Res.* 28, 27-30.

85 Bernhardt, P., Usera, A. R., and O'Connor, S. E. (2010) Biocatalytic asymmetric formation of tetrahydrobeta-carbolines. *Tetrahedron Lett.* 51, 4400−4402.

CHAPTER 3. Medium-throughput Screen of Microbially Produced Serotonin via a G-Protein-Coupled Receptor-based Sensor

3.1 Abstract

Chemical biosensors, for which chemical detection triggers a fluorescent signal, have the potential to accelerate the screening of noncolorimetric chemicals produced by microbes, enabling the high-throughput engineering of enzymes and metabolic pathways. Here, we engineer a G-protein-coupled receptor (GPCR)-based sensor to detect serotonin produced by a producer microbe in the producer microbe's supernatant. Detecting a chemical in the producer microbe's supernatant is nontrivial because of the number of other metabolites and proteins present that could interfere with sensor performance. We validate the two-cell screening system for medium-throughput applications, opening the door to the rapid engi-neering of microbes for the increased production of serotonin. We focus on serotonin detection as serotonin levels limit the microbial production of hydroxystrictosidine, a modified alkaloid that could accelerate the semisynthesis of camptothecin-derived anticancer pharmaceuticals. This work shows the ease of generating GPCR-based chemical sensors and their ability to detect specific chemicals in

complex aqueous solutions, such as microbial spent medium. In addition, this work sets the stage for the rapid engineering of serotonin-producing microbes.

3.2 Introduction

Detecting and quantifying the levels of noncolorimetric chemicals synthesized by engineered microbes relies on low-throughput chromatography-based technologies (~100 samples per day), such as gas chromatography and liquid chromatography with mass spectrometry (LC/MS). Chemical biosensors that convert a chemical signal into a fluorescent output enable the use of high-throughput screening technologies (up to 10^7 samples per day), such as microtiter plates or fluorescence activated cell sorting (FACS), for chemical detection. Such throughput can fast-track the engineering of microbes for the synthesis of noncolorimetric chemicals to achieve industrially relevant titers, yields, and productivities.

Previously, we engineered the yeast *Saccharomyces cerevisiae* for the production of the modified monoterpene indole alkaloid hydroxystrictosidine, a potential advanced intermediate in the semisynthesis of the anticancer agents irinotecan and topotecan.[1,2] Specifically, the engineered yeast converts simple sugars to serotonin, and strictosidine synthase couples serotonin with exogenously added secologanin to produce hydroxystrictosidine. As secologanin is fed to the engineered strain for the synthesis of hydroxystrictosidine, serotonin becomes the *de facto* rate-limiting substrate in the process. Serotonin is not colorimetric and LC/MS was used for the detection and quantification of this molecule.[1]

Interested in engineering an improved serotonin-producing microbe, we sought to develop a serotonin biosensor to detect serotonin in the spent medium of a serotonin-producing microbe in a medium-throughput fashion (10^3-10^4 samples per day) (Figure 3.1). We prefer to detect serotonin non-invasively in the spent medium of the serotonin producer microbe as this setup allows us to decouple serotonin production from serotonin sensing. Advantages of such a system include (1) the use of the same sensor as serotonin titers increase by simply diluting the spent medium so that the serotonin concentration is in the linear range of the sensor, (2) enabling the use of random, genomewide mutagenesis strategies to engineer the producer microbe without detrimental effects on the sensor function, and (3) the future potential to high-throughput screen producer microbes by encapsulating the producer and sensor cells and using FACS.

Recently, we developed G-protein-coupled receptor (GPCR)-based sensors in yeast by expressing a GPCR known to bind the chemical of interest on the yeast cell surface and coupling it to the yeast mating pathway, resulting in the expression of green fluorescent protein (GFP) upon chemical detection.[3] The proof-of-principle GPCR-based sensor detected decanoic acid using the GPCR OR1G1. We hypothesized that simply swapping OR1G1 with a GPCR known to bind serotonin, keeping the rest of the sensor cell intact, would result in a serotonin sensor. Additionally, previous GPCR-based sensors have not been shown (1) to detect specific analytes in complex medium, such as microbial spent medium, or (2) to have the statistical parameters necessary to be used in medium-throughput screening applications. These challenges need to be addressed prior to using GPCR-based sensors for the rapid engineering of microbes for the production of chemicals, in this particular case serotonin.

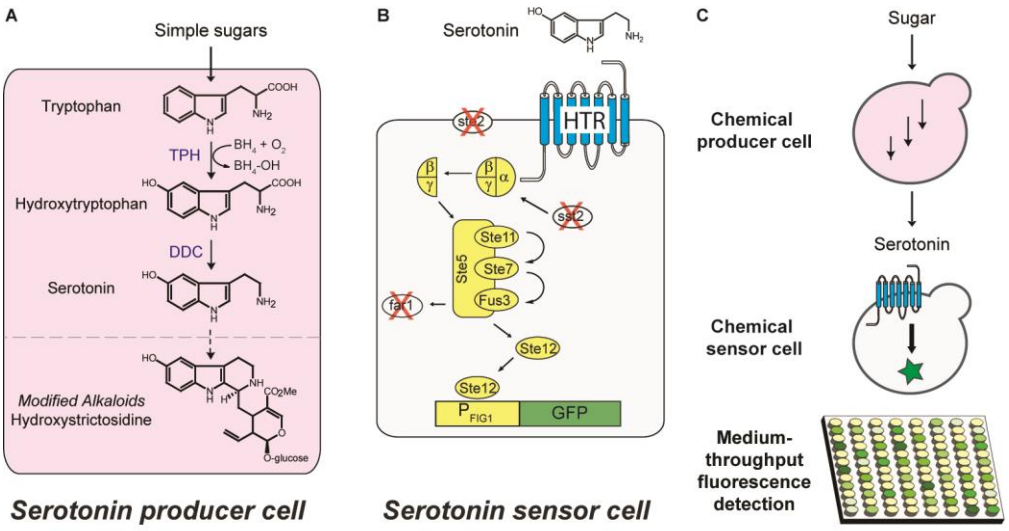

Figure 3.1. Detecting microbially produced serotonin via the G-protein coupled receptor (GPCR)-based serotonin sensor. (A) Engineered yeast produces serotonin from simple sugars.[1] (B) Serotonin sensor. A known human serotonin GPCR (HTR) is expressed in a GPCR-based sensor cell (W303 Δ*ste2*, Δ*far1*, Δ*sst2*).[3] Binding of serotonin to HTR on the cell surface stimulates the yeast mating pathway (yellow), ultimately activating expression of the reporter gene, green fluorescent protein (GFP). (C) The serotonin sensor cell detects serotonin in the spent medium of the serotonin producer cell in a medium-throughput fashion (96-well plates). Abbreviations: TPH, tryptophan hydroxylase; DDC, aromatic amino acid decarboxylase; BH_4, tetrahydrobiopterin; BH_4-OH, pterin 4a-carbinolamine.

Of the 12 serotonin GPCRs expressed in humans,[4] GPCRs 5-HT_{1a} and 5-HT_{1d} have been previously used to generate serotonin sensors in yeast.[5,6] Using a yeast/human Gα subunit chimera (Gpa1/$G_{αi3}$) and the lacZ reporter gene, the 5-HT_{1a}-based sensor had a K_D of 7 μM while the 5-HT_{1d}-based sensor had a K_D of 2 μM; albeit, no dynamic range was reported.[6] The 5-HT_{1a}-based and the 5-HT_{1d}-based sensors showed negligible or no response when using the native yeast Gα subunit, Gpa1.[6] More recently, a 5-HT_{1a}-based sensor using Gpa1 and GFP as the reporter gene resulted in a 1.25-fold increase in the intensity of the signal after activation with serotonin and a K_D of ~50 μM.[5] Swapping Gpa1 for Gpa1/$G_{αi3}$ and GFP for ZsGreen resulted in a sensor with a ~4-fold increase in the intensity of signal after activation with serotonin and a K_D of ~20 μM[5]. Given that our

previously engineered serotonin-producing strain yielded 5 mg of serotonin/L, we needed a sensor with a K_D of ~28 μM and with a significant increase in the intensity of signal after activation.

Here, we engineer a GPCR-based serotonin sensor that can detect serotonin in microbial spent medium. We demonstrate that, after medium optimization, the sensor can be used in 96-well plate format with reliable statistical parameters that set the stage for the sensor to be used in the evolution of an improved serotonin-producing microbe. The optimization of the spent medium and 96-well plate sensor validation workflow presented in this work are likely to mirror optimizations that would be needed to adapt other GPCR-based sensors for the detection of microbially produced chemicals in the spent medium in a medium throughput fashion.

3.3 Results

3.3.1 Serotonin Sensor

Previously, we engineered a GPCR-based sensor strain (W303 *Δfar1*, *Δsst2*, *Δste2*, pRS415-P_{Fig1}-GFP) that relies on Gpa1 to transmit the signal from a GPCR on the cell surface to the yeast mating pathway, which ultimately activates expression of a reporter gene. Using this sensor strain, we screened six known human serotonin GPCRs: 5-HT_{1a}, 5-HT_{1d}, 5-HT_{2b}, 5-HT_4, 5-HT_{5a}, and 5-HT_6. GPCR 5-HT_4 has at least 11 known isoforms, and all but one vary at the C-terminus,[7] which is where the GPCR interacts with the Gα subunit. We tested 5-HT_4 isoform b, the canonical isoform. GPCR 5-HT_6 has two isoforms; however, only one is functional,[8] and we tested the functional isoform. All other serotonin GPCRs tested only have one isoform.[8] Without any changes to the

original sensor strain, expression of 5-HT_4 isoform b in the sensor strain resulted in a ~3-fold increase in the intensity of the signal after activation upon exogenous addition of 100 mg/L serotonin (Figure 3.2A). The 5-HT_4 GPCR is found in both the nervous system and the gut,[4] where 90% of the body's serotonin is found.[9] No response was seen upon expression of the reporter gene in the sensor strain in the absence of 5-HT_4, confirming that 5-HT_4 is needed for serotonin detection (Figure 3.3). No response was seen upon expression of 5-HT_4 in the sensor strain in the absence of the reporter gene, confirming that serotonin was not increasing the cell autofluorescence levels (Figure 3.3). A dose-response curve of the 5-HT_4-based serotonin sensor showed a K_D of 8.1 mg/L (46 μM) with a linear range of 0.7-10 mg/L and a maximum 2.7-fold increase in the intensity of the signal after activation (Figure 3.2B; Figure 3.4). As the titers of microbially produced serotonin (~5 mg/L) land in the middle of the linear range of the serotonin sensor, no further engineering of the linear range was required. To increase the dynamic range of the 5-HT_4–based sensor, we swapped GFP for ZsGreen. In our plasmid-based reporter system, ZsGreen showed greater colony-to-colony variability in the increase in the intensity of the signal after serotonin activation (from 6.5- to 20-fold) than GFP did (from 2- to 3-fold) (Figure 3.5). To make a more reliable sensor and reduce the number of false positives in our medium-throughput screen, we kept GFP as the reporter gene.

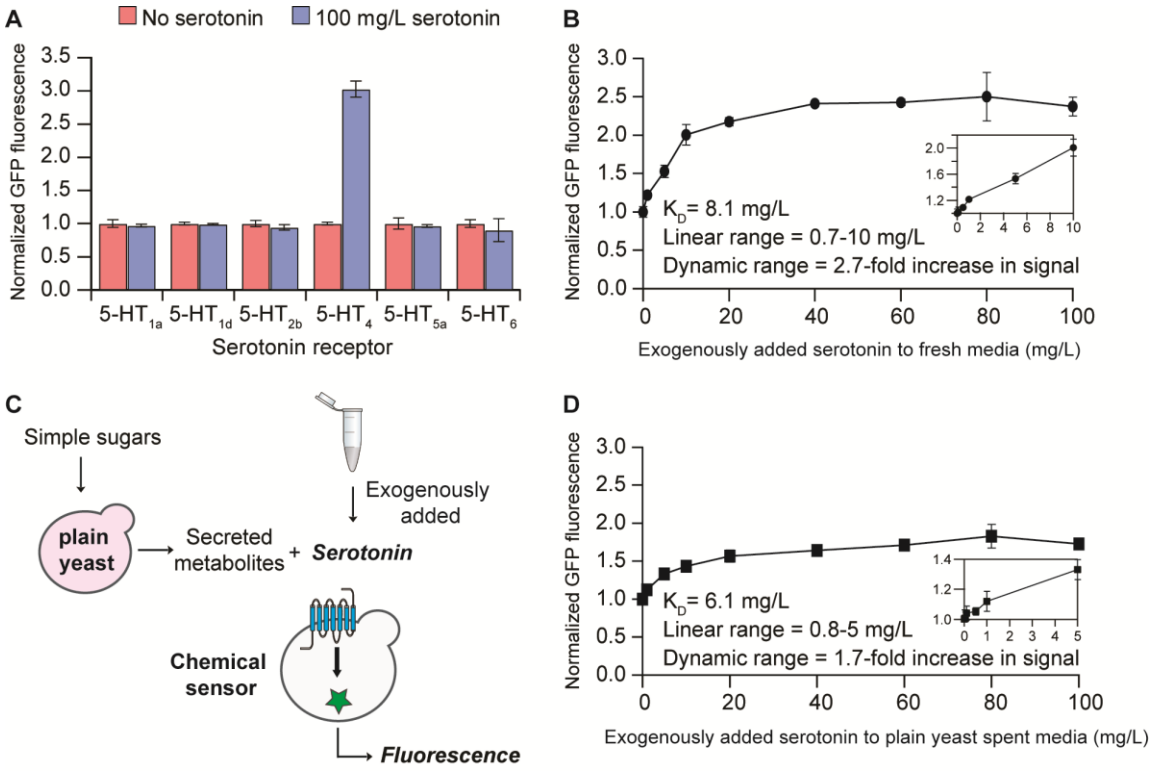

Figure 3.2. Serotonin sensor engineering. (A) Screening of serotonin GPCRs in the GPCR-based sensor strain for response to serotonin in fresh medium. (B) 5-HT_4-based serotonin sensor dose-response curve in fresh medium with exogenously added serotonin. (C) Detection of serotonin exogenously added to plain yeast spent medium. The plain yeast cell carries four blank plasmids instead of the serotonin pathway. (D) 5-HT_4-based serotonin sensor dose-response curve in plain yeast spent medium with exogenously added serotonin. All experiments were performed in triplicate, and the error bars represent the standard deviation from the mean. In all cases, the fluorescence was normalized to the sensor response in the absence of serotonin. Insets show the linear range of the response.

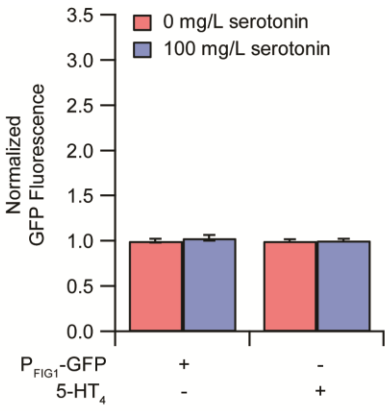

Figure 3.3. Serotonin sensor controls. Response to serotonin in cells expressing either reporter construct (P_{FIG1}-GFP) and not 5-HT_4 or 5-HT_4 and not P_{FIG1}-GFP. Experiments were carried out in triplicate and the error bars represent the standard deviation from the mean. Fluorescence was normalized to the response of the sensor to 0 mg/L serotonin.

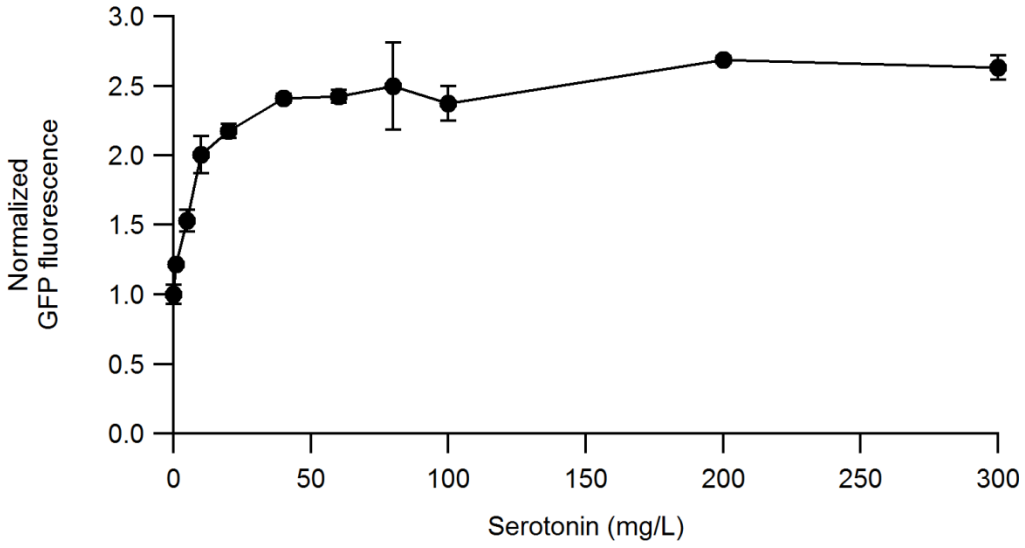

Figure 3.4. 5-HT_4-based sensor full dose response curve with exogenously added serotonin.

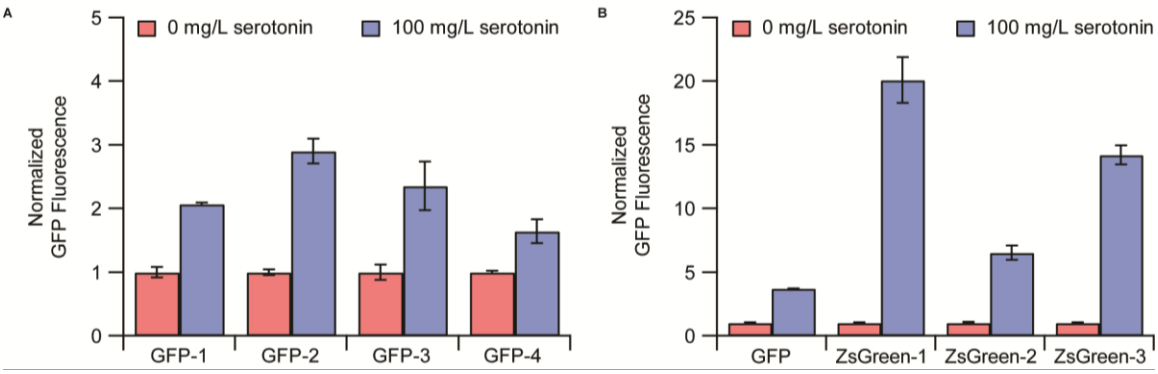

Figure 3.5. Serotonin sensor colony-to-colony variation when using GFP or ZsGreen as the reporter gene. (A) Serotonin sensor response of four different colonies using GFP as the reporter gene. (B) Serotonin sensor response of three different colonies using ZsGreen as the reporter gene. Experiments were carried out in triplicate and the error bars represent the standard deviation from the mean. Fluorescence was normalized to the response of the sensor to 0 mg/L serotonin.

3.3.2 Detection of Exogenously Added Serotonin in Plain Microbial Spent Medium

As the 5-HT_4-based sensor detected exogenously added serotonin in fresh medium, we determined if the sensor could also detect exogenously added serotonin in the spent medium of plain yeast, i.e. yeast carrying empty plasmids rather than the serotonin production pathway (Figure 3.2C). Indeed, the sensor detected serotonin with a K_D of 6.1 mg/L, a linear range of 0.8-5 mg/L, and a 1.7-fold increase in the intensity of the signal after activation (Figure 3.2D). Interestingly, the linear and dynamic range of the sensor decreased when serotonin was detected in spent rather than fresh medium. We speculate that the presence of yeast produced metabolites or the fact that some nutrients were consumed by the cell over time disturbed either the binding of serotonin to 5-HT_4 or the GPCR-based signaling process. To achieve a larger dynamic range to better distinguish producer microbes yielding different levels of serotonin, we examined the compositional differences between fresh and spent medium to adjust the nutritional constituents of the spend medium to optimize serotonin detection.

3.3.3 Effect of Nutrient Composition on Serotonin Sensing

The glucose concentration can affect the yeast mating pathway signaling process.[10] As the serotonin-producing microbe uses galactose as the carbon source[1], we determined the effect of different glucose and galactose concentrations on serotonin sensing in fresh medium. The highest serotonin sensor signal intensity was achieved in the presence of 2% glucose, the standard glucose concentration in yeast medium (Figure 3.6A). In the absence of glucose and presence of galactose or in the absence of both glucose and galactose, no sensor signal was observed, demonstrating the dependence of the serotonin sensor on glucose. Serotonin detection was restored upon addition of 0.4% glucose. Next, we analyzed the difference in nutrient composition between the sensor medium, which lacks histidine and leucine, and the serotonin producer medium, which lacks tryptophan and uracil in addition to histidine and leucine. In the absence of tryptophan and in the presence of 100 mg/L serotonin, we saw no sensor response (Figure 3.6B). The sensor response to serotonin was rescued upon addition of 20 mg/L tryptophan, the standard tryptophan concentration in fresh medium. Further addition of 20 mg/L uracil, the standard uracil concentration in fresh medium, had a slightly positive effect on serotonin detection. We attribute the improvement in sensor performance upon addition of uracil to the reduced metabolic burden on the sensor. To ensure that the serotonin sensor responds to serotonin and not tryptophan or the pathway intermediate hydroxytryptophan, we measured the serotonin sensor response to each of these compounds in the presence and absence of tryptophan (Figure 3.6C). Additionally, we measured the sensor response to 5-hydroxyindoleacetic acid (5-HIAA), a product of serotonin catabolism (Figure 3.7). The sensor showed no response in the presence of up to 100 mg/L tryptophan,

hydroxytryptophan, or 5-HIAA. The sensor responded to serotonin only in the presence of tryptophan. We speculate that tryptophan is acting as an allosteric modulator of 5-HT_4, helping to enhance the sensor signal. Indeed, allosteric modulation of the serotonin-mediated response has been seen in mammalian cells with 5-HT_{2A} in the presence of oleamide[11] and 5-$HT_{1B/1D}$ desensitization in the presence of the peptide moduline.[12] More generally, ions, lipids, amino acids, and peptides have been shown to be modulators of GPCR activity.[13] Taking these results into account, we adjusted the plain yeast spent medium to 0.4% glucose and added 100 mg/L tryptophan before serotonin detection. After adjustment, the linear range of the sensor increased from 0.8-5 to 1-10 mg/L (Figure 3.6D). Although the increase in the dynamic range was not as dramatic (2-fold vs 1.7-fold in non-adjusted spent media), the K_D stayed the same at ~6.1 mg/L. The improvement in the serotonin sensor linear range makes it suitable to screen for microbially produced serotonin.

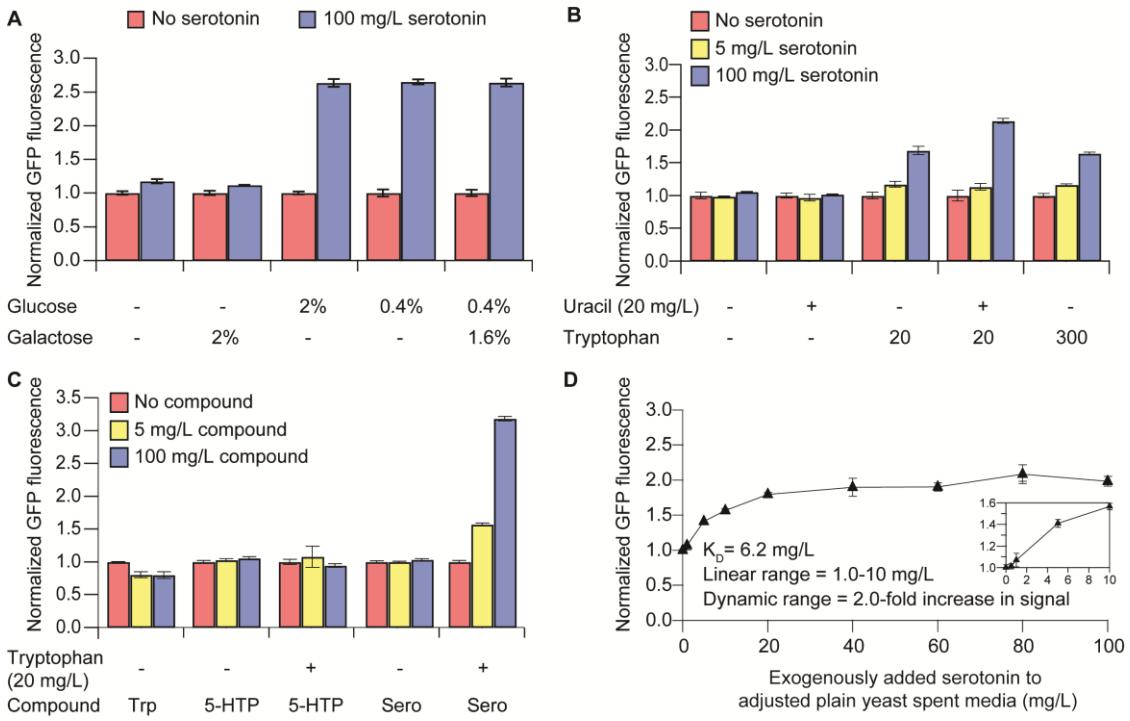

Figure 3.6. Serotonin sensor optimization. (A) Serotonin sensor dependence on glucose. (B) Serotonin sensor dependence on uracil and tryptophan. (C) Sensor response to serotonin pathway intermediates tryptophan, hydroxytryptophan, and serotonin in the presence or absence of tryptophan. Abbreviations: Trp, tryptophan; 5-HTP, hydroxytryptophan; Sero, serotonin. Experiments depicted in panels A-C were performed in fresh medium. (D) Dose-response curve of the serotonin sensor detecting serotonin exogenously added to plain yeast spent medium that had been adjusted for glucose (0.4%) and tryptophan (100 mg/L) content. All experiments were performed in triplicate and the error bars represent the standard deviation from the mean. In all cases, fluorescence was normalized to the response of the sensor to no serotonin or no pathway intermediates. Inset shows the linear range of the response.

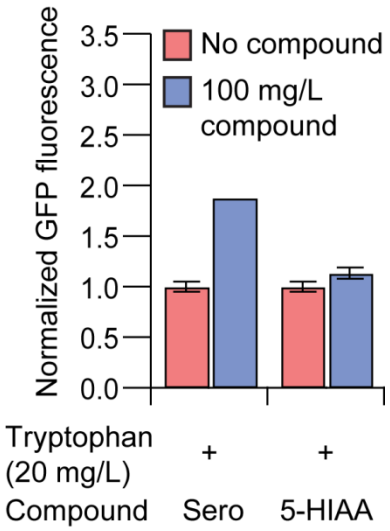

Figure 3.7. Serotonin sensor response to serotonin (Sero) and 5-hydroxyindoleacetic acid (5-HIAA). Samples fed 100 mg/L serotonin were run in duplicate. All other experiments were done in triplicate and the error bars represent the standard deviation from the mean. Fluorescence was normalized to the response of the sensor to no serotonin or 5-HIAA.

3.3.4 Detecting Microbially Produced Serotonin in a Medium-throughput Assay

The serotonin sensor resulted in a 1.3-fold increase in the intensity of the signal after activation when detecting microbially produced serotonin in the producer's spent medium. Upon adjusting the glucose and tryptophan concentrations of the producer's spent medium, we saw an additive improvement in response resulting in a 1.8-fold increase in the intensity of the signal after activation (Figure 3.8A-C). To validate the use of the serotonin sensor for medium-throughput screening applications using 96-well plates, we performed a 3 day plate uniformity experiment[14] in both fresh medium and producer spent medium adjusted with tryptophan and glucose (Figure 3.8D-F). Using two statistical parameters for assay acceptance, a Z factor of > 0.5[15] and coefficient of variation (CV) of < 10%,[16] the assay met the criteria for use in both media (average Z

factor of 0.7, average CV of 4.9%). We did see a slight interplate drift, which could be optimized by accelerating the collection time or staggering the activation times.

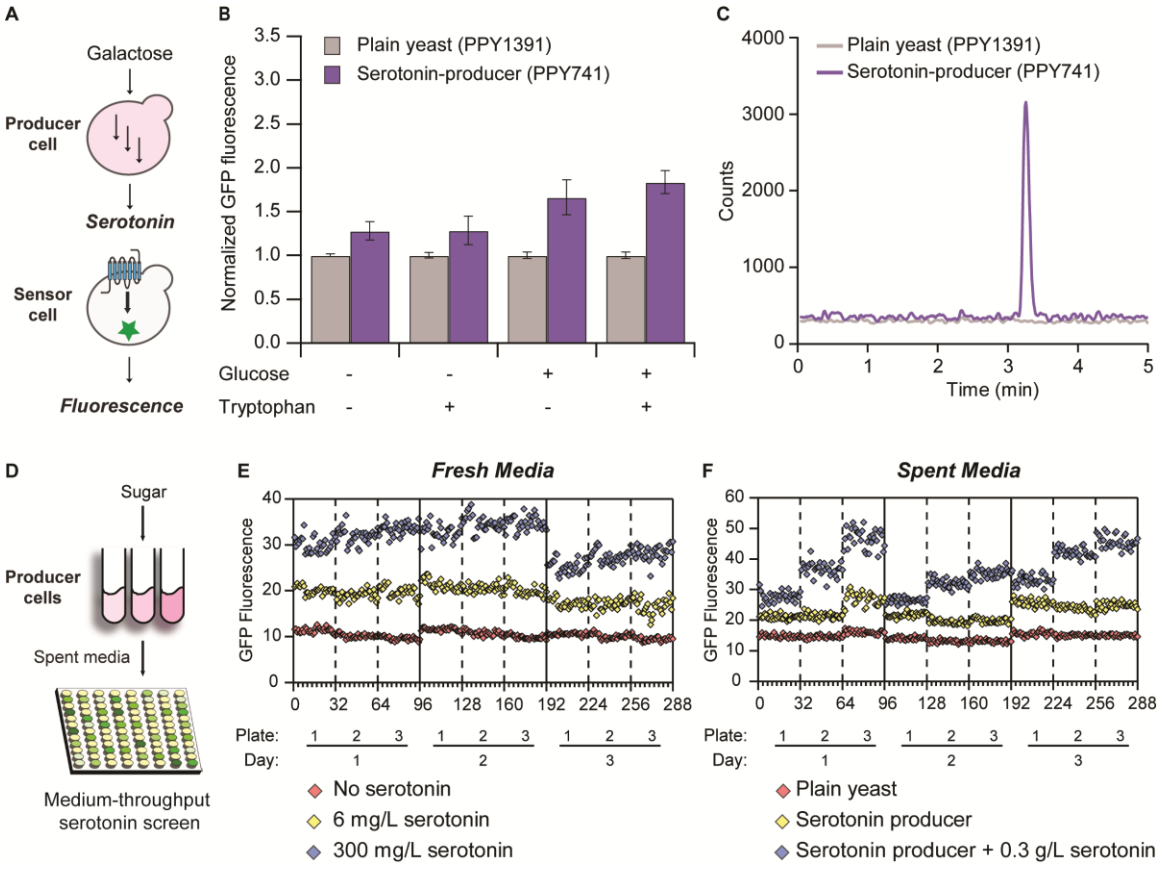

Figure 3.8. Detection of microbially-produced serotonin. (A) Schematic of microbially produced serotonin detection. (B) Serotonin sensor response upon incubation with spent medium from plain yeast (PPY1391) and the serotonin producer strain (PPY741). Experiments were performed in triplicate, and error bars represent the standard deviation from the mean. The fluorescence was normalized to the response in nonproducer spent medium for each condition. (C) Representative LC/MS (multiple-reaction monitoring) traces of the spent media from strains PPY1391 (gray) and PPY741 (purple). Shown is the serotonin transition from 176.80 to 160.00. (D) Schematic of the medium-throughput serotonin screen. (E and F) Serotonin sensor response in fresh or spend medium, respectively, over a 3 day experiment.

3.4 Discussion

We have developed a serotonin sensor capable of detecting microbially produced serotonin in the producer spent medium that has been validated for use in a medium-throughput 96-well plate assay. To generate a serotonin sensor, we screened known human serotonin GPCRs by expressing them in the yeast sensor strain for serotonin detection. No other genetic modifications to the sensor strain were needed, demonstrating the ease with which GPCR-based chemical sensors can be generated. To use the serotonin sensor for the rapid engineering of chemical-producing microbes, we demonstrate that the sensor can detect serotonin in the spent medium of the serotonin producer microbe and has the statistical parameters necessary to be used in a medium-throughput 96-well plate screen. The nutritional adjustments of the spent medium revealed in this work will likely be needed when using other GPCR-based sensors for the detection of chemicals in microbial spent medium. The 96-well plate workflow is applicable to other GPCR-based medium-throughput screens, and the workflow should also be amenable to the 384-well plate format pending assay validation.

Upon detection of microbially produced serotonin in the producer microbe's spent medium, the sensor response was ~2-fold. Although the signal was statistically significant (P =0.005), the sensor response would benefit from improvement. Coupling of 5-HT_4 to the yeast Gα subunit could be optimized by swapping 5-HT_4's cytoplasmatic domain with that of the S. cerevisiae GPCR Ste2 or using Gpa1/human Gα chimeras.[17] However, these strategies do not always result in an improvementin the signal.[3] Using ZsGreen as the reporter gene and integrating it into the chromosome should also increase the intensity of the sensor signal.[5] Alternatively, a feed forward loop could be introduced

into the sensor strain to increase the intensity of the signal only in the presence of serotonin. Such a loop could generally increase the intensity of the signal of GPCR-based sensors. Finally, although the linear range of the 5-HT_4–based serotonin sensor is narrow, the two-cell screening system allows for the producer microbe supernatant to be diluted so that the serotonin concentration lands in the linear range of the sensor.

Validation of the sensor for two key statistical parameters, Z factor and CV, shows that the sensor is suitable for 96-well plate screening, and it is now poised to be used in the engineering of improved serotonin-producing microbes. Given that serotonin is the limiting substrate in the production of hydroxystrictosidine, a potential advanced intermediate in the semisynthesis of the anticancer agents irinotecan and topotecan, the medium-throughput serotonin assay will likely enable the future increased production of hydroxystrictosidine as well as other modified monoterpene indole alkaloids.

3.5 Materials and Methods

3.5.1 Reagents

Serotonin hydrochloride was purchased from TCI (S0370). Tryptophan was purchased from Sigma (T0254). Hydroxytryptophan was purchased from Selleck Chemicals. 5-chlorotryptamine was from Ark Pharm, Inc. (AK-32281). 5-Hydroxyindoleacetic acid was purchased from Sigma (H8876).

3.5.2 Exogenous Serotonin Detection in Fresh Media

Overnight cultures of strains expressing serotonin receptors (PPY1384-7,PPY1390,PPY1444-5) in synthetic complete media lacking histidine and leucine with

2% glucose (SCglu(HL-)) were used to inoculate 20 mL of fresh SCglu(HL-) to an OD_{600}= 0.06. After incubation at 15°C (150 rpm) for 18 h for receptor expression, the sensor cells were centrifuged, resuspended in 3 mL water, and used to inoculate 200 µL of SCglu(HL-) to OD_{600}= 0.1. Serotonin was added to a final concentration of 0-300 mg/L. Plates were covered with Breathe Easy Sealing Membrane (Electron Microscopy Sciences) and samples were incubated for 4 h at 30 °C (250 rpm) for serotonin sensing. Fluorescence from 5,000 cells was measured using a Millipore Guava easyCyte HT flow cytometer. Data analysis was completed using FlowJo. For initial receptor screening and 5-HIAA screening, PPY1385 was used to express 5-HT_4. For subsequent experiments PPY1390, which expresses mCherry in addition to 5-HT_4, was used.

3.5.3 Serotonin Detection Controls

Overnight cultures of strains PPY1388 and PPY1389 in SCglu(HL-) were used to inoculate 20 mL of fresh SCglu(HL-) to an OD_{600}= 0.06 and incubated for 18 h at 15°C (150 rpm). The cells were centrifuged, resuspended in 3 mL water, and used to inoculate 200 µL of fresh SCglu(HL-) to OD_{600} = 0.1 in flat-bottom 96-well plates. Serotonin was added to a final concentration of 0 or 100 mg/L, plates were covered with Breathe Easy Sealing Membrane, and samples were incubated for 4 h at 30 °C (250 rpm). Fluorescence from 5,000 cells was measured using a Millipore Guava easyCyte HT flow cytometer. Data analysis was completed using FlowJo.

3.5.4 Colony Variation Using GFP vs. ZsGreen as Reporter Genes

Overnight cultures of multiple colonies of the serotonin sensor strain carrying GFP (PPY1390) or ZsGreen (PPY1446) as the reporter gene in SCglu(HL-) were used to

inoculate 100 or 20 mL, respectively, of fresh in SCglu(HL-) to an OD_{600}= 0.06 and incubated for 18 h at 15°C (150 rpm). The cells were centrifuged, resuspended in 20 or 3 mL water, respectively, and used to inoculate 200 μL of SCglu(HL-) to OD_{600}= 0.1 in flat-bottom 96-well plates. Serotonin was added to a final concentration of 0 or 100 mg/L, plates were covered with Breathe Easy Sealing Membrane, and samples were incubated for 4 h at 30 °C (250 rpm). Fluorescence from up to 5,000 cells was measured using a Millipore Guava easyCyte HT flow cytometer. Data analysis was completed using FlowJo.

3.5.5 Exogenous Serotonin Detection in Adjusted Fresh Media

Overnight cultures of PPY1390 in SCglu(HL-) were used to inoculate 100 mL of fresh SCglu(HL-) to an OD_{600}= 0.06 and incubated for 18 h at 15°C (150 rpm). The cells were centrifuged at 3500 rpm for 10 min, resuspended in 20 mL water, and used to inoculate 200 μL of synthetic media with various glucose, galactose, uracil, and amino acid contents to OD_{600}= 0.1 in flat-bottom 96 well plates. Serotonin, tryptophan, or hydroxytryptophan were added to final concentrations between 0-300 mg/L. Plates were covered with Breathe Easy Sealing Membrane and incubated for 4 h at 30°C (250 rpm). Fluorescence from 5,000 cells was measured using a Millipore Guava easyCyte HT flow cytometer and the data was analyzed using FlowJo.

Overnight cultures of PPY1385 in SCglu(HL-) were used to inoculate 20 mL of fresh SCglu(HL-) to an OD_{600} = 0.06 and incubated for 18 h at 15°C (150 rpm). The cells were centrifuged at 3500 rpm for 10 min, resuspended in 3 mL SCglu(HL-), and used to inoculate 5 mL SCglu(HL-) to OD_{600} = 0.05. Serotonin or 5-hydroxyindoleacetic acid

was added to final concentrations of 0 or 100 mg/L. Tubes were incubated for 4 h at 30°C (250 rpm). Fluorescence from 10,000 cells was measured using a BD LSR II flow cytometer and the data was analyzed using FlowJo.

3.5.6 Spent Media Preparation

Overnight cultures of yeast carrying empty vectors (PPY1391) and serotonin-producing yeast (PPY741) in synthetic media lacking histidine, tryptophan, leucine, and uracil with 2% glucose (SCglu(HWLU-)) were each used to inoculate three flasks of 50 mL of fresh synthetic media lacking histidine, tryptophan, leucine, and uracil with 2% galactose (SCgal(HWLU-)) to an OD_{600} = 0.1. Flasks were incubated for 69 h at 30°C (250 rpm) for serotonin production. Cells were centrifuged at 1100 x *g* for 6 min. Samples were taken from each flask and stored at -20°C for sensor and mass spectrometry analysis. Remaining spent media for each strain was pooled together for sensor validation.

3.5.7 Exogenous Serotonin Detection in Spent Media

Resuspended sensor cells were used to inoculate 200 µL of spent media to OD_{600}= 0.1 in flat-bottom 96 well plates. For adjusted spent media, solutions were added to reach final concentrations of 0.4% glucose and/or 100 mg/L tryptophan. For the dose-response curve, serotonin was added to final concentrations of 0-300 mg/L. Samples were incubated for 4 h at 30°C (250 rpm) for serotonin sensing, data was collected using Millipore Guava easyCyte HT flow cytometer and analyzed using FlowJo.

3.5.8 Medium-Throughput Serotonin Screening Validation

Three day plate uniformity experiments were completed using the interleaved-signal format[11]. For fresh media, resuspended sensor cells were used to inoculate 200 μL of SCglu(HL-) to OD_{600}= 0.1 in flat-bottom 96 well plates. Serotonin was added to final concentrations of 300, 6, or 0 mg/L corresponding to maximum, middle, and minimum signals, respectively. For spent media, resuspended sensor cells were used to inoculate 200 μL of spent media from PPY1391 and PPY741 adjusted to 0.4% glucose and 100 mg/L tryptophan to OD_{600}= 0.1 in flat-bottom 96 well plates. For spent media, maximum, middle, and minimum signals referred to PPY741 spent media and 300 mg/L serotonin, PPY741 spent media, and PPY1391 spent media, respectively. Spent media was stored at 4°C over the three-day experiment. Data was collected using Millipore Guava easyCyte HT flow cytometer and analyzed using FlowJo. Validation calculations were performed using the Excel template provided by Iversen, et al.[11] using settings for an activation study with single replicates.

3.5.9 Flow Cytometry Data Analysis

Geometric mean of the GFP-area channel was calculated for each sample using FlowJo. All fluorescence values were normalized to basal levels (0 mg/L serotonin or non-producer spent media) for all conditions tested. Student T-tests were performed using Microsoft Excel. K_D and fold increase in signal after activation for dose-response curves were obtained by fitting the experimental data to the Hill equation using Igor Pro. The lower limit of the linear range was the concentration corresponding to 10% signal saturation from the fitted model. The upper limit was determined through linear

regression analysis of experimental data until R^2 was no longer ≥ 0.95. For the adjusted spent media curve, the smallest linear regression possible (3 data points) resulted in R^2=0.93.

3.5.10 Microbially Produced Serotonin Identification

Multiple Reaction Monitoring (MRM) of serotonin was performed at the Mass Spectrometry Facility at Georgia Tech. MRM was done using a Waters Quattro LC Mass Spectrometer with a Gemini 2 x 150mm C18 column. LC conditions: Solvent A: 95%:5%:0.1% water:acetonitrile:formic acid; Solvent B: 100%:0.1% acetonitrile:formic acid. Gradient: 7 min at 100%:0% (A:B), 37 min ramp to 0%:100%, 8 min at 0%:100%, 0.1 min ramp to 100%:0%, and 7.9 min at 100%:0%. Flow rate was 0.2 mL/min. Serotonin standard curve was prepared in PPY1391 spent media. 5-Chlorotryptamine was used as an internal standard. MRM parameters: serotonin- transition 176.80 → 160.00, cone voltage 20V, collision energy 30eV; transition 176.80 → 115.00, cone voltage 20V, collision energy 30eV; 5-chlorotryptamine- transition 194.90 → 177.90, cone voltage 25V, collision energy 10eV; transition 194.90 → 142.80, cone voltage 25V, collision energy 30eV.

3.5.11 Plasmid Construction

Receptors 5-HT_{2b}, 5-HT_4, 5-HT_{5a}, and 5-HT_6 were yeast codon optimized, commercially synthesized, amplified using primers AME544/AME519, AME538/AME519, AME542/AME519, or AME536/AME519, respectively, and cloned into pKM111 at *Bam*HI/*Sac*II to generate plasmids pTMC14, pTMC18, pTMC22, and pTMC26. Receptors 5-HT_{1d} and 5-HT_{1a} were yeast codon optimized, commercially

synthesized, and directly cloned into pKM111 at *Bam*HI/*Sac*II to generate plasmids pAME142 and pAME144, respectively. The plasmids were sequence verified using primers AME397 and AME105. To construct pESC-P_{TEF1}-5-HT_4-P_{ADH1}-mCherry-His3 (pTMC40), mCherry was amplified from pmCherry using primers AME570/AME571, cloned into pTMC18 at *Sac*I/*Not*I, and sequence verified using primer AME229. To construct pRS415-P_{FIG1}-ZsGreen-Leu2 (pAME143), ZsGreen was yeast codon optimized, commercially synthesized, amplified using primers AME519/AME648, and cloned into pKM586 at *Nhe*I/*Nco*I. The construct was sequence verified using primer AME105.

3.6 References

1 Ehrenworth, A. M., Sarria, S., and Peralta-Yahya, P. (2015) Pterin-dependent mono-oxidation for the microbial synthesis of a modified monoterpene indole alkaloid. *ACS Synth. Biol*. 4, 1295-1307.

2 Ehrenworth, A. M. and Peralta-Yahya, P. (2017) Accelerating the semisynthesis of alkaloid-based drugs through metabolic engineering *Nat. Chem. Biol*. 13, 249-258.

3 Mukherjee, K., Bhattacharyya, S., and Peralta-Yahya, P. (2015) GPCR-based chemical biosensors for medium-chain fatty acids. *ACS Synth. Biol*. 4, 1261-1269.

4 McCorvy, J. D. and Roth, B. L. (2015) Structure and function of serotonin G protein-coupled receptors. *Pharmacol. Ther.*150, 129-142.

5 Nakamura, Y., Ishii, J., and Kondo, A. (2015) Applications of yeast-based signaling sensor for characterization of antagonist and analysis of site-directed mutants of the human serotonin 1A receptor. *Biotechnol. Bioeng.* 112, 1906-1915.

6 Brown, A. J., Dyos, S. L., Whiteway, M. S., White, J. H., Watson, M. A., Marzioch, M., Clare, J. J., Cousens, D. J., Paddon, C., Plumpton, C., Romanos, M. A., and Dowell, S. J. (2000) Functional coupling of mammalian receptors to the yeast mating pathway using novel yeast/mammalian G protein alpha-subunit chimeras. *Yeast.* 16, 11-22.

7 Coupar, I. M., Desmond, P. V., and Irving H. R. (2007) Human 5-HT_4 and 5-HT_7 Receptor Splice Variants: Are they Important? *Curr. Neuropharmacol.* 5, 224–231.

8 Bockaert, J., Claeysen, S., Bécamel, C., Dumuis, A., and Marin, P. (2006) Neuronal 5-HT metabotropic receptors: fine-tuning of their structure, signaling, and roles in synaptic modulation. *Cell Tissue Res.* 326, 553–572.

9 Yano, J. M., Yu, K., Donaldson, G. P., Shastri, G. G., Ann, P., Ma, L., Nagler, C. R., Ismagilov, R. F., Mazmanian, S. K., and Hsiao, E. Y. (2015) Indigenous bacteria from the gut microbiota regulate host serotonin biosynthesis. *Cell.* 161, 264-276.

10 Willhite, D. G., Brigati, J. R., Selcer, K. E., Denny, J. E., Duck, Z. A., and Wright, S. E. (2014) Pheromone responsiveness is regulated by components of the Gpr1p-mediated glucose sensing pathway in *Saccharomyces cerevisiae*. *Yeast.* 31, 361-374.

11 Thomas, E. A., Carson, M. J., Neal, M. J., and Sutcliffe, J. G. (1997) Unique allosteric regulation of 5-hydroxytryptamine receptor-mediated signal transduction by oleamide. *Proc. Natl. Acad. Sci. U.S.A.* 94, 14115-14119.

12 Fillion, G. (2000) Potential of 5-HT-moduline as a drug target for affective disorders. *Curr. Opin. Investig. Drugs*. 1, 104-109.

13 van der Westhuizen, E. T., Valant, C., Sexton, P. M., and Christopoulos, A. (2015) Endogenous allosteric modulators of G protein-coupled receptors. *J. Pharmacol. Exp. Ther*. 353, 246-260.

14 Iversen, P., W., Benoit, B., Chen, Y-F., Dere, W., Devanarayan, V., Eastwood, B. J., Farmen, M. W., Iturria, S. J., Montrose, C., Moore, R. A., Weidner, J. R., and Sittampalam, G. S. (2012) in *Assay Guidance Manual [Internet]* (Sittampalam, G. S., Coussens, N. P., Brimacombe, K., Grossman, A., Arkin, M., Auld, D., Austin, C., Baell, J., Bejcek, B., Chung, T. D. Y., Dahlin, J. L., Devanaryan, V., Foley, T. L., Glicksman, M., Hall, M. D., Hass, J. V., Inglese, J., Iversen, P. W., Kahl, S. D., Kales, S. C., Lal-Nag, M., Li, Z., McGee, J., McManus, O, Riss, T., Trask Jr, O. J., Weidner, J. R., Xia, M., and Xu, X., Eds.) pp 937-968, Eli Lilly and Company and the National Center for Advancing Translational Sciences, Bethesda, MD.

15 Zhang, J. H., Chung, T. D., and Oldenburg, K. R. (1999) A simple statistical parameter for use in evaluation and validation of high throughput screening assays. *J. Biomol. Screen.* 4, 67-73.

16 Mishra, A., Dobritsa, S. V., Crouch, M. L., Rabenstein, J., Lee, J. X., and Dhakshinamoorthy, S. (2015) Establishment and validation of a 384-well antibacterial assay amenable for high-throughput screening and combination testing. *J. Microbiol. Methods.* 118, 173-175.

17 Xue, C. Y., Hsueh, Y. P., and Heitman, J. (2008) Magnificent seven: roles of G protein-coupled receptors in extracellular sensing in fungi. *FEMS Microbiol. Rev.* 32, 1010-1032.

CHAPTER 4. Quantifying the Efficiency of *Saccharomyces cerevisiae* Translocation Tags

4.1 Abstract

Compartmentalization of metabolic pathways into organelles of the yeast *Saccharomyces cerevisiae* has been used to improve chemical production. Pathway compartmentalization aids chemical production by bringing enzymes into close proximity to one another, placing enzymes near key starting metabolites or essential co-factors, increasing the effective concentration of metabolic intermediates, and providing a more suitable chemical environment for enzymatic activity. Although several translocation tags have been used to localize enzymes to different yeast organelles, their translocation efficiencies have not been quantified. Here, we systematically quantify the translocation efficiencies of the ten commonly used *S. cerevisiae* tags by localizing green fluorescent protein into three yeast organelles: the mitochondrion (4 tags), the vacuole (3 tags), and the peroxisome (3 tags). Further, we investigate whether plasmid copy number or mRNA levels vary with tag translocation efficiency. Quantification efficiencies of *S. cerevisiae* translocation tags provides an important resource for bioengineering practitioners when choosing a tag to compartmentalize their desired protein. Finally, these efficiencies can be used to determine the percentage of enzyme compartmentalization and, thus, help better quantify effects of compartmentalization on metabolic pathway efficiency.

4.2 Introduction

Compartmentalization of metabolic pathways is an important strategy to increase chemical production[1]. Pathway compartmentalization aids chemical production by 1) bringing enzymes into close proximity of one another, enabling the handing of intermediates from one active site to another one, 2) placing enzymes near key metabolites or essential co-factors, 3) increasing the effective concentration of pathway intermediates, thus accelerating reaction rates, and 4) sometimes providing a more suitable chemical environment for enzymatic activity. Enzyme compartmentalization has increased chemical production in plants[2], filamentous fungi[3,4], and in the yeast *Saccharomyces cerevisiae*, an important chassis for chemical production due to its robustness to industrial conditions[5]. The *S. cerevisiae* mitochondrion has been leveraged for the production of steroids[6,7], terpenes[8,9], and biofuels[10]. Enzymes localized to the mitochondria gain proximity to the electron transport chain and key metabolites, such as acetyl-CoA and citric acid cycle intermediates. Targeting enzymes to the *S. cerevisiae* vacuole has been exploited for the production of methyl halides, by capitalizing on the accumulation of halide ions and the co-factor *S*-adenosyl methionine[11]. Enzyme localization to the vacuole could also take advantage of its low pH, which may provide a better environment for some enzymes, such as plant alkaloid pathway enzymes[12]. The *S. cerevisiae* peroxisome has been used to improve the production of polyhydroxyalkanoate[13], fatty acids[14], and fatty acid-derived chemicals[15]. Enzyme localization to the *S. cerevisiae* peroxisome takes advantage of fatty acid degradation intermediates. Additionally, the peroxisome may provide a more suitable environment for enzymes with a high pH optimum, such as those in β-lactam biosynthesis[16].

Several *S. cerevisiae* translocation tags have been used to localize proteins to the mitochondrion, vacuole and peroxisome. Despite the extensive knowledge on the mitochondrial, vacuolar, and peroxisomal tags' translocation mechanisms, there is no quantitative data on their translocation efficiencies, thus making the choice of translocation tags for metabolic engineering applications arbitrary. We hypothesized that translocation tags with different translocation mechanisms have different efficiencies. Here, we quantify the translocation efficiencies of four mitochondrial, three vacuolar, and three peroxisomal tags. The data presented in this work will enable metabolic engineers to rationally choose translocation tags for the compartmentalization of metabolic pathway enzymes to yeast organelles and to understand the limitations of the chosen tag. Further, the measured efficiencies of these tags will aid in approximating the percentage of protein localized to the desired compartment. This will allow more than yes/no predictions of whether a protein or a pathway has been localized to a compartment, and will instead enable calculation of the percentage of protein or pathway localized.

4.3 Results

To quantify the efficiency of translocation tags we fused enhanced green fluorescent protein (GFP) to ten commonly used *S. cerevisiae* tags: four mitochondrial tags, three vacuolar tags, and three peroxisomal tags. Each of tag-GFP fusions was expressed from the strong galactose-inducible promoter P_{GAL1} in either a single- or a multi-copy plasmid. Using confocal microscopy, we determined the effectiveness of the translocation tags to localize GFP. To determine if the translocation efficiency was cargo dependent, we also visualized the effectiveness of the translocation tags to localize mKate2, a fluorescent protein with 21.5% sequence similarity to GFP (Figure 4.1). As GFP fluorescence is pH

dependent[17], we ensured that pH difference did not affect our observation of GFP localization to the mitochondria (pH=7.5[18]) and peroxisomes (pH=8[19]) by using pH=7 media, resulting in a cytosol pH~7[20]. Likewise, we ensured that pH difference did not affect our observation of GFP localization to the vacuole (pH=6[21]) by using pH=4.5 media, resulting in a cytosol pH~6[20].

```
eGFP        MVSKGEELFTGVVPILVELDGDVNGHKFSVSGEGEGDATYGKLTLKFIC-TTGKLPVPWP       59
mKate2      ---MVSELIKENMHMKLYMEGTVNNHHFKCTSEGEGKPYEGTQTMRIKAVEGGPLPFAFD       57
                 .**:.  : : : ::* **.*:*. :.****.   *. *::: .   * **. :

eGFP        TLVTTLTYGVQCFSRYPDHMKQHDFFKSAMPEGYVQERTIFFKDDGNYKTRAEVKFEGDT       119
mKate2      ILATSFMYGSKTFINHT--QGIPDFFKQSFPEGFTWERVTTYEDGGVLTATQDTSLQDGC       115
             *.*:: ** : * .:       ****.::***:. **.  ::*.*  .:  :..::..

eGFP        LVNRIELKGIDFKEDGNILGHKL-EYNYNSHNVYIMADKQKNGIKVNFKIRHNIEDGSV-       177
mKate2      LIYNVKIRGVNFPSNGPVMQKKTLGWEASTETLYPADGGLEGRADMALK----LVGGGHL       171
            *: .::::*::* .:* :: :*   :: .:..:*   .  :.  .: :*    : .*.

eGFP        --QLADHYQQNTPIGDGPVLLPDNHYLSTQSALSKDPNE----KRDHMVLLEFVTAAGIT       231
mKate2      ICNLKTTYRSKKPAK--NLKMPGVYYVDRRLERIKEADKETYVEQHEVAVARYC-DLPSK       228
              :*   *:.:.*     : :*. :*:. :    *: ::    ::..:.: .:      .

eGFP        LGMDELYK    239
mKate2      LGHR----    232
            **
```

Figure 4.1. Alignment of eGFP and mKate2 created with Clustal Omega.

4.3.1 Localization to the Mitochondria

Mitochondrial presequence tags work by interacting with the Translocase of the Outer Membrane (TOM) complex[22,23]. We chose mitochondrial translocation tags based on their previous use to localize proteins to the yeast mitochondria (T_{COX4}[8,10], T_{OLI1}[24]), their ability to bind Tom20 (T_{HSP60}[25]), or their commercial use (T_{PDA1}[26]). To identify the mitochondria we used MitoTracker Red CMXRos, which localizes to the mitochondrial matrix. We found that GFP localization to the mitochondria is tag dependent and independent of whether GFP was expressed from a single- or a multi-copy plasmid. T_{COX4}-GFP had the highest mitochondria translocation efficiency at ~78% (Figure 4.2). $T_{HSP60,}$ $T_{PDA1,}$ and T_{OLI1} fused GFP localized to the mitochondria and the cytosol almost

evenly, similarly to the localization pattern seen with untagged GFP. T_{COX4}-mKate2 showed similar results to T_{COX4}-GFP (Figure 4.3). Interestingly, T_{HSP60} and T_{PDA1} fused mKate2 did localize to the mitochondria efficiently, which was not the case with the GFP cargo. Thus, mitochondria translocation efficiency using presequences is context dependent, confirming a phenomenon previously seen[27] and attributed to protein structure[28]. T_{OLI1}-mKate2 showed no fluorescence, however we attribute this to the low brightness compared to GFP[29].

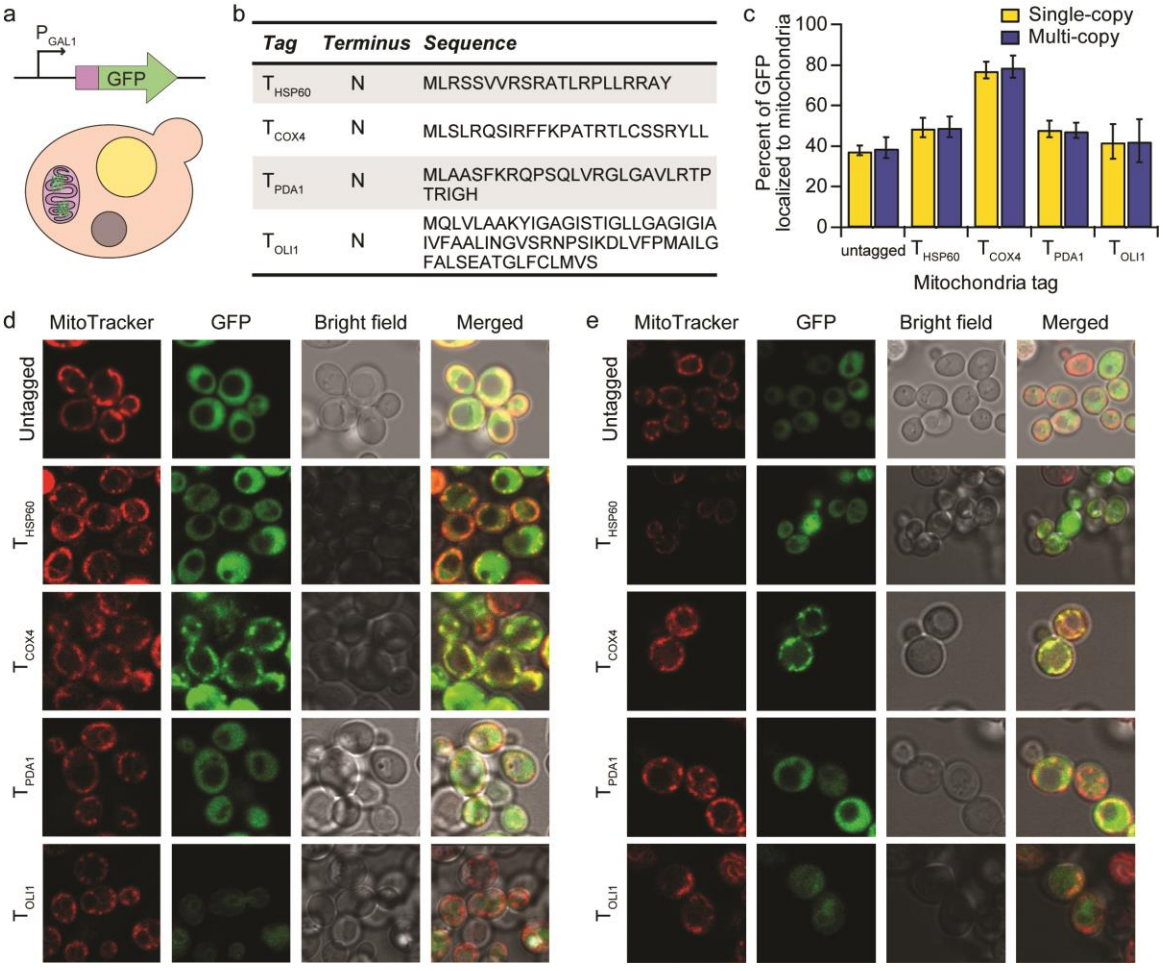

Figure 4.2. Mitochondrial localization of GFP. a. Schematic of GFP mitochondrial localization. b. Table of mitochondrial translocation tags used in this study. c. Translocation efficiency of untagged and tagged GFP to the mitochondrion in GFP positive cells with average GFP fluorescence. Percent of GFP localized to the

mitochondrion is the ratio of the mean GFP fluorescence in the mitochondrion over the mean GFP fluorescence of the mitochondria and cytosol. A 50% distribution means equal distribution in the organelle and the cytosol. Error bars represent standard deviation of 18-35 cells. d, e. Confocal microscope images of GFP positive cells with average fluorescence from single-copy (d) or multi-copy (e) plasmids showing separate images for the mitochondrial dye MitoTracker Red CMXRos, GFP, bright field, and merged images.

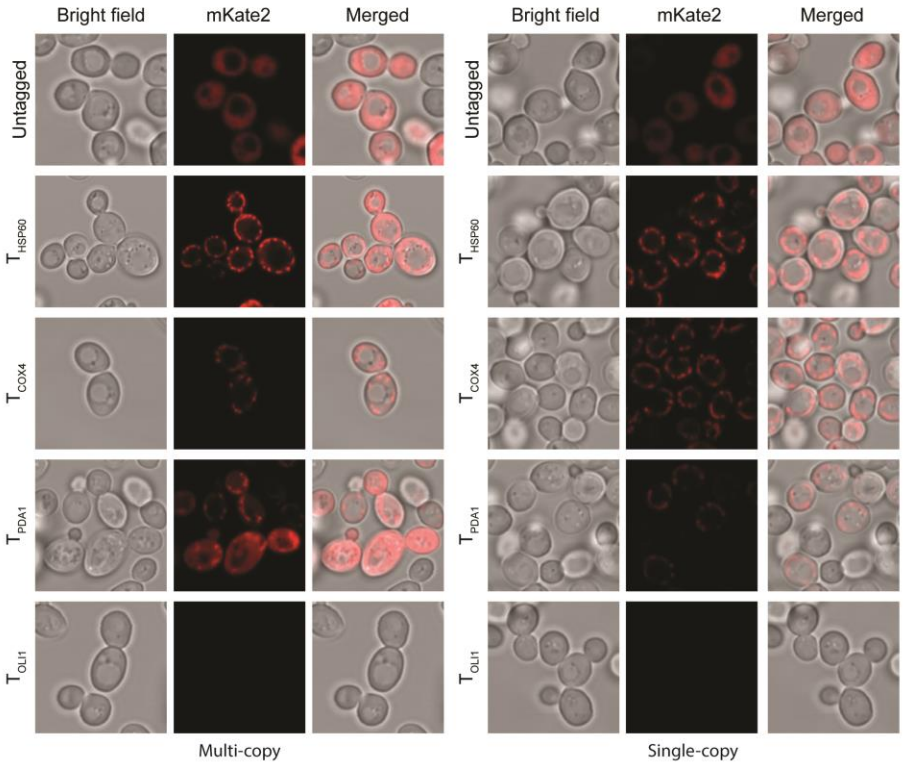

Figure 4.3. Mitochondrial localization of mKate2. Confocal microscope images of mKate2 positive cells with average fluorescence from multi-copy (left) or single-copy (right) plasmids showing separate images for mKate2, bright field, and merged images.

4.3.2 Localization to the Vacuole

The vacuole can be targeted directly from the cytosol (aminopeptidase pathway)[30] or via the secretory pathway[31], either through pre-vacuolar compartments (carboxypeptidase Y pathway) or directly from the Golgi (alkaline phosphatase pathway). We selected the vacuolar translocation tags commonly used for each vacuolar targeting mechanism: pre-

vacuolar compartments (carboxypeptidase Y: T_{PRC1}[32]), direct translocation from the Golgi (alkaline phosphatase: T_{PHO8}[33]), and direct translocation from the cytosol (aminopeptidase I: T_{APE1}[34]). To identify the vacuole, we used FM4-64 stain, which localizes to the vacuolar membrane. Similar to mitochondrial tags, localization to the vacuole is tag dependent and plasmid copy number did not affect the percentage of GFP localized to the vacuole (Figure 4.4). T_{PRC1}-GFP had the highest translocation efficiency to the vacuole at ~75%. T_{APE1} and T_{PHO8} did not localize GFP to the vacuole, with ~70% of the GFP localized to the cytosol, similar to the localization pattern of untagged GFP. T_{APE1}-mKate2 and T_{PHO8}-mKate2 had a similar localization pattern to untagged GFP (Figure 4.5) and T_{PRC1}-mKate2 did not show fluorescence, which we attribute to the low brightness compared to GFP[29]. Based on this data, we conclude that translocation to the vacuole via pre-vacuoles is the most efficient targeting mechanism.

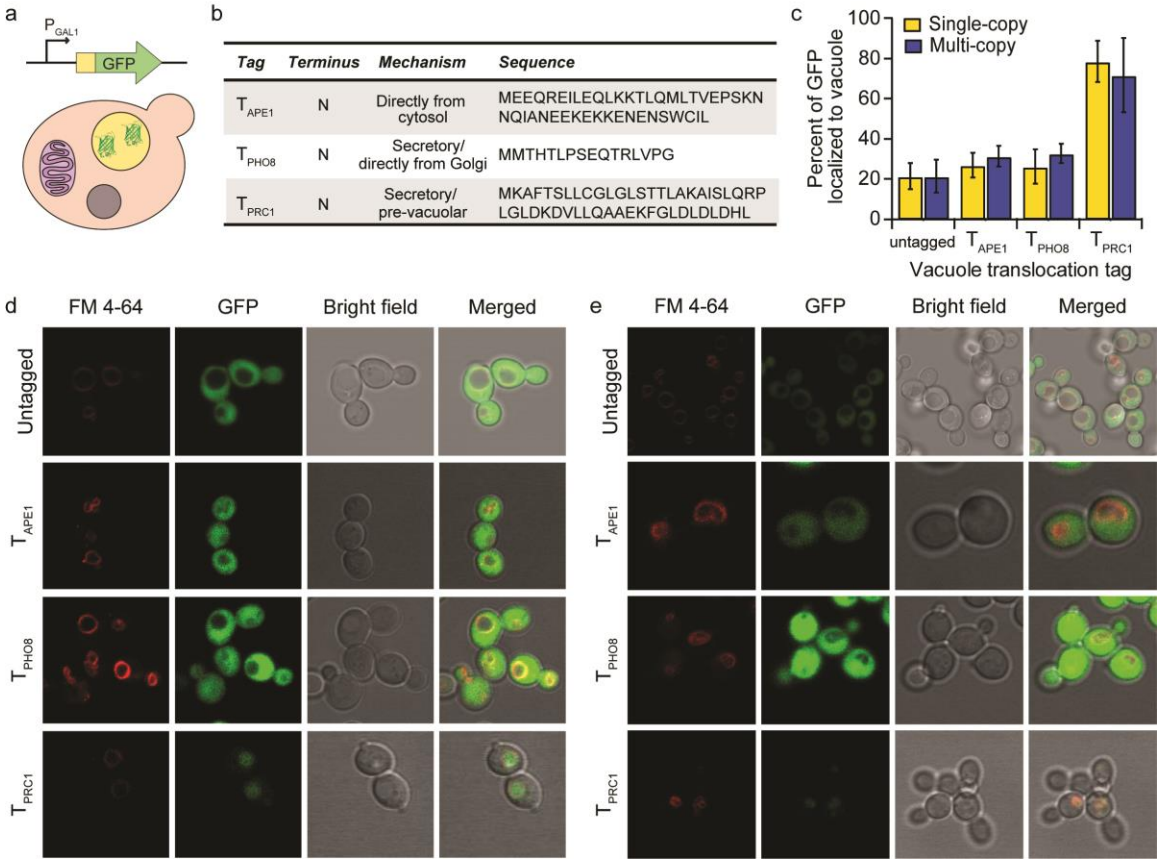

Figure 4.4. Vacuolar localization of GFP. a. Graphical representation of vacuolar localization. b. Table of vacuolar translocation tags used in this study. c. Quantitative localization of untagged and tagged GFP to the vacuole in GFP positive cells with average fluorescence. Percent GFP localized to the vacuole is the ratio of the mean GFP fluorescence in the vacuole over the mean GFP fluorescence of the vacuole and cytosol. A 50% distribution means equal distribution in the organelle and the cytosol. Error bars represent standard deviation of 15-50 cells. d, e. Confocal microscope images of GFP positive cells with average fluorescence from single-copy (d) or multi-copy (e) plasmids showing separate images for the vacuolar dye FM 4-64, GFP, bright field, and merged images.

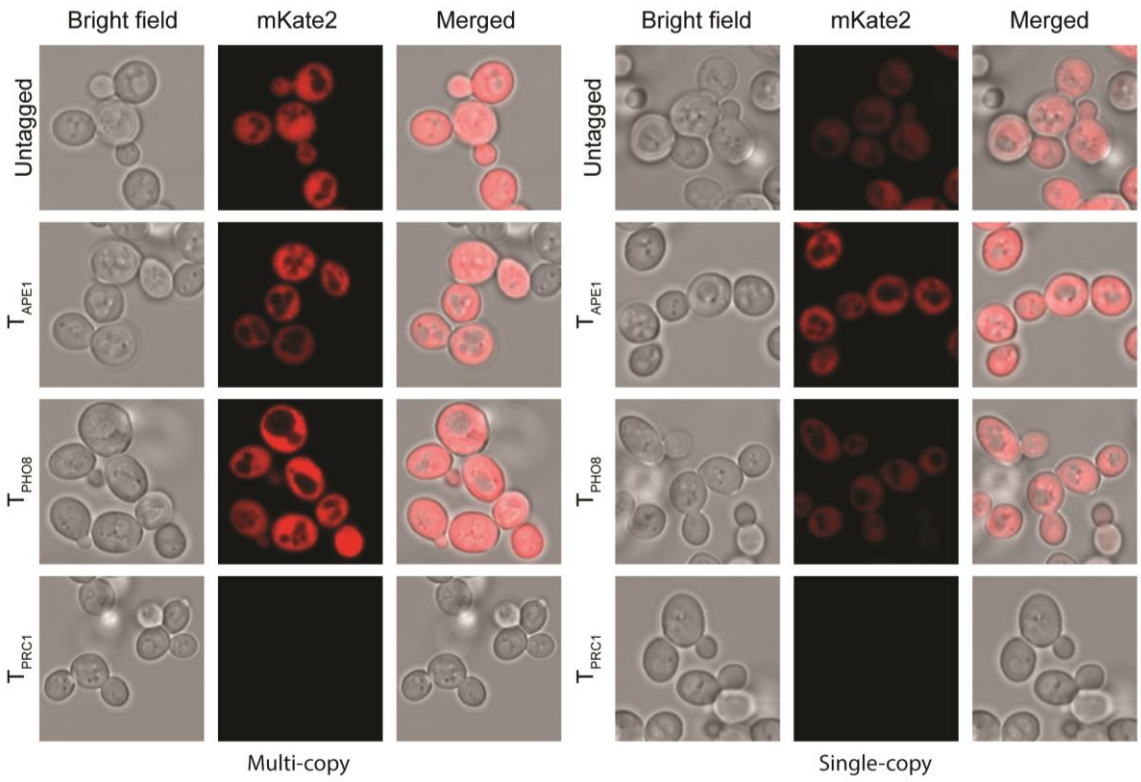

Figure 4.5. Vacuolar localization of mKate2. Confocal microscope images of mKate2 positive cells with average fluorescence from multi-copy (left) or single-copy (right) plasmids showing separate images for mKate2, bright field, and merged images.

4.3.3 Localization to the Peroxisome

Translocation to the peroxisome can be achieved using two types of peroxisomal targeting sequences (PTSs): C-terminal PTS1, which binds the Pex5 receptor, and N-terminal PTS2, which binds the Pex7 receptor[35]. We chose a canonical (T_{LUC}[36]) and a non-canonical (T_{CAT}[37]) PTS1 tag and a PTS2 tag (T_{POT1}[38]). Given the lack of stains to identify the peroxisome, we used peroxisome apparent localization based on the GFP signal and bright field images. Similarly to mitochondrial and vacuolar tags, translocation to the peroxisomes was dependent only on the translocation tag and not on the plasmid copy number (Figure 4.6). Both PTS1 tags (T_{LUC} and T_{CAT}) resulted in a GFP translocation efficiency to the peroxisome of ~99% and ~93%, respectively. T_{POT1}-GFP

localized to the peroxisome and the cytosol almost evenly. mKate2 translocation efficiencies with T_{LUC} and T_{CAT} were comparable to GFP translocation efficiencies (Figure 4.7). Based on these results, C-terminal PTS1 translocation tags T_{LUC} and T_{CAT} are more efficient at translocating payloads to the peroxisomes than the PTS2 tag T_{POT1}. While PTS1 is highly efficient as a tripeptide tag, recent work has resulted in enhanced PTS1 tags based on sequence context[39].

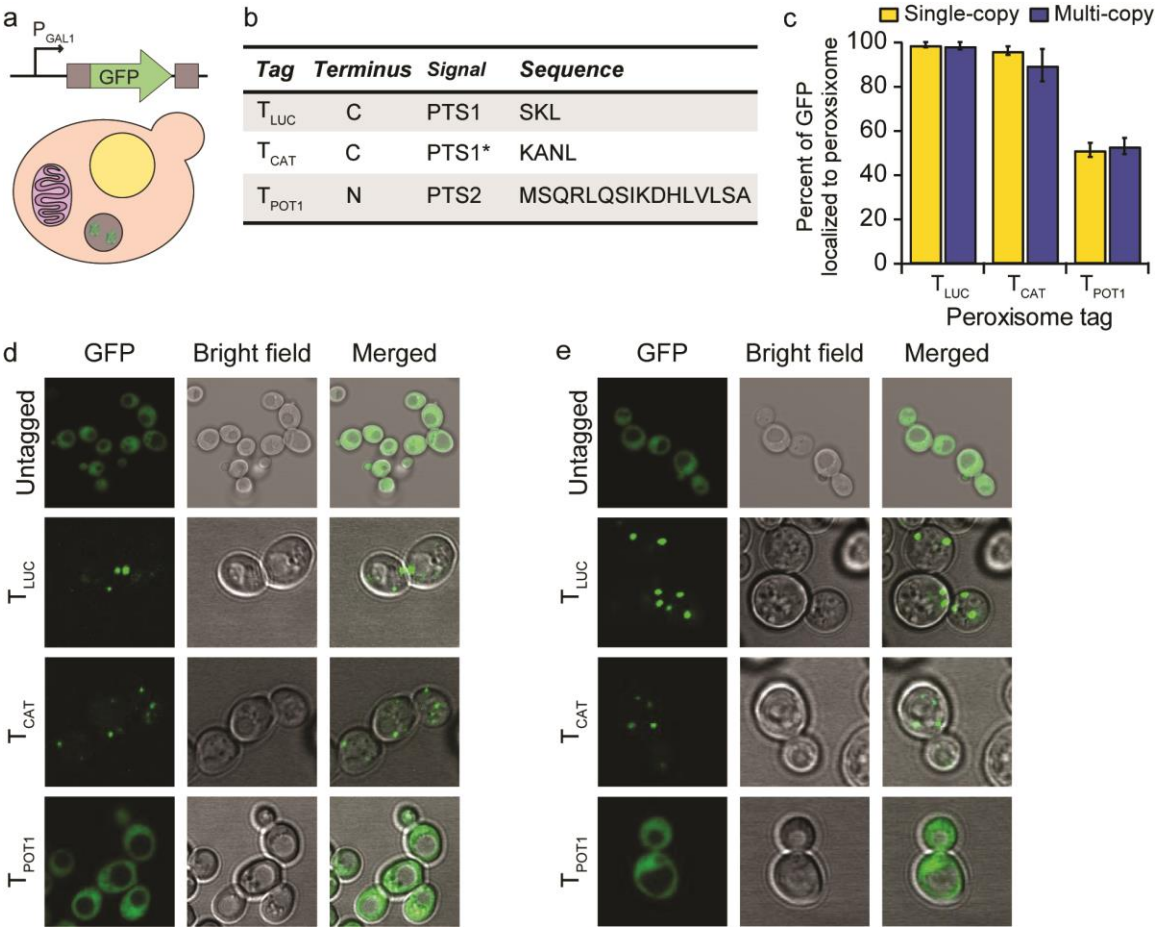

Figure 4.6. Peroxisomal localization of GFP. a. Schematic of GFP peroxisome localization. b. Table of peroxisomal translocation tags used in this study. c. Translocation efficiency of tagged GFP to the peroxisome in GFP positive cells with average GFP fluorescence. Percent of GFP localized to the peroxisome is the ratio of the mean GFP fluorescence in the peroxisome over the mean GFP fluorescence of the peroxisome and cytosol. A 50% distribution means equal distribution in the organelle and the cytosol. Error bars represent standard deviation of 20-28 cells. d, e. Confocal microscope images of GFP positive cells with average fluorescence from

single-copy (d) or multi-copy (e) plasmids showing separate images for GFP, bright field, and merged images.

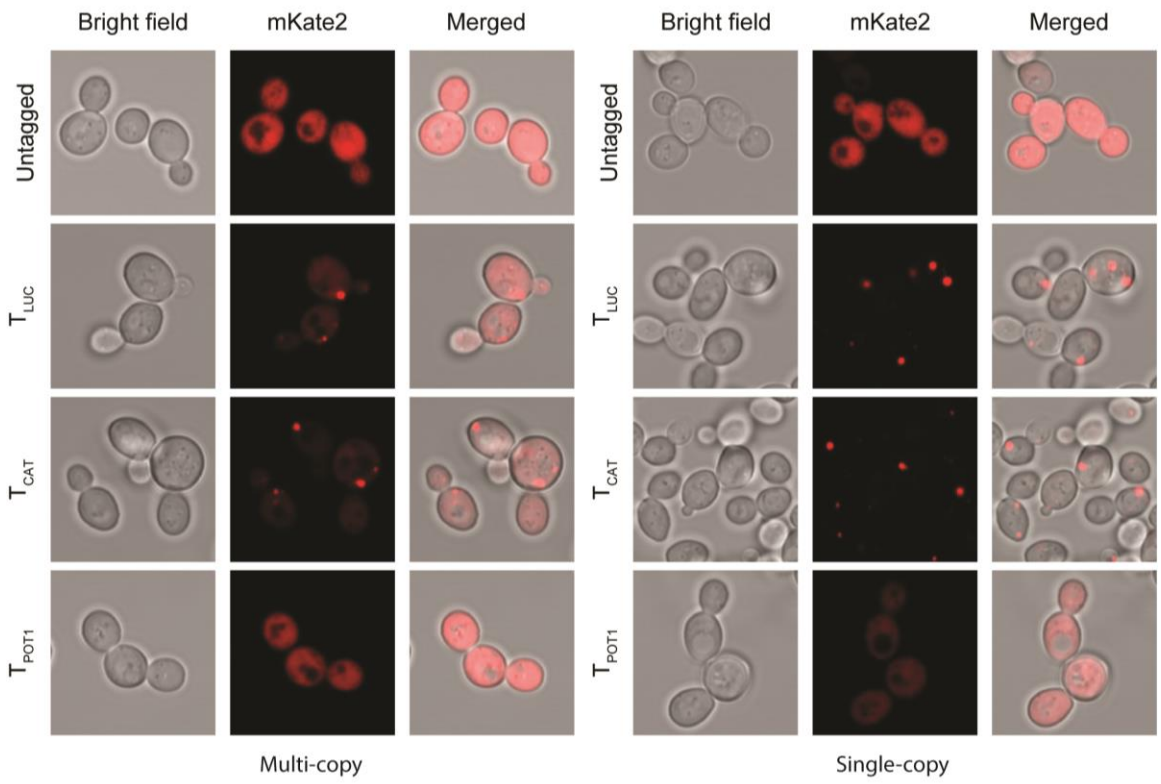

Figure 4.7. Peroxisomal localization of mKate2. Confocal microscope images of mKate2 positive cells with average fluorescence from multi-copy (left) or single-copy (right) plasmids showing separate images for mKate2, bright field, and merged images.

4.3.4 Analysis of mRNA and GFP expression

Concerned about the translocation tag disturbing the cargo mRNA levels, and potentially having an impact on the translocation efficiencies, we measured the relative mRNA levels of tagged and untagged GFP when expressed from a single- and multi-copy plasmid (Figure 4.8a). Expression of GFP from a single-copy plasmid resulted in similar GFP mRNA levels whether GFP was tagged or untagged. A similar trend was seen when GFP was expressed from a multi-copy plasmid. Thus, we conclude that there is no correlation between tag translocation efficiency and cargo mRNA levels. Comparing the

impact of plasmid copy number, the mean relative expression of GFP expressed from a single-copy plasmid was mostly (8 out of 11 samples) within error of GFP expressed from a multi-copy plasmid. We attribute this finding to the use of the strong galactose promoter (P_{Gal1}) for GFP expression.

To determine if the translocation tags altered the GFP protein expression levels, we measured GFP fluorescence of tagged and untagged GFP when expressed from single- and multi-copy plasmids using flow cytometry. When GFP was tagged to reach the mitochondria, vacuole or peroxisome and expressed from a single-copy plasmid, this resulted in a unimodal distribution of GFP fluorescence (Figure 4.8b). However, expressing the same constructs from a multi-copy plasmid resulted in a bimodal, wider distribution of GFP fluorescence (Figure 4.8c). Overall, tagged GFP expressed from a single-copy plasmid resulted in ~90% GFP positive cells, that is cells showing either low, medium or high GFP levels. Expression of tagged GFP from a multi-copy plasmid on the other hand resulted in ~70% GFP positive cells (Figure 4.8d). The single-cell level data is in accordance to the visual inspection of cells in the microscopy data.

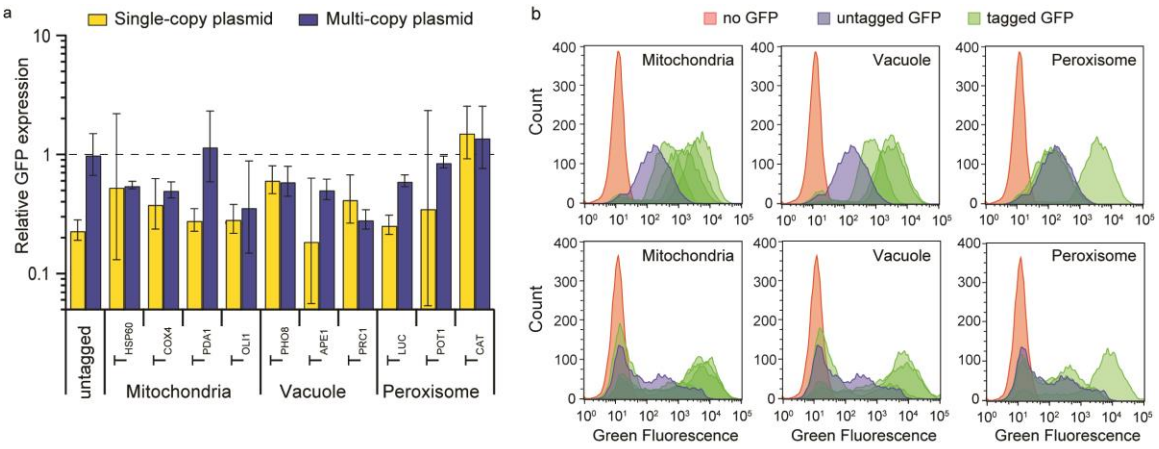

c

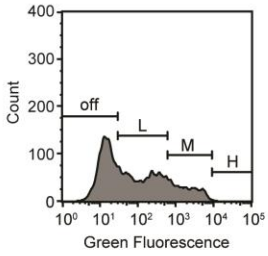

Percent of live cells expressing GFP

	Single-copy plasmid				Multi-copy plasmid			
sample	**off**	**low**	**medium**	**high**	**off**	**low**	**medium**	**high**
untagged	7	81	12	0	39	41	19	0
T_{HSP60}	3	11	79	6	12	19	49	20
T_{COX4}	1	3	74	21	16	20	40	25
T_{PDA1}	5	25	69	2	19	21	44	17
T_{OLI1}	8	57	35	0	53	26	21	0
T_{LUC}	12	80	8	0	37	45	18	0
T_{POT1}	2	5	75	18	9	13	45	33
T_{CAT}	9	82	9	0	29	46	25	0
T_{PHO8}	2	8	79	11	9	16	46	29
T_{APE1}	2	4	80	14	13	19	42	26
T_{PRC1}	9	37	54	0	50	29	19	2
blank	98	2	0	0	97	3	0	0

Figure 4.8. Analysis of GFP mRNA levels and GFP protein expression at the single cell level. a. Relative GFP mRNA levels of tagged and untagged GFP when expressed from single- and multi-copy plasmids. Experiment was performed in triplicate and analyzed using the comparative C_T method with GFP levels normalized to the levels of the housekeeping gene ACT1. Bars represent the range of expression. b. Overlaid flow cytometry histograms of live cells by organelle with GFP expressed from *top*: single- or *bottom*: multi-copy plasmids. c. Variability of GFP protein expression levels across cells expressing different tags. Left: The gates used to determine cells not expressing GFP (off), and expressing low (L), medium (M), or high (H) levels of GFP are shown on the histogram. Right: Percent of live cells expressing GFP at different levels.

4.4 Discussion

Here, we quantified the translocation efficiencies of three sets of tags for protein localization to the *S. cerevisiae* mitochondrion, vacuole, and peroxisome (Table 4-1,Table 4-2). For mitochondrial translocation, T_{COX4} shows the highest translocation efficiency with two different cargo proteins, making it the preferred translocation tag for metabolic engineering applications. When choosing vacuolar or peroxisomal tags, T_{PRC1}

(~75% of GFP localized to the vacuole) or T_{LUC} (~99% of GFP localized to the peroxisomes) are the most suitable choices, respectively. Overall, plasmid copy number does not correlate with translocation efficiency of GFP; however, copy number appears to slightly affect mKate2 translocation efficiency. This effect could be further studied using a weaker promoter than P_{Gal1}. Additionally, we show that mRNA levels do not significantly vary with translocation tag and are relatively consistent in all GFP-expressing strains. Finally, we find that, at the protein level, GFP expressed from a single-copy plasmid results in a unimodal cell distribution with more GFP positive cells than GFP expressed from a multi-copy plasmid. This is attributed to differences in plasmid stability and has been observed previously[40].

We expect the quantification of translocation efficiency and mRNA levels of translocation tags will be a valuable tool to synthetic biologists and metabolic engineers looking to localize a single protein or complete pathways to yeast organelles. Further, quantification of the translocation efficiency of these tags will enable researchers to calculate the translocation efficiency of their enzymes. It is important to note that every situation is different and pathway analysis is first required to determine whether there would be a potential advantage to the localization of a protein(s) to a compartment before tagging. If the practitioner has determined that there is a potential advantage to localize a pathway protein to a compartment (e.g. metabolite precursor, pH, metal concentration, toxic intermediates), there should be a resource that the researcher can quickly point to in order to identify what tag to use. This manuscript aims to be that resource.

Table 4-1. Translocation tag origin

Organelle	Tag	Sequence	Protein of origin	Original organism	Reference
Mitochondria	T_{HSP60}	MLRSSVVRSRATLRP LLRRAY	Heat shock protein 60	*S. cerevisiae*	25
	T_{COX4}	MLSLRQSIRFFKPATR TLCSSRYLL	Subunit IV of cytochrome c oxidase	*S. cerevisiae*	8,10
	T_{PDA1}[a]	MLAASFKRQPSQLVR GLGAVLRTPTRIGH	E1 α subunit of pyruvate dehydrogenase complex	*S. cerevisiae*	26 (human sequence)
	T_{OLI1}	MQLVLAAKYIGAGIS TIGLLGAGIGIAIVFA ALINGVSRNPSIKDLV FPMAILGFALSEATGL FCLMVS	F0-ATP synthase subunit c	*S. cerevisiae*	24
Vacuole	T_{PHO8}	MMTHTLPSEQTRLVP G	Alkaline phosphatase	*S. cerevisiae*	33
	T_{APE1}	MEEQREILEQLKKTL QMLTVEPSKNNQIAN EEKEKKENENSWCIL	Aminopeptidase I	*S. cerevisiae*	34
	T_{PRC1}	MKAFTSLLCGLGLST TLAKAISLQRPLGLD KDVLLQAAEKFGLDL DLDHL	Carboxypeptidase Y	*S. cerevisiae*	32
Peroxisome	T_{LUC}	SKL	Luciferase	*Photinus pyralis*	36
	T_{POT1}[b]	MSQRLQSIKDHLVLS A	3-ketoacyl-CoA thiolase	*S. cerevisiae*	38
	T_{CAT}	KANL	Catalase	*Homo sapiens*	37

[a] Tested 29 amino acids based on the length of the presequence in the human protein.
[b] Tag differs from reference at E14L

Table 4-2. Translocation tag descriptors

		% Translocation efficiency		mRNA levels[a]		% GFP positive cells	
Organelle	**Tag**	**Plasmid copy number**					
		Single-copy	Multi-copy	Single-copy	Multi-copy	Single-copy	Multi-copy
Mitochondria	T_{HSP60}	49.2	49.6	0.54	0.56	97.0	87.6
	T_{COX4}	77.6	79.3	0.38	0.50	99.0	84.0
	T_{PDA1}	48.4	47.7	0.28	1.17	95.1	81.2
	T_{OLI1}	42.3	42.5	0.29	0.36	91.9	46.0
Vacuole	T_{PHO8}	26.3	32.9	0.62	0.60	97.8	91.1
	T_{APE1}	27.1	31.3	0.19	0.51	98.1	86.7
	T_{PRC1}	78.5	71.7	0.42	0.28	90.4	49.0
Peroxisome	T_{LUC}	99.0	98.5	0.26	0.60	87.7	63.0
	T_{POT1}	51.5	53.2	0.35	0.86	98.1	91.2
	T_{CAT}	96.2	89.6	1.54	1.40	90.8	70.8

[a] relative expression levels compared to untagged GFP expressed from a multi-copy plasmid, normalized to the housekeeping gene ACT1

4.5 Materials and Methods

4.5.1 Confocal Microscopy for GFP

Viewing and organelle staining protocols were adapted from published protocols[41] or from manufacturer's instructions. For mitochondrial tags, overnight cultures of strains PPY370, 371, 377, 378, 382, 431, 432, 433 in synthetic complete media lacking leucine with 2% glucose (SD(L^-)) were used to inoculate 5 mL cultures in synthetic complete media lacking leucine with 2% galactose buffered with 25 mM potassium phosphate (SCgal(L^-) pH 7) to an OD_{600} = 0.05. Cultures were incubated at 30°C (250 rpm) for 21 h to OD_{600} = 0.4-1.0. Mitotracker® Red CMXRos (Molecular Probes, 1 mM solution in

DMSO) was added to a final concentration of 250nM. Cultures were incubated at 30°C (covered with foil, 250 rpm) for 15 min, pelleted, and resuspended in 100 µL phosphate buffer (PBS: 135 mM NaCl, 2.7 mM KCl, 4.3 mM Na_2HPO_4, 1.4 mM KH_2PO_4) pH = 7.4 with 2% glucose. For vacuolar tags, overnight cultures of strains PPY373, 374, 375, 384, 385, 386 in SD(L^-) were used to inoculate 5 mL cultures in non-buffered SCgal(L^-) to an OD_{600} = 0.01. Cultures were incubated at 30°C (250 rpm) for 19 h to OD_{600} = 0.3-1.0. Cells were pelleted and resuspended in 5 mL YPD. 1 mL of cells were pelleted and suspended in 50 µL freshly prepared FM4-64 (Molecular Probes) solution (32.9 µM FM4-64 in YPD). Samples were incubated at 30°C for 15 min. 1 mL of prewarmed (30°C) YPD was added to the samples. Cells were pelleted and washed twice with YPD, incubating 30°C 15-60 s between each wash (thermomixer). Samples were incubated at 30°C (thermomixer) for 60 min, pelleted, and resuspended in 100 µL PBS pH=4.6 with 2% glucose. For peroxisomal tags, overnight cultures of strains PPY1015, 1016, 372, 1018, 1019, 383 in SD(L^-) were used to inoculate 5 mL cultures in SCgal(L^-) pH 7 to an OD_{600} = 0.08. Cultures were incubated at 30°C (250 rpm) for 19 h to OD_{600} = 0.6-0.9. 1 M Tris-Cl pH = 7.5 was added to a final concentration of 10 mM and cells were incubated 5 min at 30°C (250 rpm). 1 mL of culture was pelleted and cells were resuspended in 50 µL PBS pH = 7.4 with 2% glucose. After induction and staining protocols, cells were mounted on poly-L-lysine coated slides and visualized using a 63X oil immersion objective lens on a Zeiss 510 UV confocal microscope with an Argon 488 nm laser, a HeNe 543 nm laser, and FITC and Rhodamine filters. Untagged GFP samples were similarly treated as stated above but viewed on a Zeiss LSM 780 with an Argon 488 nm laser and a HeNe 561 nm laser.

4.5.2 Confocal Microscopy for mKate2

Viewing and organelle staining protocols were adapted from manufacturer's instructions. For mitochondrial tags, overnight cultures of strains PPY1343-1347, 1354-1358 in SD(L^-) were used to inoculate 5 mL cultures in SCgal(L^-) pH 7 to an OD_{600} = 0.02. Cultures were incubated at 30°C (250 rpm) for 18 h to OD_{600} = 0.3-1.3. Mitotracker® Green (Molecular Probes, 1 mM solution in DMSO) was added to a final concentration of 200 nM. Cultures were incubated at 30°C (covered with foil, 250 rpm) for 45 min, pelleted, and resuspended in 200 µL PBS pH = 7.4 with 2% glucose. For vacuolar tags, overnight cultures of strains PPY1347, 1351-1353, 1358, 1362-1364 in SD(L^-) were used to inoculate 5 mL cultures in non-buffered SCgal(L^-) to an OD_{600} = 0.02. Cultures were incubated at 30°C (250 rpm) for 16 h to OD_{600} = 0.2-0.5. Cells were pelleted and resuspended in 5 mL PBS pH=7.4 with 2% glucose. Yeast Vacuole Marker MDY-64 (Molecular Probes, 50 mM solution in DMSO) was added to a final concentration of 10 µM. Samples were incubated at room temperature for 3-5 min. Cells were pelleted and resuspended in 200 µL PBS pH = 7.4 with 2% glucose. For peroxisomal tags, overnight cultures of strains PPY1347-1350,1358-1361 in SD(L^-) were used to inoculate 5 mL cultures in SCgal(L^-) pH 7 to an OD_{600} = 0.02. Cultures were incubated at 30°C (250 rpm) for 17 h to OD_{600} = 0.3-0.7. 1 M Tris-Cl pH = 7.5 was added to a final concentration of 10 mM and cells were incubated 5 min at 30^{o}C (250 rpm). 1 mL of culture was pelleted and cells were resuspended in 50-100 µL PBS pH = 7.4 with 2% glucose. After induction and staining protocols, cells were mounted on poly-L-lysine coated slides and mKate2 was visualized using a 63X oil immersion objective lens on a Zeiss LSM 780 confocal microscope with an Argon 458 nm laser and a HeNe

594 nm laser. Some staining was unsuccessful and therefore mKate2 data was used for qualitative purposes only.

4.5.3 Quantification of GFP Localization

GFP localization was quantified using ImageJ software[42]. Using the rhodamine channel image, organelles were manually outlined and saved as individual regions of interest (ROIs). Using the bright field image, an area in the cytosol was saved as a cytosol ROI. Mean fluorescence intensity was measured for each ROI in the FITC channel image. For each tag, 15-50 GFP positive cells with average fluorescence were analyzed with each cell having 1-5 ROIs corresponding to separate organelles. For each cell, the mean intensity for organelle ROIs and cytosol ROIs were calculated and added together to get a total intensity. The organelle intensity was divided by the total intensity and multiplied by 100 to obtain the percent of GFP localized to the organelle. Percent of GFP localized to an organelle for at least 15 cells were used to obtain the average and standard deviation. For peroxisomal tags, the peroxisome was not chemically labeled, thus no rhodamine channel signal was acquired; ROIs were chosen based on apparent localization using the FITC channel and bright field image.

$$Mean\ intensity_{organelles} + Mean\ intensity_{cytosol} = Mean\ intensity_{total}$$

$$\frac{Mean\ intensity_{organelles}}{Mean\ intensity_{total}} * 100 = percent\ efficiency$$

4.5.4 mRNA Quantification

Overnight cultures of strains in SD(L-) were used to inoculate 5 mL cultures of SCgal(L-) to an OD_{600} = 0.01. Cultures were incubated for 19 h at 30°C (250 rpm) to OD_{600} = 0.2-0.9. Cultures were pelleted and total RNA was extracted using a RNeasy Mini kit (Qiagen). RNA quantity was measured using NanoDrop Lite and samples were stored at -80°C. 1 µg of total RNA was taken from each strain and converted into cDNA using a QuantiTect Reverse Transcription kit (Qiagen). RT-PCR reactions were set up using a QuantiTect SYBR Green PCR kit (Qiagen) with 3 µL cDNA (cDNA from 150 ng mRNA) per strain. Triplicate reactions were set up for each strain. Amplification was completed using a StepOnePlus Real-time PCR system (Applied Biosystems) with primers AMEGFP-F/AMEGFP-R and AMEACT-F/AMEACT-R. GFP expression was normalized to reference gene ACT1, a gene that encodes actin, and relative expression was compared to untagged GFP expressed from a multi-copy plasmid determined using the comparative C_T method[43].

$$\Delta C_{T_{sample}} = avgC_{T_{GFP}} - avgC_{T_{actin}}$$

$$\Delta\Delta C_T = \Delta C_{T_{sample}} - \Delta C_{T_{untagged\ GFP\ multi-copy}}$$

$$2^{-\Delta\Delta C_T} = Mean\ relative\ expression\ of\ GFP\ compared\ to\ untagged\ GFP\ expressed\ from\ a\ multi-copy\ plasmid$$

$$2^{-(\Delta\Delta C_T \pm s)} = Range\ of\ fold\ change\ in\ GFP\ expression\ level\ relative\ to\ untagged\ GFP\ expressed\ from\ a\ multi-copy\ plasmid$$

$$s = standard\ deviation\ of\ \Delta C_{T_{sample}}$$

4.5.5 Protein Expression Analysis Using Flow Cytometry

Overnight cultures of strains in SD(L-) were used to inoculate 5 mL cultures of SCgal(L-) to an OD_{600} = 0.01. Cultures were incubated at 30°C (250 rpm) to OD_{600} = 0.2-0.8 and diluted 10-fold with SCgal(L-) media. GFP fluorescence for 10,000 cells was measured using a Guava easyCyte HT (Millipore). Data was analyzed using FlowJo. First, we gated for live cells (by forward and side scatter), selecting >86% of cells in all cases (Figure 4.9). Then we gated for GFP positive cells (Figure 4.8).

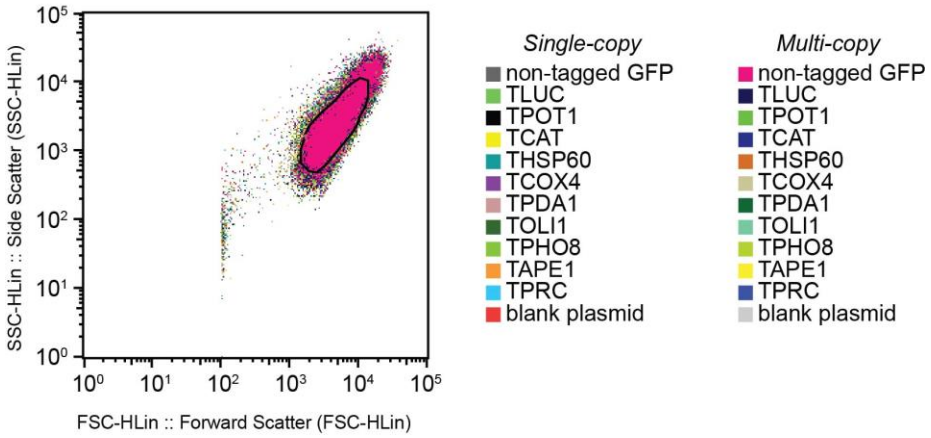

Figure 4.9. Live cell gating for flow cytometry analysis. To account for dead and outlier cells, we gated samples using forward- and side-scatter. An example gate is shown in black. In all cases, ≥ 86% of cells were chosen in the gated population.

4.5.6 Plasmid Construction

To construct pAME3s-5s, and 9, eGFP was amplified from pEGFP using primers AME440/AME103, AME440/AME121, AME440/AME122, or AME133/AME124, respectively, and cloned into pESC-Leu2 at *Bam*HI/*Hind*III. To construct pAME7-8 and pAME10-12, signal tags were amplified from pCR2.1-AME_1 using primers AME108/AME109 (T_{HSP60}), AME110/AME111 (T_{COX4}), AME114/AME115 (T_{PHO8}), AME116/AME117 (T_{APE1}), or AME118/AME119 (T_{PRC1}) and cloned into pAME3 at *Bam*HI/*Nco*I. To construct pAME14 and pAME15, signal tags were amplified from

pCR2.1-tags2.0 using primers AME155/AME156 (T_{PDA1}) or AME157/AME158 (T_{OLI1}), respectively, and cloned into pAME3 at *Bam*HI/*Nco*I. Inserts were sequenced with primers AME104/AME105.

Vectors for pAME92-95, and 99-102 were amplified using respective templates and primers (template/primer/primer): pAME7/AME231/AME484 (pAME92), pAME8/AME231/AME232 (pAME93), pAME14/AME231/AME489 (pAME94), pAME15/AME231/AME490 (pAME95), pAME9/AME231/AME485 (pAME99), pAME10/AME231/AME486 (pAME100), pAME11/AME231/AME487 (pAME111), pAME12/AME231/AME488 (pAME112). Amplified vectors were digested with *Dpn*I and PCR purified. Vectors for pAME96 and pAME97-98 were created via digestion of pAME3s with *Bam*HI/*Hind*III or *Bam*HI/*Sac*II, respectively. mKate2 was amplified from pKM1032 with primers AME491/AME493 (pAME92, 94-95, 99-102), AME494/AME493 (pAME93), AME492/AME493 (pAME96), AME492/AME496 (pAME97), or AME492/AME495 (pAME98) and cloning into their respective vectors. Inserts were sequenced with primer AME104.

The region between terminators tADH1 and tCYC1 was amplified from pAME3s-5s, 7-12, 14-15, and 92-102 using primers AME184/AME185 and cloned into pRS415 at *Bam*HI/*Hind*III. Inserts were sequenced with primers AME104 and either MH100 or AME415.

4.6 References

1 DeLoache, W. C. and Dueber, J. E. (2013) Compartmentalizing metabolic pathways in organelles. *Nat. Biotechnol.* 31, 320-321.

2 Wu, S. Q., Schalk, M., Clark, A., Miles, R. B., Coates, R. and Chappell, J. (2006) Redirection of cytosolic or plastidic isoprenoid precursors elevates terpene production in plants. *Nat. Biotechnol.* 24, 1441-1447.

3 Blumhoff, M. L., Steiger, M. G., Mattanovich, D. and Sauer, M. (2013) Targeting enzymes to the right compartment: Metabolic engineering for itaconic acid production by *Aspergillus niger*. *Metab. Eng.* 19, 26-32.

4 Herr, A. and Fischer, R. (2014) Improvement of *Aspergillus nidulans* penicillin production by targeting AcvA to peroxisomes. *Metab. Eng.* 25, 131-139.

5 Peralta-Yahya, P. P., Zhang, F. Z., del Cardayre, S. B. and Keasling, J. D. (2012) Microbial engineering for the production of advanced biofuels. *Nature* 488, 320-328.

6 Dumas, B., Cauet, G., Lacour, T., Degryse, E., Laruelle, L., Ledoux, C., Spagnoli, R. and Achstetter, T. (1996) 11 beta-hydroxylase activity in recombinant yeast mitochondria - *In vivo* conversion of 11-deoxycortisol to hydrocortisone. *Eur. J. Biochem.* 238, 495-504.

7 Szczebara, F. M., Chandelier, C., Villeret, C., Masurel, A., Bourot, S., Duport, C., Blanchard, S., Groisillier, A., Testet, E., Costaglioli, P., Cauet, G., Degryse, E., Balbuena, D., Winter, J., Achstetter, T., Spagnoli, R., Pompon, D. and Dumas, B. (2003) Total biosynthesis of hydrocortisone from a simple carbon source in yeast. *Nat. Biotechnol.* 21, 143-149.

8 Farhi, M., Marhevka, E., Masci, T., Marcos, E., Eyal, Y., Ovadis, M., Abeliovich, H. and Vainstein, A. (2011) Harnessing yeast subcellular compartments for the production of plant terpenoids. *Metab. Eng.* 13, 474-481.

9 Yuan J. and Ching, C.-B. (2016) Mitochondrial acetyl-CoA utilization pathway for terpenoid productions. *Metab. Eng.* 38, 303-309.

10 Avalos, J. L., Fink, G. R. and Stephanopoulos, G. (2013) Compartmentalization of metabolic pathways in yeast mitochondria improves the production of branched-chain alcohols. *Nat. Biotechnol.* 31,335-341.

11 Bayer, T. S., Widmaier, D. M., Temme, K., Mirsky, E. A., Santi, D. V. and Voigt, C. A. (2009) Synthesis of methyl halides from biomass using engineered microbes. *J. Am. Chem. Soc.* 131, 6508-6515.

12 Mizukami, H., Nordlov, H., Lee, S. L. and Scott, A. (1979) I. Purification and properties of strictosidine synthetase (an enzyme condensing tryptamine and secologanin) from *Catharanthus-roseus* cultured-cells. *Biochemistry* 18, 3760-3763.

13 Poirier, Y., Erard, N. and Petetot, J. M. C. (2001) Synthesis of polyhydroxyalkanoate in the peroxisome of *Saccharomyces cerevisiae* by using intermediates of fatty acid beta-oxidation. *Appl. Environ. Microb.* 67, 5254-5260.

14 Sheng, J., Stevens, J., and Feng, X. (2016) Pathway compartmentalization in peroxisome of *Saccharomyces cerevisiae* to produce versatile medium chain fatty alcohols. *Sci. Rep.* 6, 26884.

15 Zhou, Y. J, Buijs, N. A., Zhu, Z., Gómez, D.-O., Boonsombuti, A., Siewers, V. and Nielsen, J. (2016) Harnessing yeast peroxisomes for biosynthesis of fatty-acid-derived biofuels and chemicals with relieved side-pathway competition. *J. Am. Chem. Soc.* 138, 15368-15377.

16 Li, D. C., Cheng, S. W., Wei, D. Z., Ren, Y. H. and Zhang, D. R. (2007) Production of enantiomerically pure (*S*)-beta-phenylalanine and (*R*)-beta-phenylalanine by penicillin G acylase from *Escherichia coli* in aqueous medium. *Biotechnol. Lett.* 29, 1825-1830.

17 Bizzarri, R., Serresi, M., Luin, S. and Beltram, F. (2009) Green fluorescent protein based pH indicators for *in vivo* use: a review. *Anal. Bioanal. Chem.* 393, 1107-1122.

18 Orij, R., Postmus, J., Ter Beek, A., Brul, S. and Smits, G. J. (2009) In vivo measurement of cytosolic and mitochondrial pH using a pH-sensitive GFP derivative in *Saccharomyces cerevisiae* reveals a relation between intracellular pH and growth. *Microbiology* 155, 268-278.

19 van Roermund, C. W. T., de Jong, M., Ijist, L., van Marle, J., Dansen, T. B., Wanders, R. J. A. and Waterham, H. R. (2004) The peroxisomal lumen in *Saccharomyces cerevisiae* is alkaline. *J. Cell Sci.* 117, 4231-4237.

20 Valli, M., Sauer, M., Branduardi, P., Borth, N., Porro, D. and Mattanovich, D. (2005) Intracellular pH distribution in *Saccharomyces cerevisiae* cell populations, analyzed by flow cytometry. *Appl. Environ. Microb.* 71,1515-1521.

21 Preston, R. A., Murphy, R. F. and Jones, E. W. (1989) Assay of vacuolar ph in yeast and identification of acidification-defective mutants. *Proc. Natl. Acad. Sci. U.S.A.* 86,7027-7031.

22 Neupert, W. and Herrmann, J. M. (2007) Translocation of proteins into mitochondria. *Annu. Rev. Biochem.* 76,723-749.

23 Schmidt, O., Pfanner, N. and Meisinger, C. (2010) Mitochondrial protein import: from proteomics to functional mechanisms. *Nat. Rev. Mol. Cell. Bio.* 11,655-667.

24 Rafelski, S. M., Viana, M. P., Zhang, Y., Chan, Y. H. M., Thorn, K. S., Yam, P., Fung, J. C., Li, H., Costa, L. D. and Marshall, W. F. (2012) Mitochondrial network size scaling in budding yeast. *Science* 338,822-824.

25 Muto, T., Obita, T., Abe, Y., Shodai, T., Endo, T. and Kohda, D. (2001) NMR identification of the Tom20 binding segment in mitochondrial presequences. *J. Mol. Biol.* 306, 137-143.

26 ThermoFischer. CellLight Fluorescent Protein Labeling, (https://tools.thermofisher.com/content/sfs/manuals/mp10582.pdf) (accessed August 27 2015).

27 van Steeg, H., Oudshoorn, P., van Hell, B., Polman, J. E. and Grivell, L. A. (1986) Targeting efficiency of a mitochondrial pre-sequence is dependent on the passenger protein. *EMBO J.* 5, 3643-3650.

28 Wilcox, A. J., Choy, J., Bustamante, C. and Matouschek, A. (2005) Effect of protein structure on mitochondrial import. *Proc. Natl. Acad. Sci. U.S.A.* 102, 15435-15440.

29 Shcherbo, D., Murphy, C. S., Ermakova, G. V., Solovieva, E. A., Cherpurnykh, T. V., Shcheglov, A. S., Verkhusha, V. V., Pletnev, V. Z., Hazelwood, K. L., Roche, P. M., Lukyanov, S., Zaraisky, A. G., Davidson, M. W. and Chudakov, D. M. (2009) Far-red fluorescent tags for protein imaging in living tissues. *Biochem. J.* 418, 567-574.

30 Klionsky, D. J., Cueva, R. and Yaver, D. S. (1992) Aminopeptidase-I of *Saccharomyces-cerevisiae* is localized to the vacuole independent of the secretory pathway. *J. Cell. Biol.* 119, 287-299.

31 Bowers, K. and Stevens, T. H. (2005) Protein transport from the late Golgi to the vacuole in the yeast *Saccharomyces cerevisiae. Biochim. Biophys. Acta.* 1744, 438-454.

32 Johnson, L. M., Bankaitis, V. A. and Emr, S. D. (1987) Distinct sequence determinants direct intracellular sorting and modification of a yeast vacuolar protease. *Cell* 48, 875-885.

33 Cowles, C. R., Snyder, W. B., Burd, C. G. and Emr, S. D. (1997) Novel Golgi to vacuole delivery pathway in yeast: Identification of a sorting determinant and required transport component. *EMBO J.* 16, 2769-2782.

34 Oda, M. N., Scott, S. V., HefnerGravink, A., Caffarelli, A. D. and Klionsky, D. J. (1996) Identification of a cytoplasm to vacuole targeting determinant in aminopeptidase I. *J. Cell. Biol.* 132, 999-1010.

35 Martin, J. F., Ullan, R. V. and Garcia-Estrada, C. (2012) Role of peroxisomes in the biosynthesis and secretion of beta-lactams and other secondary metabolites. *J. Ind. Microbiol. Biotechnol.* 39, 367-382.

36 Gould, S. J., Keller, G. A., Hosken, N., Wilkinson, J. and Subramani, S. (1989) A conserved tripeptide sorts proteins to peroxisomes. *J. Cell. Biol.* 108, 1657-1664.

37 Purdue, P. E. and Lazarow, P. B. (1996) Targeting of human catalase to peroxisomes is dependent upon a novel COOH-terminal peroxisomal targeting sequence. *J. Cell. Biol.* 134, 849-862.

38 Glover, J. R., Andrews, D. W., Subramani, S. and Rachubinski, R. A. (1994) Mutagenesis of the amino targeting signal of *Saccharomyces-cerevisiae* 3-ketoacyl-CoA thiolase reveals conserved amino-acids required for import into peroxisomes *in-vivo*. *J. Biol. Chem.* 269**,** 7558-7563.

39 DeLoache, W. C., Russ, Z. N., and Dueber, J. E. (2016) Towards repurposing the yeast peroxisome for compartmentalizing heterologous metabolic pathways. *Nat. Commun.* 7, 11152.

40 Trenchard, I. J. and Smolke, C. D. (2015) Engineering strategies for the fermentative production of plant alkaloids in yeast. *Metab. Eng.* 30, 96-104.

41 Baggett, J. J., Shaw, J. D., Sciambi, C. J., Watson, H. A. and Wendland, B. (2003) Fluorescent labeling of yeast. *Curr. Prot. Cell Biology* Chapter 4, Unit 4 13.

42 Schneider, C.A., Rasband, W.S., and Eliceiri, K.W. (2012) NIH Image to ImageJ: 25 years of image analysis. *Nat. Methods* 9, 671-675.

43 Livak, K. J., and Schmittgen, T. D. (2001) Analysis of relative gene expression data using real-time quantitative PCR and the $2^{-\Delta\Delta CT}$ method. *Methods* 25, 402-408.

CHAPTER 5. Conclusions and Future Direction

5.1 General Conclusions

The work presented in this thesis represents the first production of a modified monoterpene indole alkaloid in the yeast *Saccharomyces cerevisiae*. Further, it serves as a resource to the synthetic biology community through the unique analysis of current pharmaceuticals put forth in chapter 1 as well as through the analysis of translocation tag efficiencies in chapter 4. Additionally, the development of a medium-throughput GPCR-based sensing assay to sense a microbially-produced chemical is likely to mirror optimizations that would be needed to develop similar sensors in the future.

5.2 Future Directions

5.2.1 Bioproduction of Other Alkaloid Families

While the work in this thesis focused on microbial production of a modified monoterpene indole alkaloid (MIA), similar work can be done involving other alkaloid families. Benzylisoquinoline alkaloids (BIAs) have been the subject of a majority of microbial metabolic engineering works in the field due to the vast knowledge of their biosynthetic pathways[1,2]. Increasing works have involved other families including ergots[3-6] and more recently xanthines[7]. Analyses such as the one showcased in chapter 1, which focused on alkaloids derived from tyrosine and tryptophan, can be done on other families of alkaloids with different biosynthetic origins or on other classes of natural products in general. This type of analysis would supply researchers with an application-based roadmap for target identification. Once beneficial targets are determined, metabolic

engineering, pathway elucidation, and protein engineering can be used to develop microbes to produce the products of interest in a rapid and renewable fashion.

5.2.2 Bioproduction of Advanced MIAs

The work in chapter 2 resulted in the microbial production of hydroxystrictosidine, a hydroxylated early intermediate in the monoterpene indole alkaloid (MIA) pathway leading to camptothecin. Advancement of hydroxystrictosidine through the camptothecin pathway would result in hydroxycamptothecin, which can potentially accelerate the semisynthesis of current anti-cancer drugs topotecan and irinotecan as well as novel anti-cancer agents. Modified MIA precursors have been shown to convert to their corresponding modified alkaloids in plant cultures, which is promising for microbial production of compounds such as hydroxycamptothecin once the downstream plant enzymes are expressed in yeast. A key challenge that remains regarding this goal is biosynthetic pathway elucidation, as no further downstream enzymes in the camptothecin pathway are currently known and very few downstream enzymes are known in other advanced MIA pathways. I believe that the most significant development in the area of microbial production of advanced MIAs, and other natural products, will be rapid pathway elucidation. With increasing advances in synthetic biology and metabolic engineering tools and technologies, I am confident that once this knowledge is obtained there will be a substantial increase in the microbial production of useful modified alkaloids, including current pharmaceuticals and novel drug leads.

5.2.3 Screening of Serotonin-Producer Libraries

With the engineering of a serotonin-producing microbe (chapter 2) and a serotonin-sensing microbe (chapter 3), the stage is set to rapidly engineer a better serotonin-producer. A variety of approaches can be used to create libraries of producer mutants, including random or rational designs targeted at key enzymes in the pathway, competing enzymes, precursor production, or product transport. Chapter 3 established a medium-throughput assay that can rapidly screen these producer mutants using a GPCR-based sensor. Once positive hits are obtained, serotonin levels can be verified and quantified using LC/MS. Improved serotonin producers can then be used to engineer improved alkaloid producers.

5.2.4 Expansion of Signal Tag Studies

The work in chapter 4 focused on quantifying the translocation efficiencies of a subset of translocation tags to three organelles (mitochondria, vacuole, and peroxisome). This study can be expanded to investigate larger suites of tags as well as other organelle targets, such as the nucleus. It would be interesting to examine further the context dependency of various tags, such as that seen for mitochondrial tags in chapter 4. The results and techniques in chapter 4 and expanded studies could additionally aid in the construction of improved signal tags.

5.3 References

1 Diamond, A. and Desgagné-Penix, I. (2016) Metabolic engineering for the production of plant isoquinoline alkaloids. *Plant Biotechnol. J.* 14, 1319–1328.

2 Narcross, L., Fossati, E., Bourgeois, L., Dueber, J.E. and Martin, V.J. (2016) Microbial factories for the production of benzylisoquinoline alkaloids. *Trends Biotechnol.* 34, 228–241.

3 Ryan, K.L., Moore, C.T. and Panaccione, D.G. (2013) Partial reconstruction of the ergot alkaloid pathway by heterologous gene expression in *Aspergillus nidulans*. *Toxins (Basel)* 5, 445–455.

4 Wallwey, C., Matuschek, M. and Li, S.M. (2010) Ergot alkaloid biosynthesis in *Aspergillus fumigatus*: conversion of chanoclavine-I to chanoclavine-I aldehyde catalyzed by a short-chain alcohol dehydrogenase FgaDH. *Arch. Microbiol.* 192, 127–134.

5 Cheng, J.Z., Coyle, C.M., Panaccione, D.G. and O'Connor, S.E. (2010) Controlling a structural branch point in ergot alkaloid biosynthesis. *J. Am. Chem. Soc.* 132, 12835–12837.

6 Robinson, S.L. and Panaccione, D.G. (2014) Heterologous expression of lysergic acid and novel ergot alkaloids in *Aspergillus fumigatus*. *Appl. Environ. Microbiol.* 80, 6465–6472.

7 McKeague, M., Wang, Y.H., Cravens, A., Win, M.N. and Smolke, C.D. (2016) Engineering a microbial platform for *de novo* biosynthesis of diverse methylxanthines. *Metab. Eng.* 38, 191–203.

APPENDIX A. Tables of Plasmids

Table A-1. Plasmids used in chapter 2

Strain #	Plasmid Name	Description	Source
PPY13	pRS413	YC-type (centromeric) shuttle vector	ATCC® 87518
PPY14	pRS414	YC-type (centromeric) shuttle vector	ATCC® 87519
PPY15	pRS415	YC-type (centromeric) shuttle vector	ATCC® 87520
PPY34	pESC-His3	Yeast shuttle vector with divergent Gal1/Gal10 promoter	Agilent #217451
PPY35	pESC-Ura3	Yeast shuttle vector with divergent Gal1/Gal10 promoter	Agilent #217454
PPY36	pESC-Trp1	Yeast shuttle vector with divergent Gal1/Gal10 promoter	Agilent #217453
PPY38	pEGFP	Enhanced Green Fluorescent Protein	F. Storici lab
PPY39	pESC-Leu2	Yeast shuttle vector with divergent Gal1/Gal10 promoter	Agilent #217452
PPY40	pAME3	pESC-P_{GAL1}-eGFP-Leu2	Chapter 2; Ehrenworth et al. (2015) *ACS Synth. Biol.* 4, 1295-1307
PPY154	pCR2.1_HGTPCH	Codon optimized* GTPCH from *H. sapiens*	Chapter 2; Ehrenworth et al. (2015) *ACS Synth. Biol.* 4, 1295-1307
PPY156	pCR2.1_MaGTPCH	Codon optimized* GTPCH from *M.alpinas*	Chapter 2; Ehrenworth et al. (2015) *ACS Synth. Biol.* 4, 1295-1307
PPY166	pAME20	pESC-P_{GAL1}-His_6-*H.sapiens*_GTPCH-Leu2	Chapter 2; Ehrenworth et al. (2015) *ACS Synth. Biol.* 4, 1295-1307

Table A-1. continued

Strain #	Plasmid Name	Description	Source
PPY168	pAME18	pESC-P_{GAL1}-His_6-*M.alpina*_GTPCH-Leu2	Chapter 2; Ehrenworth et al. (2015) *ACS Synth. Biol.* 4, 1295-1307
PPY171	pCR2.1_MaPTS	Codon optimized* PTPS from *M. alpinas*	Chapter 2; Ehrenworth et al. (2015) *ACS Synth. Biol.* 4, 1295-1307
PPY172	pCR2.1_SPTS	Codon optimized* PTPS from *S. salar*	Chapter 2; Ehrenworth et al. (2015) *ACS Synth. Biol.* 4, 1295-1307
PPY173	pCR2.1_RubPTS	Codon optimized* PTPS from *S. ruber*	Chapter 2; Ehrenworth et al. (2015) *ACS Synth. Biol.* 4, 1295-1307
PPY174	pCR2.1_PmPTS	Codon optimized* PTPS from *P. mikurensis*	Chapter 2; Ehrenworth et al. (2015) *ACS Synth. Biol.* 4, 1295-1307
PPY181	pCR2.1_MaSR	Codon optimized* SR from *M. alpina* with N-terminal His_6-tag	Chapter 2; Ehrenworth et al. (2015) *ACS Synth. Biol.* 4, 1295-1307
PPY182	pCR2.1_PseudoSR	Codon optimized* SR from *T. pseudonana* with N-terminal His_6-tag	Chapter 2; Ehrenworth et al. (2015) *ACS Synth. Biol.* 4, 1295-1307
PPY183	pAME17	pESC-P_{GAL1}-His_6-*E.coli*_GTPCH-Leu2	Chapter 2; Ehrenworth et al. (2015) *ACS Synth. Biol.* 4, 1295-1307
PPY184	pAME19	pESC-P_{GAL1}-His_6-*S.cerevisiae*_GTPCH-Leu2	Chapter 2; Ehrenworth et al. (2015) *ACS Synth. Biol.* 4, 1295-1307
PPY186	pAME22	pESC-P_{GAL1}-His_6-*M.alpina*_PTPS-Trp1	Chapter 2; Ehrenworth et al. (2015) *ACS Synth. Biol.* 4, 1295-1307
PPY187	pAME23	pESC-P_{GAL1}-His_6-*S.salar*_PTPS-Trp1	Chapter 2; Ehrenworth et al. (2015) *ACS Synth. Biol.* 4, 1295-1307
PPY188	pAME24	pESC-P_{GAL1}-His_6-*S.ruber*_PTPS-Trp1	Chapter 2; Ehrenworth et al. (2015) *ACS Synth. Biol.* 4, 1295-1307

Table A-1. continued

Strain #	Plasmid Name	Description	Source
PPY189	pAME25	pESC-P_{GAL1}-His_6-*P.mikurensis* _PTPS-Trp1	Chapter 2; Ehrenworth et al. (2015) *ACS Synth. Biol.* 4, 1295-1307
PPY190	pAME26	pESC-P_{GAL1}-His_6-*M.alpina*_SR-His3	Chapter 2; Ehrenworth et al. (2015) *ACS Synth. Biol.* 4, 1295-1307
PPY191	pAME28	pESC-P_{GAL1}-His_6-*T.pseudonana*_SR-His3	Chapter 2; Ehrenworth et al. (2015) *ACS Synth. Biol.* 4, 1295-1307
PPY241	pAME27	pESC-P_{GAL1}-His_6-*S.cerevisiae*_SR-His3	Chapter 2; Ehrenworth et al. (2015) *ACS Synth. Biol.* 4, 1295-1307
PPY242	pAME29	pESC-P_{GAL1}-eGFP-Trp1	Chapter 2; Ehrenworth et al. (2015) *ACS Synth. Biol.* 4, 1295-1307
PPY243	pAME30	pESC-P_{GAL1}-eGFP-His3	Chapter 2; Ehrenworth et al. (2015) *ACS Synth. Biol.* 4, 1295-1307
PPY338	pSS102	pESC-Ura3 with divergent P_{HXT7}/ P_{TEF1} promoter	Chapter 2; Ehrenworth et al. (2015) *ACS Synth. Biol.* 4, 1295-1307
PPY435	pCR2.1_DHPR	Codon optimized* DHPR from *H. sapiens*	Chapter 2; Ehrenworth et al. (2015) *ACS Synth. Biol.* 4, 1295-1307
PPY442	pSS42	Codon optimized (for *E. coli)* STR from *O. pumila*	Commercially synthesized for Ehrenworth et al. (2015) *ACS Synth. Biol.* 4, 1295-1307 Sequence from Bernhardt et al. (2010) *Tetrahedron Lett.* 51, 4400-4402
PPY443	pSS43	pESC-Trp1 with divergent P_{TEF1}/P_{ADH1} promoter	Chapter 2; Ehrenworth et al. (2015) *ACS Synth. Biol.* 4, 1295-1307
PPY444	pSS44	Codon optimized* TPH from *H. sapiens*	Chapter 2; Ehrenworth et al. (2015) *ACS Synth. Biol.* 4, 1295-1307

Table A-1. continued

Strain #	Plasmid Name	Description	Source
PPY465	pSS48	Codon optimized* PCD from *H. sapiens*	Chapter 2; Ehrenworth et al. (2015) *ACS Synth. Biol.* 4, 1295-1307
PPY520	pAME22PCD	pESC-P_{GAL1}-His_6-*M.alpina*_PTPS-P_{GAL10}-*H.sapiens*_PCD-Trp1	Chapter 2; Ehrenworth et al. (2015) *ACS Synth. Biol.* 4, 1295-1307
PPY538	pSS61	pESC-P_{GAL1}-STR-Ura3	Chapter 2; Ehrenworth et al. (2015) *ACS Synth. Biol.* 4, 1295-1307
PPY539	pSS62	Codon optimized* DDC from *S. scrofa*	Chapter 2; Ehrenworth et al. (2015) *ACS Synth. Biol.* 4, 1295-1307
PPY555	pAME26DHPR	pESC-P_{GAL1}-His_6-*M.alpina*_SR- P_{GAL10}-*H.sapiens*_DHPR-His3	Chapter 2; Ehrenworth et al. (2015) *ACS Synth. Biol.* 4, 1295-1307
PPY563	pSS64	Codon optimized* TH from *M. musculus*	Chapter 2; Ehrenworth et al. (2015) *ACS Synth. Biol.* 4, 1295-1307
PPY572	pSS66	pESC-P_{GAL1}-His_6-*E.coli*_GTPCH-P_{GAL10}-DDC-Leu2	Chapter 2; Ehrenworth et al. (2015) *ACS Synth. Biol.* 4, 1295-1307
PPY573	pSS67	pESC-P_{GAL1}-NCS-P_{GAL10}-TH-Ura3	Chapter 2; Ehrenworth et al. (2015) *ACS Synth. Biol.* 4, 1295-1307
PPY574	pSS68	pESC-P_{GAL10}-TH-Ura3	Chapter 2; Ehrenworth et al. (2015) *ACS Synth. Biol.* 4, 1295-1307
PPY630	pSS70	pESC-P_{GAL1}-TPH-Ura3	Chapter 2; Ehrenworth et al. (2015) *ACS Synth. Biol.* 4, 1295-1307
PPY631	pSS71	pESC-P_{GAL1}-STR-P_{GAL10}-TPH-Ura3	Chapter 2; Ehrenworth et al. (2015) *ACS Synth. Biol.* 4, 1295-1307
PPY667	pAME54	pRS414-P_{GAL1}-His_6-*M.alpina*_PTPS-Trp1	Chapter 2; Ehrenworth et al. (2015) *ACS Synth. Biol.* 4, 1295-1307

Table A-1. continued

Strain #	Plasmid Name	Description	Source
PPY668	pAME55	pRS415-P_{GAL1}-His_6-*E.coli*_GTPCH-Leu2	Chapter 2; Ehrenworth et al. (2015) *ACS Synth. Biol.* 4, 1295-1307
PPY670	pAME53	pRS413-P_{GAL1}-His_6-*M.alpina*_SR-His3	Chapter 2; Ehrenworth et al. (2015) *ACS Synth. Biol.* 4, 1295-1307
PPY700	pAME56	pESC-P_{HXT7}-DDC-P_{TEF1}-TPH- P_{ADH1}-STR-Trp1	Chapter 2; Ehrenworth et al. (2015) *ACS Synth. Biol.* 4, 1295-1307
PPY701	pAME58	pESC-P_{HXT7}-PCD- P_{TEF1}-DHPR-Ura3	Chapter 2; Ehrenworth et al. (2015) *ACS Synth. Biol.* 4, 1295-1307
PPY704	pAME57	pESC-P_{HXT7}-PTPS-P_{TEF1}-GTPCH-P_{ADH1}-SR-His3	Chapter 2; Ehrenworth et al. (2015) *ACS Synth. Biol.* 4, 1295-1307
PPY723	pAME63	pESC-P_{GAL10}-DDC-Leu2	Chapter 2; Ehrenworth et al. (2015) *ACS Synth. Biol.* 4, 1295-1307
PPY822	pAME64	pESC-P_{GAL1}-STR-His_6-Ura3	Chapter 2; Ehrenworth et al. (2015) *ACS Synth. Biol.* 4, 1295-1307

*"Codon optimized" references commercial codon optimization for *S. cerevisiae* unless otherwise noted (Operon)

Table A-2. Plasmids used in chapter 3

Strain #	Plasmid Name	Description	Source
----	----	DNA fragments of yeast codon optimized 5-HT_{1a}, 5-HT_{1d}, 5-HT_{2b},5-HT_4, 5-HT_{5a}, 5-HT_6, and ZsGreen	Life Technologies
PPY2	pmCherry	Vector carrying mCherry fluorescent protein	Y. Chenoff lab
PPY34	pESC-His3	Yeast shuttle vector with divergent Gal1/Gal10 promoter	Agilent #217451

Table A-2. continued

Strain #	Plasmid Name	Description	Source
PPY35	pESC-Ura3	Yeast shuttle vector with divergent Gal1/Gal10 promoter	Agilent #217454
PPY36	pESC-Trp1	Yeast shuttle vector with divergent Gal1/Gal10 promoter	Agilent #217453
PPY39	pESC-Leu2	Yeast shuttle vector with divergent Gal1/Gal10 promoter	Agilent #217452
PPY111	pKM111	pESC-His3 with divergent P_{TEF1}/P_{ADH1} promoters	Mukherjee et al. (2015) *ACS Synth. Biol.* 4, 1261-1269
PPY186	pAME22	pESC-P_{GAL1}-His_6-*M.alpina*_PTPS-Trp1	Chapter 2; Ehrenworth et al. (2015) *ACS Synth. Biol.* 4, 1295-1307
PPY190	pAME26	pESC-P_{GAL1}-His_6-*M.alpina*_SR-His3	Chapter 2; Ehrenworth et al. (2015) *ACS Synth. Biol.* 4, 1295-1307
PPY572	pSS66	pESC-P_{GAL1}-His_6-*E.coli*_GTPCH-P_{GAL10}-DDC-Leu2	Chapter 2; Ehrenworth et al. (2015) *ACS Synth. Biol.* 4, 1295-1307
PPY586	pKM586	pRS415- P_{FIG1}-eGFP-Leu2	Mukherjee et al. (2015) *ACS Synth. Biol.* 4, 1261-1269
PPY630	pSS70	pESC-P_{GAL1}-TPH-Ura3	Chapter 2; Ehrenworth et al. (2015) *ACS Synth. Biol.* 4, 1295-1307
PPY1191	pTMC14	pESC-P_{TEF1}-5-HT_{2b}-His3	Chapter 3
PPY1192	pTMC18	pESC-P_{TEF1}-5-HT_4-His3	Chapter 3
PPY1193	pTMC22	pESC-P_{TEF1}-5-HT_{5a}-His3	Chapter 3
PPY1194	pTMC26	pESC-P_{TEF1}-5-HT_6-His3	Chapter 3
PPY1378	pTMC40	pESC-P_{TEF1}-5-HT_4-P_{ADH1}-mCherry-His3	Chapter 3
PPY1421	pAME142	pESC-P_{TEF1}-5-HT_{1d}-His3	Chapter 3
PPY1422	pAME144	pESC-P_{TEF1}-5-HT_{1a}-His3	Chapter 3
PPY1443	pAME143	pRS415- P_{FIG1}-ZsGreen-Leu2	Chapter 3

Table A-3. Plasmids used in chapter 4

Strain #	Plasmid Name	Description	Source
PPY15	pRS415	YC-type (centromeric) shuttle vector	ATCC® 87520
PPY32	pCR2.1-AME_1	Commercially synthesized tags T_{HSP60}, T_{COX4}, T_{PHO8}, T_{APE1}, and T_{PRC1}	Eurofins Operon
PPY38	pEGFP	Enhanced Green Fluorescent Protein	F. Storici lab
PPY39	pESC-Leu2	Yeast shuttle vector with divergent Gal1/Gal10 promoter	Agilent Technologies
PPY40	pAME3	pESC-P_{GAL1}-eGFP-Leu2	Chapter 2; Ehrenworth et al. (2015) *ACS Synth. Biol.* 4, 1295-1307
PPY48	pAME7	pESC-P_{GAL1}-T_{HSP60}-eGFP-Leu2	Chapter 4; Ehrenworth et al. (2017) *Biotechnol. Bioeng.*
PPY49	pAME11	pESC-P_{GAL1}-T_{APE1}-eGFP-Leu2	Chapter 4; Ehrenworth et al. (2017) *Biotechnol. Bioeng.*
PPY50	pAME12	pESC-P_{GAL1}-T_{PRC1}-eGFP-Leu2	Chapter 4; Ehrenworth et al. (2017) *Biotechnol. Bioeng.*
PPY71	pAME10	pESC- P_{GAL1}-T_{PHO8}-eGFP-Leu2	Chapter 4; Ehrenworth et al. (2017) *Biotechnol. Bioeng.*
PPY98	pAME9	pESC- P_{GAL1}-T_{POT1}-eGFP-Leu2	Chapter 4; Ehrenworth et al. (2017) *Biotechnol. Bioeng.*
PPY170	pCR2.1-tags2.0	Commercially synthesized tags T_{PDA1} and T_{OLI1}	Eurofins Operon
PPY296	pMH9	pRS415-P_{GAL1}-T_{POT1}-eGFP-Leu2	Chapter 4; Ehrenworth et al. (2017) *Biotechnol. Bioeng.*
PPY297	pMH10	pRS415-P_{GAL1}-T_{PHO8}-eGFP-Leu2	Chapter 4; Ehrenworth et al. (2017) *Biotechnol. Bioeng.*

Table A-3. continued

Strain #	Plasmid Name	Description	Source
PPY298	pMH11	pRS415-P_{GAL1}-T_{APE1}-eGFP-Leu2	Chapter 4; Ehrenworth et al. (2017) *Biotechnol. Bioeng.*
PPY299	pMH12	pRS415-P_{GAL1}-T_{PRC1}-eGFP-Leu2	Chapter 4; Ehrenworth et al. (2017) *Biotechnol. Bioeng.*
PPY308	pMH7	pRS415-P_{GAL1}-T_{HSP60}-eGFP-Leu2	Chapter 4; Ehrenworth et al. (2017) *Biotechnol. Bioeng.*
PPY313	pAME8	pESC-P_{GAL1}-T_{COX4}-eGFP-Leu2	Chapter 4; Ehrenworth et al. (2017) *Biotechnol. Bioeng.*
PPY314	pAME14	pESC-P_{GAL1}-T_{PDA1}-eGFP-Leu2	Chapter 4; Ehrenworth et al. (2017) *Biotechnol. Bioeng.*
PPY315	pAME15	pESC-P_{GAL1}-T_{OLI1}-eGFP-Leu2	Chapter 4; Ehrenworth et al. (2017) *Biotechnol. Bioeng.*
PPY401	pMH8	pRS415-P_{GAL1}-T_{COX4}-eGFP-Leu2	Chapter 4; Ehrenworth et al. (2017) *Biotechnol. Bioeng.*
PPY402	pMH14	pRS415-P_{GAL1}-T_{PDA1}-eGFP-Leu2	Chapter 4; Ehrenworth et al. (2017) *Biotechnol. Bioeng.*
PPY403	pMH15	pRS415-P_{GAL1}-T_{OLI1}-eGFP-Leu2	Chapter 4; Ehrenworth et al. (2017) *Biotechnol. Bioeng.*
PPY931	pAME3s	pESC-P_{GAL1}-eGFP-Leu2	Chapter 4; Ehrenworth et al. (2017) *Biotechnol. Bioeng.*
PPY932	pAME4s	pESC-P_{GAL1}-eGFP-T_{LUC}-Leu2	Chapter 4; Ehrenworth et al. (2017) *Biotechnol. Bioeng.*
PPY933	pAME5s	pESC-P_{GAL1}-eGFP-T_{CAT}-Leu2	Chapter 4; Ehrenworth et al. (2017) *Biotechnol. Bioeng.*

Table A-3. continued

Strain #	Plasmid Name	Description	Source
PPY934	pMH3s	pRS415-P_{GAL1}-eGFP-Leu2	Chapter 4; Ehrenworth et al. (2017) *Biotechnol. Bioeng.*
PPY935	pMH5s	pRS415-P_{GAL1}-eGFP-T_{CAT}-Leu2	Chapter 4; Ehrenworth et al. (2017) *Biotechnol. Bioeng.*
PPY994	pMH4s	pRS415-P_{GAL1}-eGFP-T_{LUC}-Leu2	Chapter 4; Ehrenworth et al. (2017) *Biotechnol. Bioeng.*
PPY1032	pKM1032	pESC-P_{FIG1}-mKate2-P_{TEF1}-eGFP-Leu2	Peralta-Yahya lab
PPY1043	pAME94	pESC-P_{GAL1}-T_{PDA1}-mKate2-Leu2	Chapter 4; Ehrenworth et al. (2017) *Biotechnol. Bioeng.*
PPY1044	pAME97	pESC-P_{GAL1}-mKate2-T_{LUC}-Leu2	Chapter 4; Ehrenworth et al. (2017) *Biotechnol. Bioeng.*
PPY1045	pAME98	pESC-P_{GAL1}-mKate2-T_{CAT}-Leu2	Chapter 4; Ehrenworth et al. (2017) *Biotechnol. Bioeng.*
PPY1046	pAME95	pESC-P_{GAL1}-T_{OLI1}-mKate2-Leu2	Chapter 4; Ehrenworth et al. (2017) *Biotechnol. Bioeng.*
PPY1047	pAME96	pESC-P_{GAL1}-mKate2-Leu2	Chapter 4; Ehrenworth et al. (2017) *Biotechnol. Bioeng.*
PPY1048	pAME100	pESC-P_{GAL1}-T_{PHO8}-mKate2-Leu2	Chapter 4; Ehrenworth et al. (2017) *Biotechnol. Bioeng.*
PPY1049	pAME101	pESC-P_{GAL1}-T_{APE1}-mKate2-Leu2	Chapter 4; Ehrenworth et al. (2017) *Biotechnol. Bioeng.*
PPY1052	pAME92	pESC-P_{GAL1}-T_{HSP60}-mKate2-Leu2	Chapter 4; Ehrenworth et al. (2017) *Biotechnol. Bioeng.*

Table A-3. continued

Strain #	Plasmid Name	Description	Source
PPY1053	pAME102	pESC-P_{GAL1}-T_{PRC1}-mKate2-Leu2	Chapter 4; Ehrenworth et al. (2017) *Biotechnol. Bioeng.*
PPY1057	pAME99	pESC-P_{GAL1}-T_{POT1}-mKate2-Leu2	Chapter 4; Ehrenworth et al. (2017) *Biotechnol. Bioeng.*
PPY1058	pAME93	pESC-P_{GAL1}-T_{COX4}-mKate2-Leu2	Chapter 4; Ehrenworth et al. (2017) *Biotechnol. Bioeng.*
PPY1061	pAME103	pRS415-P_{GAL1}-T_{HSP60}-mKate2-Leu2	Chapter 4; Ehrenworth et al. (2017) *Biotechnol. Bioeng.*
PPY1062	pAME105	pRS415-P_{GAL1}-T_{PDA1}-mKate2-Leu2	Chapter 4; Ehrenworth et al. (2017) *Biotechnol. Bioeng.*
PPY1063	pAME107	pRS415-P_{GAL1}-mKate2-Leu2	Chapter 4; Ehrenworth et al. (2017) *Biotechnol. Bioeng.*
PPY1064	pAME108	pRS415-P_{GAL1}-mKate2-T_{LUC}-Leu2	Chapter 4; Ehrenworth et al. (2017) *Biotechnol. Bioeng.*
PPY1065	pAME109	pRS415-P_{GAL1}-mKate2-T_{CAT}-Leu2	Chapter 4; Ehrenworth et al. (2017) *Biotechnol. Bioeng.*
PPY1066	pAME111	pRS415-P_{GAL1}-T_{PHO8}-mKate2-Leu2	Chapter 4; Ehrenworth et al. (2017) *Biotechnol. Bioeng.*
PPY1067	pAME112	pRS415-P_{GAL1}-T_{APE1}-mKate2-Leu2	Chapter 4; Ehrenworth et al. (2017) *Biotechnol. Bioeng.*
PPY1068	pAME113	pRS415-P_{GAL1}-T_{PRC1}-mKate2-Leu2	Chapter 4; Ehrenworth et al. (2017) *Biotechnol. Bioeng.*
PPY1070	pAME110	pRS415-P_{GAL1}-T_{POT1}-mKate2-Leu2	Chapter 4; Ehrenworth et al. (2017) *Biotechnol. Bioeng.*

Table A-3. continued

Strain #	Plasmid Name	Description	Source
PPY1072	pAME104	pRS415-P_{GAL1}-T_{COX4}-mKate2-Leu2	Chapter 4; Ehrenworth et al. (2017) *Biotechnol. Bioeng.*
PPY1073	pAME106	pRS415-P_{GAL1}-T_{OLI1}-mKate2-Leu2	Chapter 4; Ehrenworth et al. (2017) *Biotechnol. Bioeng.*

APPENDIX B. Tables of Strains

Table B-1. Yeast strains used in chapter 2

Strain #	Name	Description	Source
PPY11	W303	*Saccharomyces cerevisiae* MATa ade2-1 ura3-1 his3-11 trp1-1 leu2-3 leu2-112 can1-100	ATCC® 20835
PPY568	W303-Ade2^{+}	*S. cerevisiae* W303 with a T190G mutation in *Ade2* gene	Chapter 2; Ehrenworth et al. (2015) *ACS Synth. Biol.* 4, 1295-1307
PPY646	W303A-646	W303-Ade2^{+} transformed with pAME17, pAME22PCD, pAME26DHPR, and pSS68	Chapter 2; Ehrenworth et al. (2015) *ACS Synth. Biol.* 4, 1295-1307
PPY649	W303A-649	W303-Ade2^{+} transformed with pSS66, pAME22PCD, pAME26DHPR, and pSS70	Chapter 2; Ehrenworth et al. (2015) *ACS Synth. Biol.* 4, 1295-1307
PPY650	W303A-650	W303-Ade2^{+} transformed with pSS66, pAME22PCD, pAME26DHPR, and pSS71	Chapter 2; Ehrenworth et al. (2015) *ACS Synth. Biol.* 4, 1295-1307
PPY658	W303A-658	W303-Ade2^{+} transformed with pSS66, pAME22PCD, pAME26DHPR, and pSS68	Chapter 2; Ehrenworth et al. (2015) *ACS Synth. Biol.* 4, 1295-1307
PPY679	W303A-679	W303-Ade2^{+} transformed with pAME17, pAME22, pAME26, and pSS68	Chapter 2; Ehrenworth et al. (2015) *ACS Synth. Biol.* 4, 1295-1307
PPY740	W303A-740	W303 Ade2^{+} transformed with pAME56 and pAME57	Chapter 2; Ehrenworth et al. (2015) *ACS Synth. Biol.* 4, 1295-1307
PPY741	W303A-741	W303-Ade2^{+} transformed with pSS66, pAME22, pAME26, and pSS70	Chapter 2; Ehrenworth et al. (2015) *ACS Synth. Biol.* 4, 1295-1307
PPY743	W303A-743	W303 Ade2^{+} transformed with pSS66, pAME22, pAME26, and pSS68	Chapter 2; Ehrenworth et al. (2015) *ACS Synth. Biol.* 4, 1295-1307
PPY744	W303A-744	W303 Ade2^{+} transformed with pAME56, pAME57, and pAME58	Chapter 2; Ehrenworth et al. (2015) *ACS Synth. Biol.* 4, 1295-1307

Table B-1. continued

Strain #	Name	Description	Source
PPY748	W303A-748	W303Ade2^{+} transformed with pAME56, pAME57, and pESC-Ura3	Chapter 2; Ehrenworth et al. (2015) *ACS Synth. Biol.* 4, 1295-1307
PPY749	W303A-57	W303-Ade2^{+} transformed with pAME57	Chapter 2; Ehrenworth et al. (2015) *ACS Synth. Biol.* 4, 1295-1307
PPY750	W303A-555453	W303-Ade2^{+} transformed with pAME55, pAME54, and pAME53	Chapter 2; Ehrenworth et al. (2015) *ACS Synth. Biol.* 4, 1295-1307
PPY751	W303-2226	W303 transformed with pAME22, and pAME26	Chapter 2; Ehrenworth et al. (2015) *ACS Synth. Biol.* 4, 1295-1307
PPY752	W303-172226	W303 transformed with pAME17, pAME22, and pAME26	Chapter 2; Ehrenworth et al. (2015) *ACS Synth. Biol.* 4, 1295-1307
PPY753	W303-172227	W303 transformed with pAME17, pAME22, and pAME27	Chapter 2; Ehrenworth et al. (2015) *ACS Synth. Biol.* 4, 1295-1307
PPY754	W303-172228	W303 transformed with pAME17, pAME22, and pAME28	Chapter 2; Ehrenworth et al. (2015) *ACS Synth. Biol.* 4, 1295-1307
PPY755	W303-172326	W303 transformed with pAME17, pAME23, and pAME26	Chapter 2; Ehrenworth et al. (2015) *ACS Synth. Biol.* 4, 1295-1307
PPY756	W303-172327	W303 transformed with pAME17, pAME23, and pAME27	Chapter 2; Ehrenworth et al. (2015) *ACS Synth. Biol.* 4, 1295-1307
PPY757	W303-172328	W303 transformed with pAME17, pAME23, and pAME28	Chapter 2; Ehrenworth et al. (2015) *ACS Synth. Biol.* 4, 1295-1307
PPY758	W303-172426	W303 transformed with pAME17, pAME24, and pAME26	Chapter 2; Ehrenworth et al. (2015) *ACS Synth. Biol.* 4, 1295-1307
PPY759	W303-172427	W303 transformed with pAME17, pAME24, and pAME27	Chapter 2; Ehrenworth et al. (2015) *ACS Synth. Biol.* 4, 1295-1307

Table B-1. continued

Strain #	Name	Description	Source
PPY760	W303-172428	W303 transformed with pAME17, pAME24, and pAME28	Chapter 2; Ehrenworth et al. (2015) *ACS Synth. Biol.* 4, 1295-1307
PPY761	W303-172526	W303 transformed with pAME17, pAME25, and pAME26	Chapter 2; Ehrenworth et al. (2015) *ACS Synth. Biol.* 4, 1295-1307
PPY762	W303-172527	W303 transformed with pAME17, pAME25, and pAME27	Chapter 2; Ehrenworth et al. (2015) *ACS Synth. Biol.* 4, 1295-1307
PPY763	W303-172528	W303 transformed with pAME17, pAME25, and pAME28	Chapter 2; Ehrenworth et al. (2015) *ACS Synth. Biol.* 4, 1295-1307
PPY764	W303-182226	W303 transformed with pAME18, pAME22, and pAME26	Chapter 2; Ehrenworth et al. (2015) *ACS Synth. Biol.* 4, 1295-1307
PPY765	W303-182227	W303 transformed with pAME18, pAME22, and pAME27	Chapter 2; Ehrenworth et al. (2015) *ACS Synth. Biol.* 4, 1295-1307
PPY766	W303-182228	W303 transformed with pAME18, pAME22, and pAME28	Chapter 2; Ehrenworth et al. (2015) *ACS Synth. Biol.* 4, 1295-1307
PPY767	W303-182326	W303 transformed with pAME18, pAME23, and pAME26	Chapter 2; Ehrenworth et al. (2015) *ACS Synth. Biol.* 4, 1295-1307
PPY768	W303-182327	W303 transformed with pAME18, pAME23, and pAME27	Chapter 2; Ehrenworth et al. (2015) *ACS Synth. Biol.* 4, 1295-1307
PPY769	W303-182528	W303 transformed with pAME18, pAME25, and pAME28	Chapter 2; Ehrenworth et al. (2015) *ACS Synth. Biol.* 4, 1295-1307
PPY770	W303-192427	W303 transformed with pAME19, pAME24, and pAME27	Chapter 2; Ehrenworth et al. (2015) *ACS Synth. Biol.* 4, 1295-1307
PPY771	W303-192428	W303 transformed with pAME19, pAME24, and pAME28	Chapter 2; Ehrenworth et al. (2015) *ACS Synth. Biol.* 4, 1295-1307

Table B-1. continued

Strain #	Name	Description	Source
PPY772	W303-192526	W303 transformed with pAME19, pAME25, and pAME26	Chapter 2; Ehrenworth et al. (2015) *ACS Synth. Biol.* 4, 1295-1307
PPY773	W303-192527	W303 transformed with pAME19, pAME25, and pAME27	Chapter 2; Ehrenworth et al. (2015) *ACS Synth. Biol.* 4, 1295-1307
PPY774	W303-192528	W303 transformed with pAME19, pAME25, and pAME28	Chapter 2; Ehrenworth et al. (2015) *ACS Synth. Biol.* 4, 1295-1307
PPY775	W303-202226	W303 transformed with pAME20, pAME22, and pAME26	Chapter 2; Ehrenworth et al. (2015) *ACS Synth. Biol.* 4, 1295-1307
PPY776	W303-202227	W303 transformed with pAME20, pAME22, and pAME27	Chapter 2; Ehrenworth et al. (2015) *ACS Synth. Biol.* 4, 1295-1307
PPY777	W303-202228	W303 transformed with pAME20, pAME22, and pAME28	Chapter 2; Ehrenworth et al. (2015) *ACS Synth. Biol.* 4, 1295-1307
PPY778	W303-202326	W303 transformed with pAME20, pAME23, and pAME26	Chapter 2; Ehrenworth et al. (2015) *ACS Synth. Biol.* 4, 1295-1307
PPY779	W303-202327	W303 transformed with pAME20, pAME23, and pAME27	Chapter 2; Ehrenworth et al. (2015) *ACS Synth. Biol.* 4, 1295-1307
PPY780	W303-202328	W303 transformed with pAME20, pAME23, and pAME28	Chapter 2; Ehrenworth et al. (2015) *ACS Synth. Biol.* 4, 1295-1307
PPY781	W303-202426	W303 transformed with pAME20, pAME24, and pAME26	Chapter 2; Ehrenworth et al. (2015) *ACS Synth. Biol.* 4, 1295-1307
PPY782	W303-202427	W303 transformed with pAME20, pAME24, and pAME27	Chapter 2; Ehrenworth et al. (2015) *ACS Synth. Biol.* 4, 1295-1307
PPY783	W303-202428	W303 transformed with pAME20, pAME24, and pAME28	Chapter 2; Ehrenworth et al. (2015) *ACS Synth. Biol.* 4, 1295-1307

Table B-1. continued

Strain #	Name	Description	Source
PPY784	W303-202526	W303 transformed with pAME20, pAME25, and pAME26	Chapter 2; Ehrenworth et al. (2015) *ACS Synth. Biol.* 4, 1295-1307
PPY785	W303-202527	W303 transformed with pAME20, pAME25, and pAME27	Chapter 2; Ehrenworth et al. (2015) *ACS Synth. Biol.* 4, 1295-1307
PPY786	W303-202528	W303 transformed with pAME20, pAME25, and pAME28	Chapter 2; Ehrenworth et al. (2015) *ACS Synth. Biol.* 4, 1295-1307
PPY787	W303A-172226	W303-Ade2^{+} transformed with pAME17, pAME22, and pAME26	Chapter 2; Ehrenworth et al. (2015) *ACS Synth. Biol.* 4, 1295-1307
PPY788	W303A-172252	W303-Ade2^{+} transformed with pAME17, pAME22, and pAME52	Chapter 2; Ehrenworth et al. (2015) *ACS Synth. Biol.* 4, 1295-1307
PPY789	W303A-175426	W303-Ade2^{+} transformed with pAME17, pAME54, and pAME26	Chapter 2; Ehrenworth et al. (2015) *ACS Synth. Biol.* 4, 1295-1307
PPY790	W303A-552226	W303-Ade2^{+} transformed with pAME55, pAME22, and pAME26	Chapter 2; Ehrenworth et al. (2015) *ACS Synth. Biol.* 4, 1295-1307
PPY791	W303A-555426	W303-Ade2^{+} transformed with pAME55, pAME54, and pAME26	Chapter 2; Ehrenworth et al. (2015) *ACS Synth. Biol.* 4, 1295-1307
PPY792	W303A-552253	W303-Ade2^{+} transformed with pAME55, pAME22, and pAME53	Chapter 2; Ehrenworth et al. (2015) *ACS Synth. Biol.* 4, 1295-1307
PPY793	W303A-175453	W303-Ade2^{+} transformed with pAME17, pAME54, and pAME53	Chapter 2; Ehrenworth et al. (2015) *ACS Synth. Biol.* 4, 1295-1307
PPY797	W303-182328	W303 transformed with pAME18, pAME23, and pAME28	Chapter 2; Ehrenworth et al. (2015) *ACS Synth. Biol.* 4, 1295-1307
PPY798	W303-182426	W303 transformed with pAME18, pAME24, and pAME26	Chapter 2; Ehrenworth et al. (2015) *ACS Synth. Biol.* 4, 1295-1307

Table B-1. continued

Strain #	Name	Description	Source
PPY799	W303-182427	W303 transformed with pAME18, pAME24, and pAME27	Chapter 2; Ehrenworth et al. (2015) *ACS Synth. Biol.* 4, 1295-1307
PPY800	W303-182428	W303 transformed with pAME18, pAME24, and pAME28	Chapter 2; Ehrenworth et al. (2015) *ACS Synth. Biol.* 4, 1295-1307
PPY801	W303-182526	W303 transformed with pAME18, pAME25, and pAME26	Chapter 2; Ehrenworth et al. (2015) *ACS Synth. Biol.* 4, 1295-1307
PPY802	W303-182527	W303 transformed with pAME18, pAME25, and pAME27	Chapter 2; Ehrenworth et al. (2015) *ACS Synth. Biol.* 4, 1295-1307
PPY803	W303-192226	W303 transformed with pAME19, pAME22, and pAME26	Chapter 2; Ehrenworth et al. (2015) *ACS Synth. Biol.* 4, 1295-1307
PPY804	W303-192227	W303 transformed with pAME19, pAME22, and pAME27	Chapter 2; Ehrenworth et al. (2015) *ACS Synth. Biol.* 4, 1295-1307
PPY805	W303-192228	W303 transformed with pAME19, pAME22, and pAME28	Chapter 2; Ehrenworth et al. (2015) *ACS Synth. Biol.* 4, 1295-1307
PPY806	W303-192326	W303 transformed with pAME19, pAME23, and pAME26	Chapter 2; Ehrenworth et al. (2015) *ACS Synth. Biol.* 4, 1295-1307
PPY807	W303-192327	W303 transformed with pAME19, pAME23, and pAME27	Chapter 2; Ehrenworth et al. (2015) *ACS Synth. Biol.* 4, 1295-1307
PPY808	W303-192328	W303 transformed with pAME19, pAME23, and pAME28	Chapter 2; Ehrenworth et al. (2015) *ACS Synth. Biol.* 4, 1295-1307
PPY809	W303-192426	W303 transformed with pAME19, pAME24, and pAME26	Chapter 2; Ehrenworth et al. (2015) *ACS Synth. Biol.* 4, 1295-1307
PPY810	W303-032930	W303 transformed with pAME3, pAME29, and pAME30	Chapter 2; Ehrenworth et al. (2015) *ACS Synth. Biol.* 4, 1295-1307

Table B-1. continued

Strain #	Name	Description	Source
PPY827	W303A-64	W303 Ade2$^+$ transformed with pAME64	Chapter 2; Ehrenworth et al. (2015) *ACS Synth. Biol.* 4, 1295-1307
PPY828	W303A-ura	W303 Ade2$^+$ transformed with pESC-Ura3	Chapter 2; Ehrenworth et al. (2015) *ACS Synth. Biol.* 4, 1295-1307
PPY835	W303-835	W303 transformed with pAME22, pAME26, and pSS68	Chapter 2; Ehrenworth et al. (2015) *ACS Synth. Biol.* 4, 1295-1307
PPY836	W303-836	W303 transformed with pAME17, pAME22, pAME26, and pSS68	Chapter 2; Ehrenworth et al. (2015) *ACS Synth. Biol.* 4, 1295-1307
PPY946	W303A-946	W303-Ade2$^+$ transformed with pSS68, pESC-Leu2, pESC-His3, and pESC-Trp1	Chapter 2; Ehrenworth et al. (2015) *ACS Synth. Biol.* 4, 1295-1307
PPY947	W303A-947	W303 Ade2$^+$ transformed with pAME63, pSS68, pESC-His3, and pESC-Trp1	Chapter 2; Ehrenworth et al. (2015) *ACS Synth. Biol.* 4, 1295-1307
PPY948	W303A-948	W303 Ade2$^+$ transformed with pAME63, pSS70, pESC-His3, and pESC-Trp1	Chapter 2; Ehrenworth et al. (2015) *ACS Synth. Biol.* 4, 1295-1307
PPY949	W303A-17	W303-Ade2+ expressing pAME17	Chapter 2; Ehrenworth et al. (2015) *ACS Synth. Biol.* 4, 1295-1307
PPY950	W303A-55	W303-Ade2+ expressing pAME55	Chapter 2; Ehrenworth et al. (2015) *ACS Synth. Biol.* 4, 1295-1307
PPY951	W303A-22	W303-Ade2+ expressing pAME22	Chapter 2; Ehrenworth et al. (2015) *ACS Synth. Biol.* 4, 1295-1307
PPY952	W303A-54	W303-Ade2+ expressing pAME54	Chapter 2; Ehrenworth et al. (2015) *ACS Synth. Biol.* 4, 1295-1307
PPY953	W303A-26	W303-Ade2+ expressing pAME26	Chapter 2; Ehrenworth et al. (2015) *ACS Synth. Biol.* 4, 1295-1307

Table B-1. continued

Strain #	Name	Description	Source
PPY954	W303A-53	W303-Ade2+ expressing pAME53	Chapter 2; Ehrenworth et al. (2015) *ACS Synth. Biol.* 4, 1295-1307
PPY955	W303A-955	W303-Ade2^{+} transformed with pSS66, pAME22, pAME26, and pSS71	Chapter 2; Ehrenworth et al. (2015) *ACS Synth. Biol.* 4, 1295-1307

Table B-2. Yeast strains used in chapter 3.

Strain #	Name	Description	Source
PPY140	W303-3Δ	*Saccharomyces cerevisiae* MATa ade2-1 ura3-1 his3-11 trp1-1 leu2-3 leu2-112 can1-100 Δ*far1*, Δ*sst2*, Δ*ste2*	Mukherjee et al. (2015) *ACS Synth. Biol.* 4, 1261-1269
PPY568	W303-Ade2^{+}	*S. cerevisiae* W303 with a T190G mutation in *Ade2* gene	Chapter 2; Ehrenworth et al. (2015) *ACS Synth. Biol.* 4, 1295-1307
PPY741	W303A-741	W303-Ade2^{+} transformed with pSS66, pAME22, pAME26, and pSS70	Chapter 2; Ehrenworth et al. (2015) *ACS Synth. Biol.* 4, 1295-1307
PPY1384	W303-3Δ-1384	PPY140 carrying pTMC14 and pKM586	Chapter 3
PPY1385	W303-3Δ-1385	PPY140 carrying pTMC18 and pKM586	Chapter 3
PPY1386	W303-3Δ-1386	PPY140 carrying pTMC22 and pKM586	Chapter 3
PPY1387	W303-3Δ-1387	PPY140 carrying pTMC26 and pKM586	Chapter 3
PPY1388	W303-3Δ-TMC40	PPY140 carrying pTMC40	Chapter 3
PPY1389	W303-3Δ-KM586	PPY140 carrying pKM586	Chapter 3
PPY1390	W303-3Δ-1390	PPY140 carrying pTMC40 and pKM586	Chapter 3
PPY1391	W303-3Δ-1391	PPY568 carrying pESC-His3, pESC-Ura3, pESC-Trp1, and pESC-Leu2	Chapter 3
PPY1444	W303-3Δ-1444	PPY140 carrying pAME142 and pKM586	Chapter 3
PPY1445	W303-3Δ-1445	PPY140 carrying pAME144 and pKM586	Chapter 3
PPY1446	W303-3Δ-1446	PPY140 carrying pTMC40 and pAME143	Chapter 3

Table B-3. Yeast strains used in chapter 4

Strain #	Name	Description	Source
PPY11	W303	*Saccharomyces cerevisiae* MATa ade2-1 ura3-1 his3-11 trp1-1 leu2-3 leu2-112 can1-100	ATCC® 20835
PPY370	W303-7	W303 transformed with pAME7	Chapter 4; Ehrenworth et al. (2017) *Biotechnol. Bioeng.*
PPY371	W303-8	W303 transformed with pAME8	Chapter 4; Ehrenworth et al. (2017) *Biotechnol. Bioeng.*
PPY372	W303-9	W303 transformed with pAME9	Chapter 4; Ehrenworth et al. (2017) *Biotechnol. Bioeng.*
PPY373	W303-10	W303 transformed with pAME10	Chapter 4; Ehrenworth et al. (2017) *Biotechnol. Bioeng.*
PPY374	W303-11	W303 transformed with pAME11	Chapter 4; Ehrenworth et al. (2017) *Biotechnol. Bioeng.*
PPY375	W303-12	W303 transformed with pAME12	Chapter 4; Ehrenworth et al. (2017) *Biotechnol. Bioeng.*
PPY377	W303-14	W303 transformed with pAME14	Chapter 4; Ehrenworth et al. (2017) *Biotechnol. Bioeng.*
PPY378	W303-15	W303 transformed with pAME15	Chapter 4; Ehrenworth et al. (2017) *Biotechnol. Bioeng.*
PPY382	W303-M7	W303 transformed with pMH7	Chapter 4; Ehrenworth et al. (2017) *Biotechnol. Bioeng.*
PPY383	W303-M9	W303 transformed with pMH9	Chapter 4; Ehrenworth et al. (2017) *Biotechnol. Bioeng.*
PPY384	W303-M10	W303 transformed with pMH10	Chapter 4; Ehrenworth et al. (2017) *Biotechnol. Bioeng.*
PPY385	W303-M11	W303 transformed with pMH11	Chapter 4; Ehrenworth et al. (2017) *Biotechnol. Bioeng.*

Table B-3. continued

Strain #	Name	Description	Source
PPY386	W303-M12	W303 transformed with pMH12	Chapter 4; Ehrenworth et al. (2017) *Biotechnol. Bioeng.*
PPY431	W303-M8	W303 transformed with pMH8	Chapter 4; Ehrenworth et al. (2017) *Biotechnol. Bioeng.*
PPY432	W303-M14	W303 transformed with pMH14	Chapter 4; Ehrenworth et al. (2017) *Biotechnol. Bioeng.*
PPY433	W303-M15	W303 transformed with pMH15	Chapter 4; Ehrenworth et al. (2017) *Biotechnol. Bioeng.*
PPY1014	W303-3s	W303 transformed with pAME3s	Chapter 4; Ehrenworth et al. (2017) *Biotechnol. Bioeng.*
PPY1015	W303-4s	W303 transformed with pAME4s	Chapter 4; Ehrenworth et al. (2017) *Biotechnol. Bioeng.*
PPY1016	W303-5s	W303 transformed with pAME5s	Chapter 4; Ehrenworth et al. (2017) *Biotechnol. Bioeng.*
PPY1017	W303-M3s	W303 transformed with pMH3s	Chapter 4; Ehrenworth et al. (2017) *Biotechnol. Bioeng.*
PPY1018	W303-M4s	W303 transformed with pMH4s	Chapter 4; Ehrenworth et al. (2017) *Biotechnol. Bioeng.*
PPY1019	W303-M5s	W303 transformed with pMH5s	Chapter 4; Ehrenworth et al. (2017) *Biotechnol. Bioeng.*
PPY1020	W303-pESCLeu2	W303 transformed with pESC-Leu2	Chapter 4; Ehrenworth et al. (2017) *Biotechnol. Bioeng.*
PPY1021	W303-pRS415	W303 transformed with pRS415	Chapter 4; Ehrenworth et al. (2017) *Biotechnol. Bioeng.*
PPY1343	W303-pAME92	W303 transformed with pAME92	Chapter 4; Ehrenworth et al. (2017) *Biotechnol. Bioeng.*

Table B-3. continued

Strain #	Name	Description	Source
PPY1344	W303-pAME93	W303 transformed with pAME93	Chapter 4; Ehrenworth et al. (2017) *Biotechnol. Bioeng.*
PPY1345	W303-pAME94	W303 transformed with pAME94	Chapter 4; Ehrenworth et al. (2017) *Biotechnol. Bioeng.*
PPY1346	W303-pAME95	W303 transformed with pAME95	Chapter 4; Ehrenworth et al. (2017) *Biotechnol. Bioeng.*
PPY1347	W303-pAME96	W303 transformed with pAME96	Chapter 4; Ehrenworth et al. (2017) *Biotechnol. Bioeng.*
PPY1348	W303-pAME97	W303 transformed with pAME97	Chapter 4; Ehrenworth et al. (2017) *Biotechnol. Bioeng.*
PPY1349	W303-pAME98	W303 transformed with pAME98	Chapter 4; Ehrenworth et al. (2017) *Biotechnol. Bioeng.*
PPY1350	W303-pAME99	W303 transformed with pAME99	Chapter 4; Ehrenworth et al. (2017) *Biotechnol. Bioeng.*
PPY1351	W303-pAME100	W303 transformed with pAME100	Chapter 4; Ehrenworth et al. (2017) *Biotechnol. Bioeng.*
PPY1352	W303-pAME101	W303 transformed with pAME101	Chapter 4; Ehrenworth et al. (2017) *Biotechnol. Bioeng.*
PPY1353	W303-pAME102	W303 transformed with pAME102	Chapter 4; Ehrenworth et al. (2017) *Biotechnol. Bioeng.*
PPY1354	W303-pAME103	W303 transformed with pAME103	Chapter 4; Ehrenworth et al. (2017) *Biotechnol. Bioeng.*
PPY1355	W303-pAME104	W303 transformed with pAME104	Chapter 4; Ehrenworth et al. (2017) *Biotechnol. Bioeng.*
PPY1356	W303-pAME105	W303 transformed with pAME105	Chapter 4; Ehrenworth et al. (2017) *Biotechnol. Bioeng.*

Table B-3. continued

Strain #	Name	Description	Source
PPY1357	W303-pAME106	W303 transformed with pAME106	Chapter 4; Ehrenworth et al. (2017) *Biotechnol. Bioeng.*
PPY1358	W303-pAME107	W303 transformed with pAME107	Chapter 4; Ehrenworth et al. (2017) *Biotechnol. Bioeng.*
PPY1359	W303-pAME108	W303 transformed with pAME108	Chapter 4; Ehrenworth et al. (2017) *Biotechnol. Bioeng.*
PPY1360	W303-pAME109	W303 transformed with pAME109	Chapter 4; Ehrenworth et al. (2017) *Biotechnol. Bioeng.*
PPY1361	W303-pAME110	W303 transformed with pAME110	Chapter 4; Ehrenworth et al. (2017) *Biotechnol. Bioeng.*
PPY1362	W303-pAME111	W303 transformed with pAME111	Chapter 4; Ehrenworth et al. (2017) *Biotechnol. Bioeng.*
PPY1363	W303-pAME112	W303 transformed with pAME112	Chapter 4; Ehrenworth et al. (2017) *Biotechnol. Bioeng.*
PPY1364	W303-pAME113	W303 transformed with pAME113	Chapter 4; Ehrenworth et al. (2017) *Biotechnol. Bioeng.*

APPENDIX C. Table of Primers

Table C-1. Table of primers used in this work

Name	Sequence (5' -> 3')	Chapters used in
ACT1-F	TTGGATTCCGGTGATGGTGT	2
ACT1-R	CGGCCAAATCGATTCTCAAA	2
AME103	TCTTAGCTAGCCGCGGTACCAAGCTTTTACAAACTCAAGAAGGACCATG	4
AME104	CACTTTAACTAATACTTTCAAC	2; 4
AME105	TAAATAACGTTCTTAATACTAAC	2; 3; 4
AME108	CGTCAAGGAGAAAAAACCCCGGATCCATGTTGAGATCATCCGTTGT	4
AME109	AGCTCCTCGCCCTTGCTCACGTAAGCACGACGCAATAAAG	4
AME110	CGTCAAGGAGAAAAAACCCCGGATCCATGCTTTCACTACGTCAATC	4
AME111	AGCTCCTCGCCCTTGCTCACAAGCAGATATCTAGAGCTAC	4
AME114	CGTCAAGGAGAAAAAACCCCGGATCCATGATGACTCACACATTACCA	4
AME115	AGCTCCTCGCCCTTGCTCACTCCAGGAACAAGACGTGTC	4
AME116	CGTCAAGGAGAAAAAACCCCGGATCCATGGAGGAACAACGTGAAAT	4
AME117	AGCTCCTCGCCCTTGCTCACGAGGATGCACCACGAATTT	4
AME118	CGTCAAGGAGAAAAAACCCCGGATCCATGAAAGCATTCACCAGTTTA	4
AME119	AGCTCCTCGCCCTTGCTCACGAGATGATCCAGGTCGAG	4
AME121	TCTTAGCTAGCCGCGGTACCTTATAATTTGGACTTGTACAGCTCGTCCATG	4
AME122	TCTTAGCTAGCCGCGGTACCTTACAAATTAGCTTTCTTGTACAGCTCGTCCATG	4
AME123	CGTCAAGGAGAAAAAACCCCGGATCCATCACGTGCACCATGGTGAGCAAGGGCGAG	2

Table C-1. continued

Name	Sequence (5' -> 3')	Chapters used in
AME124	TCTTAGCTAGCCGCGGTACCAAGCTTTTACTTGTAC AGCTCGTCC	2; 4
AME128	CTGGAGAAGGGTAAATTTTTA	2
AME133	CGTCAAGGAGAAAAAACCCCGGATCCATGTCTCAA AGACTACAAAGTATCAAGGATCATTTGGTGTTGAG CGCCGTGAGCAAGGGCGAGG	4
AME135	TCTTAGCTAGCCGCGGTACCAAGCTTTTAGTTGTGA TGACGCACAGC	2
AME137	TCTTAGCTAGCCGCGGTACCAAGCTTTTAAATACTT CTTCTTCCTAAAAG	2
AME139	TCTTAGCTAGCCGCGGTACCAAGCTTTTAAGATCTA ATCAAAGTCAAG	2
AME140	CGTCAAGGAGAAAAAACCCCGGATCCATCACGTGC ACCATGCATCACCATCACCATCACCCATCACTCAGT AAAGAAGC	2
AME141	CGTCAAGGAGAAAAAACCCCGGATCCATCACGTGC ACCATGCATCACCATCACCATCACGAGAAAGGTCC AGTTAGAG	2
AME142	CGTCAAGGAGAAAAAACCCCGGATCCATCACGTGC ACCATGCATCACCATCACCATCACCATAACATCCA ATTAGTGCAA	2
AME143	CGTCAAGGAGAAAAAACCCCGGATCCATCACGTGC ACCATGCATCACCATCACCATCACTCCCATACTCCA ACCTCTC	2
AME144	TCTTAGCTAGCCGCGGTACCAAGCTTTTAAACACCT CTTCTTCTAATC	2
AME147	CGTCAAGGAGAAAAAACCCCGGATCCATCACGTGC ACCATGCATCACCATCACCATCACGCTCAAGCTGA TTCCAGAA	2
AME148	TCTTAGCTAGCCGCGGTACCAAGCTTTTATTCACCT CTGTAGACAAC	2
AME149	CGTCAAGGAGAAAAAACCCCGGATCCATCACGTGC ACCATGCATCACCATCACCATCACACCTCCTCAACT CCAGTTA	2
AME150	TCTTAGCTAGCCGCGGTACCAAGCTTTTATTCACCT CTGTAAACGAC	2

Table C-1. continued

Name	Sequence (5' -> 3')	Chapters used in
AME151	CGTCAAGGAGAAAAAACCCCGGATCCATCACGTGC ACCATGCATCACCATCACCATCACTCCACCGTTTAC ATTACCAG	2
AME152	TCTTAGCTAGCCGCGGTACCAAGCTTTTATTCACCT CTGTATTCAAC	2
AME153	CGTCAAGGAGAAAAAACCCCGGATCCATCACGTGC ACCATGCATCACCATCACCATCACTTTGAATTGACT AGAACTTTAAG	2
AME154	TCTTAGCTAGCCGCGGTACCAAGCTTTTAACCACCT CTATAAGCAC	2
AME155	CGTCAAGGAGAAAAAACCCCGGATCCATGCTTGCT GCTTCATTCAA	4
AME156	AGCTCCTCGCCCTTGCTCACATGACCTATCCTGGTG GG	4
AME157	CGTCAAGGAGAAAAAACCCCGGATCCATGCAATTA GTATTAGCAGC	4
AME158	AGCTCCTCGCCCTTGCTCACTGAAACCATTAAACAG AATAAAC	4
AME161	CATAACATCCAATTAGTGCAA	2
AME162	AATACTTCTTCTTCCTAAAAG	2
AME163	CCATCACTCAGTAAAGAAGC	2
AME164	GTTGTGATGACGCACAGC	2
AME165	CGTCAAGGAGAAAAAACCCCGGATCCATCACGTGC ACCATGCATCACCATCACCATC	2
AME166	TCTTAGCTAGCCGCGGTACCAAGCTTTTATTCATCG TAGAAATCAATAT	2
AME167	TCTTAGCTAGCCGCGGTACCAAGCTTTTAAACATCG AAGTAATCAACA	2
AME168	GGTAAAGTTATTTTAGTTACAG	2
AME169	AGGCATAAAGTCCGCCAAG	2
AME180	TCTTAGCTAGCCGCGGTACCAAGCTTTTAAGGCATA AAGTCCGCCAAG	2
AME183	CGTCAAGGAGAAAAAACCCCGGATCCATCACGTGC ACCATGCATCACCATCACCATCACGGTAAAGTTATT TTAGTTACAG	2
AME184	TCGAGGTCGACGGTATCGATAAGCTTGAGCGACCT CATGCTATAC	2; 4

Table C-1. continued

Name	Sequence (5' -> 3')	Chapters used in
AME185	GCGGCCGCTCTAGAACTAGTGGATCCCTTCGAGCG TCCCAAAAC	2; 4
AME229	ACGTATCTACCAACGATTTG	2; 3
AME230	GTATATGGATATGTATATGGTG	2
AME231	AAGCTTGGTACCGCGGC	4
AME232	AAGCAGATATCTAGAGCTAC	4
AME241	AATTCAACCCTCACTAAAGGGCGGCCGCATGGCAG CTGCTGCAGC	2
AME242	GGCGAAGAATTGTTAATTAAGAGCTCTTAGAAATA AGCTGGAGTCAA	2
AME245	GGCTCCTTTTCCAATCCTCTTGATATCGAAAAACTA GCTGAAAAATGTGATGTGCTAACGATTGAGATTGA GCATGTTGA	2
AME246	TCAACATGCTCAATCTCAATCGTTAGCACATCACAT TTTTCAGCTAGTTTTTCGATATCAAGAGGATTGGAA AAGGAGCC	2
AME247	AAGACGGTAATACTAGATGC	2
AME363	TGTAATCCATCGATACTAGTTTATTCACCTCTGTAA ACGAC	2
AME364	ATTTTAATCAAAAAGCGACCATGACCTCCTCAACTC CAG	2
AME365	GGTCGCTTTTTGATTAAAATTAAAAAAACTTT	2
AME366	GGTGGCTGTAATTAAAACTTAGATTAGATT	2
AME367	AAGTTTTAATTACAGCCACCATGCCATCACTCAGTA AAGA	2
AME368	TTAATAAAAGTGTTCGCAAATTAGTTGTGATGACG CACAG	2
AME369	TTTGCGAACACTTTTATTAATTC	2
AME370	TCTTTAAAGTTTCTTTGTCTCC	2
AME371	AGACAAAGAAACTTTAAAGAATCCTTTTGTTGTTTC CGGG	2
AME372	GGTCGGTGTATATGAGATAGTTGATTGT	2
AME373	CTATCTCATATACACCGACCATGTCATCCAAAGAA CATCAT	2
AME374	CCTATAGTGAGTCGTATTACTTATTCATCGTAGAAA TCAATATG	2

Table C-1. continued

Name	Sequence (5' -> 3')	Chapters used in
AME375	TGTAATCCATCGATACTAGTTTAAGTCATGGAGAC AGCG	2
AME376	ATTTTAATCAAAAAGCGACCATGGCTGGTAAAGCT CATAG	2
AME377	AAGTTTTAATTACAGCCACCATGGCAGCTGCTGCA GC	2
AME378	TTAATAAAAGTGTTCGCAAATTAGAAATAAGCTGG AGTCAA	2
AME383	CCTATAGTGAGTCGTATTACTGTATATGAGATAGTT GATTGT	2
AME384	TGTAATCCATCGATACTAGTTTAAGATTTAATTTCA GCTTTAC	2
AME385	ATTTTAATCAAAAAGCGACCATGAATGCTTCTGATT TTAGAA	2
AME386	AAGTTTTAATTACAGCCACCATGGAAGAATTGGAA GATGTT	2
AME387	TTAATAAAAGTGTTCGCAAATTAAGTATCCTTCAAA ATTTCAA	2
AME388	CTATCTCATATACACCGACCATGGGCTCTCCTGAGT TTT	2
AME389	CCTATAGTGAGTCGTATTACTTAAGATCCAAACGA AGAGAA	2
AME394	GTAATACGACTCACTA	2
AME395	ACTAGTATCGATGGATTACAA	2
AME396	CATTTGCAGCTATTGTAAAATA	2
AME397	CTCAAGTTTCAGTTTCATTTTT	2; 3
AME406	TCTTAGCTAGCCGCGGTACCTTAGTGATGGTGATGG TGATGAGATCCAAACGAAGAGAAC	2
AME415	GTGACTCTTAGGTTTTAAAAC	4
AME440	CGTCAAGGAGAAAAAACCCCGGATCCATGGTGAGC AAGGGCGAG	4
AME441	CACAAGGGTCCATAACAGC	2
AME442	ACGGTCATAATTACAAGGTTG	2
AME443	CGATGAAATGGTCACCGTG	2
AME444	GACAGACCGATCACCGAAT	2
AME445	CTGGCAAGAAGCTAGATCC	2

Table C-1. continued

Name	Sequence (5' -> 3')	Chapters used in
AME446	GTTCTATGATCTGGATATTGTT	2
AME484	TGTTCTCCTTAATCAGCTCGCTCACGTAAGCACGACGCAATAAAG	4
AME485	TGTTCTCCTTAATCAGCTCGCTCACGGCGCTCAACACCAAATG	4
AME486	TGTTCTCCTTAATCAGCTCGCTCACTCCAGGAACAAGACGTGTC	4
AME487	TGTTCTCCTTAATCAGCTCGCTCACGAGGATGCACCACGAATTT	4
AME488	TGTTCTCCTTAATCAGCTCGCTCACGAGATGATCCAGGTCGAG	4
AME489	TGTTCTCCTTAATCAGCTCGCTCACATGACCTATCCTGGTGGG	4
AME490	TGTTCTCCTTAATCAGCTCGCTCACTGAAACCATTAAACAGAATAAAC	4
AME491	GTGAGCGAGCTGATTAAGG	4
AME492	TTTAACGTCAAGGAGAAAAAACCCCGGATCCATGGTGAGCGAGCTGATTA	4
AME493	CTTAGCTAGCCGCGGTAC	4
AME494	TTTGTGTAGCTCTAGATATCTGCTTGTGAGCGAGCTGATTAAGG	4
AME495	GAGCGGATCTTAGCTAGCCGCGGTACCTTACAAATTAGCTTTTCTGTGCCCCAGTTTGCT	4
AME496	TTAGAGCGGATCTTAGCTAGCCGCGGTACCTTATAATTTGGATCTGTGCCCCAGTTTGCT	4
AME519	TTCGGTTAGAGCGGATCTT	3
AME536	ATCTAATCTAAGTTTTAATTACAAAGGATCCATGGTTCCAGAACCAGGTC	3
AME538	ATCTAATCTAAGTTTTAATTACAAAGGATCCATGGATAAGTTGGATGCTAAC	3
AME542	ATCTAATCTAAGTTTTAATTACAAAGGATCCATGGATTTGCCAGTTAACTTG	3
AME544	ATCTAATCTAAGTTTTAATTACAAAGGATCCATGGCTTTGTCCTATAGAGT	3
AME570	ATACAATCAACTATCTCATATACAGCGGCCGCATGGTGAGCAAGGGCGAG	3

Table C-1. continued

Name	Sequence (5' -> 3')	Chapters used in
AME571	CTGGCGAAGAATTGTTAATTAAGAGCTCTTATAATTTGGACTTGTACAGC	3
AME648	ACAAAAAAAAAAAAAAAAAAGGATCCATGGCTCAATCTAAGCATGG	3
AMEACT-F	TTCTGAGGTTGCTGCTTTGG	4
AMEACT-R	ACCGACGATAGATGGGAAGAC	4
AMEGFP-F	TCAAGATCCGCCACAACATC	4
AMEGFP-R	GTGCTCAGGTAGTGGTTGTC	4
MH100	ACGTTGTAAAACGACGGCC	2; 4
MH101	CTATGACCATGATTACGCC	2; 4
SS112	GACAACCTTGATTGGAGA	2
SS152	GGCGAAGAATTGTTAATTAATTAAGTCATGGAGACAGC	2
SS153	AATTCAACCCTCACTAAAGGATGGCTGGTAAAGCTC	2
SS157	TGGCGAAGAATTGTTAATTAATTAAGATTTAATTTCAGCTTTACCTTC	2
SS158	GAATTCAACCCTCACTAAAGGATGAATGCTTCTGATTTTAGAAG	2
SS159	CGTCAAGGAGAAAAAACCCCATGGGCTCTCCTGAG	2
SS160	TCTTAGCTAGCCGCGGTACCTTAAGATCCAAACGAAGAGA	2
SS177	GGCGAAGAATTGTTAATTAATTAAGTATCCTTCAAAATTTCAATG	2
SS178	AATTCAACCCTCACTAAAGGATGGAAGAATTGGAAGATGT	2
SS179	GGCGAAGAATTGTTAATTAATTAAGAAATAGCAGACAATGCT	2
SS180	AATTCAACCCTCACTAAAGGATGCCAACTCCATCC	2
SS207	CGTCAAGGAGAAAAAACCCCATGGAAGAATTGGAAGATGT	2
SS208	TCTTAGCTAGCCGCGGTACCTTAAGTATCCTTCAAAATTTCAATG	2

APPENDIX D. DNA Sequences

DNA synthesized for chapter 2:

Escherichia coli GTP cyclohydrolase I (P0A6T5)

```
ATGCCATCACTCAGTAAAGAAGCGGCCCTGGTTCATGAAGCGTTAGTTGCGCGAGGACT
GGAAACACCGCTGCGCCCGCCCGTGCATGAAATGGATAACGAAACGCGCAAAAGCCTTA
TTGCTGGTCATATGACCGAAATCATGCAGCTGCTGAATCTCGACCTGGCTGATGACAGT
TTGATGGAAACGCCGCATCGCATCGCTAAAATGTATGTCGATGAAATTTTCTCCGGTCT
GGATTACGCCAATTTCCCGAAAATCACCCTCATTGAAAACAAAATGAAGGTCGATGAAA
TGGTCACCGTGCGCGATATCACTCTGACCAGCACCTGTGAACACCATTTTGTTACCATC
GATGGCAAAGCGACGGTGGCCTATATCCCGAAAGATTCGGTGATCGGTCTGTCAAAAAT
TAACCGCATTGTGCAGTTCTTTGCCCAGCGTCCGCAGGTGCAGGAACGTCTGACGCAGC
AAATTCTTATTGCGCTACAAACGCTGCTGGGCACCAATAACGTGGCTGTCTCGATCGAC
GCGGTGCATTACTGCGTGAAGGCGCGTGGCATCCGCGATGCAACCAGTGCCACGACAAC
GACCTCTCTTGGTGGATTGTTCAAATCCAGTCAGAATACGCGCCACGAGTTTCTGCGCG
CTGTGCGTCATCACAACTAA
```

Mortierella alpina GTP cyclohydrolase I (G3FNL6)

```
ATGTCCCATACTCCAACCTCTCCAAAGACCGCTTCCTCTGTTGAATTGGTTCATCCAAC
CGCAAAGCAAGCATTGTTGAACCACGCTTTGACTGGTCATTCCCATTCCTCTGGTAGAT
CCTACTTGAAGTCCGAATCTCCAGAAGGTAGATCCGCTACTCCAATTGATTTCGACGGT
TTATCCTTTCCATCCATTGGTGCTAGAGATAGAAGAGAAGATACCGAAGAACAAAGAGC
TGCTAGAATTGAGAAGATAGCTGGTTCCGTTAGAACCATTTTGGAGTGTATTGGTGAAG
ATCCAGATAGAGAAGGTTTGTTGAAGACTCCAGAAAGATACGCTAAGGCATTGATGTTC
TTCTCCAAAGGTTACGAAGAATCCGTTACTCATTTGATGAATAAGGCATTATTTCAAGA
AGATCACGACGAAATGGTTATTGTTAAAGATATTGACGTTTTCTCCTTGTGTGAACATC
ATATGGTTCCATTTACTGGTAAGATTCATATTGGTTACATTCCAAAGAACGGTAAGGTT
GTTGGTTTGTCCAAAATTGCTAGATTGGCTGAAATGTTTTCCAGAAGATTGCAAGTTCA
AGAAAGATTGACCAAACAAGTTGCTATGGCTTTGCAAGAATTGTTAGATCCATTGGGTG
TTGCTGTTGTTATGGAAGCATCTCATTTCTGTATGGTTATGAGAGGTGTTCAAAAGCCA
GGTTCTCAAACCATTACCTCCTCTATGTTTGGTTGTTTTAGAGATCAAGGTAAAACCAG
AGAAGAGTTCTTGTCCTTGATTAGAAGAAGAGGTGTTTAA
```

Saccharomyces cerevisiae GTP cyclohydrolase I (P51601）

```
ATGCATAACATCCAATTAGTGCAAGAGATAGAAAGACATGAAACCCCGTTAAACATTAG
ACCTACCTCTCCATACACTTTAAACCCTCCTGTCGAGAGAGATGGGTTTTCTTGGCCAA
GTGTGGGTACAAGACAACGTGCAGAGGAAACTGAAGAGGAGGAAAAGGAACGAATTCAA
CGCATTTCAGGCGCTATCAAGACAATTTTGACCGAACTGGGTGAAGATGTCAACAGAGA
AGGTCTACTAGATACTCCACAAAGATACGCTAAAGCCATGCTTTATTTCACTAAAGGTT
ACCAAACGAACATTATGGACGATGTCATTAAGAATGCTGTCTTTGAAGAAGATCATGAT
GAAATGGTTATTGTTCGTGATATTGAAATTTACTCGTTATGTGAACATCATTTGGTGCC
```

ATTTTTCGGCAAGGTTCATATCGGGTATATACCAAATAAAAAAGTCATCGGGTTAAGTA
AGTTGGCCAGATTGGCAGAAATGTATGCGAGAAGGCTCCAAGTTCAAGAAAGACTTACA
AAGCAAATTGCAATGGCCCTAAGTGATATTCTAAAACCATTAGGTGTAGCCGTTGTTAT
GGAAGCTTCTCATATGTGCATGGTTTCAAGAGGCATTCAAAAAACGGGATCTTCTACGG
TAACTTCTTGTATGCTTGGAGGGTTTAGGGCTCATAAAACAAGAGAAGAGTTTTTAACT
CTTTTAGGAAGAAGAAGTATTTAA

Homo sapiens GTP cyclohydrolase I (P30793-1)

ATGGAGAAAGGTCCAGTTAGAGCTCCAGCAGAGAAGCCAAGAGGTGCTAGATGTTCTAA
CGGATTTCCAGAAAGAGATCCTCCAAGACCAGGTCCTTCTAGACCAGCTGAGAAACCAC
CTAGACCAGAAGCTAAATCTGCTCAACCAGCTGACGGTTGGAAAGGTGAAAGACCAAGA
TCTGAAGAGGACAACGAATTGAATCTACCAAATCTAGCTGCCGCTTATTCATCTATCTT
GTCTTCCTTGGGAGAGAATCCACAAAGACAAGGTCTATTGAAGACTCCTTGGAGAGCTG
CCTCTGCTATGCAATTCTTTACTAAAGGTTATCAAGAAACTATTTCTGACGTTTTGAAC
GACGCAATCTTCGACGAGGATCACGACGAGATGGTTATTGTCAAAGATATTGATATGTT
CTCTATGTGTGAACACCACTTGGTTCCATTTGTTGGTAAAGTTCACATTGGTTATTTGC
CTAATAAGCAAGTTTTGGGTTTGTCTAAATTGGCTAGAATTGTTGAAATCTATTCTAGA
AGATTGCAAGTTCAAGAAAGATTGACTAAACAAATTGCTGTTGCTATTACTGAAGCATT
GAGACCAGCAGGTGTTGGTGTTGTCGTTGAAGCTACTCACATGTGTATGGTTATGAGAG
GTGTTCAGAAGATGAACTCTAAGACTGTTACTTCTACTATGTTGGGTGTCTTTAGAGAA
GATCCAAAGACTAGAGAAGAGTTCTTGACTTTGATTAGATCTTAA

Mortierella alpina 6-pyruvoyl tetrahydrobiopterin synthase (G3FNL7)

ATGACCTCCTCAACTCCAGTTAGAACTGCTTACGTTACCAGAATTGAACATTTCTCCGC
TGCTCATAGATTGAATTCCGTTCATTTGTCTCCTGCTGAAAACGTTAAGTTGTTCGGTA
AGTGTAATCATACTTCCGGTCACGGTCATAATTACAAGGTTGAAGTTACCATTAAAGGT
CAAATTAATCCACAATCCGGTATGGTTATTAACATTACCGATTTGAAGAAGACCTTGCA
AGTTGCTGTTATGGACCCTTGTGATCATAGAAATTTGGATATTGATGTTCCATACTTCG
AATCCAGACCATCCACCACTGAAAACTTGGCTGTCTTCTTGTGGGAAAACATTAAGTCC
CATTTGCCACCATCCGATGCTTACGATTTGTACGAAATTAAGTTGCACGAAACCGATAA
GAACGTTGTCGTTTACAGAGGTGAATAA

Salmo salar 6-pyruvoyl tetrahydrobiopterin synthase (B5XE18)

ATGGCTCAAGCTGATTCCAGAAACGAAGTTGCTGAAAGAATTGGTTACATTACCAGAGT
TCAATCCTTCTCCGCTTGTCATAGATTGCATTCCCCAACCTTGTCCGATGAAGTCAACA
AGAGAATCTTCGGTAAGTGTAACAATCCAAACGGTCACGGTCATAACTACAAGGTTGAA
GTCACCGTCAGAGGTAAGATTGATAGACATACTGGTATGGTCATGAACATTACCGATTT
GAAGCAACATATTGAAGAAGTCATTATGATTCCATTGGATCATAAGAATTTGGATAAGG
ACGTTCCATACTTTGCTAACGTTGTCTCTACTACCGAAAACGTTGCTGTCTACATTTGG
GATAACATGGTTAAGCAATTGCCAGCTAACTTGTTGTACGAAGTTAAGATTCACGAAAC
CGATAAGAACATTGTTGTCTACAGAGGTGAATAA

Salinibacter ruber 6-carboxy-5,6,7,8-tetrahydropterin synthase (Q2RYU6)

ATGTCCACCGTTTACATTACCAGAAAGGTTCATTTCAACGCTGCTCATAGATTGCATAA
TCCAAATAAGTCCGATGCTTGGAACGAAGATACCTACGGTAAGGATAACAATCCAAACT
GGCATGGTCATAACTACGAATTGGAAGTCACCGTTGCTGGTGAACCAGATCCAGAAACC
GGTTACGTTGTCGATTTGGGTGTCTTGAAGGATATTTTGCATGATAGAGTTTTGGATAA
GGTTGATCATAAGAACTTGAACTTGGAAGTCGATTTCATGGATGGTGTTATTCCTTCCT
CTGAAAACTTCGCTATTGCTATTTGGAATGAAATTGAAGATGCTTTGCCAAACGGTGAA
TTGCATTGTGTCAGATTGTACGAAACTCCAAGAAACTTCGTTGAATACAGAGGTGAATA
A

Phycisphaera mikurensis Putative 6-pyruvoyl tetrahydrobiopterin synthase (I0IIJ5)

ATGTTTGAATTGACTAGAACTTTAAGATTTTGTCCATCTGGTGATCCAGGTGCTCCAAG
AGATAACGCTCATGCTGCTTGGCCACCACCAAGAGGTTTAGCAGGTGTATTATCTTTAG
ATTTGACTATTGCTGGTAGACCAGATCCAGGTACTGGTGTTTTATTGAACGTTAAAGAT
TTAGATGCAGCTTTTGCTGCCGCTGCATTACCAAGATTCAGAGCAGCTGCAGGTGCTGA
ACCAGCAGGTTTATTGAGAGGTGTTGCTCAAGCATTAGCTCCTACTTTACCATTTCCAT
TGTTAAGATTGAGATTATCTGCATCTGCTTCAGCTTCTACTGAATTGAGACCAGCTGAT
ATGTCTAGAGTTATTTTGAGACAAAGATTCTCTTTCTCTGCTGCTCATAGATTACAAGC
TGATGCTTTGTCTGAAGAGGAAAATAGAACATTGTTTGGTAAGTGTAATAGACCATCTT
TTCATGGTCATAATTACGAATTAGAAGTTGCTGCAGCCGCTGCTATTGCTCCAGATGGT
AGATCTTTAGAACCAGCTGCATTAGATGCTGCTGTTAGAACTAGAGTCATTGATACTTT
AGATCATAGAAATTTGAATACTGATGTTGCTGCTTTTGCTACTAGAAATCCAACTGTTG
AACATATTGCTCAAACTTGTTGGGATTTGTTAGCTGGTGGTTTACCAGAAGGTGCAGAA
TTACAAGAAGTTGTAGTTTGGGAAACTGATAGAACATCTTGTGCTTATAGAGGTGGTTA
A

Mortierella alpina Sepiapterin reductase (G3FNL8)

ATGTCATCCAAAGAACATCATTTGGTTATTATTAACGGTGTTAATAGAGGTTTTGGTCA
TTCCGTTGCATTGGATTACATAAGACATTCAGGTGCTCATGCTGTTTCCTTTGTTTTGG
TTGGTAGAACTCAACATTCCTTGGAACAAGTTTTGACTGAATTGCATGAAGCTGCATCT
CATGCTGGTGTTGTCTTCAAGGGTGTCGTTGTCTCCGAAGTTGATTTGGCTCATTTGAA
CTCTTTGGATTCTAATTTGGCTAGAATACAATCTGCTGCAGCTGATTTGAGAGACGAAG
CTGCACAATCTACCAGAACTATTACTAAGTCTGTTTTGTTTAATAACGCTGGTTCATTG
GGTGATTTGTCCAAGACTGTTAAGGAATTTACCTGGCAAGAAGCTAGATCCTACTTGGA
TTTCAACGTCGTTTCCTTAGTTGGTTTGTGTTCCATGTTCTTGAAGGATACCTTGGAAG
CATTTCCAAAGGAACAATATCCAGATCATAGAACTGTTGTCGTTTCCATTTCTTCCTTG
TTAGCTGTTCAAGCATTCCCAAATTGGGGTTTGTACGCTGCAGGTAAGGCAGCTAGAGA
TAGATTGTTAGGTGTTATTGCTTTGGAAGAAGCAGCTAATAACGTTAAGACCTTGAATT
ACGCTCCAGGTCCATTGGATAACGAAATGCAAGCTGATGTTAGAAGAACCTTGGGTGAT
AAAGAACAATTGAAGATTTACGATGATATGCATAAGTCTGGTTCCTTGGTTAAGATGGA
AGATTCCTCTAGAAAGTTGATTCATTTGTTAAAGGCTGATACCTTCACCTCCGGTGGTC
ATATTGATTTCTACGATGAATAA

Saccharomyces cerevisiae Putative cytoplasmic short-chain dehydrogenase/reductase (P40579)

ATGGGTAAAGTTATTTTAGTTACAGGTGTTTCCAGAGGTATCGGTAAGTCCATCGTGGA
TGTTCTTTTCAGTTTGGACAAGGACACGGTTGTTTACGGTGTAGCCAGGTCTGAGGCAC
CCTTGAAGAAGTTGAAAGAGAAGTATGGCGACAGGTTTTTTTACGTTGTCGGTGATATT
ACCGAGGATTCCGTGTTGAAGCAGTTGGTTAACGCTGCTGTTAAGGGCCACGGCAAGAT
CGACTCCTTGGTTGCCAACGCTGGTGTCCTAGAGCCCGTGCAAAATGTCAACGAGATTG
ATGTCAACGCTTGGAAGAAGCTGTATGACATCAACTTCTTCAGCATTGTTTCCTTGGTT
GGCATTGCGTTACCTGAATTGAAGAAGACCAACGGTAACGTGGTATTCGTCAGTTCGGA
CGCCTGTAACATGTACTTCAGCAGTTGGGGAGCTTACGGTTCTTCAAAAGCCGCTCTGA
ACCACTTCGCCATGACTCTGGCCAACGAGGAAAGGCAAGTGAAAGCCATTGCCGTCGCC
CCAGGTATTGTGGACACAGATATGCAAGTTAACATTAGGGAGAACGTGGGGCCTTCCTC
CATGAGTGCAGAGCAATTGAAGATGTTTAGAGGTTTAAAGGAGAATAACCAGTTGCTGG
ATAGCTCTGTGCCAGCTACAGTTTATGCCAAATTGGCCCTTCATGGTATTCCTGACGGT
GTTAATGGACAGTACTTGAGCTATAATGACCCTGCCTTGGCGGACTTTATGCCTTAA

Thalassiosira pseudonana Sepiapterin reductase (B8BVR3)

ATGCAAAACAAGGAAAACGATGAAACCTCCATTGTTGTCGATATTCATGAAATGGATTT
GTCCGATTTGGATATTTTGGCTGTTAACATGAAGTTGTTGTTTGAATTCTACACCAAGG
TTACCAAGTACAATCAATGTTGGTTGTTCAACAATGCTGGTTCCTTGGGTCCATTGGGT
CCAACCTTGTCCTTGTGTAACGGTGATCCATTGAGATTAATGCAAGATTTGAAGAAAGC
TGTTGATTTGAACGTTACCTCCGCTACCTGGATTTCCTCACAATTCGTTTCCACCTTTG
GTTCCTCTCATAAGGACGATACTCCACCATTGGTTAGAATTGTTAACATTTCTTCCTTG
TGTGCTATTGAACCATTCCAAACTATGGCTGTTTACTGTATGGGTAAGGCTGCAAGAGA
TATGTACCATTTGGTTTTGGCTAAAGAACATAAGGATTCCGATACTATGAAAGTTTTGA
ACTACGCTCCAGGTCCTTGTGATACTGAAATGACTGATGTTTTGGCTGGTTCTGCTGTT
TTGGATTGGGATTTGCATCAATATTACGCTACATCCAAGAGAGATCAAAAGTTGGTTGA
TCCTTTGGATTCTGCTAAGAAATTGATTGAATTGTTAGAAAAGGATGAATTCACCACAG
GTTCCCATGTTGATTACTTCGATGTTTAA

Homo sapiens Pterin-4-alpha-carbinolamine dehydratase (P61457)

ATGGCTGGTAAAGCTCATAGATTGTCTGCTGAAGAAAGAGATCAATTGTTGCCAAACTT
GAGAGCTGTTGGTTGGAACGAATTGGAAGGTAGAGATGCTATTTTCAAGCAATTCCATT
TCAAAGATTTCAATAGAGCCTTCGGTTTCATGACTAGAGTTGCCTTGCAAGCTGAAAAG
TTAGATCATCATCCAGAATGGTTCAACGTCTACAATAAGGTCCATATTACCTTGTCCAC
TCATGAATGTGCTGGTTTGTCTGAAAGAGATATTAACTTGGCATCCTTCATTGAACAAG
TCGCTGTCTCCATGACTTAA

Homo sapiens Dihydropteridine reductase (P09417)

ATGGCAGCTGCTGCAGCCGCTGGTGAAGCTAGAAGAGTTTTGGTTTACGGTGGTAGAGG
TGCTTTGGGTTCTAGATGTGTCCAAGCATTCAGAGCTAGAAATTGGTGGGTTGCTTCTG
TTGATGTCGTTGAAAACGAAGAAGCATCTGCTTCTATTATTGTTAAAATGACTGATTCT
TTTACTGAACAAGCTGATCAAGTTACTGCTGAAGTTGGTAAATTGTTAGGTGAAGAGAA
AGTTGATGCTATTTTGTGTGTTGCTGGTGGTTGGGCTGGTGGTAACGCTAAATCTAAAT
CTTTGTTTAAGAATTGTGATTTGATGTGGAAACAATCTATTTGGACTTCTACTATTTCT
TCTCATTTGGCTACTAAACATTTGAAAGAAGGTGGTTTGTTAACTTTGGCAGGTGCTAA
AGCTGCTTTGGATGGTACTCCAGGTATGATTGGTTACGGTATGGCTAAAGGTGCAGTTC

ATCAATTGTGTCAATCTTTGGCTGGTAAGAACTCTGGTATGCCACCTGGTGCAGCTGCT
ATTGCTGTTTTGCCAGTTACTTTGGATACACCAATGAATAGAAAATCTATGCCAGAAGC
TGATTTCTCTTCTTGGACTCCATTGGAATTCTTGGTTGAAACTTTTCATGATTGGATTA
CTGGAAAGAATAGACCATCTTCTGGTTCTTTGATTCAAGTTGTTACTACTGAAGGTAGA
ACTGAATTGACTCCAGCTTATTTCTAA

Mus musculus Tyrosine 3-monooxygenase (P24529)

ATGCCAACTCCATCCGCTTCCTCCCCACAACCAAAGGGTTTCAGACGCGCTGTGTCTGA
ACAAGATACTAAGCAAGCTGAAGCTGTTACTTCCCCAAGATTCATCGGTAGAAGACAAT
CTTTGATTGAAGATGCTAGAAAGGAAAGAGAAGCTGCAGCTGCAGCCGCTGCAGCCGCT
GTTGCTTCTGCTGAACCAGGTAATCCATTGGAAGCTGTTGTCTTCGAAGAAAGAGATGG
TAATGCTGTTTTGAATTTGTTGTTCTCTTTGAGAGGTACTAAGCCATCTTCCTTGTCTA
GAGCTCTAAAGGTATTCGAAACTTTCGAAGCTAAGATTCATCATTTGGAAACTAGACCT
GCACAAAGACCATTGGCTGGTTCCCCACATTTGGAATACTTCGTTAGATTTGAAGTTCC
ATCCGGTGATTTGGCTGCTTTGTTGTCTTCCGTTAGAAGAGTTTCTGATGATGTTAGAT
CCGCTAGAGAAGATAAGGTTCCTTGGTTTCCAAGAAAGGTTTCTGAATTGGATAAGTGT
CATCATTTGGTTACTAAGTTTGATCCAGATTTGGATTTGGATCATCCAGGTTTCTCCGA
TCAAGCATACAGACAAAGAAGAAAGTTGATTGCTGAAATTGCTTTCCAATACAAGCAAG
GTGAACCAATTCCACATGTTGAATACACTAAGGAAGAAATTGCTACTTGGAAGGAAGTT
TACGCTACTTTGAAGGGTTTGTACGCTACTCATGCTTGTAGAGAACATTTGGAAGCATT
TCAATTGTTGGAAAGATACTGTGGTTACAGAGAAGATTCTATTCCACAATTGGAAGATG
TTTCTCATTTCTTGAAGGAAAGAACTGGTTTCCAATTGAGACCAGTTGCTGGTTTGTTG
TCCGCTAGAGATTTCTTGGCTTCCTTGGCTTTCAGAGTTTTCCAATGTACTCAATACAT
TAGACATGCTTCCTCCCCAATGCATTCTCCAGAACCAGATTGTTGTCATGAATTGTTGG
GTCATGTTCCAATGTTGGCTGATAGAACTTTCGCTCAATTCTCTCAAGATATTGGTTTG
GCTTCTTTGGGTGCTTCTGATGAAGAAATTGAAAAGTTGTCCACTGTTTACTGGTTTAC
TGTTGAATTTGGTTTGTGTAAGCAAAATGGTGAATTGAAGGCTTACGGTGCCGGATTGT
TGTCCTCTTACGGTGAATTGTTGCATTCTTTGTCTGAAGAACCAGAAGTTAGAGCTTTC
GATCCAGATACTGCTGCTGTTCAACCATACCAAGATCAAACTTACCAACCAGTTTACTT
CGTTTCTGAATCTTTCTCTGATGCTAAGGATAAGTTGAGAAATTACGCTTCTAGAATCC
AAAGACCATTCTCTGTTAAGTTTGATCCATACACTTTGGCTATTGATGTCTTGGATTCT
CCACATACTATTAGAAGATCTTTGGAAGGTGTTCAAGATGAATTGCATACTTTGACTCA
AGCATTGTCTGCTATTTCTTAA

Homo sapiens Tryptophan-5-hydroxylase 2 isoform 1 AA145-460 (Q8IWU9-1)

ATGGAAGAATTGGAAGATGTTCCTTGGTTCCCAAGAAAGATTTCCGAATTGGATAAGTG
TTCCCATAGAGTTTTGATGTATGGTTCCGAATTGGATGCTGATCATCCAGGTTTCAAGG
ATAATGTTTACAGACAAAGAAGAAAGTACTTCGTTGATGTTGCTATGGGTTACAAGTAC
GGTCAACCAATTCCAAGAGTTGAATACACTGAAGAAGAAACTAAGACTTGGGGCGTTGT
GTTCAGAGAATTGTCCAAGTTGTACCCAACTCATGCTTGTAGAGAATACTTGAAGAATT
TCCCATTGTTGACTAAGTACTGTGGTTACAGAGAAGATAATGTTCCACAATTGGAAGAT
GTTTCCATGTTCTTGAAGGAAAGATCCGGTTTCACTGTTAGACCAGTTGCTGGTTACTT
GTCCCCAAGAGATTTCTTGGCTGGTTTGGCTTACAGAGTCTTCCATTGTACTCAATACA
TTAGACATGGTTCCGATCCATTGTACACTCCAGAACCAGATACTTGTCATGAATTGTTG
GGTCATGTTCCATTGTTGGCTGATCCAAAGTTCGCTCAATTCTCCCAAGAAATTGGTTT
GGCTTCCTTGGGTGCTTCCGATGAAGATGTTCAAAAGTTGGCTACTTGTTACTTCTTCA

CTATTGAATTCGGTTTGTGTAAGCAAGAAGGTCAATTGAGAGCTTACGGTGCTGGTTTG
TTATCCTCTATTGGTGAATTGAAGCACGCTTTGTCCGATAAGGCTTGTGTTAAGGCTTT
CGACCCAAAGACTACTTGTTTGCAAGAATGTTTGATTACTACTTTCCAAGAAGCATACT
TCGTTTCCGAATCCTTCGAAGAAGCTAAGGAGAAGATGAGAGATTTCGCTAAGTCCATT
ACTAGACCATTCTCCGTTTACTTCAATCCATACACTCAATCCATTGAAATTTTGAAGGA
TACTTAA

Sus scrofa Aromatic-L-amino-acid decarboxylase (P80041)

ATGAATGCTTCTGATTTTAGAAGGAGAGGTAAAGAAATGGTTGACTACATGGCTGATTA
CTTGGAAGGTATTGAAGGTAGACAAGTTTACCCAGATGTTCAACCAGGTTACTTGAGAC
CATTGATTCCAGCTACTGCTCCACAAGAACCAGATACTTTTGAAGATATTTTGCAAGAT
GTTGAGAAGATTATTATGCCAGGTGTCACACATTGGCACTCGCCATACTTCTTTGCTTA
CTTCCCAACTGCTTCCTCCTACCCAGCTATGTTGGCTGATATGTTGTGTGGTGCTATTG
GTTGTATTGGTTTCTCCTGGGCTGCTTCCCCAGCTTGTACTGAATTGGAAACTGTTATG
ATGGATTGGTTGGGTAAAATGTTGCAATTGCCAGAAGCCTTCTTGGCTGGTGAAGCTGG
TGAAGGTGGTGGTGTTATTCAAGGTTCCGCTTCCGAAGCTACTTTGGTTGCTTTGTTGG
CTGCTAGAACTAAAGTTACTAGAAGATTGCAAGCTGCTTCTCCAGGTTTGACTCAAGGT
GCTGTTTTGGAGAAGTTGGTTGCTTACGCCTCCGACCAAGCTCATTCCTCCGTTGAAAG
AGCTGGTTTGATTGGTGGTGTTAAATTGAAAGCTATTCCATCCGATGGTAAATTTGCTA
TGAGAGCTTCCGCTTTGCAAGAAGCCTTGGAAAGAGATAAAGCTGCTGGTTTGATTCCA
TTCTTCGTTGTTGCTACTTTGGGTACTACTTCCTGTTGTTCCTTTGATAATTTGTTGGA
AGTTGGTCCAATTTGTCATGAAGAAGATATTTGGTTGCATGTTGATGCTGCTTACGCTG
GTTCCGCTTTCATTTGTCCAGAATTTAGACATTTGTTGAATGGTGTTGAATTTGCTGAT
TCCTTTAATTTCAATCCACATAAATGGTTGTTGGTTAATTTTGATTGTTCCGCTATGTG
GGTTAAAAGAAGAACTGATTTGACTGGTGCTTTTAAATTGGACCCAGTTTACTTGAAAC
ATTCCCATCAAGGTTCCGGTTTGATTACTGATTACAGACATTGGCAATTGCCATTGGGT
AGAAGATTTAGATCCTTGAAAATGTGGTTTGTCTTCAGAATGTACGGTGTTAAAGGTTT
GCAAGCCTACATTAGAAAGCATGTTCAATTGTCCCATGAATTTGAAGCCTTTGTTTTGC
AAGATCCAAGATTTGAAGTTTGTGCTGAAGTTACTTTGGGTTTGGTTTGTTTTAGATTG
AAAGGTTCCGATGGTTTGAATGAGGCTTTGTTGGAAAGAATTAATTCCGCTAGAAAGAT
TCATTTGGTTCCATGTAGATTGAGAGGTCAATTTGTTTTGAGATTTGCTATTTGTTCCA
GAAAAGTTGAATCCGGTCATGTTAGATTGGCTTGGGAACATATTAGAGGTTTGGCTGCT
GAATTGTTGGCTGCTGAAGAAGGTAAAGCTGAAATTAAATCTTAA

Ophiorrhiza pumila Strictosidine synthase (6x-His tag underlined) (Q94LW9) (Sequence from Bernhardt et al. (2010) *Tetrahedron Lett.* 51, 4400-4402)

ATGGGCTCTCCTGAGTTTTTCGAATTTATTGAAGCACCGTCTTATGGTCCAAATGCGTA
TGCGTTCGACAGCGACGGCGAGTTGTATGCGAGCGTGGAAGACGGTCGTATTATCAAGT
ACGACAAGCCTTCTAACAAATTCCTGACTCATGCTGTTGCCAGCCCGATCTGGAACAAT
GCCCTGTGTGAGAATAATACCAACCAAGACCTGAAGCCGCTGTGCGGTCGCGTCTACGA
CTTTGGTTTTCATTATGAAACGCAGCGCCTGTACATTGCAGATTGCTACTTCGGCTTGG
GCTTTGTTGGTCCGGACGGCGGTCACGCGATTCAACTGGCAACCTCCGGTGATGGCGTT
GAGTTCAAGTGGCTGTACGCGTTGGCGATCGACCAACAGGCAGGCTTCGTCTACGTGAC
GGACGTTTCTACTAAGTACGATGATCGTGGTGTTCAGGACATTATTCGCATTAATGATA
CCACGGGTCGCCTGATTAAGTATGACCCTTCGACCGAAGAGGTGACCGTGCTGATGAAA
GGCCTGAATATTCCGGGCGGTACCGAGGTTAGCAAAGACGGTAGCTTTGTGCTGGTTGG

TGAGTTCGCGTCGCATCGTATCCTGAAGTACTGGCTGAAGGGTCCGAAGGCCAATACCA
GCGAGTTTCTGCTGAAGGTGCGCGGTCCAGGTAATATCAAACGTACCAAAGATGGTGAT
TTCTGGGTTGCGTCCAGCGATAACAACGGCATCACGGTGACGCCACGTGGTATCCGCTT
CGATGAGTTTGGCAACATTCTGGAGGTCGTTGCTATTCCGCTGCCGTATAAAGGTGAAC
ATATCGAGCAGGTCCAAGAACACGACGGCGCCCTGTTCGTGGGTAGCCTGTTTCATGAG
TTCGTCGGCATCCTGCATAACTATAAGAGCAGCGTTGACCATCATCAGGAAAAGAACTC
GGGTGGTCTGAACGCGAGCTTCAAGGAGTTCTCTTCGTTTGGATCTCATCACCATCACC
ATCACTAG

DNA synthesized for chapter 3:

Homo sapiens 5-Hydroxytryptamine receptor 1A (P08908)

ATGGATGTTCTATCTCCAGGTCAAGGTAACAACACTACTTCTCCACCAGCTCCATTCGA
AACTGGTGGTAACACTACTGGTATCTCTGATGTTACTGTCTCTTATCAAGTCATTACTT
CCTTGTTGTTAGGTACATTGATCTTCTGTGCTGTCTTAGGTAATGCTTGTGTTGTTGCT
GCTATTGCACTAGAAAGATCCTTACAAAACGTTGCTAACTACTTGATTGGATCTTTGGC
TGTTACTGATTTGATGGTTTCTGTCTTAGTCTTACCAATGGCTGCTTTGTATCAAGTCT
TGAACAAATGGACATTGGGTCAAGTTACTTGTGATTTGTTCATAGCTTTGGATGTCTTA
TGTTGTACTTCATCTATCTTACATTTGTGTGCTATTGCTTTGGATAGATACTGGGCTAT
CACTGATCCAATTGATTACGTTAACAAGAGAACTCCAAGAAGAGCAGCTGCATTGATAT
CATTGACTTGGTTGATTGGTTTCTTGATTTCCATTCCACCTATGTTAGGTTGGAGAACA
CCAGAAGATAGATCTGATCCAGATGCTTGTACTATCTCTAAAGATCATGGTTACACTAT
CTACTCTACTTTCGGTGCTTTCTACATTCCATTGCTATTGATGTTGGTTCTATACGGTA
GAATCTTCAGAGCTGCTAGATTCAGAATCAGAAAGACAGTTAAGAAAGTTGAAAAGACT
GGTGCTGATACTAGACATGGTGCTTCTCCAGCTCCACAACCAAAGAAGTCTGTTAACGG
TGAATCTGGTTCTAGAAACTGGAGATTAGGTGTTGAATCTAAAGCTGGTGGTGCTTTGT
GTGCAAACGGTGCTGTTAGACAAGGTGACGACGGTGCTGCTTTGGAAGTCATTGAAGTT
CATAGAGTTGGTAACTCTAAGGAACATTTGCCATTACCATCTGAAGCTGGTCCAACTCC
ATGTGCTCCAGCATCATTCGAAAGAAAGAACGAAAGAAACGCTGAAGCTAAGAGAAAGA
TGGCTTTGGCTAGAGAAAGGAAGACTGTCAAGACTTTGGGTATCATCATGGGAACTTTC
ATCTTGTGTTGGTTACCTTTCTTCATTGTTGCTTTGGTCCTACCATTCTGTGAATCATC
TTGTCATATGCCAACTTTGTTGGGTGCTATCATCAACTGGTTGGGTTACTCTAACTCAT
TGCTTAACCCAGTTATCTATGCTTACTTCAACAAGGATTTCCAAAACGCTTTCAAGAAG
ATCATCAAGTGTAAGTTCTGTAGACAATAA

Homo sapiens 5-Hydroxytryptamine receptor 1D (P28221)

ATGTCTCCATTGAACCAATCTGCTGAAGGTTTGCCACAAGAAGCATCCAACAGATCCTT
GAACGCTACTGAAACTTCTGAAGCATGGGACCCAAGAACTTTGCAAGCTCTAAAGATCT
CCTTGGCTGTTGTCTTGTCAGTCATTACTCTAGCTACTGTCTTGTCTAACGCTTTCGTC
TTGACTACTATCTTGTTGACTAGAAAGTTGCATACTCCAGCTAACTACTTGATTGGATC
ATTGGCTACAACTGATTTGCTAGTTTCCATCTTGGTTATGCCAATCTCCATTGCTTACA
CTATCACTCATACTTGGAACTTTGGTCAAATCTTGTGTGATATCTGGTTGTCATCTGAC
ATCACTTGTTGTACTGCTTCTATCTTGCATTTGTGTGTCATTGCTTTGGATAGATACTG
GGCTATTACTGATGCTTTGGAATACTCTAAGAGAAGAACTGCTGGTCATGCTGCTACTA

TGATTGCTATTGTCTGGGCTATCTCCATTTGTATCTCTATTCCACCTTTGTTCTGGAGA
CAAGCTAAGGCTCAAGAAGAAATGTCTGATTGTTTGGTTAACACTTCTCAAATCTCCTA
TACTATCTACTCTACTTGTGGTGCTTTCTACATTCCATCTGTTTTGTTGATCATTCTAT
ACGGTAGAATCTACAGAGCAGCTAGAAACAGAATCTTGAATCCACCATCATTGTATGGT
AAGAGATTCACTACTGCTCATTTGATTACTGGTTCAGCAGGTTCTTCATTGTGTTCCTT
GAACTCATCTTTGCATGAAGGTCATTCTCATTCTGCTGGTTCTCCATTGTTCTTCAATC
ATGTTAAGATCAAGTTGGCTGATTCTGCATTGGAAAGAAAGAGAATCTCCGCTGCTAGA
GAAAGAAAGGCTACTAAGATTCTAGGTATCATTCTAGGTGCTTTCATCATTTGTTGGTT
GCCATTCTTTGTCGTTTCCTTGGTCTTGCCAATCTGTAGAGATTCTTGTTGGATTCATC
CAGCTTTGTTCGACTTCTTCACTTGGTTGGGATACCTTAACTCTCTTATCAATCCAATC
ATCTACACTGTCTTCAACGAAGAATTCAGACAAGCATTCCAAAAGATTGTTCCATTCAG
AAAGGCTTCTTAA

<u>*Homo sapiens* 5-Hydroxytryptamine receptor 2B (P41595)</u>

ATGGCTTTGTCCTATAGAGTCTCCGAATTGCAATCTACCATTCCAGAACATATCTTGCA
ATCAACCTTCGTTCATGTTATCTCCTCTAACTGGTCAGGTCTACAAACTGAATCCATCC
CAGAAGAAATGAAGCAAATCGTCGAAGAACAAGGTAACAAGTTGCATTGGGCTGCTCTA
TTGATCTTGATGGTCATCATTCCAACCATTGGTGGTAACACCTTGGTCATCTTGGCTGT
CTCCTTGGAAAAGAAGTTGCAATACGCTACCAACTACTTCCTAATGTCTCTAGCTGTCG
CTGATTTGTTGGTTGGTCTATTCGTCATGCCAATCGCACTATTGACTATCATGTTCGAA
GCTATGTGGCCACTACCATTGGTCTTGTGTCCAGCTTGGTTGTTCCTGGATGTCTTGTT
CTCTACCGCTTCCATCATGCATTTGTGTGCTATCTCTGTTGACAGATACATCGCTATTA
AGAAGCCAATTCAAGCTAATCAATACAACTCTAGAGCTACAGCTTTCATTAAGATCACT
GTTGTCTGGTTGATTTCTATTGGTATTGCTATTCCAGTTCCAATCAAAGGTATTGAAAC
TGATGTTGATAATCCAAACAACATTACTTGTGTCTTGACTAAGGAAAGATTCGGAGATT
TCATGTTGTTCGGTTCCTTGGCTGCTTTCTTCACTCCATTGGCTATTATGATTGTCACC
TACTTCTTGACCATCCATGCTTTGCAAAAGAAGGCTTACCTAGTCAAGAACAAACCACC
ACAAAGATTGACTTGGTTGACTGTCTCCACTGTCTTCCAAAGAGATGAAACTCCTTGTT
CATCACCAGAAAAGGTTGCTATGTTGGATGGTTCTAGAAAGGATAAGGCTTTGCCAAAC
TCTGGTGACGAAACCTTGATGAGAAGAACTTCTACCATCGGTAAGAAGTCTGTTCAAAC
CATCTCTAACGAACAAAGAGCTTCCAAAGTCTTGGGTATTGTCTTCTTCTTGTTCTTGT
TGATGTGGTGTCCATTCTTCATTACTAACATTACCCTAGTCTTGTGTGATTCCTGTAAC
CAAACTACCTTGCAAATGTTGTTGGAAATCTTCGTCTGGATTGGTTACGTCTCTTCAGG
TGTTAATCCATTGGTTTACACTTTGTTCAACAAGACTTTCAGAGATGCTTTCGGAAGAT
ACATAACTTGTAACTACAGAGCTACCAAGTCTGTTAAGACTTTGAGAAAGAGATCTTCT
AAGATTTACTTTAGAAATCCAATGGCTGAAAACTCTAAGTTCTTCAAGAAGCATGGTAT
TAGAAACGGTATTAATCCAGCTATGTATCAATCACCAATGAGATTGAGATCTTCAACTA
TTCAATCTTCATCTATCATCTTGTTGGATACTCTATTGTTGACTGAAAACGAAGGTGAT
AAGACTGAAGAGCAAGTCTCTTACGTTTAA

<u>*Homo sapiens* 5-Hydroxytryptamine receptor 4, isoform B (Q13639-1)</u>

ATGGATAAGTTGGATGCTAACGTTTCTTCCGAAGAAGGTTTCGGTTCTGTTGAAAAGGT
TGTCTTGCTAACATTCTTGTCTACTGTCATCTTGATGGCTATCTTGGGTAACTTGTTGG
TTATGGTTGCTGTTTGTTGGGATAGACAATTGAGAAAGATTAAGACTAACTACTTCATT
GTTTCCTTGGCTTTCGCTGATTTGTTGGTCTCTGTCTTGGTTATGCCATTCGGTGCTAT
TGAATTGGTTCAAGATATCTGGATTTACGGTGAAGTCTTCTGTTTGGTTAGAACTTCTT

TGGATGTCTTGTTGACTACTGCTTCTATCTTCCATTTGTGTTGTATTTCCTTGGATAGA
TATTACGCTATCTGTTGTCAACCATTGGTTTACAGAAACAAGATGACTCCATTGAGAAT
TGCTTTGATGTTGGGTGGTTGTTGGGTCATTCCTACTTTCATCTCTTTCTTGCCAATCA
TGCAAGGTTGGAACAACATTGGTATCATCGATTTGATTGAAAAGAGAAAGTTCAACCAA
AACTCTAACTCTACTTACTGTGTCTTCATGGTTAACAAGCCATACGCTATTACTTGTTC
CGTCGTTGCTTTCTACATTCCATTCCTATTGATGGTCTTGGCTTACTACAGAATCTACG
TTACTGCTAAGGAACATGCTCATCAAATCCAAATGTTGCAAAGAGCTGGTGCTTCCTCT
GAATCTAGACCACAATCTGCTGATCAACATTCTACTCATAGAATGAGAACTGAAACTAA
GGCTGCTAAGACCTTGTGTATCATCATGGGATGTTTCTGTTTGTGTTGGGCTCCATTCT
TCGTTACTAACATCGTTGATCCATTCATCGATTACACTGTTCCAGGTCAAGTTTGGACT
GCTTTCTTGTGGTTGGGTTACATCAACTCTGGTTTGAATCCATTCTTGTACGCATTCTT
GAACAAGTCTTTCAGAAGAGCTTTCTTGATCATCTTGTGTTGTGATGATGAAAGATACA
GAAGACCATCTATCCTAGGTCAAACTGTTCCTTGTTCTACTACTACTATCAACGGTTCC
ACACATGTCTTGAGAGATGCTGTTGAATGTGGTGGACAATGGGAATCTCAATGTCATCC
ACCAGCTACTTCTCCATTGGTTGCAGCTCAACCATCTGATACCTAA

<u>*Homo sapiens* 5-Hydroxytryptamine receptor 5A (P47898)</u>

ATGGATTTGCCAGTTAACTTGACTTCTTTCTCTTTGTCCACTCCATCTCCATTGGAAAC
TAATCATTCCTTGGGTAAAGATGATTTGAGACCATCTTCACCATTGCTATCAGTCTTCG
GTGTCTTGATCTTGACTTTGTTGGGTTTCTTGGTTGCAGCTACTTTCGCTTGGAACTTG
CTAGTCTTGGCTACTATCTTGAGAGTTAGAACTTTCCATAGAGTTCCACATAACTTGGT
TGCTTCCATGGCTGTCTCTGACGTCTTGGTCGCTGCATTGGTTATGCCATTGTCCTTGG
TTCACGAATTGTCTGGTAGGAGATGGCAATTGGGTAGAAGATTGTGTCAATTGTGGATT
GCTTGTGATGTCTTGTGTTGTACTGCTTCCATCTGGAACGTTACTGCTATTGCTTTGGA
TAGATATTGGTCCATTACTAGACATATGGAATACACATTGAGAACTAGAAAGTGTGTTT
CCAACGTTATGATTGCTTTGACTTGGGCTTTGTCTGCTGTCATTTCCTTGGCTCCATTG
TTGTTTGGTTGGGGTGAAACTTACTCTGAAGGTTCAGAAGAATGTCAAGTTTCTAGAGA
ACCATCTTACGCTGTCTTCTCTACTGTTGGTGCTTTCTATTTGCCATTGTGTGTTGTCT
TGTTTGTCTATTGGAAGATTTACAAAGCTGCTAAGTTTAGAGTTGGTTCTAGAAAGACT
AATTCTGTTTCTCCAATCTCTGAAGCTGTTGAAGTCAAAGATTCTGCTAAACAACCACA
AATGGTTTTCACTGTTAGACATGCTACTGTTACTTTCCAACCAGAAGGTGATACTTGGA
GAGAACAAAAGGAACAAAGAGCTGCTTTGATGGTTGGTATCTTGATTGGTGTTTTCGTC
CTATGTTGGATTCCATTCTTCTTGACTGAATTGATTTCTCCATTGTGTTCATGTGATAT
TCCAGCTATCTGGAAATCTATCTTCTTGTGGTTGGGTTATTCCAATTCCTTCTTCAATC
CATTGATCTATACTGCATTCAATAAGAACTACAATTCTGCTTTCAAGAACTTCTTCTCT
AGACAACATTAA

<u>*Homo sapiens* 5-Hydroxytryptamine receptor 6 (P50406)</u>

ATGGTTCCAGAACCAGGTCCAACTGCTAACTCTACTCCAGCTTGGGGTGCTGGTCCACC
ATCTGCTCCAGGAGGTTCTGGTTGGGTTGCTGCTGCTTTGTGTGTTGTTATTGCTTTAA
CTGCTGCAGCTAATTCTCTATTGATTGCTCTAATTTGTACTCAACCAGCTTTGAGAAAC
ACTTCTAACTTCTTCTTGGTTTCATTGTTCACTTCTGATTTGATGGTTGGTTTGGTTGT
CATGCCACCAGCTATGTTGAACGCTTTGTACGGTAGATGGGTTTTGGCTAGAGGTTTGT
GTTTGTTATGGACTGCTTTCGATGTTATGTGTTGTTCTGCTTCTATCTTGAACTTGTGT
TTGATTTCTTTGGATAGATACTTGTTGATTTTGTCTCCTTTGAGATACAAGTTAAGAAT
GACTCCATTGAGAGCATTAGCTCTAGTTTTGGGAGCTTGGTCTTTGGCTGCTTTGGCAT

CTTTCTTACCTTTGCTATTGGGTTGGCATGAATTAGGTCATGCTAGACCACCAGTTCCA
GGTCAATGTAGATTGTTAGCTTCTTTACCATTTGTCTTGGTTGCTTCCGGTTTGACTTT
CTTCTTGCCATCTGGTGCTATTTGTTTCACTTACTGTAGAATTTTGTTAGCTGCTAGAA
AACAAGCTGTTCAAGTTGCTTCTTTAACTACTGGTATGGCTTCTCAAGCATCTGAAACT
TTACAAGTTCCAAGAACTCCAAGACCAGGTGTTGAATCTGCTGATTCTAGAAGATTGGC
TACTAAACATTCTAGAAAGGCTTTGAAAGCATCCTTAACTTTGGGTATCTTGTTAGGTA
TGTTCTTTGTTACTTGGTTACCATTCTTTGTTGCTAACATTGTTCAAGCTGTTTGTGAT
TGTATTTCTCCAGGTTTGTTTGATGTTTTGACTTGGTTAGGATATTGTAATTCTACTAT
GAATCCAATCATCTATCCATTGTTTATGAGAGATTTCAAGAGAGCTTTAGGTAGATTCT
TGCCTTGTCCAAGATGTCCAAGAGAAAGACAAGCATCTTTGGCTTCTCCATCTTTGAGA
ACTTCTCATTCTGGTCCAAGACCTGGTTTGTCTTTACAACAAGTTTTGCCATTACCATT
ACCACCAGATAGTGATTCAGATTCTGATGCTGGTTCAGGTGGTTCATCTGGTTTGAGAT
TAACTGCTCAATTGTTGTTACCAGGTGAAGCTACTCAAGATCCTCCTTTGCCAACAAGA
GCTGCCGCTGCAGTTAATTTCTTCAACATTGATCCTGCTGAACCTGAATTGAGACCACA
TCCATTAGGTATTCCAACTAATTAA

ZsGreen

ATGGCTCAATCTAAGCATGGTTTGACTAAGGAAATGACTATGAAGTACAGAATGGAAGG
TTGTGTTGACGGTCATAAGTTCGTTATCACTGGTGAAGGAATTGGTTATCCATTCAAAG
GTAAGCAGGCTATCAACTTGTGTGTTGTTGAAGGTGGTCCATTGCCATTCGCTGAAGAC
ATCTTGTCTGCTGCTTTCATGTACGGTAACAGAGTCTTCACTGAATACCCACAAGACAT
TGCTGATTACTTCAAGAACTCTTGTCCAGCTGGTTACACTTGGGATAGATCCTTCTTGT
TTGAAGATGGTGCTGTTTGTATCTGTAATGCTGATATCACTGTTTCTGTTGAAGAAAAC
TGTATGTATCATGAATCTAAGTTCTATGGTGTCAACTTCCCAGCTGATGGTCCAGTTAT
GAAGAAGATGACTGATAACTGGGAACCATCTTGTGAAAAGATCATTCCAGTTCCAAAGC
AAGGTATCTTGAAAGGTGATGTTTCTATGTACTTGCTATTGAAAGATGGTGGTAGATTG
AGATGTCAATTCGATACTGTCTACAAAGCTAAGTCTGTTCCAAGAAAGATGCCAGATTG
GCATTTCATTCAACATAAGTTGACTAGAGAAGATAGATCTGATGCTAAGAATCAAAAGT
GGCATCTAACTGAACATGCTATTGCTTCTGGTTCTGCTTTGCCATAA